Periodically driven topological non-interacting and interacting quantum lattice systems

Dissertation
zur
Erlangung des Doktorgrades (Dr. rer. nat.)
der
Mathematisch-Naturwissenschaftlichen Fakultät
der
Rheinischen Friedrich-Wilhelms-Universität Bonn

von
Qiu, Haixin
aus
Chengdu, P.R.China

Bonn, 2022

Dieser Forschungsbericht wurde als Dissertation von der Mathematisch-Naturwissenschaftlichen Fakultät der Universität Bonn angenommen und ist auf dem Hochschulschriftenserver der ULB Bonn https://nbn-resolving.org/urn:nbn:de:hbz:5-66481 elektronisch publiziert.

1. Gutachter:	Prof. Dr. Johann Kroha
2. Gutachter:	Prof. Dr. David Luitz
Tag der Promotion:	13.04.2022
Erscheinungsjahr:	2022

Abstract

Periodically driven quantum lattice systems are nowadays reachable in the laboratory. Those systems, which can host exotic non-equilibrium phases and phenomena, attract intensive theoretical studies. In this thesis, we use field theoretical Keldysh-Floquet methods to study periodically driven topological lattice systems, especially the non-interacting and interacting Rice-Mele models that can support topological transports. With the theoretical understanding of the periodically driven topological phases, we found dissipative stabilized quantized non-adiabatic charge pumps in a non-interacting lattice model. This dissipative charge pump is observed in the wave-guide experiments. Further, we studied the strongly correlated driven topological lattice systems through the non-equilibrium Floquet-Keldysh dynamical mean-field theory. In our studies, we covered the adiabatic to high-frequency regimes and weakly interacting to strongly interacting regimes for the interacting systems. This may give us a qualitative picture of the strongly correlated quantum phases in periodically driven topological lattice models.

Acknowledgements

I would like to thank my advisor Prof. Johann Kroha sincerely and deeply. His encouragements and supports make this thesis possible. Over the years I learn a lot from Hans through lectures and discussions.

I would like to thank my Ph.D. examination committee, Prof. Johann Kroha, Prof. David Luitz, Prof. Stefan Linden, and Prof. Olav Schiemann.

I would like to thank the staff of the physics institute of University of Bonn, especially Andreas Wißkirchen, Petra Weiß, Patricia Zündorf and Christa Börsch.

I would like to thank Zlata Fedorova and Prof. Stefan Linden for the collaboration on the plasmonic wave-guide and non-adiabatic Thouless pump.

I would like to thank Oliver Freyermuth and Peter Wienemann and Philip Bechtle, for their work, the second generation of the Bonn Analysis Facility (BAF2) which is the computer cluster in the physics institute. The BAF2 is user friendly. It greatly helped me with numerical computations and saved me a ton of time.

I would like to thank all the group people in the condensed matter theory group of Prof. Kroha. We had many discussions on various topics. I thank Lai Zhong Yuan for many discussions at the early stage of my thesis. Special thank Tim Bode, for the discussions of the Keldysh method. I would like to thank Francisco Meirinhos, and Marvin Lenk for the discussions of numerical methods, and the equilibrium NCA code. I thank Michael Turaev, Aya Abouelela, Ulli Pohl, Kateryna Zatsarynna, Michael Kajan, Sayak Ray, Lukas Köbbing, Christopher Lietmeyer, Krzysztof Piotr Wójcik, Farzaneh Zamani, Pierre Seyb, Paul Züge, Bastian Havers, Fulya Koc, Johannes Rentrop, Ammar Nejati, Soroush Arabi, Mert Bozkurt for discussions and helps.

I would like to thank Prof. Imke Schneider, my advisor inside the SFB 185 OSCAR. I thank SFB 185 OSCAR secretary Ruth Ellen Bischoff. I also would like to thank all the students and professors in SFB 185 OSCAR. I learned a lot from the lectures and talks from professors. The discussions with Maximilian Kiefer-Emmanouilidis, Christoph Dauer, Rui Li, Christopher Mink, and many other students are very useful. I can still clearly remember the OSCAR student school in 2018 and many other events, and dinners, where I learned and enjoyed a lot.

I would like to thank the lecturers in Bonn-Cologne Graduate School of Physics and Astronomy (BCGS), and also the lecturers in the Bonn physics institute series, that is PI, BCTP, HISKP, and IAP as well as the colloquiums, such as the Physics Colloquium and Bethe Colloquium. I listened and learned a lot from them. I also enjoyed the discussions with my BCGS classmates, and they helped me many times. The BCGS also gives many quality lectures from outside of Bonn, for instance, the BCGS intensive week on topological insulators by Janos Asboth. Also, I would like to thank Prof. Hartmut Monien for his encouragements.

I am grateful that I have many opportunities to attend meetings and schools with the support of group Prof. Kroha. I would like to thank the all lecturers there that stimulated questions and discussions,

including Prof. Jean Zinn-Justin, Prof. Jürg Fröhlich. This also reminded me that I hope the corona (COVID-19) time will pass soon, I miss DPG centre Bad Honnef where I listened to a lot of great talks, and I hope relaxed discussion sessions on physics with beer are again possible, without worries.

I would like to thank the online resources, and the people behind them, on Wikipedia, Stack Overflow, Github, Zhihu, and many other platforms. They helped and continue to help me a lot.

I would like to thank Hoid Bai Long, Du Meng Lin, Pang Jin Yi, Wang Yi Fan, Zhang Zhong Yi, Zhang Rui, Zhao Rong Chuan, Shi Meng, Xu Yong, Wang Xin, Zhang Si Nuo, Du Peng, Wang Yang, Zhang Jia Ju, Liu Liu Ming, Wang Qian, Yang Di, Dong Xiao Yu, He shu, Lan Mu, and many others (a complete list would be too long), for discussions of physics. Surely I can also remember the events besides physics, the enjoyable parties, sports, and dinners, with people living in Bonn, in Germany, and even in other places in Europe. To avoid making another thesis of acknowledgements I will stop here.

I would like to thank my wife Cao Lu.

I would like to thank my parents for their understanding.

Contents

CHAPTER 1

Introduction

1.1 Introduction

Real-time dynamics and non-equilibrium phenomena appear in all areas of physics, including cosmology [1], particle and nuclear physics [2], atomic physics, condensed matter physics [3], chemical and biological systems [4] and many other areas. The examples are the inflation model of the early universe, the quark-gluon plasma, the optical lattice dynamics, ultrafast dynamics of electronic systems, molecular dynamics, and so on.

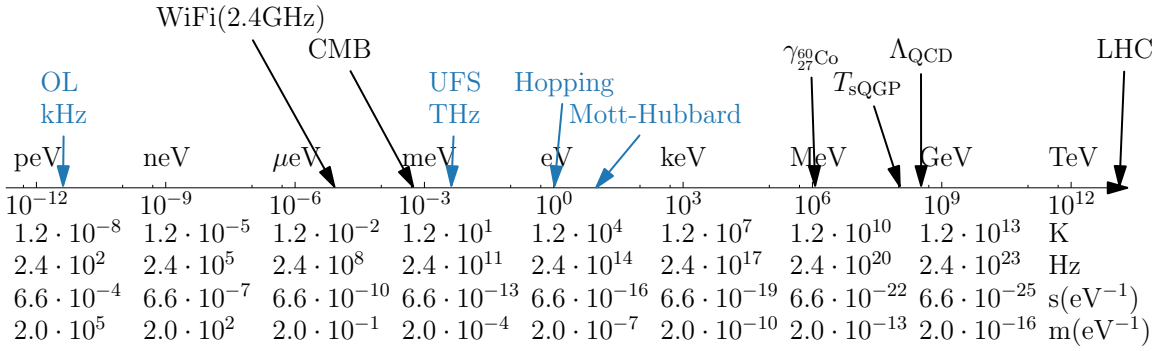

Figure 1.1: A scale graph for the energy scales in nature. The optical lattice (OL) is at kHz, where the tunneling rate or the hopping in fermionic atoms are about [5] 10^2 to 10^3 Hz, the interaction strength is tunable by the Feshbach resonance. The Wi-Fi frequency, 2.4 GHz. The ultrafast spectroscopy [6] (UFS) at THz. The plasmonic wave-guide has the hopping amplitude $J_0 = 0.144\mu\text{m}^{-1} = 1.44\times10^5\text{m}^{-1} \sim 0.03$eV which is near THz. The spectral radiance peak value of the cosmic microwave background (CMB) [7] which is about 160 GHz, the corresponding temperature is about 3 K. The hopping energy and the on-site Hubbard interaction energy is around eV, here we use [8] $4t^2/U \sim 0.13$ eV where t is the hopping and U is the on-site interaction. The strongly coupled quark-gluon plasma (sQGP) [2] critical temperature which is about 155 MeV. The quantum chromodynamics energy scale [9] $\Lambda_{\rm QCD} \sim 332$ MeV. The Higgs boson is about [10, 11] 125 GeV. The large hadron collider (LHC) [12] center-of-mass energy, about 13 TeV. The labels are translated to Kelvin (K), Hertz (Hz), second (s), and meter (m) for quick references.

Two areas become especially active in recent years: atomic, molecule, and optical physics that studies the light-matter interaction, and condensed matter physics that traditionally study dense matter, solids, liquids, and gases. The representative platforms are optical lattices in the kiloHertz (kHz) region and electronic systems in several electron volts (eV) regions. These activities are majorly triggered by recent year's experimental advances, which allow us to drive quantum systems in the lab far from their static or equilibrium states and reach novel phases. Many theoretical works are also motivated and are continuously improving our understanding of far-from-equilibrium quantum systems. The energy scale of those two platforms can be found in Fig. 1.1 among other scales.

There are usually two ways to drive quantum systems. One way is to apply a short but strong pulse that brings the system out of the previously static state at a certain time point or suddenly switch on/off the external field. Another way is to continuously drive the system, usually periodically. Nowadays, both of them are reachable in the lab, and in many cases, they belong to the different time scales of the same experiment realization. In this thesis, we will majorly focus on the second case, that is, to apply a periodic drive [3, 6, 13–15].

Periodically driven systems are so common that vast examples exist even in our daily life, such as engines, fans, etc. For microscopic systems that are quantum mechanical with time-periodic Hamiltonian, these systems are usually called Floquet systems. The name "Floquet" is from the French mathematician, Gaston Floquet, who purposed a theorem, the Floquet theorem, to solve the ordinary differential equations which have time-periodic parameters. The external periodical drive is thus commonly called Floquet drive.

One of the strong motivations for applying the periodical drive is that in this way experimentalists can create and control a system in a state that is inaccessible without drive. Many experiment achievements are reached in recent years. For instance, in the optical lattice [15, 16] where model parameters can be modulated by directly tuning the strength of the applied laser, the dynamical localization and photon assistant tuning are realized through Floquet drive. With the periodic drives, coherent controls, for instance, the control of the Bose-Hubbard model for superfluid to Mott insulator transition in the optical lattices, are realized and achieved in various spatial dimensions $d_s = 1, 2, 3$. Even gauge fields can be introduced through driving. People find that [17] the periodic drive can create gauge fields, e.g., magnetic fields, artificially. Those gauge fields can be thought of as a realization of lattice gauge theory, and can be used to realize topological states [15]. Although currently unreachable, if some more sophisticated setup can be done in the future, a quantum simulation, i.e., analogue quantum computing, for some very hard problems such as lattice quantum chromodynamics (QCD) would be exciting.

In electronic systems [3, 6], similar effects can be observed like those in optical lattices, which is not a surprise that one of the motivations to construct optical lattices is to quantum simulate the electronic many-body systems in a cleaner system where theoretical understanding or prediction can be verified or excluded in a conclusive way. There are interesting electronic systems, including the materials that host the Mott-Hubbard transition, the heavy-fermion Kondo systems with strong electron-impurity correlation, the topological insulators, the conventional superconductor, the high-temperature superconductor and so on, can be driven by lasers out of the equilibrium. All those electronic systems can be potentially studied by using Floquet drive, either to observe known phenomena in a "new axis" or create some new phenomena. Especially the topological systems such as topological insulators can have periodically driven extensions, and exotic phases are found, e.g., the anomalous Floquet topological insulator [13], and Floquet time-crystal [18]. They are examples that the periodically driven systems can have unique phases that static or equilibrium systems hardly reach.

All those realizations are often called "Floquet engineering" [6, 13]. As the name suggests, controlling systems with periodic drives are practical and flexible.

Theoretically, many works have been done to understand Floquet systems for non-interacting systems [6] and further for interacting and strongly correlated systems [3]. Those systems are studied by various theoretical and numerical methods. For instance, numerically, the time-dependent density matrix renormalization group [19] (t-DMRG), the non-equilibrium dynamical mean-field theory [3] (neq-DMFT), the continuous-time quantum monte-carlo [20] (ct-QMC) and others. And analytically or semi-analytically, they are studied by Bethe ansatz, perturbative and non-perturbative renormalization group. Many challenges are still there for those techniques even without drive and near equilibrium. And in the non-equilibrium and strongly periodically driven systems those problems, such as the Monte Carlo sign problem [21, 22], are even amplified. An example is that the ct-QMC for DMFT can only reach a very limited short time for the non-equilibrium real-time dynamics [3].

In this work, we study the periodically driven systems with topological structure through specific lattice models by focusing on the field theoretical method [23–28], and Green's function method [29]. Especially, we use Schwinger-Keldysh real-time Green's function and self-consistent method, e.g., the dynamical mean-field theory. These theoretical tools will give us an accessible and clear way to study Floquet systems. Some more introductions can be found in the separated chapters.

1.2 Outline

Here we give a short outline of this thesis. Chapters 1-5 are reviews and derivations of theoretical methods. Chapters 5 and 6 include computations of models and numerical results. Chapter 2-7 will be organized as follows:

Chapter 2 We review some theoretical tools that are commonly used for studying strongly correlated systems, especially the basics of the Dyson-Schwinger equations and their extensions, and many of the useful equations. I focus on the correlation functions to make the chapter concrete and in a finite length. That means we will skip many details, for instance, the path/functional integral construction or operator/second quantization.

Chapter 3 We review the so-called Keldysh method or real-time Green's functions which allow a field theoretical description for far-from-equilibrium quantum systems. The Keldysh method will allow us to compute observables from the n-point correlation functions of the non-equilibrium systems, mostly within the usual field theoretical framework.

Chapter 4 We review the topological insulators and their periodically driven generalizations, Floquet topological insulators by using geometry and topology.

Chapter 5 We discuss the Floquet theorem and its applications, especially the Floquet representations of real-time Green's functions. We also discuss the heating problems of Floquet systems briefly.

Chapter 6 We use the Rice-Mele model as an example, we reviewed the Thouless pump and its properties in the Floquet picture. Then in collaboration with the experimental group, we studied a

novel dissipative Thouless pump in photonic waveguides in detail, which is based on our understanding of the usual Thouless pump.

Chapter 7 We study the Rice-Mele Fermi Hubbard model as an example of the periodically driven strongly correlated interacting quantum many-body systems. The tool we choose is the Floquet-Keldysh dynamical mean-field theory with iterated perturbation theory (IPT) solver. In this chapter, we also discuss the slave-boson technique and non-crossing approximation (NCA) for the single impurity Anderson model and its Floquet-Keldysh form. The formalism is re-derived. We give some outlooks for this thesis at the end of this chapter.

CHAPTER 2

General field theory: Dyson-Schwinger equations

The quantum theory with many degrees of freedom can be defined in different ways, one of those ways is to define all n-point correlation functions and their relations to each other. Key equations are the celebrated Dyson-Schwinger equations (DSE) and their generalizations, such as n-particle-irreducible (n-PI) methods and functional renormalization groups (FRG). One can regard those Dyson-Schwinger equations as a set of exact "quantum equations of motion". Formally, they are infinitely coupled and truncations are needed in practical computations. I will briefly review those general field theoretical methods, DSE, n-PI, and FRG, here.

2.1 Generating functional and correlation functions

Here I use condensed notations which follows [30] for simplicity and clarity.

The generating functional of the n-point time-ordering correlation functions [30, 31] is the central and basic quantity of the quantum field theory and quantum statistical field theory. One can write the generating functional Z in a compact form as

$$Z = \mathrm{Tr}\left[\rho_0 \hat{T}_C \exp\left\{\mathrm{i}\int_{\boldsymbol{x},C(x^0)} J^{\alpha}(x)\hat{\phi}_{\boldsymbol{\alpha}}[\hat{\varphi}](x)\right\}\right] \tag{2.1}$$

Here we use the interacting picture of the full Hamiltonian without external source. Correlation functions can be generated by first applying suitable functional derivatives of the J and then set $J = 0$. The summation of same indices $\boldsymbol{\alpha}$ are implied. The $x = (x^0, x^i)$ is the space-time coordinate. The ρ_0 is the density matrix at the initial time $x^0 = t = t_0$. The $\int_{\boldsymbol{x},C(x^0)}$ is the shorthand notation of $\int_{C(t)} \mathrm{d}t\, \mathrm{d}^{d_s}x$, where $d_s = d - 1$ is the spatial dimension. Here we used the general integration contour $C(t)$ on the complex time plane $t \in \mathbb{C}$ for later convenience.[1] The Heisenberg operator $\hat{\phi}$ represents the fundamental field $\hat{\varphi}(x)$ and all their composites $\hat{\phi}[\hat{\varphi}]$. The set of fundamental field $\hat{\varphi}$ can be so-called superfield, i.e. a vector of all fields that are included in the action $S[\hat{\varphi}]$. For instance, if we include only one fundamental fermion field, $\hat{\phi}[\hat{\varphi}] = \hat{\varphi} = (\psi, \bar{\psi})$, where $\bar{\psi}$ is the canonical conjugate of ψ.

[1] We will discuss Z again in the Keldysh theory chapter, there the contour time is used.

The product $J^{\alpha}\hat{\phi}_{\alpha} = J^{\alpha}\gamma_{\alpha\beta}\hat{\phi}^{\beta}$ and the metric γ will be defined later. We also define[2]

$$J^{\alpha}\hat{\phi}_{\boldsymbol{\alpha}} = \sum_{i=1}^{i=N} J^{\alpha_1,\cdots,\alpha_{n_i}}\hat{\phi}_{\alpha_1,\cdots,\alpha_{n_i}} \tag{2.3}$$

where N is the number of the tensorial field, and n_i is the number of the tensor index of the i-th tensorial field. It is clear that the index $\boldsymbol{\alpha}$ can represent not only one vector component α_1, but also a set of tensorial components with different number of indices $\{\alpha_1, \alpha_1\alpha_2, \cdots\}$. An example would be $N = 2$ with $n_1 = 1$ and $n_2 = 2$, where

$$J^{\alpha}\hat{\phi}_{\boldsymbol{\alpha}} = J^{\alpha_1}\hat{\phi}_{\alpha_1} + J^{\alpha_1\alpha_2}\hat{\phi}_{\alpha_1\alpha_2} \tag{2.4}$$

Note the symmetries of J^{α} and $J^{\alpha_1\alpha_2}$ needs to be consistent with the symmetries of $\hat{\phi}_{\alpha}$ and $\hat{\phi}_{\alpha_1\alpha_2}$. We can simplify the notation even further by defining

$$\int_{\boldsymbol{x},C(x)} J^{\alpha}(x)\hat{\phi}_{\boldsymbol{\alpha}}(x) \equiv \boldsymbol{J^{a}}\hat{\phi}_{\boldsymbol{a}} \tag{2.5}$$

and [30] the ultra-local metric $\gamma^{\boldsymbol{a}}{}_{\boldsymbol{b}} = \delta_C(x - x')\gamma^{\alpha}{}_{\beta}$. Where the metric for $\hat{\phi}_{\boldsymbol{a}}$ is

$$\oplus_{i=1}^{N}\left(\otimes^{n_i}\gamma\right) \tag{2.6}$$

The metric should take care of the statistics of the fields, where the order of the indices and the number of indices for Bose/Fermi fields are taken into account. To achieve those proper ordering, we will use the following definitions

$$\hat{\phi}^{\boldsymbol{a}} = \gamma^{\boldsymbol{ab}}\hat{\phi}_{\boldsymbol{b}} \quad \text{and} \quad \hat{\phi}_{\boldsymbol{a}} = \hat{\phi}^{\boldsymbol{b}}\gamma_{\boldsymbol{ba}} \tag{2.7}$$

$$\gamma_{\boldsymbol{b}}{}^{\boldsymbol{a}} = \gamma^{\boldsymbol{ac}}\gamma_{\boldsymbol{cb}} = \delta^{\boldsymbol{a}}_{\boldsymbol{b}} \quad \text{and} \quad \gamma^{\boldsymbol{a}}{}_{\boldsymbol{b}} = \gamma^{\boldsymbol{ac}}\gamma_{\boldsymbol{cb}} = (-1)^{\boldsymbol{ab}}\delta^{\boldsymbol{a}}_{\boldsymbol{b}} \tag{2.8}$$

$$(-1)^{\boldsymbol{ab}} = (-1)^{\text{number of fermionic indices in } \boldsymbol{a}} \tag{2.9}$$

We used in (2.7) the Northwest-Southeast notation, i.e., the lower indices are on the right-hand side. The above metric is diagonal for bosons or gauge (boson) fields. And it is anti-symmetric for fermion, $\gamma_{ab} = -\gamma_{ab}$ with a, b fermionic indices.

As an example, we can consider the case for a single fermionic field $\boldsymbol{a} = a$, and $\hat{\varphi}_a = (\hat{\psi}, \hat{\bar{\psi}})$. In this case, the contraction can be written down explicitly

$$\hat{\varphi}_a = (\hat{\psi}, \hat{\bar{\psi}}), \qquad J_a = (J_{\hat{\psi}}, J_{\hat{\bar{\psi}}}), \qquad \gamma^{ab} = \begin{pmatrix} 0 & -1 \\ 1 & 0 \end{pmatrix} \tag{2.10}$$

[2] This is so-called deWitt's condensed notation [32]. The full version is

$$\frac{\delta A[J]}{\delta J_{\boldsymbol{a}}} \equiv A^{,\boldsymbol{a}}, \quad A^{\boldsymbol{a}}B_{\boldsymbol{a}} \equiv \int_{x\in M}\sum_{\alpha} A^{\alpha}(x)B_{\alpha}(x)\mathrm{d}^d x \tag{2.2}$$

With suitable normalization assumed. However, to use a comma, for instance, $A^{,\boldsymbol{a}}$, to represent the functional derivative is not always convenient, and I will mostly avoid to use it, but use variation symbol δ or ∂, and use the superscript $A^{(n)}$ to represent n-th derivatives.

$$J^a\hat{\varphi}_a = \gamma^{ab}J_b\hat{\varphi}_a = \hat{\varphi}^a J_a = \int_{C(x)} J_{\hat{\bar{\psi}}}(x)\hat{\psi}(x) - J_{\hat{\psi}}(x)\hat{\bar{\psi}}(x) \tag{2.11}$$

Clearly the number of the fermionic index in the above is 1, because there is only one index and it is fermionic. The source terms here share the statistics of the corresponding fields, which are anti-commuting. We can also write down the metric for the vector "super field" $\hat{\phi}_a = (\hat{\varphi}, \hat{A}, \hat{\psi}, \hat{\bar{\psi}})$ and $\hat{\phi}^a = \gamma^{ab}\hat{\phi}_b = (\hat{\varphi}, \hat{A}, \hat{\bar{\psi}}, -\hat{\psi})$.

$$\gamma^{ab} = \begin{pmatrix} 1 & 0 & 0 & 0 \\ 0 & 1 & 0 & 0 \\ 0 & 0 & 0 & -1 \\ 0 & 0 & 1 & 0 \end{pmatrix} \tag{2.12}$$

Where $\gamma = \gamma_\varphi \oplus \gamma_A \oplus (\gamma_\psi \otimes \gamma_{\bar{\psi}})$ is understood.

With the above notations, the path integral representation can be written done immediately [30, 33] in a very compact form

$$e^{\mathrm{i}W} = Z = \mathrm{Tr}\left[\rho(t_0)\int \mathrm{d}[\hat{\varphi}]\exp\left\{\mathrm{i}S[\hat{\varphi}] + \mathrm{i}J^{\boldsymbol{a}}\hat{\phi}_{\boldsymbol{a}}[\hat{\varphi}]\right\}\right] \tag{2.13}$$

Where the $\mathrm{d}[\hat{\varphi}]$ is the path/functional integral measure. The W is sometimes called Schwinger functional [30]. Note that here the fields in the path integral (functional integral) should be understood as the bosonic coherent state eigenvalues or the Grassmann numbers.

Although the path integral quantization or the canonical quantization are very useful, the general structure of all correlation functions, and thus the full quantum problem, can be formally written down through the Schwinger functional and functional calculus. Those relations for correlations function are then free of quantization schemes.

As we already defined, the Schwinger functional reads

$$W[J] = -\mathrm{i}\ln Z[J] \tag{2.14}$$

Diagrammtically, it is the sum of all connect vacuum diagrams [34]. Here I keep the "i" rather than use the Euclidean notation in the reference [30]. In later sections we will also use the Euclidean notation. We summarize the noations in the Table. 2.1. It is not essential for the general properties of the generating functional or the correlation functions. Here, to transfer to Pawlowski's notation, we can Wick rotate $t \to \mathrm{i}t$ and flip the sign of the sources (current), the definition of the Schwinger functional also needs to be changed accordingly. For practical uses, the real time and imaginary time have some important differences, which we will not discuss here.

With the above definition of W, the normalized expectation value of operator $\hat{I}$ can be written as

$$I[J] = \langle\hat{I}[J]\rangle = e^{-\mathrm{i}W[J]}\hat{I}[J, \frac{\delta}{\mathrm{i}\delta J}]e^{\mathrm{i}W[J]} \tag{2.15}$$

All quantities in the quantum field theory can be defined through a proper choice of operator $\hat{I}[J, \frac{\delta}{\mathrm{i}\delta J}]$ and its expectation values $I = \langle\hat{I}[J]\rangle$.

Now we can define many important quantities in field theories. The normalized n-point correlation

functions can be written as

$$\langle \hat{I}^{(N)}_{\boldsymbol{a}_1\cdots\boldsymbol{a}_n} \rangle = \langle \prod_{i=1}^{N} \hat{\phi}_{\boldsymbol{a}_i} \rangle \tag{2.16}$$

which can be generated by the functional derivatives

$$I^{(N)}_{\boldsymbol{a}_1\cdots\boldsymbol{a}_n} = \langle \hat{I}^{(N)}_{\boldsymbol{a}_1\cdots\boldsymbol{a}_n} \rangle = e^{-\mathrm{i}W[J]} \left(\prod_{i=1}^{N} \frac{\delta}{\mathrm{i}\delta J^{\boldsymbol{a}_i}} \right) e^{\mathrm{i}W[J]} \tag{2.17}$$

The operator $\hat{I}^{(N)}$ is then $\prod_{i=1}^{N} \frac{\delta}{\mathrm{i}\delta J^{\boldsymbol{a}_i}}$.

Moreover, we can define the second functional derivation of the Schwinger functional $W[J]$

$$\mathrm{i}G_{\boldsymbol{ab}} \equiv \mathrm{i}W^{(2)}_{\boldsymbol{ab}} \equiv \frac{\delta}{\mathrm{i}\delta J_{\boldsymbol{a}}} \frac{\delta}{\mathrm{i}\delta J_{\boldsymbol{b}}} \mathrm{i}W[J] = I^{(2)}_{\boldsymbol{a}_1\boldsymbol{a}_2} - I^{(1)}_{\boldsymbol{a}_1} I^{(1)}_{\boldsymbol{a}_2} \tag{2.18}$$

It is the two-point connected Green's function. The one-point mean-field $\phi = \langle \hat{\phi} \rangle$ can be also reached by

$$\phi_{\boldsymbol{a}}[J] \equiv \frac{\delta}{\delta J_{\boldsymbol{a}}} W[J] \tag{2.19}$$

The chain rule can be written down as well

$$\frac{\delta}{\mathrm{i}\delta J^{\boldsymbol{a}}} = \frac{\delta \phi_{\boldsymbol{b}}}{\mathrm{i}\delta J_{\boldsymbol{a}}} \frac{\delta}{\delta \phi_{\boldsymbol{b}}} = \mathrm{i}G_{\boldsymbol{ab}} \frac{\delta}{\delta \phi_{\boldsymbol{b}}} \tag{2.20}$$

$$\frac{\delta^2 W[J]}{\delta J^{\boldsymbol{a}} \delta J^{\boldsymbol{c}}} \frac{\delta^2 \Gamma[\phi]}{\delta \phi_{\boldsymbol{c}} \delta \phi_{\boldsymbol{b}}} = \gamma^{\boldsymbol{b}}_{\boldsymbol{a}} \tag{2.21}$$

With all those definitions we can derive many useful equations for n-point correlation functions and vertices.

2.2 Dyson-Schwinger equations

Dyson-Schwinger equations (DSEs), as a set of quantum equations of motion can be used to define the field theory and represent a full description if without truncation. Here I briefly review DSEs.

2.2.1 Dyson-Schwinger equations

We highly follow [30] and [35, 36] and [34], the derivation can be found in many other books, articles and reviews, for instance [26, 28, 33, 37].

Use the partition function (2.13) the standard Dyson-Schwinger equation (DSE) is a "quantum

Real time notations	Euclidean notations
$e^{\mathrm{i}W} = Z = \int \mathrm{d}\mu[\hat{\varphi}] \exp\left\{\mathrm{i}S[\hat{\varphi}] + \mathrm{i}J^{\boldsymbol{a}}\hat{\phi}_{\boldsymbol{a}}[\hat{\varphi}]\right\}$	$e^{W} = Z = \int \mathrm{d}\mu[\hat{\varphi}] \exp\left\{-S[\hat{\varphi}] + J^{\boldsymbol{a}}\hat{\phi}_{\boldsymbol{a}}[\hat{\varphi}]\right\}$
$I[J] = \langle \hat{I}[J] \rangle = e^{-\mathrm{i}W[J]} \hat{I}[J, \frac{\delta}{\mathrm{i}\delta J}] e^{\mathrm{i}W[J]}$	$I[J] = \langle \hat{I} \rangle = e^{-W[J]} \hat{I}[J, \frac{\delta}{\delta J}] e^{W[J]}$
$I^{(n)}_{\boldsymbol{a}_1\cdots\boldsymbol{a}_n} = \langle \hat{I}^{(n)}_{\boldsymbol{a}_1\cdots\boldsymbol{a}_n} \rangle = e^{-\mathrm{i}W[J]} \left(\prod_{i=1}^{n} \frac{\delta}{\mathrm{i}\delta J^{\boldsymbol{a}_i}}\right) e^{\mathrm{i}W[J]}$	$I^{(n)}_{\boldsymbol{a}_1\cdots\boldsymbol{a}_n} = \langle \hat{I}^{(n)}_{\boldsymbol{a}_1\cdots\boldsymbol{a}_n} \rangle = e^{-W[J]} \left(\prod_{i=1}^{n} \frac{\delta}{\delta J^{\boldsymbol{a}_i}}\right) e^{W[J]}$
$\mathrm{i}G_{\boldsymbol{ab}} \equiv \mathrm{i}W^{(2)}_{\boldsymbol{ab}} \equiv \frac{\delta}{\mathrm{i}\delta J^{\boldsymbol{a}}} \frac{\delta}{\mathrm{i}\delta J^{\boldsymbol{b}}} \mathrm{i}W[J] = I^{(2)}_{\boldsymbol{a}_1\boldsymbol{a}_2} - I^{(1)}_{\boldsymbol{a}_1} I^{(1)}_{\boldsymbol{a}_2}$	$G_{\boldsymbol{ab}} \equiv W^{(2)}_{\boldsymbol{ab}} \equiv \frac{\delta}{\delta J^{\boldsymbol{a}}} \frac{\delta}{\delta J^{\boldsymbol{b}}} W[J] = I^{(2)}_{\boldsymbol{a}_1\boldsymbol{a}_2} - I^{(1)}_{\boldsymbol{a}_1} I^{(1)}_{\boldsymbol{a}_2}$
$\frac{\delta W}{\delta J^{\boldsymbol{a}}} = \phi_{\boldsymbol{a}}$	$\frac{\delta W}{\delta J^{\boldsymbol{a}}} = \phi_{\boldsymbol{a}}$
$\frac{\delta}{\mathrm{i}\delta J^{\boldsymbol{a}}} = \frac{\delta \phi_{\boldsymbol{b}}}{\mathrm{i}\delta J^{\boldsymbol{a}}} \frac{\delta}{\delta \phi_{\boldsymbol{b}}} = \mathrm{i}G_{\boldsymbol{ab}} \frac{\delta}{\delta \phi_{\boldsymbol{b}}}$	$\frac{\delta}{\delta J^{\boldsymbol{a}}} = \frac{\delta \phi_{\boldsymbol{b}}}{\delta J^{\boldsymbol{a}}} \frac{\delta}{\delta \phi_{\boldsymbol{b}}} = G_{\boldsymbol{ab}} \frac{\delta}{\delta \phi_{\boldsymbol{b}}}$
$W[J(\phi)] = \phi_{\boldsymbol{a}} \frac{\delta \Gamma[\phi]}{\delta \phi_{\boldsymbol{a}}} + \Gamma[\phi] = \phi_{\boldsymbol{a}} J^{\boldsymbol{a}} + \Gamma[\phi]$	$W[J(\phi)] = \phi_{\boldsymbol{a}} \frac{\delta \Gamma[\phi]}{\delta \phi_{\boldsymbol{a}}} - \Gamma[\phi] = \phi_{\boldsymbol{a}} J^{\boldsymbol{a}} - \Gamma[\phi]$
$\frac{\delta \Gamma[\phi]}{\delta \phi} = -J$	$\frac{\delta \Gamma[\phi]}{\delta \phi} = J$
$W^{(2)}_{\boldsymbol{ac}} = \frac{\delta^2 W[J]}{\mathrm{i}\delta J^{\boldsymbol{a}} \mathrm{i}\delta J^{\boldsymbol{c}}} = -\frac{\delta \phi^{\boldsymbol{c}}}{\delta J^{\boldsymbol{a}}}$	$W^{(2)}_{\boldsymbol{ac}} = \frac{\delta^2 W[J]}{\delta J^{\boldsymbol{a}} \delta J^{\boldsymbol{c}}} = \frac{\delta \phi^{\boldsymbol{c}}}{\delta J^{\boldsymbol{a}}}$
$\Gamma^{(2)}_{\boldsymbol{cb}} = \frac{\delta^2 \Gamma[\phi]}{\delta \phi_{\boldsymbol{c}} \delta \phi_{\boldsymbol{b}}} = -\frac{\delta J^{\boldsymbol{b}}}{\delta \phi^{\boldsymbol{c}}}$	$\Gamma^{(2)}_{\boldsymbol{cb}} = \frac{\delta^2 \Gamma[\phi]}{\delta \phi_{\boldsymbol{c}} \delta \phi_{\boldsymbol{b}}} = \frac{\delta J^{\boldsymbol{b}}}{\delta \phi^{\boldsymbol{c}}}$
$\frac{\delta^2 W[J]}{\mathrm{i}\delta J^{\boldsymbol{a}} \mathrm{i}\delta J^{\boldsymbol{c}}} \frac{\delta^2 \Gamma[\phi]}{\delta \phi_{\boldsymbol{c}} \delta \phi_{\boldsymbol{b}}} = (-1)^2 \frac{\delta \phi^{\boldsymbol{c}}}{\delta J^{\boldsymbol{a}}} \frac{\delta J^{\boldsymbol{b}}}{\delta \phi^{\boldsymbol{c}}} = \gamma^{\boldsymbol{b}}_{\boldsymbol{a}}$	$\frac{\delta^2 W[J]}{\delta J^{\boldsymbol{a}} \delta J^{\boldsymbol{c}}} \frac{\delta^2 \Gamma[\phi]}{\delta \phi_{\boldsymbol{c}} \delta \phi_{\boldsymbol{b}}} = \frac{\delta \phi^{\boldsymbol{c}}}{\delta J^{\boldsymbol{a}}} \frac{\delta J^{\boldsymbol{b}}}{\delta \phi^{\boldsymbol{c}}} = \gamma^{\boldsymbol{b}}_{\boldsymbol{a}}$

Table 2.1: Summary of conventions for the real time notation and the Euclidean notation.

continuity equation"[3]

$$\frac{\delta Z[J_a]}{\delta \hat{\phi}_a} = \int \mathrm{d}[\hat{\phi}] \frac{\delta}{\delta \hat{\phi}_a} e^{\mathrm{i}S[\hat{\phi}] + \mathrm{i}J^a \hat{\phi}_a} = \mathrm{i} \int \mathrm{d}[\hat{\phi}] \frac{\delta}{\delta \hat{\phi}_a} e^{\mathrm{i}S[\hat{\phi}] + \mathrm{i}J^a \hat{\phi}_a} \left(\frac{\delta S}{\delta \hat{\phi}_a} + J^a\right) = 0 \tag{2.23}$$

Here we restrict ourselves to the (1PI) case, with only one index per field $\mathbf{a} = a$ and the measure is $\mathrm{d}\mu[\hat{\varphi}] = \mathrm{d}[\hat{\phi}]$. Define operator $\hat{I}_{\mathrm{DSE}}$ of the Dyson-Schwinger equation

$$\hat{I}_{\mathrm{DSE}} = J + \left.\frac{\delta S}{\delta \hat{\phi}}\right|_{\hat{\phi} = \frac{\delta}{\delta J}} \tag{2.24}$$

Now the Dyson-Schwinger equation is

$$\langle \hat{I}_{\mathrm{DSE}} \rangle = 0 \tag{2.25}$$

[3] The general DSE is defined as [30]

$$\int \mathcal{G}[\hat{\varphi}] \left(\mathrm{d}[\hat{\varphi}] \hat{\Psi}[\hat{\phi}] e^{\mathrm{i}S[\hat{\varphi}] + \mathrm{i}J^{\mathrm{a}} \hat{\phi}_{\mathrm{a}}[\hat{\varphi}]}\right) = 0 \tag{2.22}$$

where $\mathcal{G}$ generates the symmetry of the path-integral and $\hat{\Psi}$ is an operator composited by $\hat{\phi}$.

Remind that $\langle \ldots \rangle = e^{-\mathrm{i}W[J]} \ldots e^{\mathrm{i}W[J]}$.

Alternatively DSEs can be reached by using functional derivatives [36] of the 1-PI effective actions

$$\Gamma = W[J_a] - \phi_a J^a \tag{2.26}$$

and

$$\frac{\delta\Gamma[\phi]}{\delta\phi_a} = -\gamma^a_b J^b \tag{2.27}$$

Using the chain rule we have

$$\frac{\delta\Gamma[\phi]}{\delta\phi_a} = \frac{\delta S[\hat{\phi}]}{\delta\hat{\phi}_a}\bigg|_{\hat{\phi}_a=\phi_a+\mathrm{i}G_{ab}\delta/\delta\phi_b} = -\gamma^a_b J^b \tag{2.28}$$

If we set $J = 0$, we have a closed equation.

One can find that any n-point correlation function can be represented by some m-point vertices and 2-point correlation/Green's functions through functional derivatives of the above equation (2.28). The computations of those derivatives are in principle straightforward, but still, need a lot of labour. Fortunately, there are some Mathematica packages to help us, for instance [4] the DoFun [35, 36, 38].

Note that if we write out the γ_{ab} metric explicitly, for anti-commute fields, the functional derivatives from the right or from the left will be different, and the order will affect the resulting DSEs. In DoFun 3.0 package choose left derivatives [36]

$$\Gamma^{(4)}_{ijkl} = \Gamma^{(\bar{\psi}\bar{\psi}\psi\psi)}_{ijkl} = \frac{\delta^4\Gamma}{\delta\bar{\psi}_i\delta\bar{\psi}_j\delta\psi_k\delta\psi_l} \equiv= -\frac{\overrightarrow{\delta}^2}{\delta\bar{\psi}_i\delta\bar{\psi}_j}\frac{\overrightarrow{\delta}^2}{\delta\psi_k\delta\psi_l}\Gamma\bigg|_{\bar{\psi}_{\mathrm{phys}},\psi_{\mathrm{phys}}} \tag{2.29}$$

that is the fermion ψ from the right, the anti-fermion $\bar{\psi}$ from the left. Which we will follow here.

The (2.28) is still very abstract. To give an example, we consider the Gross-Neveu model. The Gross-Neveu model is a pure fermionic model with Dirac fermions and a four-fermion interaction term [39, 40]

$$S(\hat{\psi},\psi) = -\int \mathrm{d}^d x \left[\bar{\psi}\cdot\partial\!\!\!/\psi + \frac{1}{2N_f}g(\bar{\psi}\cdot\psi)^2\right] = -\int \mathrm{d}^d x \left[\bar{\psi}_a\partial\!\!\!/\psi_a + \frac{1}{2N_f}g(\bar{\psi}_a\psi_a)^2\right] \tag{2.30}$$

The integer N_f is the total flavor number. The real number g is a coupling parameter. In momentum space [35] the action reads

$$\begin{aligned} S[\bar{\psi},\psi] = &\sum_{j=1}^{N_f}\int \frac{\mathrm{d}^d q}{(2\pi)^d}\bar{\psi}_j(q)(-q\!\!\!/)\psi_j(q) \\ &+ \sum_{i,j=1}^{N_f}\int \frac{\mathrm{d}^d q_1}{(2\pi)^d}\frac{\mathrm{d}^d q_2}{(2\pi)^d}\frac{\mathrm{d}^d q_3}{(2\pi)^d}\bar{\psi}_i\left(q_1\right)\psi_i\left(q_2\right)\frac{g}{2N_f}\bar{\psi}_j\left(q_3\right)\psi_j\left(-q_1-q_3-q_2\right) \end{aligned} \tag{2.31}$$

where the internal momentum q_1, q_2, q_3 are used. The Dyson-Schwinger equations for $\Gamma^{(2)}$ and $\Gamma^{(4)}$

[4] In DoFun the Euclidean notation is used.

of Gross-Neveu model are shown in the Fig. 2.1 and in the Fig. 2.2 respectively. From the figures, one can see that the $\Gamma^{(2)}$ is depending on $\Gamma^{(4)}$ and the $\Gamma^{(4)}$ is depending on $\Gamma^{(6)}$. Therefore, although the Dyson-Schwinger equations are exact, they are infinitely coupled. In practice, a truncation is needed. For a truncation many studies set $\Gamma^{(6)} = 0$.

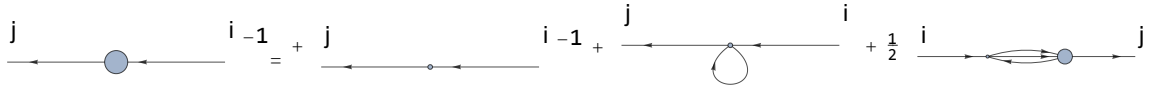

Figure 2.1: $\Gamma^{(2)} = \Gamma^{(\bar{\psi}\psi)} = S_0^{(\bar{\psi}\psi)} + \Sigma$ for the Gross-Neveu model (2.31). The small dots are bare vertices, the big dots are full vertices. One can see that the last graph depends on the $\Gamma^{(4)}$. Generated from the DoFun [36].

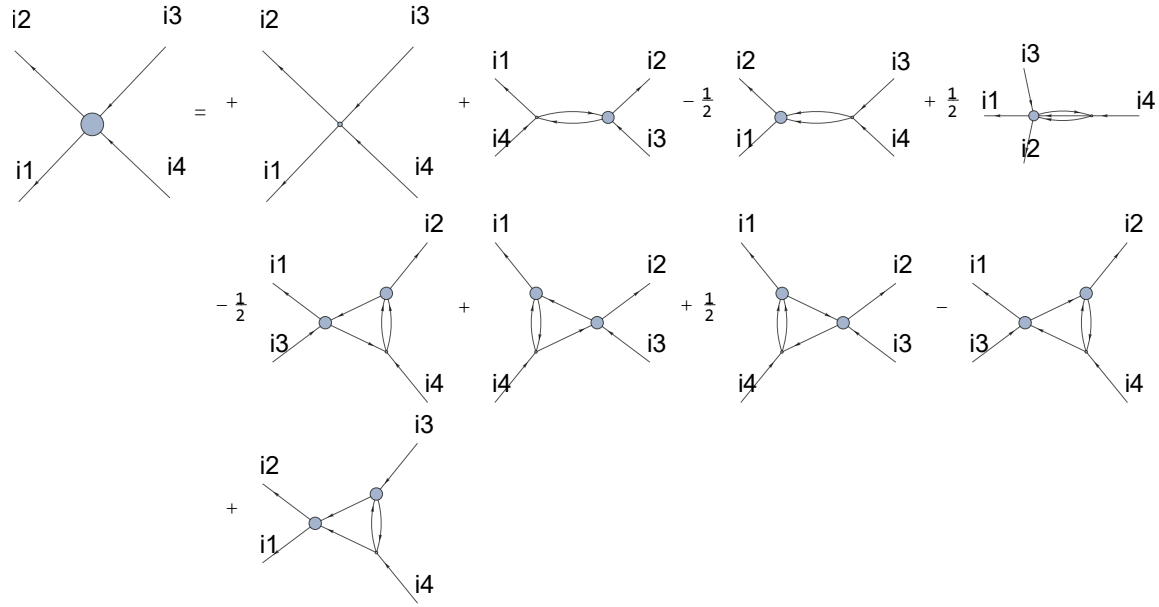

Figure 2.2: $\Gamma^{(4)} = \Gamma^{(\bar{\psi}\bar{\psi}\psi\psi)}$ for the Gross-Neveu model (2.31). The small dots are bare vertices, the big dots are full vertices $\Gamma^{(n)}$ where n is equals to the lags they have. One can see that the top rightmost graph depends on the $\Gamma^{(6)}$. Generated from DoFun [36].

2.2.2 Bethe-Salpeter equations

The Bethe-Salpeter equation [41] is a Dyson-Schwinger like equation which is frequently used in quantum mechanical bound state problems. For simplicity, we consider the Gross-Neveu model [39] with a partial bosonization through the Hubbard-Stratonovich transformation. This will give us a fermionic fields Yukawa coupling with the auxiliary field[5] σ

$$S_N(\bar{\psi}, \psi, \sigma) = \int_x \left[-\bar{\psi} \cdot (\partial\!\!\!/ + \sigma)\psi + \tilde{m}\sigma^2 \right] \tag{2.32}$$

[5] Note the hats are omitted, $\hat{\psi} \to \psi$.

$\tilde{m} = \Lambda^{d-4}\frac{m^2}{2g^2}$. Here we focus on the structure of the Bethe-Salpeter equation, regardless the origin of this action. For simplicity we can assume ψ only has one component

$$S_N(\bar{\psi},\psi,\sigma) = \int_x \left[-\bar{\psi}\partial\!\!\!/\psi - \bar{\psi}\psi\sigma + \tilde{m}\sigma^2\right] \tag{2.33}$$

where the "sigma" field is from the Lagrange multiplier $\sigma(x)\left((\bar{\psi}(x)\cdot\psi(x) - N\rho(x)\right)$ where we set $N = 1$ and integrated out ρ.

Now attach source J_ψ to ψ ($J_{\bar{\psi}}$ to $\bar{\psi}$) and J_σ to σ field, the Dyson-Schwinger equation reads [26, 30]

$$e^{-W}\left[J_\psi - \frac{\delta S[\psi,\bar{\psi},\sigma]}{\delta\bar{\psi}}\right]_{\psi=\frac{\delta}{\delta J_\psi},\sigma=\frac{\delta}{\delta J_\sigma}} e^W = 0 \tag{2.34}$$

and $\frac{\delta S[\psi,\bar{\psi},\sigma]}{\delta\bar{\psi}} = -\partial\!\!\!/\psi - \psi\sigma$, thus

$$\left[J_\psi(x) - \left(-\partial\!\!\!/_x - \frac{\delta}{\delta J_\sigma(x)}\right)\frac{\delta}{\delta J_\psi(x)}\right] W[J_\psi, J_{\bar{\psi}}, J_\sigma] = 0 \tag{2.35}$$

Partial once by $J_\psi(x')$ gives us the DSE for two-point propagator $W^{(2)}$. We can also go two steps further, that is, to apply three derivatives of J_ψ

$$\frac{\delta^3}{\delta J_\psi(x')\delta J_\psi(y)\delta J_\psi(y')}\left[J_\psi(x) - \left(-\partial\!\!\!/_x - \frac{\delta}{\delta J_\sigma(x)}\right)\frac{\delta}{\delta J_\psi(x)}\right] W[J_\psi, J_{\bar{\psi}}, J_\sigma] = 0 \tag{2.36}$$

Use that $\delta J(x)/\delta J(y) = \delta(x-y)$ and

$$\frac{\delta}{\delta J_\psi(x)}\frac{\delta}{\delta J_{\bar{\psi}}(x')} W = W^{(2)}_{xx'} \tag{2.37}$$

We reach the equation for $W^{(4)}$ after setting $J_\psi = J_{\bar{\psi}} = 0$, it reads

$$\left[-\left(-\partial\!\!\!/^x - \frac{\delta}{\delta J_\sigma(x)}\right)\right] W^{(4)}_{x'yy'x} + \delta_{xy'}W^{(2)}_{x'y} - \delta_{xy}W^{(2)}_{x'y'} + \delta_{xx'}W^{(2)}_{yy'} = 0 \tag{2.38}$$

Here the shorthand notation $\delta_{xy} = \delta(x-y)$ is used. Now assume the incoming two particles have different starting space-time positions $x \neq x'$, then $\delta_{xx'} = 0$, the minus sign before δ_{yx} is from switching the order of the $\delta_{J(y)}$ and $\delta_{J(y')}$, since they are fermionic sources. Befor the next step, notice that $[(-\partial\!\!\!/_x - \Sigma)W^{(2)}]_{xy} = \delta_{xy}$. Reminding this, we can first subtract and add a ψ self-energy Σ in front of $W^{(4)}$

$$\left[-\left(-\partial\!\!\!/^x - \Sigma + \Sigma - \frac{\delta}{\delta J_\sigma(x)}\right)\right] W^{(4)}_{x'yy'x} + \delta_{xy'}W^{(2)}_{x'y} - \delta_{xy}W^{(2)}_{x'y'} = 0 \tag{2.39}$$

And then we multiply[6] $(-\partial\!\!\!/_{x'} - \Sigma)$ and reorder the terms and indices. As a result, we arrive the

[6] This can be chosen differently.

Bethe-Salpeter equation [26]

$$(-\not{\partial}^{x'} - \Sigma)(-\not{\partial}^{x} - \Sigma)W^{(4)}_{xx'yy'} = -\delta_{xy'}\delta_{x'y} + \delta_{xy}\delta_{x'y'} + (-\not{\partial}_{x'} - \Sigma)\left(-\Sigma + \frac{\delta}{\delta J_\sigma(x)}\right)W^{(4)}_{xx'yy'}\Big|_{J_\sigma=0} \tag{2.40}$$

Through a definition of the Bethe-Salpeter kernel $K_{xx'yy'}$ the above equation can be written into an integro-differential form

$$(-\not{\partial}_{x'} - \Sigma)(-\not{\partial}_{x} - \Sigma)W^{(4)}_{xx'yy'} = -\delta_{xy'}\delta_{x'y} + \delta_{xy}\delta_{x'y'} + \int_{yy'} K_{xx'yy'}W^{(4)}_{yy'zz'} \tag{2.41}$$

Where $\delta_{xy} = \delta(x - y)$.

One can also move $(-\not{\partial} - \Sigma) = (W^{(2)})^{-1}$ to the right hand side. Integrate by part to move the acting variables of the partial ∂, and reaches

$$W^{(4)}_{xx'yy'} = -W_{xy'}W_{x'y} + W_{xy}W_{x'y'} + (-\not{\partial}_{x} - \Sigma)^{-1}\left(-\Sigma + \frac{\delta}{\delta J_\sigma(x_1)}\right)W^{(4)}_{xx'yy'}\Big|_{J_\sigma=0} \tag{2.42}$$

The right most term contains the Bethe-Salpeter kernel. This kernel can be better understood by an example as the following. First we neglect the derivative δ_{J_σ}. We have

$$(-\not{\partial}_{x} - \Sigma)^{-1}(-\Sigma) \tag{2.43}$$

Where $G = (-\not{\partial}_{x} - \Sigma)^{-1}$ is a full propagator. The G^{-1} removes one fermionic propagator line from the self-energy Σ, and gives two more indices where two more propagators can be attached. For instance, the lowest fermionic self-energy has the form

$$[\Sigma_1]_{xy} = [\nu^{(3)}W^{(2)}D\nu^{(3)}]_{xy} \tag{2.44}$$

where D is the σ field propagator, and $\nu^{(3)}$ is the bare vertex tensor. Then $(W^{(2)})^{-1}_{x'y'}[\Sigma_1]_{xy} = [\nu^{(3)}D\nu^{(3)}]_{xx'yy'}$ gives

$$V_{xx'yy'} = [\nu^{(3)}D\nu^{(3)}]_{xx'yy'} \tag{2.45}$$

Which is the lowest order kernel, a single σ line.

2.2.3 Ward identities

In field theory, Ward identities or Ward-Takahashi identities [42, 43] are well-known and exact relations between the n-point and $(n+1)$-point functions. It is closed related to the DSE and the classical gauge symmetries such as charge conservation. The derivation can be found in many textbooks, for instance see [34] which uses functional derivatives and see [44] for operator method.

Ward-Takahashi identity

Here we closely follow the appendix of [45], which uses functional derivatives. Let us omit the hats on the fields. Note that if a field is under functional integral, it should be understood as an eigenvalue of the corresponding coherent state.

We assume the action of the system has some global continuous symmetry, e.g., the $U(1)$ symmetry. Define the Noether current for this symmetry as

$$\partial_\mu j^\mu = 0 \tag{2.46}$$

An example model can be a non-relativistic fermionic model

$$S = -\int_x \partial_\mu \bar{\psi} \partial^\mu \psi + V(\bar{\psi}\psi)^2 = \int_x \mathcal{L} \tag{2.47}$$

where a transform $\bar{\psi} \to e^\alpha \bar{\psi}$, $\psi \to e^{-\alpha}\psi$ keeps the action invariant, α is a constant complex number which contains a global phase, the i is absorbed into α. Where $\mathcal{L}$ is the Lagrangian density. The Noether current of the $U(1)$ global symmetry for this model can be derived by applying a infinitesimal local transform $\epsilon(x)$, or equivalently by the Euler-Lagrange equation

$$j^\mu = \partial^\mu \bar{\psi}\psi - \bar{\psi}\partial^\mu \psi \tag{2.48}$$

To derive the Ward-Takahashi identity, first, we can write down the partition function with source terms J_ψ, $J_{\bar{\psi}}$, and J^μ as

$$Z[J_\psi, J_{\bar{\psi}}, J_\mu] = \langle \hat{T} \exp\left\{ -\int_x \left[J_\psi(x)\psi(x) + J_{\bar{\psi}}(x)\bar{\psi}(x) + J_\mu(x) j^\mu(x) \right] \right\} \rangle \tag{2.49}$$

Note that I used capital J for sources. The $j^\mu(x)$ is the Noether current and is a composite bosonic field. Here as an example, I consider the fermionic fields ψ and $\bar{\psi}$, this means ψ, $\bar{\psi}$, J_ψ, $J_{\bar{\psi}}$ are anti-commuting. The functional integral version of the time ordering expectation value is

$$Z[J_\psi, J_{\bar{\psi}}, J^\mu] = \int \mathrm{d}[\psi, \bar{\psi}] e^{-S[\psi, \bar{\psi}, j^\mu, J_\psi, J_{\bar{\psi}}, J_\mu]} \tag{2.50}$$

Now we apply the local infinitesimal continuous symmetry transform, here the local infinitesimal $U(1)$ transform, on the fields and sources to keep the action unchanged. The fields transform as

$$\psi'(x) = (1 + \epsilon(x))\psi(x), \quad \bar{\psi}'(x) = (1 - \epsilon(x))\psi(x), \quad j'^\mu(x) = j^\mu[\psi', \bar{\psi}'] \tag{2.51}$$

The $j^\mu[\psi', \bar{\psi}'] = \partial^\mu \bar{\psi}'\psi' - \bar{\psi}'\partial^\mu \psi'$. And the sources are transformed in the same way.

$$J'_\psi(x) = (1 + \epsilon(x))\, J_\psi(x), \quad J'_{\bar{\psi}}(x) = (1 - \epsilon(x))\, J_{\bar{\psi}}(x), \quad J'_\mu(x) = J_\mu(x) - \partial_\mu \epsilon(x) \tag{2.52}$$

The last transform for the external source is to cancel the $\partial\epsilon$ terms from the kinetic energy.

One can check that simultaneously applying (2.51) and (2.52) will keep the action unchanged, up to $O(\epsilon^2)$

$$S[\psi, \bar{\psi}, j^\mu, J_\psi, J_{\bar{\psi}}, J_\mu] = S[\psi', \bar{\psi}', j'^\mu, J'_\psi, J'_{\bar{\psi}}, J'_\mu] \tag{2.53}$$

Plug the above equation into functional integrals, we have

$$\int \mathrm{d}[\psi, \bar{\psi}] e^{-S[\psi, \bar{\psi}, j^\mu, J_\psi, J_{\bar{\psi}}, J_\mu]} = \int \mathrm{d}[\psi, \bar{\psi}] e^{-S[\psi', \bar{\psi}', j'^\mu, J'_\psi, J'_{\bar{\psi}}, J'_\mu]} \tag{2.54}$$

The right hand side can be rewritten as

$$\int \mathrm{d}[\psi,\bar{\psi}]e^{-S[\psi',\bar{\psi}',j'^{\mu},J'_{\psi},J'_{\bar{\psi}},J'_{\mu}]} = \int \mathrm{d}[\psi',\bar{\psi}']\left|\frac{\delta\psi(x)}{\delta\psi'(x)}\right|\left|\frac{\delta\bar{\psi}(x)}{\delta\bar{\psi}'(x)}\right| e^{-S[\psi',\bar{\psi}',j'^{\mu},J'_{\psi},J'_{\bar{\psi}},J'_{\mu}]} \tag{2.55}$$

Now assume the integral measures do not change (the Jacobian is identity) under this transform, i.e. $\left|\frac{\delta\psi(x)}{\delta\psi'(x)}\right| = \left|\frac{\delta\bar{\psi}(x)}{\delta\bar{\psi}'(x)}\right| = 1$ and we can rename the ψ' and $\bar{\psi}'$ to ψ and $\bar{\psi}$

$$\int \mathrm{d}[\psi,\bar{\psi}]e^{-S[\psi',\bar{\psi}',j'^{\mu},J'_{\psi},J'_{\bar{\psi}},J'_{\mu}]} = \int \mathrm{d}[\psi,\bar{\psi}]e^{-S[\psi,\bar{\psi},j^{\mu},J'_{\psi},J'_{\bar{\psi}},J'_{\mu}]} \tag{2.56}$$

Note the j'^{μ} is composite of ψ' and $\bar{\psi}'$. We can see that only the sources are transformed.

Use (2.54) and (2.56) we can find

$$\int \mathrm{d}[\psi,\bar{\psi}]\left[e^{-S[\psi,\bar{\psi},j^{\mu},J_{\psi},J_{\bar{\psi}},J_{\mu}]} - e^{-S[\psi,\bar{\psi},j^{\mu},J'_{\psi},J'_{\bar{\psi}},J'_{\mu}]}\right] = 0 \tag{2.57}$$

Now by noticing the sources are transformed (passively) under the infinitesimal symmetry transform as in (2.52), we can plug Eq. (2.52) into Eq. (2.57). We find

$$\int \mathrm{d}[\psi,\bar{\psi}]\left[1 - e^{-\int_x[\epsilon J_{\psi}\psi - \epsilon J_{\bar{\psi}}\bar{\psi} - (\partial_{\mu}\epsilon)j^{\mu}]}\right] e^{-S[\psi,\bar{\psi},j^{\mu},J_{\psi},J_{\bar{\psi}},J_{\mu}]} = 0 \tag{2.58}$$

We can expand the above equation to linear order in ϵ, and apply that inside the integral $(\partial_{\mu}\epsilon)j^{\mu} = \epsilon(\partial_{\mu}j^{\mu})$, where we get

$$\int_x \epsilon\left[J_{\psi}\psi - J_{\bar{\psi}}\bar{\psi} - (\partial_{\mu}j^{\mu})\right]\Big|_{\psi=\frac{\delta}{\delta J_{\psi}},\bar{\psi}=\frac{\delta}{\delta J_{\bar{\psi}}},j^{\mu}=\frac{\delta}{\delta J_{\mu}}} Z[J_{\psi},J_{\bar{\psi}},J_{\mu}] = 0 \tag{2.59}$$

Since the $\epsilon(x)$ is arbitrary, the arguments in the bracket should be zero to satisfy the equation. From this we find a equation for the partition function

$$\left[J_{\psi}\psi - J_{\bar{\psi}}\bar{\psi} - (\partial_{\mu}j^{\mu})\right]\Big|_{\psi=\frac{\delta}{\delta J_{\psi}},\bar{\psi}=\frac{\delta}{\delta J_{\bar{\psi}}},j^{\mu}=\frac{\delta}{\delta J_{\mu}}} Z[J_{\psi},J_{\bar{\psi}},J_{\mu}] = 0 \tag{2.60}$$

The above equation (2.60) is the master equation of the Ward identity, it allows us to derive the Ward-Takahashi identity. The derivation is now straightforward, consider the three-point time ordering correlation function, which can be reached three functional derivatives

$$Z^{(3)\mu}(x|y,z) \equiv \langle\hat{T}\left\{j^{\mu}(x)\psi(y)\bar{\psi}(z)\right\}\rangle = \frac{\delta}{\delta J_{\mu}(x)}\frac{\delta^2}{\delta J_{\psi}(y)\delta J_{\bar{\psi}}(z)}Z \tag{2.61}$$

The partial of x of the above quantity is

$$\partial^x_{\mu}Z^{(3)\mu}(x|y,z) = \frac{\delta^2}{\delta J_{\psi}(y)\delta J_{\bar{\psi}}(z)}\partial^x_{\mu}\frac{\delta}{\delta J_{\mu}(x)}Z \tag{2.62}$$

Here the ∂_μ^x means partial derivative on x. The $\partial_\mu^x \frac{\delta}{\delta J_\mu(x)}$ can be translated by using (2.60) identity

$$\begin{aligned}\partial_\mu^x Z^{(3)\mu}(x|y,z) &= \frac{\delta^2}{\delta J_\psi(y)\delta J_{\bar\psi}(z)}\left(J_\psi(x)\frac{\delta}{\delta J_\psi(x)} - J_{\bar\psi}(x)\frac{\delta}{\delta J_{\bar\psi}(x)}\right)Z \\ &= \delta^d(y-x)\frac{\delta^2 Z}{\delta J_\psi(x)\delta J_{\bar\psi}(z)} - \delta^d(z-x)\frac{\delta^2 Z}{\delta J_\psi(y)\delta J_{\bar\psi}(x)} \\ &= \delta^d(y-x)G(x,z) - \delta^d(z-x)G(y,x)\end{aligned} \tag{2.63}$$

The (2.63) is usually called Ward-Takahashi. Note that although the fields $\psi, \bar\psi$ and the sources J_ψ, $J_{\bar\psi}$ are anti-commuting, the final signs remain unchanged, since here we commuted them twice. In the end we sent $J_{\bar\psi} = J_\psi = 0$. From the derivation we can see, the Ward-Takahashi identities are an exact relations from the classical continuous symmetries.

Wöffle-Vollhardt Ward identity

The above Ward identities can be combined with some integral equations of n-point functions and generate new identities. One of them is called Vollhardt-Wölfle [46] Ward identity, which is originally purposed for using in disorder systems [47, 48]. The Wöffle-Vollhardt Ward identity is an identity between the two-point irreducible vertex and the Bethe-Salpther kernel. A non-perturbative proof can be found in [49, 50].

Following [49, 50] we can derive the Wöffle-Vollhardt Ward identity from the (2.63). First we write $Z^{(3)\mu}$ into integral of propagators and a vertex function

$$Z^{(3)\mu}(x|y,z) = \int_{y'z'} G(y,y')\Gamma^\mu(x|y',z')G(z',z) \tag{2.64}$$

We assume the vertex $\Gamma^\mu(x|y',z')$ follows[7] the integral equation

$$\Gamma^\mu(x|y',z') - \Gamma_0^\mu(x|y',z') = \int_{y_1y_2z_1z_2} G\left(y_1,y_2\right)\Gamma^\mu(x|y_1,z_1)G(z_1,z_2)K(y_2,z_2|y',z') \tag{2.65}$$

where K is the Bethe-Salpeter kernel. Act ∂_μ^x on both side of (2.64) and use the Ward-Takahashi identity (2.63), One has

$$\partial_\mu^x\Gamma^\mu(x|y,z) = G^{-1}(y-x)\delta^d(x-z) - \delta^d(y-x)G^{-1}(x-z) \tag{2.66}$$

$$\partial_\mu^x\Gamma_0^\mu(x|y,z) = G_0^{-1}(y-x)\delta^d(x-z) - \delta^d(y-x)G_0^{-1}(x-z) \tag{2.67}$$

Where we used $\int_y G^{-1}(x,y)G(y,z) = \delta(x-z)$. Now we can subtract (2.66) from (2.67), and get

$$\Sigma(y,x)\delta^d(x-z) - \delta^d(y-x)\Sigma(x-z) = \partial_\mu^x\Gamma_0^\mu(x|y,z) - \partial_\mu^x\Gamma^\mu(x|y,z) \tag{2.68}$$

Here we used the definition of the irreducible two-point vertex (self-energy) $\Sigma = G_0^{-1} - G^{-1}$. The

[7] Here subscript of y_1, y_2, z_1, and z_2 are used to name the variables, and should not be confused with the spatial components.

LHS of the above equation is already an irreducible 2-point vertex function. The RHS can be related to the Bethe-Salpeter kernel $K(y,z|y',z')$ by the following procedures. First we apply ∂^x_μ to the integral equation (2.65), then substitute (2.66), and perform two of the integrals by using $\int_y G^{-1}(x,y)G(y,z) = \delta(x-z)$. After some algebra we reach

$$\partial^x_\mu \Gamma^\mu_0(x|y,z) - \partial^x_\mu \Gamma^\mu(x|y,z) = \int_{y_1 z_1} \left[\delta^d(y_1 - x)G(x,z_1) - G(y_1,x)\delta^d(x-z_1)\right] K(y,z|y_1,z_1) \tag{2.69}$$

The (2.68) and (2.69) give the Wöffle-Vollhardt Ward identity of space-time variables

$$\begin{aligned} &\Sigma(y,x)\delta^d(x-z) - \delta^d(y-x)\Sigma(x-z) \\ &= \int_{y_1 z_1} \left[\delta^d(y_1 - x)G(x,z_1) - G(y_1,x)\delta^d(x-z_1)\right] K(y,z|y_1,z_1) \end{aligned} \tag{2.70}$$

By using the translational invariance and Fourier transform, the momentum space version can be written down as well, see for instance [46, 49, 50]. This kind of Ward identities can be used to solve self-consistent equations in disorder systems [47].

2.3 Quantum effective actions

In this section and the following sections, I choose the Euclidean notation for simplicity and clarity.

As we have seen in the previous sections, the Dyson-Schwinger equations can be derived from the 1-PI effective action which is a Legendre transformation of the Schwinger functional W respect to the one point mean field ϕ. This effective action can be cast into a form very closed to the classical action S, however, with the couplings replaced by the vertex functions (functional) that can have multiple spatial dependencies, namely non-local. This can be easily seen from the formal expansion

$$\Gamma = \sum_n c_n \Gamma^{(n)a_1\ldots a_n} \phi_{a_1} \ldots \phi_{a_n} \tag{2.71}$$

here I write out the n sum explicitly. c_n are expansion coefficients depending on n and can be fixed by the definitions. The n-point vertices are defined as

$$\Gamma^{(n)a_1\ldots a_n} = \frac{\delta^n \Gamma}{\delta\phi_{a_1}\ldots\delta\phi_{a_n}} \tag{2.72}$$

From this point of view, one can compute the $\Gamma^{(n)}$ correlation functions and the observables. Surely the $\Gamma^{(n)}$ are not easy to compute, they are in general non-local and depend on multiple space-time indices. To solve them one usually needs to solve coupled non-linear integro-differential equations, which are sometimes even difficult to solve numerically. Beside those difficulties, in the following sections, we will see that there are also many advantages to consider quantum effective actions.

2.3.1 The 1-PI quantum effective action and tree expansions

The 1-PI action is already introduced in the previous sections, see for instance (2.28).

$$\Gamma = -W + \psi_a J^a \tag{2.73}$$

$$\frac{\delta\Gamma}{\delta\phi_a} = -J^a \tag{2.74}$$

In the book of Weinberg [44], clean and clear formal derivations for the 1-PI quantum effective action are available. There, a one-loop result for the φ^4 theory is given as an example. Where one regards the one-particle irreducible (1-PI) effective action as the classical (tree) action and matches it with the sum of the vacuum 1-PI graphs. Although the non-perturbative (diagram free) definition is very simple, as a Legendre transformation about the original (connected diagrams) generating functional, it still offers an intuitive picture especially when we further truncate the action. For further studies see for instance [51].

One remarkable property of the quantum effective actions Γ is that they preserve the symmetries of the action S. On one hand, this is important for the renormalizability of theory. Since from the counter-term point of view, the allowed counter-term is restricted by the symmetries of S. So that it avoids problems that arise from some divergences which do not follow symmetries of S but are produced by truncations. On the other hand, from computing observables, the preserved symmetries will keep a certain level of conservation laws and produce a conserving approximation whenever we apply the truncation of the perturbation series order by order. The particular name "conserving approximations" is usually referred to the 2-PI quantum effective action which will be introduced in the next section.

Tree expansion

For deriving the 2-PI quantum effective action, the so-called tree expansions, or skeleton expansions [52], are needed. The tree expansions are the exact relations between the derivatives of the Schwinger functional $W[J]$ and the 1-PI effective action $\Gamma[\phi]$, namely $W(n)$ and $\Gamma^{(m)}$. The tree expansion can be directly derived through functional derivatives, the start point is the identity

$$G \equiv W^{(2)} = [\Gamma^{(2)}]^{-1} \tag{2.75}$$

we will suppress the indices here in this section for clarity.

To compute the tree expansions, first we consider $W^{(3)}$ where

$$W^{(3)} = \frac{\delta}{\delta J} W^{(2)} = \frac{\delta\phi}{\delta J}\frac{\delta}{\delta\phi}[\Gamma^{(2)}]^{-1} = -\frac{\delta\phi}{\delta J}[\Gamma^{(2)}]^{-2}\Gamma^{(2)} = -W^{(2)}[\Gamma^{(2)}]^{-2}\Gamma^{(3)} \tag{2.76}$$

Since $G = [\Gamma^{(2)}]^{-1}$, we immediately have

$$W^{(3)} = -G^3\Gamma^{(3)} \tag{2.77}$$

We can also find similar relations for the $W^{(4)}$. Use $W^{(4)} = \frac{\delta}{\delta J} W^{(3)}$, we have

$$W^{(4)} = -\frac{\delta}{\delta J}\left(\frac{\delta W^{(2)}}{\delta J}\right) = -\frac{\delta \phi}{\delta J}\left(\frac{\delta}{\delta \phi}[\Gamma^{(2)}]^{-3}\right)\Gamma^{(3)} - \frac{\delta \phi}{\delta J}[\Gamma^{(2)}]^{-3}\frac{\delta}{\delta \phi}\Gamma^{(3)} \tag{2.78}$$

Further we can use $W^{(2)} = \Gamma^{(2)}$ and reach the final result for $W^{(4)}$

$$W^{(4)} = -G^4\Gamma^{(4)} + 3G^5\Gamma^{(3)}\Gamma^{(3)} \tag{2.79}$$

Since $W^{(n)}$ is the connected n-point Green's function, the tree expansion (skeleton expansion) gives the exact relations between the connected Green's functions and the m-point vertex functions $\Gamma^{(m)}$. From the above equations, we can see that diagrammatically there are only tree graphs, namely, there is no closed loop. Indeed, the loops are absorbed into the full vertices and propagators. The tree structure is the reason of the name "tree expansions" (or skeleton expansions).

2.3.2 The 2-PI quantum effective action and the conserving approximation

The 2-PI quantum action is a direct extension of the 1-PI action, it is frequently called Luttinger-Ward functional [53]. The idea is, rather than treat a single field and a single external field (source) term as the building blocks, one can introduce 2-point sources and treat fields combination, e.g. $\hat{\phi}\hat{\phi}$ as building blocks to build expansions.

We can consider the bilinear with the form $\hat{\phi}\hat{\phi}$. It is bosonic apparently. This is bosonic nature is especially useful for studying pure fermionic models. Since the 1-point mean fields of the fermionic field $\hat{\phi} = \hat{\psi}$ vanishes identically, i.e. $\langle\hat{\psi}\rangle = 0$, because of the anti-commutation nature of the $\hat{\psi}$.

The 2-PI method has a long history, which can be tracked back to the 1960s. The work of Luttinger and Ward [53] as well as Baym and Kadanoff [54, 55], and later Cornwall, Jackiw and Tomboulis [56] and many others. This method gives us a powerful way to construct systematic self-consistent approximations for quantum field theories in and out of the equilibrium. Especially for out of equilibrium where the conservation laws are crucial.

In the rest of this section we will review the derivation of the 2-PI quantum effective action. We are strongly following the Ref. [57], where pure fermionic microscopic actions are considered. We can write down the action as[8]

$$\exp W[\eta, j] = Z[\eta, j] = \int D\hat{\psi} \exp\left\{\eta_a\hat{\psi}_a + \frac{1}{2}j_{ab}\hat{\psi}_a\hat{\psi}_b - \frac{1}{24}\lambda_{abcd}\hat{\psi}_a\hat{\psi}_b\hat{\psi}_c\hat{\psi}_d\right\} \tag{2.80}$$

Here we have the classical action S_j

$$S_j[\hat{\psi}] = -\frac{1}{2}j_{ab}\hat{\psi}_a\hat{\psi}_b + \frac{1}{24}\lambda_{abcd}\hat{\psi}_a\hat{\psi}_b\hat{\psi}_c\hat{\psi}_d \tag{2.81}$$

where λ_{abcd} and j_{ab} are totally anti-symmetric, $j_{ab} = -j_{ba}$. The $\hat{\psi}_a$ should be understood as a

[8] Note that usually it is $j = G_0^{-1} + J_2$ and J_2 is the two-point source term. It is allowed and convenient to absorb them into source j since what we need here is to get composite field $\hat{\psi}\hat{\psi}$ by derivations of j.

condensed notation, for instance

$$\hat{\psi}_a = \left(\hat{\psi}_\sigma(x^0, x^i), \hat{\bar{\psi}}_\sigma(x^0, x^i)\right) \tag{2.82}$$

The $\hat{\psi}$ means Grassmann variables if it is in the functional integral and $\hat{\bar{\psi}}$ means $\bar{\psi}$. The action S_j can represent a large class of models with four-fermion interactions, the most common examples are the Hubbard model and the lattice Gross-Neveu model.

Define the one-point mean-field ψ_a

$$\psi_a = \langle \hat{\psi}_a \rangle = \frac{\delta W}{\delta \eta_a} \tag{2.83}$$

The 1PI effective action Γ_F is the Legendre transform about a fermionic source η_a, which reads

$$\Gamma_F[\psi, j] = -W[\eta, j] + \eta_a \psi_a \tag{2.84}$$

the Γ_F gives the usual relations

$$\frac{\delta \Gamma_F}{\delta \psi_a} = \eta_a \quad \text{and} \quad \left(W_F^{(2)}\right)_{ab} = \frac{\delta^2 W}{\delta \eta_a \delta \eta_b} = (\Gamma_F^{(2)})^{-1}_{ab} = \left(\frac{\delta^2 \Gamma_F[\psi, j]}{\delta \psi \delta \psi}\right)^{-1}_{ab} \tag{2.85}$$

We can get three-point correlation function $I^{(3)}_{acd} = \langle \hat{\psi}_a \hat{\psi}_c \hat{\psi}_d \rangle$ from the DSE (2.28). We repeat it here

$$\frac{\delta \Gamma}{\delta \psi_a} - \left.\frac{\delta S[\hat{\psi}]}{\delta \hat{\psi}_a}\right|_{\hat{\psi}_a = \psi_a + G_{ac}\frac{\delta}{\delta \psi_c}} = 0 \tag{2.86}$$

Note $G = G[\eta]$, and we will only send $\eta = 0$ later. The resulting correlation function $I^{(3)}$ is

$$\begin{aligned} I^{(3)}_{acd} = \langle \hat{\psi}_a \hat{\psi}_c \hat{\psi}_d \rangle = \Bigg[& \psi_a \psi_c \psi_d + \left(\Gamma_F^{(2)}\right)^{-1}_{ac} \psi_d - \left(\Gamma_F^{(2)}\right)^{-1}_{ad} \psi_c + \left(\Gamma_F^{(2)}\right)^{-1}_{cd} \psi_a \\ & - \left(\Gamma_F^{(2)}\right)^{-1}_{aa'} \left(\Gamma_F^{(2)}\right)^{-1}_{cc'} \left(\Gamma_F^{(2)}\right)^{-1}_{dd'} \frac{\delta^3 \Gamma_F}{\delta \psi_{a'} \delta \psi_{c'} \delta \psi_{d'}} \Bigg] \end{aligned} \tag{2.87}$$

Here we keep ψ for later derivations and set it to zero at the end of the derivations.

By functional derivatives, we have

$$W_F^{(2)} = \frac{\delta^2 W}{\delta \eta_a \delta \eta_b} = \frac{\delta}{\delta \eta} \frac{\delta W}{\delta \eta} = \frac{\delta \psi}{\delta \eta} = Z^{-1} Z' + Z^{-1} Z'' = -Z^{-2} Z' Z' + Z^{-1} Z'' = -\psi_a \psi_b + \langle \hat{\psi}_a \hat{\psi}_b \rangle \tag{2.88}$$

where we defined $Z' = \delta Z / \delta \eta$, $Z'' = \delta(\delta Z / \delta \eta)/\delta \eta$. From this we can define a two-point mean field G_{ab}

$$G_{ab} = \frac{\delta W}{\delta j_{ab}} = \langle \hat{\psi}_a \hat{\psi}_b \rangle = \frac{\delta^2 W}{\delta \eta_a \delta \eta_b} + \frac{\delta W}{\delta \eta_a} \frac{\delta W}{\delta \eta_b} = \left(W_F^{(2)}\right)_{ab} + \psi_a \psi_b \tag{2.89}$$

Similarly, one can derive another useful identity

$$\begin{aligned} W_B^{(2)} =& \frac{\delta^2 W}{\delta j_{ab}\delta j_{cd}} = \left\langle \hat{\psi}_a\hat{\psi}_b\hat{\psi}_c\hat{\psi}_d\right\rangle - \left\langle \hat{\psi}_a\hat{\psi}_b\right\rangle\left\langle \hat{\psi}_c\hat{\psi}_d\right\rangle \\ =& \frac{\delta^4 W}{\delta\eta_a\delta\eta_b\delta\eta_c\delta\eta_d} + \frac{\delta^2 W}{\delta\eta_b\delta\eta_c}\frac{\delta^2 W}{\delta\eta_a\delta\eta_d} - \frac{\delta^2 W}{\delta\eta_a\delta\eta_c}\frac{\delta^2 W}{\delta\eta_b\delta\eta_d} + \Delta W_B^{(2)} \\ =& \left(W_F^{(4)}\right)_{abcd} + \left(W_F^{(2)}\right)_{bc}\left(W_F^{(2)}\right)_{ad} - \left(W_F^{(2)}\right)_{ac}\left(W_F^{(2)}\right)_{bd} + \Delta W_B^{(2)} \end{aligned} \tag{2.90}$$

where $\Delta W_B^{(2)}$ are the terms which are multiplied with at least one $\delta W/\delta\eta_a$. The $\Delta W_B^{(2)} = 0$ for $\eta_a = 0$ and $\psi_a = 0$. One can find the detailed form of the $\Delta W_B^{(2)}$ in the Ref. [57].

We can now define the 2PI effective action Γ_B through the bosonic source j and bosonic mean-field G[9]

$$\Gamma_B[G] = -W[\eta = 0, j] + \frac{1}{2}j_{ab}G_{ab} \tag{2.91}$$

where in the end $\eta = 0$, and $\frac{1}{2}j_{ab}G_{ab} = -\frac{1}{2}j_{ba}G_{ab} = -\frac{1}{2}\,\mathrm{Tr}(jG)$. The $\eta = 0$ makes the derivation here simpler than the cases with bosonic microscopic fields where the 2PI effective action is define as the double Legendre transform [33, 57, 58], $\Gamma_M[\psi, G] = -W[\eta, j] + \eta_a\psi_a + \frac{1}{2}j_{ab}G_{ab}$. For microscopic fermionic $\hat{\psi}$, the expectation value is $\langle\hat{\psi}_a\rangle = 0$, if the source $\eta_a = 0$. Note that the derivatives of the source η and the mean field ψ can be non-zero. So it is important to remember that to set them to zero not at the last line of derivations, not before.

Now we can use $\Gamma_B[G]$ to derive DSE like "equations of motions". Just like the 1-PI case, functional derivatives of Γ_B give

$$\frac{\delta\Gamma_B}{\delta G_{ab}} = j_{ab} \quad \text{and} \quad \left(\Gamma_B^{(2)}\right)_{ab,cd} = \frac{\delta^2\Gamma_B}{\delta G_{ab}\delta G_{cd}} = \left(W_B^{(2)}\right)^{-1}_{ab,cd} \tag{2.92}$$

Where the $W_B^{(2)}$ is defined as

$$\left(W_B^{(2)}\right)_{ab,cd} = \frac{\delta^2 W[0, j]}{\delta j_{ab}\delta j_{cd}} \tag{2.93}$$

Note that the inversion identity now has the form

$$\left(W_B^{(2)}\right)_{ab,a'b'}\left(W_B^{(2)}\right)^{-1}_{a'b',cd} = \frac{\delta G_{ab}}{\delta j_{a'b'}}\frac{\delta j_{a'b'}}{\delta G_{cd}} = \mathbb{1}_{ab,cd} = \delta_{ac}\delta_{bd} - \delta_{ad}\delta_{bc} \tag{2.94}$$

with $G_{ab} = -G_{ba}$.

Now, the question is how to write down the effective action $\Gamma_B[G]$ in terms of the new mean field G? This is important, because it is only practically useful once we know the expression of the action, and can further make approximations/truncation on it. This question can be addressed by computing the relations between[10] $\Gamma_B^{(2)}$ and $\Gamma_F^{(4)}$, bridged by the correlation functions $I^{(2)} = \langle\hat{\psi}\hat{\psi}\rangle$ and $I^{(4)} = \langle\hat{\psi}\hat{\psi}\hat{\psi}\hat{\psi}\rangle$.

[9] In equilibrium $\Gamma_B = F/T$ where F is the Helmholtz free energy and T is the temperature.
[10] Or equivalently $W_B^{(2)}$.

Let us get start with the first derivative of the 1PI action

$$\frac{\delta\Gamma_F}{\delta\psi_b} = -\eta_b = j_{ab}\psi_a - \frac{1}{6}\lambda_{abcd}\left\langle\hat{\psi}_a\hat{\psi}_c\hat{\psi}_d\right\rangle = j_{ab}\psi_a - \frac{1}{6}\lambda_{abcd}I^{(3)}_{acd} \tag{2.95}$$

From the (2.87) we know that $I^{(3)} = G^3\Gamma^{(3)}_F$ if we set $\eta = 0$ and $\psi = 0$. From the (2.95) we have $I^{(3)} = 0$ when $\eta = 0$ and $\psi = 0$, thus $\Gamma^{(3)}_F = G^{-3}I^{(3)} = 0$, which is compatible with the symmetry of the bare action. Thus in a shorthand notation the tree expansion of the $W^{(4)}_F$ is

$$W^{(4)}_F = G^4\Gamma^{(4)}_F - 3G^5\Gamma^{(3)}_F\Gamma^{(3)}_F = G^4\Gamma^{(4)}_F \tag{2.96}$$

For $\psi = 0$ from (2.89) we know that

$$G_{ab} = \left(\Gamma^{(2)}_F\right)^{-1}_{ab} = \left(W^{(2)}_F\right)_{ab} \tag{2.97}$$

On the other hand, the $W^{(2)}_B$ can be expressed through $W^{(2)}_F$ and $W^{(4)}_F$ by using the Eq. 2.90, that is[11]

$$W^{(2)}_B = \frac{\delta^2 W}{\delta j_{ab}\delta j_{cd}} = \left(W^{(4)}_F\right)_{abcd} + \left(W^{(2)}_F\right)_{bc}\left(W^{(2)}_F\right)_{ad} - \left(W^{(2)}_F\right)_{ac}\left(W^{(2)}_F\right)_{bd} \tag{2.98}$$

where we set $\eta = 0$ and $\psi = 0$ which lead to $\Delta W^{(2)}_B = 0$ in (2.90). The $W^{(4)}_F$ and $W^{(2)}_F$ can be expressed further into functional derivatives of the 1PI action Γ_F through the identities (2.97) and (2.96), which give us

$$\begin{aligned} W^{(2)}_B = \left(\Gamma^{(2)}_B\right)^{-1}_{ab,cd} = &-\left(\Gamma^{(4)}_F\right)_{a'b'c'd'}\left(\Gamma^{(2)}_F\right)^{-1}_{aa'}\left(\Gamma^{(2)}_F\right)^{-1}_{bb'}\left(\Gamma^{(2)}_F\right)^{-1}_{cc'}\left(\Gamma^{(2)}_F\right)^{-1}_{dd'} \\ &+ \left(\Gamma^{(2)}_F\right)^{-1}_{bc}\left(\Gamma^{(2)}_F\right)^{-1}_{ad} - \left(\Gamma^{(2)}_F\right)^{-1}_{ac}\left(\Gamma^{(2)}_F\right)^{-1}_{bd} \end{aligned} \tag{2.99}$$

Again $\eta = \psi = 0$ is applied in the end. We also defined $\left(\Gamma^{(4)}_F\right)_{a'b'c'd'} \equiv \frac{\delta^4\Gamma_F}{\delta\psi_{a'}\delta\psi_{b'}\delta\psi_{c'}\delta\psi_{d'}}$. The above equation (2.99) is the identity that we are searching for, which links the $\Gamma^{(2)}_B$ and $\Gamma^{(4)}_F$. Now we are ready to write down the 2-PI action.

Functional differentiate (2.95) by ψ_a and then set $\psi = 0$ gives

$$\left(\Gamma^{(2)}_F\right)_{ab} = -j_{ab} + \frac{1}{2}\lambda_{abcd}\left(\Gamma^{(2)}_F\right)^{-1}_{cd} + \frac{1}{6}\lambda_{be'c'd'}\left(\Gamma^{(2)}_F\right)^{-1}_{e'}\left(\Gamma^{(2)}_F\right)^{-1}_{c'}\left(\Gamma^{(2)}_F\right)^{-1}_{d'}\left(\Gamma^{(4)}_F\right)_{aecd} \tag{2.100}$$

Substitute (2.97) and (2.99) into the above equation, we have

$$G^{-1}_{ab} = -j_{ab} + \frac{1}{2}\lambda_{abcd}G_{cd} + Y_{ab} \tag{2.101}$$

[11] One can see that $W^{(2)}_B$ is the "L" in Baym and Kadanoff's old original papers [54, 55]. And "j" minus the quadratic part of the Hamiltonian is the "U" in Baym and Kadanoff's old original papers [54, 55]. Where $\pm L = \delta G/\delta U$ at $U = 0$, U is the source coupled to the density by $\int_x U(x)n(x)$. And in [54] it was shown that the L is preserving the energy, momentum, and gauge conservation laws, with three conditions (A,B,C), and later in [55] unified them into one.

Where Y_{ab} is given in terms of $\Gamma_B^{(2)}$

$$Y_{ab} = \frac{1}{6}\lambda_{nbcd}G^{-1}_{ae}\left[\left(\Gamma_B^{(2)}\right)^{-1}_{en,cd} + G_{ec}G_{nd} - G_{ed}G_{nc}\right] \tag{2.102}$$

The Y can be read off from (2.99). The above equation (2.102) implies that the self-energy part is constructed by the $W_B^{(2)} = (\Gamma_B^{(2)})^{-1}$.

Although now we have the 2PI action of the four-fermion model, Y can be still complicated. As a example, we can first truncate to the one-loop order which is at $O(\lambda G)$, by setting $Y = 0$. We then have[12]

$$G^{-1}_{ab} = -j_{ab} + \frac{1}{2}\lambda_{abcd}G_{cd} \tag{2.103}$$

This means that the corresponding effective action Γ_B reads

$$\frac{\delta\Gamma_{B1}}{\delta G_{ab}} = j_{ab} = -\left(G^{-1}\right)_{ab} + \frac{1}{2}\lambda_{abcd}G_{cd} \tag{2.104}$$

Use the identity

$$\delta G_{ab}/\delta G_{cd} = \mathbb{1}_{ab,cd} = \delta_{ac}\delta_{bd} - \delta_{ad}\delta_{bc} \tag{2.105}$$

the functional integration can be performed

$$\Gamma_{B1} = \frac{1}{2}\operatorname{Tr}\ln G + \frac{1}{8}\lambda_{abcd}G_{ab}G_{cd} + \text{const.} \tag{2.106}$$

up to a constant "const.". Note the $1/2$ includes the effect of the definition (2.105) contracting with a anti-symmetric matrix/tensor. This can be verified by functional derive the $\operatorname{Tr}\log G$ by G which gives a factor of 2.

The $Y \neq 0$ cases, namely the higher order actions, can be computed in an iterative manner. As another example we can iterate to 2-loop order $O\left(\lambda^2 G^2\right)$. We first partial twice the Γ_{B1}, this gives us

$$\left(\Gamma_{B1}^{(2)}\right)_{ab,cd} = -G^{-1}_{ac}G^{-1}_{bd} + G^{-1}_{ad}G^{-1}_{bc} + \lambda_{abcd} \tag{2.107}$$

One can check by direct computations that up to $O(\lambda^2 G^2)$, the inverse of the above functional is

$$\left(\Gamma_{B1}^{(2)}\right)^{-1}_{ab,cd} = -G_{ac}G_{bd} + G_{ad}G_{bc} - G_{ar}G_{bs}\lambda_{rstw}G_{tc}G_{wd} \tag{2.108}$$

Here we reach this inversion by completing the identity and neglecting the higher order terms.[13] Plug the expression $\left(\Gamma_{B1}^{(2)}\right)^{-1}_{ab,cd}$ into (2.102), we have

$$Y_{\alpha\beta} = -\frac{1}{6}\lambda_{atrs}\lambda_{bncd}G_{tn}G_{rc}G_{sd} \tag{2.109}$$

[12] This is the self-consistent Hartree-Fock approximation.

[13] There maybe other ways that I do not know.

The final result for the effective action at the second order now can be reached by integrating G,

$$\Gamma_{B2} = \Gamma_{B1} - \frac{1}{48}\lambda_{atrs}\lambda_{bncd}G_{ab}G_{tn}G_{rc}G_{sd} \tag{2.110}$$

Diagrammatically, this is a three-loop vacuum bubble. It is clear that we can always separate the Γ_B into a "kinetic" term and a "interacting" (or "Phi") term Γ_Φ

$$\Gamma_B = \frac{1}{2}\operatorname{Tr}\ln G + \Gamma_\Phi \tag{2.111}$$

Now use $\delta\Gamma_B/\delta G_{ab} = j_{ab}$, one finds

$$\frac{\delta\Gamma_\Phi}{\delta G_{ba}} = \frac{\delta\Gamma_B}{\delta G_{ba}} - \frac{\delta\frac{1}{2}\operatorname{Tr}\ln G}{\delta G_{ba}} = j_{ba} + G^{-1}_{ab} = -j_{ab} + \Gamma^{(2)}_{F,ab} = -G^{-1}_{0,ab} - J_{2,ab} + G^{-1}_{ab} = -\Sigma_{ab} \tag{2.112}$$

where one can now set the external source $J_2 = 0$. Here we used $[\delta \ln\det A/\delta A_{ij}] = [(A^{-1})^\intercal]_{ij}$ and cared the additional factor 2 for the anti-symmetric case. The Σ is the one-particle-irreducible part of the $\Gamma^{(2)}_F$ and thus the Γ_Φ is two-particle-irreducible (2-PI) as the name suggests. In many literature, if the self-energy Σ can be computed from the functional derivation of some approximated (truncated) Γ_Φ, it is called Φ-derivable. And this kind of approximations are called conserving approximations [59].

If we restore J_2 for $j = -G_0^{-1} + J_2$, the $\Gamma_B[G]$ can be written as

$$\Gamma_B[G] = -\frac{1}{2}\operatorname{Tr}\ln G^{-1} - \operatorname{Tr}G_0^{-1}G + \Gamma_\Phi[G] \tag{2.113}$$

where $\ln\int D\hat{\psi}D\hat{\bar{\psi}}e^{-S_0[\hat{\psi},\hat{\bar{\psi}}]} = \ln\left(\det G_0^{-1}\right) = \operatorname{Tr}\ln G_0^{-1}$, and

$$(\Sigma[G])_{ab} \equiv -\frac{\delta\Gamma_\Phi[G]}{\delta G_{ba}} \tag{2.114}$$

The minus sign is easy to understand since the functional derivative cut down one fermionic line and change the loop number by 1, and Each fermionic loop will contribute a -1. The indices order $\ldots/\delta G_{ba}$ is to produce the arrow direction which agrees with the usual Feynman rule. We should keep in mind that although Γ_B is called bosonic effective action, it is for the fermionic microscopic fields $\hat{\psi}$.

The 2-PI action of Bosonic microscopic field

The 2-PI action of bosonic microscopic fields can be derived as well, for some details see the Ref. [33, 58]. The difference is now $\langle\hat{\varphi}\rangle \neq 0$ is possible which makes the situation more complicated, the partition function and the Schwinger functional with 1-point and 2-point sources are

$$Z[J_1, J_2] = \exp\{W[J_1, J_2]\} = \int \mathrm{d}[\hat{\varphi}]\exp\left\{-S[\hat{\varphi}] + J_{1,a}\hat{\varphi}_a + \frac{1}{2}J_2\hat{\varphi}_a\hat{\varphi}_b\right\} \tag{2.115}$$

For instance the S can be a ϕ^4 theory

$$S[\hat{\varphi}] = \int_x \left\{ \frac{1}{2}\partial^\mu \hat{\varphi}(x)\partial_\mu \hat{\varphi}(x) - \frac{m^2}{2}\hat{\varphi}(x)\hat{\varphi}(x) - \frac{\lambda}{4!}\left(\hat{\varphi}(x)\hat{\varphi}(x)\right)^2 \right\} \tag{2.116}$$

The 2-PI action for bosonic microscopic field $\hat{\varphi}$ is now

$$\Gamma[\varphi, \Delta] = W[J_1, J_2] + \frac{\delta W[J_1, J_2]}{\delta J_{1,a}} J_{1,a} + \frac{\delta W[J_1, J_2]}{\delta J_{2,ab}} J_{2,ab} \tag{2.117}$$

The $\Gamma[\varphi, \Delta]$ can be written into mean fields φ and the propagator Δ, note that now $\varphi = \langle\hat{\varphi}\rangle \neq 0$ possible, the result is

$$\Gamma[\varphi, \Delta] = S[\varphi] + \frac{1}{2}\operatorname{Tr}\ln\Delta^{-1} + \frac{1}{2}\operatorname{Tr}\Delta_0^{-1}\Delta + \Gamma_\Phi[\varphi, \Delta] \tag{2.118}$$

The prefactor can be understood through the Gaussian integral of the bosonic fields for the quadratic action S_0, $\ln\int D\hat{\varphi}e^{-S_0[\hat{\varphi}]} = \ln\left(\det\Delta_0^{-1}\right)^{-\frac{1}{2}} = \frac{1}{2}\operatorname{Tr}\ln\Delta_0^{-1}$. Here we neglect the constant terms. The action (2.118) follows

$$\frac{\delta\Gamma[\varphi, \Delta]}{\delta\varphi_a} = J_{1,a} + J_{2,ab}\varphi_b \quad \text{and} \quad \frac{\delta\Gamma[\varphi, \Delta]}{\delta\Delta_{ab}} = \frac{1}{2}J_{2,ab} \tag{2.119}$$

The second equation of above gives

$$-\frac{1}{2}\Delta^{-1} + \frac{1}{2}\Delta_0^{-1} + \frac{\delta\Gamma_\Phi[\varphi, \Delta]}{\delta\Delta} = 0 \tag{2.120}$$

Set $J_2 = 0$, we have

$$\Sigma_{ab}[\varphi, \Delta] \equiv 2\frac{\delta\Gamma_\Phi[\varphi, \Delta]}{\delta\Delta_{ab}} \tag{2.121}$$

A mixed 2-PI action [57] can be defined for presenting bosonic and fermionic microscopic fields at the same time. We will review it now.

For boson-fermion interaction

Now we consider the quantum effective action for a boson-fermion interaction, for instance a simple scalar Yukawa term

$$S \sim \int g\hat{\bar{\psi}}\hat{\psi}\hat{\varphi} \tag{2.122}$$

In real time convention

$$e^{\mathrm{i}W} = Z \tag{2.123}$$

$$e^{\mathrm{i}\Gamma[\varphi,\Delta,G]} = e^{\mathrm{i}W+\ldots} \tag{2.124}$$

In the "..." are the source terms. The 2-PI effective action can be then written as [33]

$$\Gamma[\varphi, \Delta, G] = S[\varphi] + \frac{\mathrm{i}}{2}\operatorname{Tr}\ln\Delta^{-1} + \frac{\mathrm{i}}{2}\operatorname{Tr}\Delta_0^{-1}\Delta - \mathrm{i}\operatorname{Tr}\ln G^{-1} - \mathrm{i}\operatorname{Tr}G_0^{-1}G + \Gamma_\Phi[\varphi, \Delta, G] + \text{const} \tag{2.125}$$

A example can be found in [33, 58], where a chiral Yukawa term is considered for the chiral meson model. Note that here we used Δ for bosonic field, rather than in [33, 58] which is representing the fermionic field. Here we also keep the $\frac{1}{2}$ in front of the fermionic trace-log term to be consistent with previous definitions. One can see the difference between bosonic microscopic field and fermionic microscopic field through the relative minus sign of the trace-log, and the iΓ should have a "+", i.e. $+\operatorname{Tr}\ln G^{-1}$.

The Φ-functional $\Gamma_\Phi[\varphi, \Delta, G]$ is

$$\Gamma_\Phi[\varphi, \Delta, G] = \text{The vacuum diagrams that are 2-PI for } \Delta \text{ and } G. \tag{2.126}$$

where the action should not become disconnected whenever one cut up to two Δ lines, or two G lines, or one Δ and one G lines. The stationary equations are

$$\frac{\delta\Gamma[\varphi, \Delta, G]}{\delta\Delta_{ab}} = 0, \quad \frac{\delta\Gamma[\varphi, \Delta, G]}{\delta G_{ab}} = 0 \tag{2.127}$$

The self-energies are then

$$\Sigma^{(b)} = 2\mathrm{i}\frac{\delta\Gamma_\Phi[\Delta, G]}{\delta\Delta_{ab}}, \quad \Sigma^{(f)}_{ab} = -\mathrm{i}\frac{\delta\Gamma_\Phi[\Delta, G]}{\delta G_{ba}} \tag{2.128}$$

Note the relative "i" difference between the Euclidean and the real-time convention. Note the right hand side equation has a special order of indices. The "i" is from the real time convention.

2.3.3 Symmetries in the conserving approximation

To see how the action Γ_B compromises the symmetries of the microscopic Lagrangian/Hamiltonian, one can apply symmetry transformations. Here again, we follow [57].

A general unitary symmetry transform can be written as

$$\hat{\psi}_\alpha = r_{\alpha\beta}\hat{\psi}'_\beta \tag{2.129}$$

Where the $r_{\alpha\beta}$ is an invertible linear transformation of the fundamental fields. The two point source is the transformed as

$$j_{\alpha\beta} = \left(r^{-1}\right)_{\alpha'\alpha}\left(r^{-1}\right)_{\beta'\beta} j_{\alpha'\beta'} \tag{2.130}$$

the coupling for the quartic part transforms as

$$\lambda_{\alpha\beta\gamma\delta} = \left(r^{-1}\right)_{\alpha'\alpha}\left(r^{-1}\right)_{\beta'\beta}\left(r^{-1}\right)_{\gamma'\gamma}\left(r^{-1}\right)_{\delta'\delta}\lambda_{\alpha'\beta'\gamma'\delta'} \tag{2.131}$$

Recall

$$S_j[\hat{\psi}] = -\frac{1}{2}j_{ab}\hat{\psi}_a\hat{\psi}_b + \frac{1}{24}\lambda_{abcd}\hat{\psi}_a\hat{\psi}_b\hat{\psi}_c\hat{\psi}_d \tag{2.132}$$

The classical action $S_j[\hat{\psi}, j, \lambda]$, as well as the partition function $Z[j, \lambda]$ and the Schwinger functional $W[j, \lambda]$ are invariant under the changes (2.130) and (2.131), that is

$$S_j\left[\hat{\psi}', j', \lambda'\right] = S_j[\hat{\psi}, j, \lambda] \tag{2.133}$$

$$Z\left[j',\lambda'\right] = Z[j,\lambda] \tag{2.134}$$

$$W\left[j',\lambda'\right] = W\left[j,\lambda\right] \tag{2.135}$$

Note that the invariant of Z and W need the Jacobian of the functional measures are identities.[14]

Now we consider the action Γ_B. The "kinetic" trace-log term is

$$\mathrm{Tr}\ln G = \ln\det G \tag{2.136}$$

For the $G = \delta W/\delta j$ and (2.130) we have

$$G_{ab} = r_{aa'}r_{bb'}G'_{a'b'} \tag{2.137}$$

and use the identity of the determinants

$$\det G = \det rrG' = (\det r)^2 \det G \tag{2.138}$$

if the $\det r = 1$ then the trace-log term is invariant, even when the S_j is not invariant under $r_{\alpha\beta}$ transformation. This indicates that Γ_B can have even larger symmetry groups than S_j. The symmetries of Γ_B are those fulfill

$$\lambda_{a'b'c'd'}r_{a'a}r_{b'b}r_{c'c}r_{d'd} = \lambda_{abcd} \tag{2.139}$$

Also the lattice translational symmetry of the Hamiltonian and the local gauge symmetry of the quartic term of the Hamiltonian are preserved at the action level.

The advantages of the action Γ_B and in general the 2-PI quantum effective actions are not restricted to the action level invariant of the classical symmetries, but also the two-particle quantities derived from it (the $W_B^{(2)}$ and the vertices) are invariant under conservation laws. As is mentioned before it was proofed that [54, 55] the quantity

$$W_B^{(2)} = \left(\Gamma_B^{(2)}\right)^{-1} = \left(\frac{\delta\Gamma_B}{\delta G\delta G}\right)^{-1} \tag{2.140}$$

follows the conservation laws if the Γ_B is a two-particle irreducible quantum effective action. The $W_B^{(2)}$ corresponding to two particle scattering process, and the conserving nature actually ensures that many physical collision information with respect to the symmetries can be consistently computed from the 2-PI action and its corresponding equations of motions, or in another word the 2-PI Dyson-Schwinger like equations. This is especially important for non-equilibrium physics and transport problems.

Originally, Baym also [55] proved, through a simple but general example, that once G is from the Φ derivable, $W_B^{(2)}$ follows the conservation law where the integral version of the continuous equation is fulfilled. Here I follow one part of [54] to give an example.

From (2.101), $G^{-1}_{ab} = -j_{ab} + \frac{1}{2}\lambda_{abcd}G_{cd} + Y_{ab}$ we can get the left and right version of the Dyson-Schwinger equations

$$G_{ca}G^{-1}_{ab} = -G_{ca}j_{ab} + \frac{1}{2}G_{ca}\lambda_{abcd}G_{cd} + G_{ca}Y_{ab} \tag{2.141}$$

[14] There in [57], quantum anomalies are also discussed, as a term comes from the Jacobian of the functional measure under symmetry transformation. The anomalies will break certain classical symmetries. For the effective action would be something like $\Gamma_B\left[G',\lambda'\right] = \Gamma_B[G,\lambda] - \ln\det(t)$.

and

$$G_{ab}^{-1}G_{bd} = -j_{ab}G_{bd} + \frac{1}{2}\lambda_{abcd}G_{cd}G_{bd} + Y_{ab}G_{bd} \tag{2.142}$$

Now we can separate $j = -G_0^{-1} + J_2$ and subtract the above two equations, then write the abstract contractions into summation and the integrals.[15]

To make contact with the original references, we follow [55] and consider the continuous case with a central interaction potential locally in the time space. The Hamiltonian reads

$$H(x^0) = \frac{1}{2m}\int_{\boldsymbol{x}} \hat{\psi}^\dagger(x)\partial_{\boldsymbol{x}}^2\hat{\psi}(x) + \frac{1}{2}\int_{\boldsymbol{x},\boldsymbol{y},y^0} \hat{\psi}^\dagger(x)\hat{\psi}^\dagger(y)V(x-y)\hat{\psi}(y)\hat{\psi}(x) \tag{2.143}$$

With this Hamiltonian, one can find $G_0^{-1}(x,y) = (\mathrm{i}\partial_{x^0} + \partial_{\boldsymbol{x}}^2/2m)\delta(x-y) = (-\mathrm{i}\partial_{y^0} + \partial_{\boldsymbol{y}}^2/2m)\delta(x-y)$. For this example, the integrals and summations are written explicitly, and here I restrict to the fermionic case. The result after substituting (2.142) and (2.141) should be

$$\begin{aligned}&(\partial_{x^0} + \partial_{y^0})\left(\mathrm{i}G_{J_2}\right)_{xy} + \frac{1}{2\mathrm{i}m}(\partial_{\boldsymbol{x}} + \partial_{\boldsymbol{y}})(\partial_{\boldsymbol{x}} - \partial_{\boldsymbol{y}})\left(\mathrm{i}G_{J_2}\right)_{xy} \\ &\quad = \int_z \left(J_{2,xz}\left(G_{J_2}\right)_{zy} - \left(G_{J_2}\right)_{xz}J_{2,zy} - \mathrm{i}(V_{xz} - V_{yz})\left(G_{2,J_2}\right)_{xz^-,yz^+}\right)\end{aligned} \tag{2.144}$$

Where $V_{xy} = V(x-y) = \delta(x^0 - y^0)u(|\boldsymbol{x}-\boldsymbol{y}|)$ and G_2 is a functional. The VG_2 term contains the terms YG and λGG. Now set $y \to x^+ = x + 0^+$, where 0^+ is an infinitesimal positive four-vector.

$$\begin{aligned}\partial_{x^0}\left(\mathrm{i}G_{J_2}\right)_{xx^+} + \frac{1}{2\mathrm{i}m}(\partial_{\boldsymbol{x}})(\partial_{\boldsymbol{x}} - \partial_{\boldsymbol{x}^+})\left(\mathrm{i}G_{J_2}\right)_{xx^+} &= -\left(\partial_{x^0}\langle\hat{n}(x)\rangle_{J_2} + \sum_i \partial_{x^i}\langle\hat{j}^i(x)\rangle_{J_2}\right) \\ &= \int_z \left(J_{2,xz}\left(G_{J_2}\right)_{zy} - \left(G_{J_2}\right)_{xz}J_{2,zy}\right)\end{aligned} \tag{2.145}$$

In above, $V_{xy} - V_{x^+y} \to 0$ is used. Note that $\hat{n}$ is the charge density operator and $\hat{j}^i$ is the current density operator of spatial component i. If assume the external source $J_{2,xy} = \delta(x-y)J_{2,x}$ then the last line of the above equation is zero. As a result

$$\partial_\mu\langle\hat{j}^\mu\rangle_{J_2} = \partial_{x^0}\langle\hat{n}(x)\rangle_{J_2} + \sum_i \partial_{x^i}\langle\hat{j}^i(x)\rangle_{J_2} = 0 \tag{2.146}$$

This is the continuity equation of the charge conservation. The general conserving approximations are not restricted to the Hamiltonian and the interaction in this example. It is also not only can be applied to the charge conservation, but also can be applied to all one-particle conservation laws. Other symmetry related conservation law such as momentum conservation and energy conservation can be also included [54, 55, 59].

[15] This procedure is skipped here.

2.3.4 The n-PI quantum effective action

From the derivations of the 2PI effective action, we can see that the crucial part is to find the relation between the functional derivative of the source j and those of ϕ, or $\Gamma_B^{(2)}$ and $\Gamma_F^{(4)}$. Generally, the higher effective actions (n-PI, $n > 2$) can be calculated recursively from 2-PI effective actions, for a general computation and for non-Abelian gauge theory with fermions up to 4-PI action see [33, 60].

For many realistic computations, one usually truncates the effective action to a maximum loop order, say to L-loop order. Then there is an equivalent hierarchy of the n-PI actions. Define the n-point connected correlation function as V_n then when apply the effective action truncation up to 3-loop order, we have

$$\begin{aligned}\Gamma^{(3\text{loop})}[\phi] \neq \Gamma^{(3\text{loop})}[\phi, D] \neq \Gamma^{(3\text{loop})}\left[\phi, D, V_3\right] \\ = \Gamma^{(3\text{loop})}\left[\phi, D, V_3, V_4\right] = \Gamma^{(3\text{loop})}\left[\phi, D, V_3, V_4, \ldots, V_n\right]\end{aligned} \tag{2.147}$$

where ϕ is the one-point mean field $\langle\hat{\phi}\rangle$, D is the two-point and V_3 is the three-point mean field. Without truncations, the n-PI effective actions are equivalent

$$\Gamma[\phi] = \Gamma[\phi, D] = \Gamma\left[\phi, D, V_3\right] = \Gamma\left[\phi, D, V_3, V_4\right] = \Gamma\left[\phi, D, V_3, V_4, \ldots, V_n\right] \tag{2.148}$$

The detailed derivations of above relations are beyond the scope of our discussions. The crucial step is to combine the bare vertex V_{0n} with the corresponding source term [33]

$$g_n V_{0n} \longrightarrow g_n V_{0n} - R_n \equiv g_n \tilde{V}_n \tag{2.149}$$

and derive relations between V_n and $\tilde{V}_n$ through applying functional derivatives and functional identities such as DSEs. For the irreducibility, one naively expects the n-PI action gives loop $L = n$ diagrams n line irreducible, however, there is a study [61] on 5-PI for a bosonic microscopic field. There at loop order $L = 5$, the 5-PI effective action is not irreducible upon a 5 line cut, for some 5-loop vacuum diagrams. Therefore, the name 5-PI seems not true literally. Thus, in general, one may regard "n-PI" as "n-Lengendred" quantum effective action.

2.3.5 Self-consistent methods

We can see that in DSEs or the equations of motion derived from effective actions, the target quantities appear on both sides of the equations. This means they usually need to be solved recursively or through non-linear solvers for the integro-differential equations. The gap equation in the mean-field theory is the simplest example of this kind of self-consistent equations.

For instance, in the two-particle-irreducible action section, we know from (2.112) that the Dyson equation reads

$$G_0 - G^{-1} = -\frac{\delta\Gamma_\Phi}{\delta G} \tag{2.150}$$

Where to the order $O(\lambda^2 G^2)$ we have

$$\Gamma_\Phi = +\frac{1}{2}\lambda_{abcd}G_{ab}G_{cd} - \frac{1}{48}\lambda_{atrs}\lambda_{becd}G_{ab}G_{te}G_{rc}G_{sd} \tag{2.151}$$

It is clear that the equation (2.150) has the full propagator G on both side of the equation, this makes

the equation a self-consistent equation (a generalized gap equation) for the 1-particle quantity, i.e., the two-point function G. Other things in the equation are fixed in the model. Recall that the index contractions are including the possible integral and summations of all possible fields, the Eq. 2.150 is then usually an integral equation, and is difficulty to solve analytically. Numerically, it can be efficiently solved in many contexts. Some nice reviews can be found in [62] and also [33, 63].

2.4 Functional renormalization group

Quantum field theory receives understandings after Wilson's work, the renormalization group. The renormalization group solved an important puzzle in the quantum field theory, i.e., why renormalization is needed and the meaning of renormalizability. There are nice reviews written by K. G. Wilson [64–66], where Wilson used Kondo model as an example to address this problem.

It is great that there are Wilsonian ways to compute the n-point vertices and the quantum effective actions in a non-perturbative manner. One of those ways is pointed out by Polchinski in the seminal work [67], where scale dependent Schwinger functional W_k is used as the central quantity, k labels the scale. Nowadays it is usually presented in a form called Wetterich equation [68] or the (exact) functional renormalization group (FRG) equation of quantum effective actions. This method has several advantages, such as it is a non-perturbative method and we can direct extract physical quantities once the actions or vertices are obtained at the end of the flow. Here I make a very short discussion about the functional renormalization group. For more details see the references [30, 69, 70] and many other reviews [31, 36, 52, 71, 72].

2.4.1 Functional renormalization group

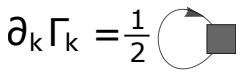

Figure 2.3: The Wetterich equation has a one loop structure. The filled box is the $\partial_k R_k$. The full line is the scale dependent propagator $[\Gamma^{(2)} + R_k]^{-1}$

The Wilsonian renormalization group [65–67, 73] regards all quantum field theories as some sort of effective field theories that have scale dependence and cutoffs. And the scale k (or Λ) low energy[16] physics can be captured by a field theory with finite number of non-divergent parameters $\lambda_i(k)$ at the given scale k.[17] The $\lambda_i(k)$ can be computed from a set of differential equations about k, the flow equations. Lowering the k is equivalent to coarse graining the resolution.

With this picture, the effective action of a system can be also regarded as scale dependent. If one knows the effective action at some initial scale Λ_0 as $\Gamma_{k=\Lambda_0}$ where an infrared (IR) cutoff is set at k, then a set of differential equations can be constructed as an analogue of the flow equations of the running coupling parameters. As long as k is lowered to zero, and the differential equation is integrated and solved, the full effective action $\Gamma = \Gamma_{k\to 0}$ is reached and the n-point vertices $\Gamma^{(n)}$ can be computed. This is the idear of the FRG.

[16] Low compare with the UV cutoff Λ_0

[17] Perturbatively the n-point functions has the limit when takes $\Lambda_0 \to \infty$ which is proven in the Ref. [67].

Let us go to some details. Consider a scale which is marked by the four momenta $k = (k_0, \boldsymbol{k})$ where $k_0 = E$ is the energy[18]. A scale dependent average action is Γ_k, which fulfils

$$\Gamma_{k=\Lambda_0} = S, \quad \lim_{k\to 0} \Gamma_k = \Gamma \tag{2.152}$$

It can be regarded as in a finite space-time volume k^{-d}. The $\Gamma = \Gamma_{k=0}$ is the full effective action. A scale dependent [30, 69] 1-PI effective action[19] is defined as

$$\Gamma_k[R] = -W_k[J] + J_a\phi^a - \Delta S'[\phi, R] \tag{2.153}$$

Note that $\phi = \langle\hat{\phi}\rangle$, where the scale dependent Schwinger functional is $W_k = \ln Z_k[J] = \ln \int D\hat{\phi} \exp\{-S[\hat{\phi}] - \Delta S'[\hat{\phi}, R] + J_a\hat{\phi}^a\}$. The cutoff is in $\Delta S'$

$$\Delta S'[\phi, R] = \frac{1}{2}\phi_a R_k^{ab}\phi_b \tag{2.154}$$

The cutoff, R_k, as a scale dependent source term that can be regarded as a k dependent mass. It should satisfy [35]

$$\begin{cases} \lim_{q^2/k^2\to 0} R_k & > 0 \\ \lim_{k^2/q^2\to 0} R_k & = 0 \\ \lim_{k\to\Lambda_0\to\infty} R_k & = \infty \end{cases} \tag{2.155}$$

The R_k is a IR cutoff where if the scale $k = \Lambda_0$ all fluctuations are suppressed, since the "mass" $R \to \infty$. For fixed k, $R \to 0$ if $q^2/k^2 \to 0$, and the high four momentum fluctuations are preserved. The fluctuations which have four-momentum lower than $q^2 \sim k^2$ are suppressed by the positive mass term R.

For example, the cutoff source term can be chosen as $R_k(q) \sim q^2/(e^{q^2/k^2} - 1)$ or $R_k(q^2) = (k^2 - q^2)\theta(k^2 - q^2)$, $\theta(x)$ is the step function. The RG results should not depend on the cutoff choices if without any approximation, however in practice the cutoff choice matters, and may need to be optimized.

Now comes to the central equation, the Wetterich equation [30, 69], it reads

$$\frac{\partial}{\partial k}\Gamma_k[\phi] = \frac{1}{2}\,\mathrm{Tr}\left\{\left[\Gamma_k^{(2)}[\phi] + R_k\right]^{-1}\frac{\partial}{\partial k}R_k\right\} \tag{2.156}$$

We also show it diagrammatically in Fig. 2.3. Again, ϕ means the $\langle\hat{\phi}\rangle$. Here the trace is defined as $\mathrm{Tr} = \sum_a \int d^dq/(2\pi)^d$ and the identity is thus $\mathbb{1} = (2\pi)^d\delta(q - q')\,\delta_{ab}$ which combines the momentum and index delta. This one-loop equation is exact and one need to solve it by integrating the flow from the initial cutoff $k = \Lambda_0$ down to the deep IR scale $k = 0$. This will return a full 1-PI effective action. It is no a surprise that to solve the full 1-PI effective action exactly is not realistic in most of the situations, and different approximation schemes should be applied. Two of them are frequently used, gradient expansions and vertex expansions [52, 69, 70]. We will review the vertex expansions here.

The vertex expansions [70] are frequently used in strongly correlated electronic systems. The

[18] One can equivalently use the "RG time", $t = \ln(k/\Lambda_0)$ to mark the scale.

[19] Here and after I restrict to the 1-PI version, all though other formalism are possible.

starting point is again the general expansion of the 1-PI effective action that is mentioned before in (2.71), but now for the scale-dependent action

$$\Gamma_k = \sum_n c_n \Gamma_k^{(n)a_1 \ldots a_n} \phi_{a_1} \ldots \phi_{a_n} \tag{2.157}$$

where c_n are constant prefactors, ϕ are 1-point mean fields, and $\Gamma^{(n)}$ are n-th functional derivatives of the Γ_k. Through functional differentiating the Wetterich equation (2.156), one can match the order n vertex $\Gamma_k^{(n)}$ order by order and write down a set of infinite coupled equations [70].

To see how those equations look like, we plot the vertex expansion for Gross-Neveu model in Fig. 2.4, again we used DoFun [36] package. And for Hubbard model see [70] and Fig. 2.5. Those diagrams give us a set of differential equations to solve. After finding the solution, the interesting data such ase critical exponents and other observables can be extracted from the n-vertices.

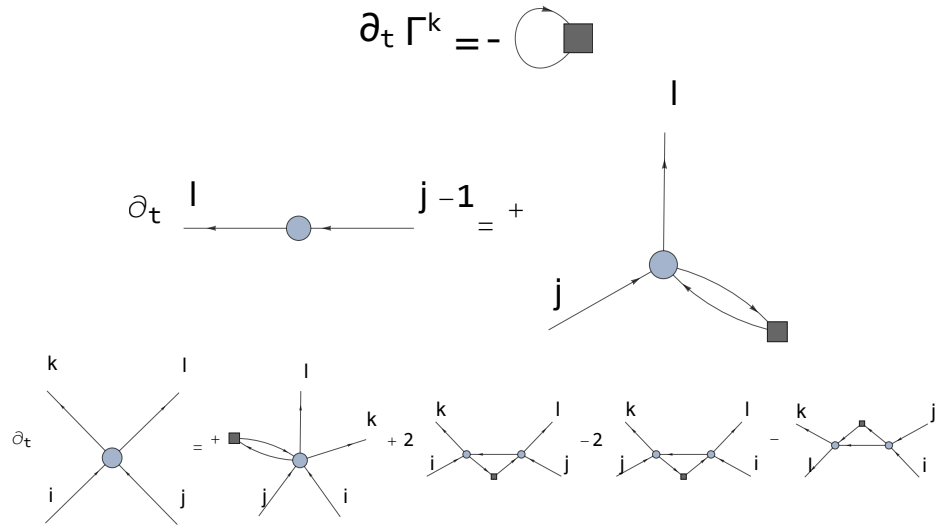

Figure 2.4: The DoFun output for the Gross-Neveu model. Flow of scale dependent effective action, two-point $\Gamma_k^{(2)}$ and four-point vertices $\Gamma_k^{(4)}$. The $t = \ln(k/\Lambda_0)$ is the RG time with Λ_0 the initial UV cutoff. The filled box is now the $\partial_t R_k$.

2.4.2 Relations between FRG and self-consistent method

The relation between the FRG equations with vertex truncation up to 4-vertex and the parquet approximation (PA) is discussed recently [74–76], the authors point out that the loss of accuracy by dropping the 6-point function and beyond, which makes the derivative incomplete, can be partially recovered by making the derivative complete through additional parquet diagrams. Then the FRG equation differential equations can be solved self-consistently and become a resummation technique that offers a new way to solve the problems in which vertex corrections are important. Especially this kind of method makes the flow regulator free and it is also promising to avoid the low energy divergences occurring in dynamical vertex approximation [77] $D\Gamma A$, which is a non-local extension of the DMFT.

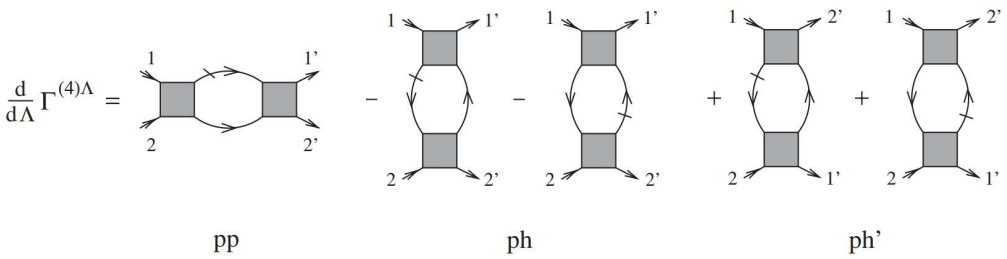

Figure 2.5: Vertex expansion for $\Gamma^{(4)}$ setting the $\Gamma^{(6)} = 0$ for Hubbard model, here the scale is Λ. The three typical channels are labeled as particle-particle (pp), particle-hole (ph) and exchanged particle-hole (ph'). Define $G_k \equiv \Gamma_k^{(2)}$. The slashed lines are the single scale propagators $S_k \sim -G_k \partial_t R_k G_k$, see [70] equation (48). Figure from [70].

2.5 Summary

In this chapter, I reviewed some basics of the integral equations of the n-point correlations functions and the n-point vertex functions in the quantum/statistical field theory, where we used functional equations to demonstrate the theoretical structure. Those equations are Dyson-Schwinger equations, tree expansions, n-particle-irreducible actions, scale dependent effective actions and their functional derivatives, i.e., vertices. They may be summarized in a graph Fig. 2.6.

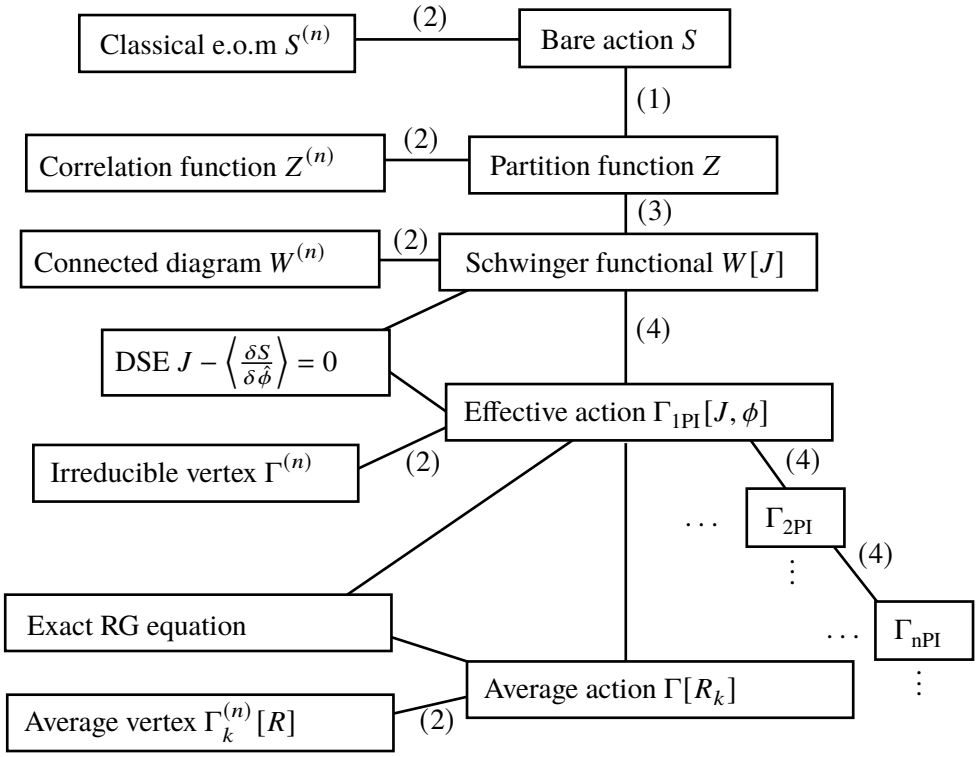

Figure 2.6: A summary of the effective actions and the equations of the correlation functions. They are related by: (1) Functional integrals, (2) Functional derivatives, (3) Legendre transforms with source terms and fields, (4) Legendre transforms with n-point mean fields.

CHAPTER 3

Non-equilibrium: Keldysh method

In this chapter, we review the Keldysh method for non-equilibrium quantum systems.

In general, the quantum mechanical systems always start their time evolution from an initial state $|\Psi_{\text{in}}\rangle$ to a final state $|\Psi_{\text{out}}\rangle$. This general setting can be described by the so-called Keldysh formalism, which can be traced back to Schwinger's [78] and Keldysh's [79] works, as well as the works of Kadanoff and Baym [59] in the 1960s. This formalism is especially convenient in the field theoretical context since almost all techniques available in the usual quantum/statistical field theory can be straightforwardly extended, and to be useful for non-equilibrium physics. It is not a surprise that the Dyson-Schwinger equations and their generalizations can be used in this manner as well. An important class of those Keldysh DSEs are frequently called Kadanoff-Baym equations [59]. These equations are formally almost identical to their equilibrium counterpart, however, the time variables are now on the contour time path (CTP) or the Schwinger-Keldysh contour, see Fig. 3.1. The feature of the Keldysh method is that it allows the distribution to also evolve dynamically and it is not necessarily related with spectral function by the Fluctuation-Dissipation theorem (FDT)[1]. Interestingly, an additional dynamical degree of freedom will arise on top of all the detailed structures of the concrete models. There are many good reviews and textbooks for the Keldysh method, including [25, 29, 33, 58, 80–83], some more details may be found in [63, 84, 85]. Many original ideas can be found in the old classic book by Kadanoff and Baym [59].

The Keldysh method is not only a technical method to compute certain observables in field theoretical way, but also a convenient "language" [82] for describing the dynamical processes, such as classical and quantum relaxation, diffusion, dissipation, coherence/decoherence, and further the integrable or chaotic systems. The Keldysh method has the following advantages: it is

1. Use complex time contour which refers only to the initial density matrix
2. Can treat Real-time without analytical continuation
3. Gives the inter-play of spectra and occupation
4. Can unify the equilibrium and non-equilibrium
5. Can derive Boltzmann equation and other kinetic equation from the “first principle”.

[1] Namely, the fields or two-point functions do not, in general, follow the Kubo-Martin-Schwinger (KMS) boundary condition. We will discuss this in a section of this chapter.

Technically, extent field-theoretical tools to the Keldysh form is simple. The extensions can be done through three steps.

1. Choose the time contour, usually the close time contour, and write down contour time equations.

2. Go to real-time by representing the products by tensor contractions of the contour indices

3. Replace contour time propagators and vertices by real-time propagators and vertices.

We will give detailed discussions in the following sections.

3.1 Field theory on closed time path (CTP) contour

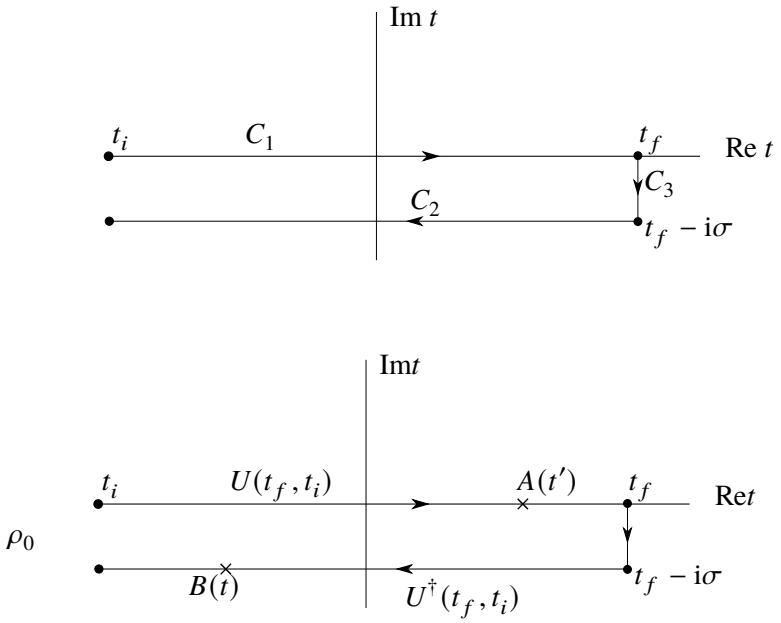

Figure 3.1: Schwinger-Keldysh closed contour time path (CTP), see also [81, 83, 86]. Usually we call C_1 the "+" part, C_2 the "−" part. Note that the C_3 contour do not contribute in most of the case we are considering.

Consider a general case in which the Hamiltonian [2] of the system has an explicit time dependence. This means in the Schrödinger picture it has time dependence through its parameters. The Schrödinger picture full Hamiltonian $H(t)$ can be separated into two parts

$$H(t) = H_1(t) + H_2(t)$$

[2] As a functional of field operators.

where $H_2(t) = \theta(t - t_i)H_2(t)$, the $\theta(t)$ is the Heaviside step function. Step of time means that the H_2 is switched on at time point t_i. Then the expectation value of any observable at time $t > t_i$ is

$$\langle \hat{O}_H(t) \rangle = \mathrm{Tr}[\rho(t_i)\hat{O}_H(t)] = \mathrm{Tr}[\rho(t)\hat{O}_S]$$

here ρ is the density matrix. The operator $O(t)$ is a Heisenberg picture operator for the observable O with respect to the total Hamiltonian $H(t)$. Now, if one uses the general time propagation of the operator $\hat{O}(t) = U(t_i, t)\hat{O}(t)U(t, t_i)$, then

$$\begin{aligned} \langle \hat{O}_H(t) \rangle &= \langle \Psi(t_i)|\hat{O}_H(t)|\Psi(t_i)\rangle \\ &= \langle \Psi(t_i)|U(t_i, t)\hat{O}_S U(t, t_i)|\Psi(t_i)\rangle = \langle \Psi(t)|\hat{O}_S|\Psi(t)\rangle \end{aligned} \tag{3.1}$$

Here, $\hat{O}_S$ is the operator in the Schrödinger picture. Now consider the interaction picture (a rotating frame) of Hamiltonian H_1. We can $U(t_i, t_f) = U^\dagger(t_f, t_i)$ and $U(t, t_i) = u_2(t, t_i)u_1(t, t_i)$ to get

$$\hat{O}_H(t) = u_2^\dagger(t, t_i)O_{H_1}(t)u_2(t, t_i) = u_2^\dagger(t, t_i)u_1^\dagger(t, t_i)O_S u_1(t, t_i)u_2(t, t_i) \tag{3.2}$$

where we assumed

$$u_1(t, t_i) = \hat{T} \exp\left\{-\mathrm{i}\int_{t_i}^{t} \mathrm{d}t' H_1(t')\right\} \tag{3.3}$$

that satisfies

$$i\frac{\mathrm{d}}{\mathrm{d}t}u_1(t, t_i) = H_1(t)u_1(t, t_i) \tag{3.4}$$

Then u_1 is the evolution operator of $H_1(t)$ and

$$\hat{O}_{H_1}(t) = u_1^\dagger(t, t_i)\hat{O}_S u_1(t, t_i) \tag{3.5}$$

From the above equations, we can see that

$$\langle \hat{O}_H(t) \rangle = \langle \Psi(t_i)|u_2^\dagger(t, t_i)\hat{O}_{H_1}(t)u_2(t, t_i)|\Psi(t_i)\rangle \tag{3.6}$$

And we can write the interaction picture [28] Schrödinger equation as

$$\begin{aligned} &\mathrm{i}\frac{\mathrm{d}}{\mathrm{d}t}|\Psi\rangle_S = H_S|\Psi\rangle_S \\ &\rightarrow \mathrm{i}\frac{\mathrm{d}}{\mathrm{d}t}\left(u_1|\Psi\rangle_1\right) = \left(H_1 + H_2\right)_S u_1|\Psi\rangle_1 \\ &\rightarrow H_1 u_1|\Psi\rangle_1 + \mathrm{i}u_1\frac{\mathrm{d}}{\mathrm{d}t}|\Psi\rangle_1 = \left(H_1 + H_2\right)_S u_1|\Psi\rangle_1 \\ &\rightarrow \mathrm{i}\frac{\mathrm{d}}{\mathrm{d}t}|\Psi\rangle_1 = u_1^\dagger\left(H_2\right)_S u_1|\Psi\rangle_1 \\ &\rightarrow \mathrm{i}\frac{\mathrm{d}}{\mathrm{d}t}|\Psi\rangle_1 = [H_2]_{H_1}|\Psi\rangle_1 \end{aligned} \tag{3.7}$$

where $|\Psi\rangle_1 = u_1^\dagger|\Psi\rangle_S$ and the interaction picture Hamiltonian is defined as

$$[H_2]_{H_1} \equiv u_1^\dagger(H_2)_S u_1 \tag{3.8}$$

Note that H_2 is originally in the Schrödinger picture.

From equation (3.7) the time propagation operator $u_2(t,t_i)$ in this specific interaction picture can be written as

$$u_2(t,t_i) = \hat{T}\exp\{-\mathrm{i}\int_{t_i}^{t} \mathrm{d}t'[H_2(t')]_{H_1}\}$$

Where the $\hat{T}$ is the time ordering operator where inside it the operators of different times commute, and they are time ordered which means that the operator of the later time are on the left. To relate this interaction picture to quantum field theory methods, we will use an alternative form of the above equation. We write the conjugate of U, i.e., $U(t_i,t_f) = U^{\dagger}(t_f,t_i)$ into an anti-time-ordering operator $\overline{T}$. The $\overline{T}$ means to order the operators with the inverse times order, i.e., the operator of the later time to the right. Now we have

$$u_2^{\dagger}(t,t_i) = \overline{T}\exp\{\mathrm{i}\int_{t_i}^{t} dt'[H_2(t')]_{H_1}\}$$

Since the incoming initial state is $|\Psi(t_i)\rangle$, one can define the initial density matrix as

$$\rho_0 \equiv |\Psi(t_i)\rangle\langle\Psi(t_i)| \tag{3.9}$$

Where $\mathrm{Tr}\,\rho_0 = 1$ and $\rho_0 = \rho_0^{\dagger}$. Note that ρ_0 is not restricted to pure state density matrices, it can also be for mixed states, e.g. the thermal density matrix. Equation (3.1) can be written as

$$\langle\hat{O}_H(t)\rangle = \mathrm{Tr}\left[\rho_0\hat{T}_C\left[e^{-\mathrm{i}\int_{C(t')}[H_2(t')]_{H_1}}\hat{O}_{H_1}(t)\right]\right]$$

Here we commuted operators inside the time-ordering. The $\int_{C(t')}$ is the contour integral on the Schwinger-Keldysh contour or close time path (CTP), see Fig. 3.1. Note that t_f is later than the measuring time t. This is always allowed since if without operator insertions, the $+/-$ (or C_1/C_2) contours cancel with each other because of the unitarity. This cancelation also guarantees normalization.

We can now define the partition function as

$$Z = \mathrm{Tr}\,\rho_0\hat{T}_C e^{-\mathrm{i}\int_{C(t)}[H_2(t)]_{H_1}} \tag{3.10}$$

We can choose H_1 and H_2 in different ways. A natural way is to choose a perturbation H_2 defined as $H_2(t) = \int_{\boldsymbol{x}} J(t,\boldsymbol{x})\hat{\phi}(\boldsymbol{x})$ which is a time-dependent external source coupled to the Schrödinger field operator $\hat{\phi}(x)$. With in mind that H_1 is the Hamiltonian of the full system where these external sources are turned off, we have

$$Z[J] = \mathrm{Tr}\left[\rho_0\hat{T}_C\exp\left\{-\mathrm{i}\int_{\boldsymbol{x},C(t)} J(x)\hat{\phi}(x)\right\}\right] \tag{3.11}$$

Here $x = (x^0,x^1,\ldots) = (t,\boldsymbol{x})$, $\hat{\phi}(x)$ is the Heisenberg operator with respect to $H_1(t)$. The (3.11) this is the equation (2.1) at the very beginning. Note that $J(x)$ and $\hat{\psi}(x)$ now have their time variables on the contour. The contour-time integration on the CTP is defined as

$$\int_{C(t)} = \int_{-\infty}^{+\infty}\mathrm{d}t_+ - \int_{-\infty}^{+\infty}\mathrm{d}t_- \tag{3.12}$$

Note the relative minus sign, which can be absorbed into a "contour metric" if one defines tensor vertices. We will discuss the tensor vertices in later sections.

One can now understand the generating functional $Z[J]$ for the Schwinger-Keldysh contour time path (CTP) as a trace of the time evolution of the ρ_0 from initial time t_i to a final time t_f. For a closer look, we can split the contour ordering in the partition function [83, 87]

$$Z[J_+, J_-] = \mathrm{Tr}[U(t_f, t_i, J_+)\rho_0 U^\dagger(t_f, t_i, J_-)] \tag{3.13}$$

With the source terms switched off, it is

$$Z = \mathrm{Tr}[\rho(t)] \tag{3.14}$$

which is the trace of the time-dependent density matrix.

In contrast to the usual partition functions, the (3.13) has two sources coupled to the operators on the upper + and lower − contours. To see this, we rewrite $u_2 = U(t_f, t_i, J_+)$. The explicit form of the partition functional is then

$$Z[J_+, J_-] = \mathrm{Tr}\left[\left(\hat{T} e^{-\mathrm{i}\int_x J_+(x)\hat{\phi}_+(x)}\right)\rho_0\left(\overline{T} e^{\mathrm{i}\int_x J_-(x)\hat{\phi}_-(x)}\right)\right] \tag{3.15}$$

Here $\int_x = \int_{-\infty}^{+\infty} \mathrm{d}x$. The correlation functions are now

$$\mathrm{Tr}[(\hat{T}\hat{\phi}_+(x)\hat{\phi}_+(y)\ldots)\rho_0(\overline{T}\hat{\phi}_-(z)\hat{\phi}_-(s)\ldots)] \tag{3.16}$$

Apply the cyclic rule of the trace, we get

$$Z[J_+, J_-] = \mathrm{Tr}\left[\rho_0 \hat{T}_C e^{-\mathrm{i}\int_x (J_+(x)\hat{\phi}_+(x) - J_-(x)\hat{\phi}_-(x))}\right] \tag{3.17}$$

where $\hat{T}_C$ is the contour time ordering operator. The Schwinger functional on the CTP then can be defined in the usual way

$$e^{\mathrm{i}W[J_+, J_-]} = Z[J_+, J_-] \tag{3.18}$$

Note that $Z[0, 0] = \mathrm{Tr}\,\rho_0 = 1$ for the Schwinger-Keldysh case, which means that one can alternatively define $W = Z$ rather than $W = -\mathrm{i}\ln Z$ and its functional derivatives will be normalized observable. This normalization property [25] is an advantage of the Keldysh method for disorder systems.

3.2 Basic two-point functions

Here we discuss some representative 2-point functions, the connected Green's functions. The connected Green's functions are functional derivatives of the generating functional, the Schwinger functional W

$$\mathrm{i}G^{ab}(x, y) = \mathrm{i}\frac{\delta W}{\delta \mathrm{i}J_a(x)\delta \mathrm{i}J_b(y)}\bigg|_{J_+=0, J_-=0} \tag{3.19}$$

where we suppressed all indices except the contour indices and the space-time. Here we majorly consider the fermionic microscopic fields; it means that

$$\frac{\delta W}{\delta J_{\pm}(x)} = \langle \psi_{\pm}(x) \rangle = 0 \tag{3.20}$$

where we have the fermionic property that the 1-point mean-field vanishes.

In a matrix form the G^{ab} reads

$$G^{ab} = \begin{pmatrix} \frac{\delta W}{\delta \mathrm{i}J_+ \delta \mathrm{i}J_+} & \frac{\delta W}{\delta \mathrm{i}J_+ \delta \mathrm{i}J_-} \\ \frac{\delta W}{\delta \mathrm{i}J_- \delta \mathrm{i}J_+} & \frac{\delta W}{\delta \mathrm{i}J_- \delta \mathrm{i}J_-} \end{pmatrix} \Bigg|_{J_+ = J_- = 0} = \begin{pmatrix} G^{++} & G^{+-} \\ G^{-+} & G^{--} \end{pmatrix} = \begin{pmatrix} G^T & G^< \\ G^> & G^{\overline{T}} \end{pmatrix} \tag{3.21}$$

Here I defined two-point functions [3, 25, 29, 33] on closed time path (CTP) contour. Although G on CTP is commonly defined in almost all literatures for the Keldysh method, including the original paper of Keldysh [79], the notations vary from author to author. It is thus worthy to define them by using uniform and consistent notations. For space-time variables, we will use $x^0 \equiv t, x \equiv (x^0, \boldsymbol{x})$.

The self-energy Σ, namely the 1-PI irreducible part of the collected two-point function, can be defined through

$$\Gamma^{(2)} = (W^{(2)})^{-1} = G^{-1} = [G_0]^{-1} - \Sigma \tag{3.22}$$

And they follow the same transformation rules as G^{-1}.

From (3.21) we see that on the CTP we have four contour Green's functions, they are defined as

$$G^{++} = G^T(x,y) = -\mathrm{i} \langle T\psi_+(x)\psi_+^\dagger(y) \rangle_{\rho_0} = \theta(x^0 - y^0)G^>(x,y) + \theta(y^0 - x^0)G^<(x,y) \tag{3.23}$$

$$G^{--} = G^{\overline{T}}(x,y) = -\mathrm{i} \langle \overline{T}\psi_-(x)\psi_-^\dagger(y) \rangle_{\rho_0} = \theta(y^0 - x^0)G^>(x,y) + \theta(x^0 - y^0)G^<(x,y) \tag{3.24}$$

$$G^{+-} = G^<(x,y) \tag{3.25}$$

$$G^{-+} = G^>(x,y) \tag{3.26}$$

The $>$ can be regarded as an "arrow" from $-$ to $+$.

We can write G^{++} and G^{--} into $G^>$ and $G^<$ with proper causal structures

$$G^{++} = G^T(x,y) = -\mathrm{i} \langle T\psi_+(x)\psi_+^\dagger(y) \rangle_{\rho_0} = \theta(x^0 - y^0)G^>(x,y) + \theta(y^0 - x^0)G^<(x,y) \tag{3.27}$$

$$G^{--} = G^{\overline{T}}(x,y) = -\mathrm{i} \langle \overline{T}\psi_-(x)\psi_-^\dagger(y) \rangle_{\rho_0} = \theta(y^0 - x^0)G^>(x,y) + \theta(x^0 - y^0)G^<(x,y) \tag{3.28}$$

The step function $\theta(t - t')$ is defined as

$$\theta(t - t') = \begin{cases} t - t' \geq 0: & 1 \\ t - t' < 0: & 0 \end{cases} \tag{3.29}$$

Although this definition is standard, its equal time point $t = t'$ is special. There are some subtleties for the equal time cases of Keldysh Green's functions, and thus is better to be treated carefully. The four elements of the Green's function are not independent

$$G^T(x,y) + G^{\overline{T}}(x,y) - G^>(x,y) - G^<(x,y) = 0 \tag{3.30}$$

Note that in the above $x^0 \neq y^0$ is assumed. To be directly related to the physical observables, we have real-time Green's functions [25]

$$G^R(x,y) = \frac{1}{2}\left(G^T - G^{\overline{T}} + G^> - G^<\right) = \theta(x^0 - y^0)\left(G^> - G^<\right) \tag{3.31}$$

$$G^A(x,y) = \frac{1}{2}\left(G^T - G^{\overline{T}} - G^> + G^<\right) = \theta(y^0 - x^0)\left(G^< - G^>\right) \tag{3.32}$$

$$G^K(x,y) = \frac{1}{2}\left(G^T + G^{\overline{T}} + G^> + G^<\right) = G^> + G^<, \quad \text{for} \quad x^0 \neq y^0 \tag{3.33}$$

Note that [25], although $G^{R/A}(t,t) \neq 0$, whenever without multiplied by the distribution function, the retarded and advanced Green's function at equal time should appear as a summation $G^R(t,t)+G^A(t,t)$. Since $G^R(t,t) + G^A(t,t) = 0$, it gives a "$\theta(0) = 0$" regularization. On the other hand, the equal time subtraction of the retarded and advanced Green's functions identically give $G^R(t,t) - G^A(t,t) = -\mathrm{i}$, which is resulting from the normalization. Moreover it is straightforward to see $G^>(t,t) = \mathrm{i}/2 = -G^<(t,t)$.

We can also define the fermionic spectral propagator $A(x,y)$ and the statistical propagator $F(x,y)$ [33] through the anticommutator of the fields and the commutator of the fields[3]

$$A(x,y) = \langle\{\psi(x), \psi^\dagger(y)\}\rangle, \quad F(x,y) = -\frac{\mathrm{i}}{2}\langle[\psi(x), \psi^\dagger(y)]\rangle \tag{3.35}$$

Note that here the definition is different from [58] by a factor "$-\mathrm{i}$", this is because of the "$-\mathrm{i}$" convention used here for Green's functions. Clearly the contour Green's functions can be decomposed by the statistical and spectral propagator [33, 58]

$$\begin{aligned} G_C(x,y) &= -\mathrm{i}\,\langle \hat{T}_C \psi(x)\psi^\dagger(y)\rangle = \theta_C(x^0 - y^0)G^>(x,y) + \theta_C(y^0 - x^0)G^<(x,y) \\ &= F(x,y) - \frac{\mathrm{i}}{2}A(x,y)\,\mathrm{sgn}_C\left(x^0 - y^0\right) \end{aligned} \tag{3.36}$$

Similarly, for the 1-PI irreducible 2-point function

$$\Sigma_C = \Sigma_{(F)}(x,y) - \frac{\mathrm{i}}{2}\Sigma_{(A)}(x,y)\,\mathrm{sgn}_C\left(x^0 - y^0\right) \tag{3.37}$$

Here the contour sign sgn_C is defined as

$$\mathrm{sgn}_C(x^0 - y^0) = \theta_C(x^0 - y^0) - \theta_C(y^0 - x^0) \tag{3.38}$$

[3] Bosonic cases are

$$A^{(\mathrm{boson})}(x,y) = \langle[\varphi(x), \varphi(y)]\rangle\,, \quad F^{(\mathrm{boson})}(x,y) = -\frac{\mathrm{i}}{2}\,\langle\{\varphi(x), \varphi(y)\}\rangle \tag{3.34}$$

The proof is simple, just rewrite $\langle\varphi_a(x)\varphi_b(y)\rangle\,\theta_C(x^0 - y^0) + \langle\varphi_b(y)\varphi_a(x)\rangle\,\theta_C(y^0 - x^0)$ by the use of $\varphi(x)\varphi(y) = \frac{1}{2}[\varphi(x), \varphi(y)] + \frac{1}{2}\{\varphi(x), \varphi(y)\}$.

The contour step function has the explicit form[4]

$$\theta_C(x^0 - y^0) = \begin{cases} x^0 \in +, y^0 \in + : & \theta(x^0 - y^0) \\ x^0 \in -, y^0 \in - : & \theta(y^0 - x^0) \\ x^0 \in +, y^0 \in - : & 1 \\ x^0 \in -, y^0 \in + : & 0 \end{cases} \tag{3.39}$$

Where the step function θ is defined in (3.29).

With the above definitions, we can rewrite the contour Green's functions by the spectral and statistical components [33, 58]

$$G^{++} = G^T(t,t') = F(x,y) - \frac{\mathrm{i}}{2}A(x,y)\,\mathrm{sgn}\left(x^0 - y^0\right) \tag{3.40}$$

$$G^{+-} = G^<(t,t') = F(x,y) + \frac{\mathrm{i}}{2}A(x,y) \tag{3.41}$$

$$G^{-+} = G^>(t,t') = F(x,y) - \frac{\mathrm{i}}{2}A(x,y) \tag{3.42}$$

$$G^{--} = G^{\widetilde{T}}(t,t') = F(x,y) + \frac{\mathrm{i}}{2}A(x,y)\,\mathrm{sgn}\left(x^0 - y^0\right) \tag{3.43}$$

The sgn function is defined as

$$\mathrm{sgn}(x^0 - y^0) = \theta(x^0 - y^0) - \theta(y^0 - x^0) \tag{3.44}$$

The spectral correlation function $A(x,y)$ and statistical correlation function $F(x,y)$ for fermions [29, 33] can be written alternatively by

$$A(x,y) = 2\left\langle \psi_{[-}\psi^\dagger_{+]}\right\rangle = \mathrm{i}(G^> - G^<)(x,y) = \mathrm{i}(G^R - G^A) \tag{3.45}$$

$$F(x,y) = -\mathrm{i}\left\langle \psi_{(-}\psi^\dagger_{+)}\right\rangle = \frac{1}{2}(G^> + G^<)(x,y) = \frac{1}{2}G^K \tag{3.46}$$

With the help of the short-hand notation $a_{[+}b_{-]} = \frac{1}{2}(a_+b_- - a_-b_+)$ and $a_{(+}b_{-)} = \frac{1}{2}(a_+b_- + a_-b_+)$. Note, under our definition the free spectral function in the momentum space is $A(\omega, \boldsymbol{k}) = 2\pi\delta(\omega - \epsilon_{\boldsymbol{k}})$, with the quasi-particle dispersion $\epsilon_{\boldsymbol{k}}$. Also from the above identities we can conclude[5]

$$G^< = \frac{1}{2}(G^K - G^R + G^A) \tag{3.47}$$

$$G^> = \frac{1}{2}(G^K + G^R - G^A) \tag{3.48}$$

Since one can always parametrize [25, 29] an anti-Hermitian matrix by a upper block triangular, a Hermitian matrix and a lower triangular matrix, the Keldysh Green's function can be decomposed into

$$G^K = G^R \circ h - h \circ G^A \tag{3.49}$$

[4] In a more compact way [81], assume that the contour time t is parametrized through a monotonically increasing τ through the parametrization $t = z(\tau)$, then $\theta_C(t - t') = \theta(\tau - \tau')$. The contour delta function is then $\delta_C(t - t') = (\frac{\partial z}{\partial \tau})^{-1}\delta(\tau - \tau')$.

[5] No confusion for A on advanced G^A and the spectral function $A(x,y)$.

The $h(t,t')$ is a two-time function. For fermions in equilibrium[6], the so-called fluctuation-dissipation theorem (FDT) applies. The Keldysh Green's function has the explicit form

$$G^K = h(\omega)(G^R - G^A) \tag{3.50}$$

Or equivalently

$$F(\omega) = \frac{\mathrm{i}}{2} h(\omega) A(\omega) \tag{3.51}$$

Where $h(\omega) \equiv \left(1 - 2n_{\mathrm{FD}}(\omega)\right) = \left(1 - \frac{2}{e^{-\beta\omega}+1}\right) = \tanh\left(\frac{\beta\omega}{2}\right)$. Equation (3.51) is called the fluctuation-dissipation theorem (FDT) and can be related to an equilibrium symmetry of the field that is called the Kubo-Martin-Schwinger (KMS) symmetry. Since KMS symmetry is a fundamental symmetry of the equilibrium, it will be further explained in the KMS section.

There are different ways to define a time-dependent effective distribution function. One simple choice is that $n = (1-h)/2$ can be defined through h

$$n(t,t') \equiv \frac{1 - h(t,t')}{2} = \frac{1}{2} - \frac{F(t,t')}{\mathrm{i}A(t,t')} \tag{3.52}$$

Or through parametrization (3.49). The n can be equivalently defined as

$$n(t,t') \equiv \mathrm{i}\frac{G^<(t,t')}{A(t,t')} \tag{3.53}$$

For convenience, we can also define the spectral broadening [29]

$$\Gamma = \mathrm{i}(\Sigma^R - \Sigma^A) = \Sigma_{(A)} \tag{3.54}$$

where $\Sigma = G_0 - G$. Note that Σ^A is the advanced self-energy, and $\Sigma_{(A)}$ is the spectral self-energy.

3.3 Keldysh functional integral

A functional integral[7] can be written down for the Schwinger-Keldysh contour in a straightforward way. Note that now the fields are doubled, and there is a relative minus sign between the upper and lower contour actions. For instance, for scalar (real) bosonic fields we have

$$S = S_+[\varphi_+] - S_-[\varphi_-] = S[\varphi_{\mathrm{cl}}, \varphi_{\mathrm{q}}] \tag{3.55}$$

And for complex fermionic fields we have

$$S = S_+[\psi_+, \bar{\psi}_+] - S_-[\psi_-, \bar{\psi}_-] = S[\psi_1, \psi_2, \bar{\psi}_1, \bar{\psi}_2] \tag{3.56}$$

The functional integral is now the integration of all field configurations that are weighted by the $e^{\mathrm{i}S}$,

[6] And equivalently [59] $G^>(\omega) = \mathrm{i}[1 - n_{\mathrm{FD}}(\omega)]A(\omega)$, and in equilibrium $G^<(\omega) = -\mathrm{i}n_{\mathrm{FD}}(\omega)A(\omega)$. Here $G^<(\omega) = -e^{-\beta\omega}G^>(\omega)$

[7] A detailed introduction can be found in the book [25]

for instance, the fermionic field, we have

$$Z = \int \mathrm{d}[\psi_1, \psi_2, \bar{\psi}_1, \bar{\psi}_2] e^{\mathrm{i}S} \tag{3.57}$$

Details about the generating functional with the path-integral form can be found in [25, 33, 81–83, 88].

We can write the action into the free part and the interacting part as

$$Z = \int \mathrm{d}[\hat{\phi}] e^{\mathrm{i}S} = \int \mathrm{d}[\hat{\phi}] e^{\mathrm{i}(S_0 + S_{\mathrm{int}})} \tag{3.58}$$

Clearly the standard perturbation theory [34] can be applied. The perturbation theory, as well as Wick's theorem, are formally unchanged, except that additional indices should be included.

For open systems, the Keldysh functional integral method works equally well, for a review see [88], where a Lindblad master equation is translated into the Keldysh field-theoretical language.

3.4 Diagrammatics and perturbation theory on CTP

Bosonic	Fermionic
$L = \frac{1}{\sqrt{2}}\left(\tau^0 - i\tau^2\right)$	$L = \frac{1}{\sqrt{2}}\left(\tau^0 - i\tau^2\right)$
$\begin{pmatrix}\varphi_{\mathrm{cl}}\\ \varphi_{\mathrm{q}}\end{pmatrix} = L\tau^3 \begin{pmatrix}\varphi_+\\ \varphi_-\end{pmatrix}$	$\begin{pmatrix}\psi_1\\ \psi_2\end{pmatrix} = L\tau^3 \begin{pmatrix}\psi_+\\ \psi_-\end{pmatrix}$
$\left(\bar{\varphi}_{\mathrm{cl}}, \bar{\varphi}_{\mathrm{q}}\right) = \left(\bar{\varphi}_+, \bar{\varphi}_-\right)\left(L\tau^3\right)^\dagger$	$\left(\bar{\psi}_1, \bar{\psi}_2\right) = \left(\bar{\psi}_+, \bar{\psi}_-\right) L^\dagger$
$\hat{D} \equiv \begin{pmatrix}\hat{D}_{++} & \hat{D}_{+-}\\ \hat{D}_{-+} & \hat{D}_{--}\end{pmatrix}$	$\hat{G} \equiv \begin{pmatrix}\hat{G}_{++} & \hat{G}_{+-}\\ \hat{G}_{-+} & \hat{G}_{--}\end{pmatrix}$
$D = \begin{pmatrix}D^K & D^A\\ D^R & 0\end{pmatrix} = -\mathrm{i}\begin{pmatrix}\langle\varphi_{\mathrm{cl}}\bar{\varphi}_{\mathrm{cl}}\rangle & \langle\varphi_{\mathrm{cl}}\bar{\varphi}_{\mathrm{q}}\rangle\\ \langle\varphi_{\mathrm{q}}\bar{\varphi}_{\mathrm{cl}}\rangle & \langle\varphi_{\mathrm{q}}\bar{\varphi}_{\mathrm{q}}\rangle\end{pmatrix}$	$G = \begin{pmatrix}G^R & G^K\\ 0 & G^A\end{pmatrix} = -\mathrm{i}\begin{pmatrix}\langle\psi_1\bar{\psi}_1\rangle & \langle\psi_1\bar{\psi}_2\rangle\\ \langle\psi_2\bar{\psi}_1\rangle & \langle\psi_2\bar{\psi}_2\rangle\end{pmatrix}$
$D = L\tau^3\hat{D}(L\tau^3)^\dagger$	$G = L\tau^3\hat{G}L^\dagger$
$D^{-1} = \begin{pmatrix}0 & [D^{-1}]^A\\ [D^{-1}]^R & [D^{-1}]^K\end{pmatrix}$	$G^{-1} = \begin{pmatrix}[G^R]^{-1} & [G^{-1}]^K\\ 0 & [G^K]^{-1}\end{pmatrix}$

Table 3.1: The usual conventions of the field rotation to real time fields. Where τ^i are Pauli matrices, $\tau^0_{ab} = \delta_{ab}$. See also [25]. Note that the fermionic convention can be chosen to be the same as the bosonic ones. Here we follow the conventions in [25].

In this section, we present several examples of the Keldysh perturbation theory. Roughly speaking

it is simply to replace vertices of the Feynman rules by tensor vertices, and the propagators by matrix propagators [25, 29].

For bosonic fields we define

$$\varphi_{\mathrm{cl}}(t) = \frac{1}{\sqrt{2}}\left(\varphi_+(t) + \varphi_-(t)\right), \quad \varphi_{\mathrm{q}}(t) = \frac{1}{\sqrt{2}}\left(\varphi_+(t) - \varphi_-(t)\right) \tag{3.59}$$

Where the φ_{cl} is the "average", or symmetric summation of the $\varphi_\pm$ and the φ_{q} is the "relative", or anti-symmetric summation of the $\varphi_\pm$.

For fermionic fields, the conventions are usually different, where we have

$$\psi_1(t) = \frac{1}{\sqrt{2}}\left(\psi_+(t) + \psi_-(t)\right), \quad \psi_2(t) = \frac{1}{\sqrt{2}}\left(\psi_+(t) - \psi_-(t)\right) \tag{3.60}$$

$$\bar{\psi}_1(t) = \frac{1}{\sqrt{2}}\left(\bar{\psi}_+(t) - \bar{\psi}_-(t)\right), \quad \bar{\psi}_2(t) = \frac{1}{\sqrt{2}}\left(\bar{\psi}_+(t) + \bar{\psi}_-(t)\right) \tag{3.61}$$

These definitions are allowed since the fermionic fields $\bar{\psi}$ and ψ are independent fields rather than complex conjugates of each other. This convention has the advantage that it simplifies the 2-point function matrices to upper triangular matrices. As we know the inverse of the upper triangular matrices are again upper triangular, many equations will become simpler.

We will call $\psi_{1/2}$ or φ_{cl} and φ_{q} are in the real-time representation, and we will call the fields with $+/-$ in the contour time representation. We summarize the contour-time and real-time conventions of the bosonic and fermionic fields in Table 3.1.

Now, we give some specific examples where the tensor vertices are derived. We can first consider a scalar-fermion (Yukawa) interaction, the Keldysh action is then simply $S_+ - S_-$ and

$$S_{\mathrm{int}} = \int_x (g^+\varphi^+\bar{\psi}^+\psi^+ - g^-\varphi^-\bar{\psi}^-\psi^-) \tag{3.62}$$

For simplicity, we choose $\varphi = \bar{\varphi}$. Microscopically we have $g^+ = g^-$ thus

$$S_{\mathrm{int}} = \int_x (g\varphi^+\bar{\psi}^+\psi^+ - g\varphi^-\bar{\psi}^-\psi^-) \tag{3.63}$$

One can then define the tensor vertices (for the fermion-boson interaction) as [89]

$$\gamma^+_{jk} = \begin{pmatrix} 1 & 0 \\ 0 & 0 \end{pmatrix} = +\frac{1}{2}(\tau^0 + \tau^3)_{jk}, \quad \gamma^-_{jk} = \begin{pmatrix} 0 & 0 \\ 0 & -1 \end{pmatrix} = -\frac{1}{2}(\tau^0 - \tau^3)_{jk} \tag{3.64}$$

This is also equivalent to mark each vertex with the contour label $+/-$ and give it a corresponding sign. We can write the above labeling in a compact form

$$S_{\mathrm{int}} = \int_x \gamma^i_{jk} g \varphi^i \bar{\psi}^j \psi^k \tag{3.65}$$

On the other hand. For the real-time basis, we have

$$\varphi_+ = \frac{1}{\sqrt{2}}(\varphi_{\rm cl} + \varphi_{\rm q}), \quad \varphi_- = \frac{1}{\sqrt{2}}(\varphi_{\rm cl} - \varphi_{\rm q}) \tag{3.66}$$

$$\psi_+ = \frac{1}{\sqrt{2}}(\psi_1 + \psi_2), \quad \psi_- = \frac{1}{\sqrt{2}}(\psi_1 - \psi_2) \tag{3.67}$$

$$\bar{\psi}_+ = \frac{1}{\sqrt{2}}(\bar{\psi}_1 + \bar{\psi}_2), \quad \bar{\psi}_- = \frac{1}{\sqrt{2}}(\bar{\psi}_2 - \bar{\psi}_1) \tag{3.68}$$

after some algebra, the interacting part of the action reads

$$S_{\rm int} = \int_x \frac{g}{\sqrt{2}}\varphi^{\rm cl}\left(\bar{\psi}_1\psi_1 + \bar{\psi}_1\psi_1\right) + \frac{g}{\sqrt{2}}\varphi^{\rm q}\left(\bar{\psi}_1\psi_2 + \bar{\psi}_2\psi_1\right) \tag{3.69}$$

Now we can define the tensor vertices [25] of the basis (ψ_1, ψ_2). They are

$$\gamma^{\rm cl} \equiv \frac{1}{\sqrt{2}}\begin{pmatrix}1 & 0\\ 0 & 1\end{pmatrix} = \frac{1}{\sqrt{2}}\tau^0, \quad \gamma^{\rm q} \equiv \frac{1}{\sqrt{2}}\begin{pmatrix}0 & 1\\ 1 & 0\end{pmatrix} = \frac{1}{\sqrt{2}}\tau^1 \tag{3.70}$$

Again τ^i are the Pauli matrices act in the Keldysh space [25]. From this we can put the interacting part into a compact form

$$S_{\rm int} = \int_x g\gamma^\alpha_{ab}\varphi^\alpha\bar{\psi}_a\psi_b \tag{3.71}$$

where the same indices are summed. $\alpha \in \{{\rm cl}, {\rm q}\}$ and $a, b \in \{1, 2\}$.

For a example, now we consider the second order expansion of $e^{{\rm i}S_{\rm int}}$ in coupling g. We also do contractions for the propagator of φ

$$\frac{{\rm i}^2}{2}g^2\int_{x,x'}\gamma^\alpha_{ab}\varphi^\alpha\bar{\psi}_a\psi_b\gamma^\beta_{cd}\varphi^\beta\bar{\psi}_c\psi_d \tag{3.72}$$

this gives

$$-\frac{1}{2}g^2\int_{x,x'}\varphi^\alpha(x)\left(\gamma^\alpha_{ab}G_{da}(x',x)G_{bc}(x,x')\gamma^\beta_{cd}\right)\varphi^\beta(x') \tag{3.73}$$

which is a fermionic loop.

Another example is the tree level contraction

$$\frac{{\rm i}^2}{2}g^2\int_{x,x'}\gamma^\alpha_{ab}\varphi^\alpha\bar{\psi}_a\psi_b\gamma^\beta_{cd}\varphi^\beta\bar{\psi}_c\psi_d \tag{3.74}$$

which gives us

$$-\frac{\rm i}{2}g^2\int_{x,x'}\bar{\psi}_a(x)\psi_b(x)\left(\gamma^\alpha_{ab}D^{\alpha\beta}(x,x')\gamma^\beta_{cd}\right)\bar{\psi}_c(x')\psi_d(x') \tag{3.75}$$

The above diagram becomes especially simple if the bosonic propagator $D(x, y)$ is in a contact pair interaction form, i.e., it is local in space and time, and it satisfies the FDT. We can assume $D^R = D^A$

in energy and momentum space[8] and write

$$D(\omega,\boldsymbol{p})=\begin{pmatrix}D^K(\omega,\boldsymbol{p}) & D^R(\omega,\boldsymbol{p})\\ D^A(\omega,\boldsymbol{p}) & 0\end{pmatrix}=u_0\begin{pmatrix}0 & 1\\ 1 & 0\end{pmatrix} \tag{3.76}$$

Note that in momentum space, the FDT implies $D^K \sim (D^R - D^A)$. Transform back to the space-time, we have

$$D(x,y)=\begin{pmatrix}D^K & D^R\\ D^A & 0\end{pmatrix}=u_0\delta_{xy}\begin{pmatrix}0 & 1\\ 1 & 0\end{pmatrix}=u_0\delta_{xy}\tau^1 \tag{3.77}$$

Using $D(x,y)$ in (3.77) we can compute the contact tensor vertex ν_{abcd}

$$u_0\delta_{xy}\nu_{abcd}=u_0\gamma^\alpha_{ab}D^{\alpha\beta}(x,x')\gamma^\beta_{cd}=u_0\delta_{xy}\gamma^\alpha_{ab}\tau^{1,\alpha\beta}\gamma^\beta_{cd} \tag{3.78}$$

Where after the contraction, it is

$$\nu_{abcd}=\frac{1}{2}(\tau^0\otimes\tau^1+\tau^1\otimes\tau^0)_{abcd}=\frac{1}{2}(\tau^0_{ab}\tau^1_{cd}+\tau^1_{ab}\tau^0_{cd}) \tag{3.79}$$

With ν_{abcd} the tree graph (3.75) becomes

$$S_{4,\text{int}}=\mathrm{i}\int_x -\frac{u_0 g^2}{2}\bar\psi_a(x)\psi_b(x)\nu_{abcd}\bar\psi_c(x)\psi_d(x) \tag{3.80}$$

Obviously it gives a four-fermion interaction action.

The normal ordered version of (3.80) with the generic coupling U_0 reads

$$S_{4,\text{int}}=\mathrm{i}\int_x -U_0\nu_{abcd}\bar\psi_a(x)\bar\psi_c(x)\psi_b(x)\psi_d(x) \tag{3.81}$$

where if $U_0>0$ it gives a repulsive interaction. We defined

$$U_0\equiv\frac{u_0 g^2}{2} \tag{3.82}$$

For the $+/-$ basis, we can do the same procedures. Note that the contraction needed now is

$$\gamma^i_{jk}\hat D^{ii'}\gamma^{i'}_{j'k'} \tag{3.83}$$

If we use $D=L\tau^3\hat D(L\tau^3)^\dagger$, for the contact interaction the bosonic propagator $\hat D$ in $+,-$ basis reads

$$\hat D(x,y)=\begin{pmatrix}D^{++} & D^{+-}\\ D^{-+} & D^{--}\end{pmatrix}_{xy}=u_0\delta_{xy}\begin{pmatrix}1 & 0\\ 0 & -1\end{pmatrix}=u_0\delta_{xy}\tau^3 \tag{3.84}$$

[8] Although this is not entirely consistent with the causal structure.

The vertex γ^i_{jk} in the contact interaction case gives

$$\nu_{ijkl} = \frac{1}{2}(\tau^0 \otimes \tau^3 + \tau^3 \otimes \tau^0)_{ijkl} = \frac{1}{2}(\tau^0_{ij}\tau^3_{kl} + \tau^3_{ij}\tau^0_{kl}) \tag{3.85}$$

This vertex is especially simple, since it is diagonal for all its containing matrices.

As a last example, let us consider a typical self-energy diagram at the second order in U_0

$$\Sigma_{ll'}(x,x') = U_0\nu_{ijkl}G_{ii'}(x,x')G_{jj'}(x,x')G_{k'k}(x',x)U_0\nu_{i'j'k'l'} \tag{3.86}$$

This can be directly read off from a Feynman diagram using the defined tensor vertex and propagators in the Schwinger-Keldysh space. The tensor contractions will produce many terms, in the real-time $1,2$ basis, this may need some algebra. The $+,-$ basis gives a simple result, the tensor contraction machinery can be done with the help of the computer algebra system[9], the final result is

$$\hat{\Sigma}(x,x') = U_0^2\begin{pmatrix} G^T(x,x')G^T(x,x')G^T(x',x) & -G^<(x,x')G^<(x,x')G^>(x',x) \\ -G^>(x,x')G^>(x,x')G^<(x',x) & G^{\overline{T}}(x,x')G^{\overline{T}}(x,x')G^{\overline{T}}(x',x) \end{pmatrix} \tag{3.87}$$

Note the minus signs form the contractions with τ^3.

Diagrammatics can also be done by marking the vertex with $+$ or $-$. If we consider $\Sigma^< = \Sigma^{+-}$, it is simply

$$\Sigma^< = -U_0^2 G^{+-}G^{+-}G^{-+} = -U_0^2 G^< G^< G^> \tag{3.88}$$

And $\Sigma^> = \Sigma^{-+}$ gives

$$\Sigma^> = -U_0^2 G^{-+}G^{-+}G^{+-} = -U_0^2 G^> G^> G^< \tag{3.89}$$

These are related to the collision processes and to the collision integral of the quantum Boltzmann equations, which we will see in the upcoming sections.

If we have space and time translational invariance, we can Fourier transform the self-energy into energy momentum space and the product becomes convolutions

$$\Sigma^{</>}(p) = -U_0^2(G^{</>}_q \circ G^{>/<}_{-q'} \circ G^{</>}_k)(p) \tag{3.90}$$

Note that the last two Green's functions have been switched to make the product more symmetric.

3.5 Dyson-Schwinger equations on CTP

We can apply Keldysh techniques to the Dyson-Schwinger equations. In this section, we consider fermionic fields and the two-point function. The equations for the bosonic fields will be almost the same. The difference will be in the form of the free dispersion, the signs, and the vacuum expectation value of microscopic fields.

The relation between the functional derivatives of the 1-PI effective action $\Gamma[\psi_1,\psi_2,\bar{\psi}_1,\bar{\psi}_2]$ and the Schwinger functional $W[J_{\psi_1},J_{\psi_2},J_{\bar{\psi}_1},J_{\bar{\psi}_2}]$ can be written in the usual way

$$[G^{-1}]_{ab}(xy) = \Gamma^{(2)}_{ab}(x,y) = [(W^{(2)})^{-1}]_{ab}(x,y) = [G_0^{-1}]_{ab}(x,y) - \Sigma_{ab}(x,y) \tag{3.91}$$

[9] For example, the Mathematica.

although the physical meaning of the source is extended to contain the dynamical statistical properties. Note this identity is also called Dyson equation.

Here for convenience we introduce a short hand notation for generalized convolutions

$$[f \circ g](x, y) \equiv \int_z f(x, z) g(z, y) \tag{3.92}$$

where for real time we have $\int_z = \int_{t\in(-\infty,\infty)} \int_{\boldsymbol{x}}$. The left and right Dyson equations can be written as

$$\left([G^{-1}]_{ab} \circ G_{bc}\right)(x, z) = \delta_{ac}\delta_{xz} \tag{3.93}$$

$$\left(G_{ab} \circ [G^{-1}]_{bc}\right)(x, z) = \delta_{ac}\delta_{xz} \tag{3.94}$$

Now one can write those matrix equations into components. Consider the left Dyson equation, we can first choose the diagonal elements $\left([G^{-1}]_{11} \circ G_{11} + [G^{-1}]_{12} \circ G_{21}\right)(x, z) = \delta_{11}\delta_{xz}$. Use $G_{21}(x, y) = 0$ and match the label, where

$$\left([G^{-1}]^R \circ G^R\right)(x, z) = \delta_{xz} \tag{3.95}$$

Equivalently we can find $\left([G^{-1}]_{21} \circ G_{11} + [G^{-1}]_{22} \circ G_{22}\right)(x, z) = \delta_{22}\delta_{xz}$ gives $\left([G^{-1}]^A \circ G^A\right)(x, z) = \delta_{xz}$.

The Keldysh component of the Dyson equation follows $[G^{-1}]_{11} \circ G_{12} + [G^{-1}]_{12} \circ G_{22} = 0$. Note that for finite Σ^K, $[G_0^{-1}]^K$ can be neglected[10], which gives us

$$[G^{-1}]^R \circ G^K \circ [G^{-1}]^A = \Sigma^K \tag{3.97}$$

This equation is also usually called the Keldysh equation.

Several different but equivalent forms of the Dyson equation appear in the literature. Although their derivations are, in principle, straightforward, we still compute the differential equations of $G^>(x, y)$ and $G^<(x, y)$ here for clarity.

Starting with (3.95). We can write $[G^{-1}] = [G_0^{-1}] - \Sigma$, then we have the equation

$$[G_0^{-1}]^{R/A} \circ G^{R/A} = \Sigma^{R/A} \circ G^{R/A} + \delta \tag{3.98}$$

Subtract $G^{R/A}$ equations and use $[G_0^{-1}]^R = [G_0^{-1}]^A = G_0^{-1}$ in the time space yields

$$G_0^{-1} \circ (G^R - G^A) = \Sigma^R \circ G^R - \Sigma^A \circ G^A \tag{3.99}$$

[10] This can be seen by direct computation

$$\begin{aligned}(G_0^{-1})^K &= -[G_0^{-1}]^R \circ G_0^K \circ [G_0^{-1}]^A = -[G_0^{-1}]^R \circ (G_0^R \circ h - h \circ G_0^A) \circ [G_0^{-1}]^A \\ &= -(h \circ [G_0^{-1}]^A - [G_0^{-1}]^R \circ h) \\ &= -([G_0^{-1}]^A - [G_0^{-1}]^R) \circ h \sim \mathrm{i}0^+ h\end{aligned} \tag{3.96}$$

Here in last steps we used the $[G_0^{-1}]^A \circ h = h \circ [G_0^{-1}]^A$ for the free Green's functions.

Here G_0^{-1} should be understood as $[G_0^{-1}]^{R/A}$ without the regulator. Similarly for the Keldysh component

$$G_0^{-1} \circ G^K = \Sigma^R \circ G^K + \Sigma^K \circ G^A \tag{3.100}$$

The above two equations are differential equations that are derived from the Dyson equation (3.93). We can also write them using $G^<$ and $G^>$. The key identities that we need are

$$G^> - G^< = G^R - G^A, \quad G^K = G^> + G^< \tag{3.101}$$

and similar relations for Σ. They are equivalent to $G^R + G^K = 2G^> + G^A$ and $\Sigma^K - G^A = 2\Sigma^> - \Sigma^R$. Inserting (3.101) into the summation of (3.99) and (3.100), we have

$$G_0^{-1} \circ G^> = \Sigma^R \circ G^> - \Sigma^> \circ G^A \tag{3.102}$$

One can see that the above equation is an equation of motion of $G^>$. For the equation of $G^<$, we can subtract (3.99) and (3.100), then apply (3.101), which will give us

$$G_0^{-1} \circ G^< = \Sigma^R \circ G^< - \Sigma^< \circ G^A \tag{3.103}$$

Same for the equation with $(<\!\!\rightarrow\!\!>)$.

On the other hand, the right Dyson equation can give two more equations, which we will only give the results, they are

$$G^{>/<} \circ G_0^{-1} = G^R \circ \Sigma^{>/<} - G^{>/<} \circ \Sigma^A \tag{3.104}$$

We can see that they agree with the well known Langreth rules, for Langreth rules see [63]. Now use that in the time domain the inverse of the bare Green's function reads

$$G_0^{-1}(x, y) = [\mathrm{i}\partial_{x^0} - H_0(x^0, \boldsymbol{x}, \boldsymbol{y})]\delta_{x^0 y^0} \tag{3.105}$$

Here $H_0(x_0, \boldsymbol{x}, \boldsymbol{y})$ is the non-interacting part of the Hamiltonian which we assumed to have a single time dependence and can be nonlocal in space. With G_0^{-1} we can write down the final equations of this section, the Kadanoff-Baym equations

$$\begin{aligned} \mathrm{i}\partial_{x^0} G^{>/<}(x, y) - \int_{\boldsymbol{r}} H_0(x^0, \boldsymbol{x}, \boldsymbol{r}) G^{>/<}(x^0, \boldsymbol{r}|y) &= [\Sigma^R \circ G^{>/<} - \Sigma^{>/<} \circ G^A](x, y) \\ \mathrm{i}\partial_{y^0} G^{>/<}(x, y) - \int_{\boldsymbol{r}} G^{>/<}(x|y^0, \boldsymbol{r}) H_0(y^0, \boldsymbol{r}, \boldsymbol{y}) &= [G^R \circ \Sigma^{>/<} - G^{>/<} \circ \Sigma^A](x, y) \end{aligned} \tag{3.106}$$

These four equations are the Dyson(-Schwinger) equations on the CTP. Usually its applications are combined with the conserving approximation of the self-energies. Those sets of integro-differential equations give the quantum equations of motions of the two-point functions that are suitable for non-equilibrium dynamics and are usually called Kadanoff-Baym equations. Those equations also have a long history back to the 1960s, and many applications [3, 58] in the real time evolution of the quantum systems.

An interesting recent application of the Kadanoff-Baym equations is in the Sachdev-Kitaev-Ye (SYK) model [90]. The SYK model is a quantum mechanical model of all-to-all random interacting Majorana fermions. It can be treated in a large N dynamical mean-field approximation where its 2-point and 4-point functions are analytical soluble. This model saturates the Lyapunov exponent, the

classical bound of chaos. As an almost minimal model of quantum chaos, it has a gravity dual, or specially AdS/CFT, which is pointed out by Kitaev. The Sachdev-Kitaev-Ye (SYK) model is intensively studied since 2015. In that case, the $G^>$ and $G^<$ obeys a special relation for Majorana fermions (real fermions $\psi^\dagger = \psi$), reads $G^>(t_1, t_2) = -G^<(t_2, t_1)$, the particle-hole symmetry which makes the Dyson-Schwinger/Kadanoff-Baym equation simpler to solve. The KMS or the above relation between $G^>$ and $G^<$ are not general properties of all quantum dynamical systems.

From the above derivations, one can expect that the higher Dyson-Schwinger equations or effective actions can be translated to CTP language straightforwardly.

The higher Dyson-Schwinger equations, especially the relations between the n-point and $(n \pm 1)$-point can be derived in the same way, and won't be present here. Moreover, the 2-PI effective actions and the functional renormalization group can be generalized to the Schwinger-Keldysh contour. namely CTP. The 2-particle-irreducible functional renormalization group on CTP can be found in references [91, 92].

3.6 Kinetic equation, Boltzmann equation, and collision integral

In this section, we will review the derivation of the (quantum) Boltzmann equation, follow [25]. It is a good example to show the physical meaning of the Keldysh method, and the Kadanoff-Baym equations.

The (collisionless) classical Boltzmann equation can be written in the form

$$\mathrm{d}_t n = \frac{\mathrm{d}n(\boldsymbol{x}, \boldsymbol{v}, t)}{\mathrm{d}t} = \left(\frac{\mathrm{d}n}{\mathrm{d}\boldsymbol{x}}\boldsymbol{v} + \frac{\mathrm{d}n}{\mathrm{d}\boldsymbol{v}}\dot{\boldsymbol{v}} + \frac{\partial n}{\partial t}\right) = 0 \tag{3.107}$$

where n is the distribution function of the particles. This can be regarded as a result from the total derivative

$$n(\boldsymbol{x} + \boldsymbol{v}\mathrm{d}t, \boldsymbol{v} + \dot{\boldsymbol{v}}\mathrm{d}t, t + \mathrm{d}t) - n(\boldsymbol{x}, \boldsymbol{v}, t) = 0 \tag{3.108}$$

and the assumption that n is only explicitly depending on the position x, the velocity vector v and the time t, where $n = n(t, \boldsymbol{x}, \boldsymbol{v})$, and $\boldsymbol{v} \equiv \dot{\boldsymbol{x}}$.

The quantum manybody version of the Boltzmann equation, the quantum Boltzmann equation, can be derived from the Keldysh method directly, and has a similar form

$$\hat{\mathrm{d}}_t[n] = I_{\mathrm{col}}[n] \tag{3.109}$$

where n is the distribution function of the quasiparticles, and $I_{\mathrm{col}}[n]$ is called the collision integral. The operator $\hat{\mathrm{d}}_t$ is similar to d_t, we will define it later in this section.

For clarity, in this section, I will write out the space-time variables and use indices to denote Keldysh indices, other indices are suppressed. Again define the short-hand notation for generalized convolution $[f \circ g](x, y) = \int_z f(x, z)g(z, y)$. This section closely follows the book [25].

To obtain the equations of effective distributions, one can use the parametrization of the Keldysh component of the Green's function $G^K = G^R \circ h - h \circ G^A$. Recall the Keldysh part of the Dyson equation on the CTP

$$[G^{-1}]^R \circ G^K \circ [G^{-1}]^A = \Sigma^K \tag{3.110}$$

Following [25], we now apply the parametrization of G^K and $G^{R/A} = [G_0^{-1}]^{R/A} - \Sigma^{R/A}$

$$\begin{aligned}&[G^{-1}]^R \circ (G^R \circ h - h \circ G^A) \circ [G^{-1}]^A = \Sigma^K \\ \rightarrow &h \circ [G_0^{-1}]^A - [G_0^{-1}]^R \circ h = \Sigma^K + h \circ \Sigma^A - \Sigma^R \circ h\end{aligned} \tag{3.111}$$

Now it is time to choose the form of the free Green's function, one can select, as an example, a standard form of nonrelativistic particle in an external potential $V(x)$

$$[G_0^{-1}]^{R/A} = [G_0^A]^{-1}(x,y) = \delta_{xy}(\mathrm{i}\partial_t + \nabla_{\boldsymbol{x}}^2/(2m) - V(y) \pm \mathrm{i}0^+) \tag{3.112}$$

In time space one can neglect the regulators $\pm\mathrm{i}0^+$, thus the (3.111) can be written into

$$\left[\left(-\mathrm{i}\partial_t - \frac{1}{2m}\nabla_{\boldsymbol{x}}^2 + V\right)\overset{\circ}{,}h\right]_- = \Sigma^K - \left(\Sigma^R \circ h - h \circ \Sigma^A\right) \tag{3.113}$$

where $([f\overset{\circ}{,}g]_\pm)_{ab} = f_{ab} \circ g_{bc} \pm g_{ab} \circ f_{bc}$ as the commutator/anti-commutator with matrix production and convolution. Note that $h = h(x,y)$ and the commutator of the differential operator should be understood as $[\partial_t \overset{\circ}{,} h(x^0, y^0)] = (\partial_{x^0} - \partial_{y^0})h(x,y)$, similarly for $\nabla_{\boldsymbol{x}}^2$. Here t is denoting the averaged time

$$t \equiv t_{\mathrm{a}} \tag{3.114}$$

Here t_{a} is the averaged time or the "center of mass" time.

In order to make the above equation closer to the kinetic equation or the Boltzmann equation one still need to do

1. Wigner transform and gradient expansion[11]
2. Quasi-particle approximation

[11] Wigner transform (See [25] starting from p.87). Define the averaged and relative coordinates $x_{\mathrm{a}} = (x_1 + x_2)/2$ and $x_{\mathrm{r}} = x - x'$, where $x = x_{\mathrm{a}} + x_{\mathrm{r}}/2$ and $x' = x_{\mathrm{a}} - x_{\mathrm{r}}/2$. The Wigner transform (WT) and the inverse Wigner transform (IWT) are

$$\mathrm{WT}: \quad a(x_{\mathrm{a}}, p) = \int_{x_{\mathrm{r}}} \mathrm{e}^{-\mathrm{i}p\cdot x_{\mathrm{r}}} a\left(x_{\mathrm{a}} + \frac{x_{\mathrm{r}}}{2}, x_{\mathrm{a}} - \frac{x_{\mathrm{r}}}{2}\right) \tag{3.115}$$

$$\mathrm{IWT}: \quad a(x,x') = \int_p \mathrm{e}^{\mathrm{i}p\cdot(x-x')} a\left(\frac{x+x'}{2}, p\right) \tag{3.116}$$

Define $\partial_x \partial_p = \nabla_{\boldsymbol{x}} \nabla_{\boldsymbol{p}} - \partial_{x^0}\partial_{p^0}$, the convolution after the Wigner transform is

$$c = a \circ b \xrightarrow{\mathrm{WT}} c(x,p) = a(x,p)\mathrm{e}^{\frac{1}{2}\left(\overleftarrow{\partial}_x \overrightarrow{\partial}_p - \overleftarrow{\partial}_p \overrightarrow{\partial}_x\right)} b(x,p) \tag{3.117}$$

The (gradient) expansion of the above is

$$c = a \circ b \xrightarrow{\mathrm{WT}} ab + \frac{\mathrm{i}}{2}\left(\partial_x a \partial_p b - \partial_p a \partial_x b\right) + \cdots \tag{3.118}$$

$$[a\overset{\circ}{,}b]_- = a \circ b - b \circ a = \xrightarrow{\mathrm{WT}} \mathrm{i}\left(\partial_x a \partial_p b - \partial_p a \partial_x b\right) + \cdots \tag{3.119}$$

The Wigner transform of product of 2-point functions is

$$c(x,x') = a(x,x')b(x,x') \xrightarrow{\mathrm{WT}} c(x,p) = \int_q a(x, p-q)b(x,q) \tag{3.120}$$

These steps [25, 29, 33, 89] have the consequence that they

1. Separate the scale.

2. Make the distribution evolution with on shell processes only.

Now we follow [25, 29] to derive the Boltzmann equation from the Keldysh method. The discussion about the limitation of the quasi-particle approximation and the semi-classical Boltzmann equation can be found, for instance, in [33].

First, by using the Wigner transform and gradient expansion, one can get the identity for the potential

$$[V^{\circ}h] \xrightarrow{\mathrm{WT}} \mathrm{i}\partial_x V(x)\partial_p h(x,p) = \mathrm{i}\nabla_{\boldsymbol{x}} V\nabla_{\boldsymbol{p}} h - \mathrm{i}\partial_t V\partial_\epsilon h \tag{3.121}$$

For the dispersion[12]

$$\left[-\nabla_{\boldsymbol{x}}^2, h\right] \xrightarrow{\mathrm{WT}} -\mathrm{i}\nabla_{\boldsymbol{p}}\boldsymbol{p}^2\nabla_{\boldsymbol{x}} h = -2\mathrm{i}\boldsymbol{p}\nabla_{\boldsymbol{x}} h \tag{3.123}$$

For the time derivative

$$\left[-\mathrm{i}\partial_t{}^{\circ}h\right] \xrightarrow{\mathrm{WT}} -\mathrm{i}\partial_\epsilon\epsilon\partial_t h = -\mathrm{i}\partial_t h \tag{3.124}$$

And for the self-energy related terms

$$\Sigma^R \circ h - h \circ \Sigma^A \xrightarrow{\mathrm{WT}} h\left(\Sigma^{\mathrm{R}} - \Sigma^{\mathrm{A}}\right) + \mathrm{i}\partial_x\left(\mathrm{Re}\,\Sigma^R\right)\partial_p h - \mathrm{i}\partial_p\left(\mathrm{Re}\,\Sigma^R\right)\partial_x h \tag{3.125}$$

The Wigner transforms (3.121) to (3.125) can be substituted to (3.113), and give us a equation that is closed to the Boltzmann equation

$$-\mathrm{i}\partial_t h - 2\mathrm{i}\boldsymbol{p}\nabla_{\boldsymbol{x}} h + \mathrm{i}\nabla_{\boldsymbol{x}} V\nabla_{\boldsymbol{p}} h - \mathrm{i}\partial_t V\partial_\epsilon h = \Sigma^K - h\left(\Sigma^{\mathrm{R}} - \Sigma^{\mathrm{A}}\right) - \left(\mathrm{i}\partial_x(\mathrm{Re}\,\Sigma^R)\partial_p h - \mathrm{i}\partial_p(\mathrm{Re}\,\Sigma^R)\partial_x h\right) \tag{3.126}$$

To make the above equation closer to the Boltzmann form, we recall that $\partial_x\partial_p = \nabla_{\boldsymbol{x}}\nabla_{\boldsymbol{p}} - \partial_t\partial_\epsilon$ and move the derivative term from the RHS to LHS, then multiply an i on both sides

$$(1 - \partial_\epsilon \mathrm{Re}\,\Sigma^R)\partial_t h + (2\boldsymbol{p} + \nabla_{\boldsymbol{p}}\mathrm{Re}\,\Sigma^R)\nabla_{\boldsymbol{x}} h - \partial_x(V + \mathrm{Re}\,\Sigma^R)\partial_p h = \mathrm{i}\Sigma^K - \mathrm{i}h\left(\Sigma^{\mathrm{R}} - \Sigma^{\mathrm{A}}\right) \tag{3.127}$$

For clarity, we can define the prefactors into "tilde" variables [25] and clean up the equation

$$\left[\tilde{Z}^{-1}\partial_t + \tilde{\boldsymbol{v}}_{\boldsymbol{p}}\nabla_{\boldsymbol{x}} - \left(\nabla_{\boldsymbol{x}}\tilde{V}\right)\nabla_{\boldsymbol{p}} + \partial_t\tilde{V}\partial_\epsilon\right] h(x,p) = I_{\mathrm{col}}[h] \tag{3.128}$$

Where $\tilde{\boldsymbol{v}}_{\boldsymbol{p}} \equiv 2\boldsymbol{p} + \nabla_{\boldsymbol{p}}\mathrm{Re}\,\Sigma^R$, $\partial_x(V + \mathrm{Re}\,\Sigma^R) \equiv \partial_x(V + \mathrm{Re}\,\Sigma^R)$. The $\tilde{Z} \equiv (1 - \partial_\epsilon \mathrm{Re}\,\Sigma^R)^{-1}$ is called quasi-particle weight, or wave-function renormalization. The collision integral $I_{\mathrm{col}}[h]$ is defined as

$$I_{\mathrm{col}}[h] = \mathrm{i}\Sigma^K(x,p) - h(x,p)\Gamma(x,p) \tag{3.129}$$

[12] For generic dispersion $\boldsymbol{p}^2 \to \omega_{\boldsymbol{p}}$ it is

$$\left[\omega_{\boldsymbol{p}}{}^{\circ}h\right] \xrightarrow{\mathrm{WT}} -\mathrm{i}\boldsymbol{v}_{\boldsymbol{p}}\nabla_{\boldsymbol{x}} h \tag{3.122}$$

Where $\boldsymbol{v}_{\boldsymbol{p}} = \nabla_{\boldsymbol{p}}\omega_{\boldsymbol{p}}$.

where $\Gamma = \mathrm{i}(\Sigma^R - \Sigma^A)$. The form of the equation (3.128) is very closed to the Boltzmann equation already, we can further rewrite it into $\hat{\mathrm{d}}_t h = I_{\mathrm{col}}[h]$ form.

Second, we apply the quasiparticle approximation to restrict the distribution to be on-shell. This means we fix the ϵ to be equal to the energy $\omega_{\boldsymbol{p}} + V + \mathrm{Re}\,\Sigma^R$ of the quasi-particle. This approximation is suitable when the quasi-particle spectrum is sharp peaked around its energy, i.e., we have a long live well-defined quasi-particle. The kinetic equation with the quasi-particle approximation will satisfy $\partial_t \tilde{V} \partial_\epsilon h = 0$. Define[13]

$$\hat{\mathrm{d}}_t[h] = \left[\tilde{Z}^{-1}\partial_t + \tilde{\boldsymbol{v}}_{\boldsymbol{p}} \nabla_{\boldsymbol{x}} - \left(\nabla_{\boldsymbol{x}} \tilde{V}\right) \nabla_{\boldsymbol{p}}\right] h \tag{3.130}$$

The kinetic equation (3.128) reads

$$\hat{\mathrm{d}}_t \left[\tilde{h}(\boldsymbol{x}, t, \boldsymbol{p})\right] = I_{\mathrm{col}}[\tilde{h}]\big|_{\epsilon = \omega_{\boldsymbol{p}} + V + \mathrm{Re}\,\Sigma^R} \tag{3.131}$$

Here we defined $\tilde{h}(t, \boldsymbol{x}, \boldsymbol{p}) = h(t, \boldsymbol{x}, \epsilon = \omega_{\boldsymbol{p}} + V + \mathrm{Re}\,\Sigma^R, \boldsymbol{p})$. The on-shell condition, as in other situation of the field theory, leads to a classical (or semi-classical) approximation. Obviously, this equation can be written into the form $\hat{\mathrm{d}}_t[n] = I_{\mathrm{col}}[n]$ by the use of $\tilde{h} = 1 - 2n$ in the fermionic case.

Now we have the quantum Boltzmann equation (3.131), but what is inside the $I_{\mathrm{col}}[n]$? The collision integral $I_{\mathrm{col}}[n]$ is represented by the self-energies that can be computed perturbatively using Feynman diagrams. Let us focus on the lowest order non-vanishing collision integral from the sunset diagram. This is a well-known example from the Fermi liquid theory. This contribution we have computed in (3.87), in space-time coordinates

$$\Sigma^{>/<}(y, y') \sim -U_0^2 G^{>/<}(y, y') G^{>/<}(y, y') G^{</>}(y', y) \tag{3.132}$$

To understand the collision integral, we can assume that $G^>$ and $G^<$ for the fermions can be written into the form

$$G^>_p = \mathrm{i}(1 - n_p(x)) A_p, \quad G^<_p = -\mathrm{i} n_p(x) A_p \tag{3.133}$$

And we can further assume a spatial translational invariance. This means the $n_p(x)$ is the average position $x \equiv x_{\mathrm{a}}$ independent, but it still can depend on the averaged time $t \equiv t_{\mathrm{a}}$

$$n_p(x) = n_p(t, \boldsymbol{x}) = n_p(t) \tag{3.134}$$

The above simplification is especially true in the equilibrium, where $G^>(\omega) = \mathrm{i}(1 - n_{\mathrm{FD}}(\omega)) A(\omega)$, $G^<(\omega) = -\mathrm{i} n_{\mathrm{FD}}(\omega) A(\omega)$, which can be seen through the relation $G^<(\omega) = -e^{-\beta\omega} G^>(\omega)$. Use (3.90)

$$\begin{aligned}
\Sigma^>_p &= -U_0^2 (G^> \circ G^< \circ G^>)_p \\
&= -U_0^2 \int_{p_1 p_2 p_3} (2\pi)^d \delta^d_{p, p_1 + p_2 - p_3} G^>_{p_1} G^<_{p_3} G^>_{p_2} \\
&= -\mathrm{i} U_0^2 \int_{p_1 p_2 p_3} (2\pi)^d \delta^d_{p, p_1 + p_2 - p_3} (1 - n_{p_1}) n_{p_3} (1 - n_{p_2}) A_{p_1} A_{p_3} A_{p_2}
\end{aligned} \tag{3.135}$$

Here the numbers 1, 2, and 3 enumerate the different momenta and should not be confused with the vector component.

[13] In many literature it is names as a "collision partial" $\left(\frac{\partial}{\partial t} f\right)_{\mathrm{col}}$.

The equation (3.135) can be regarded as part of the collision integral of the generalized quantum Boltzmann equation that the quasi-particle assumption is relaxed. This kind of construction is used [93] to discuss the non-equilibrium DMFT results, as the non-equilibrium DMFT results in some situations are very close to equilibrium DMFT spectra with a non-equilibrium distribution solved by a quantum Boltzmann equation, when the collision integral contains terms in the form of Eq. (3.135).

To reach textbook results, we can apply the quasi-particle assumption

$$A_p(x) = 2\pi\tilde{Z}\delta(\omega - \epsilon_{\boldsymbol{p}}(x)) \tag{3.136}$$

we can set $\tilde{Z} = 1$ here, to only consider the quasi-particles. By assuming a spatial translational invariant and averaged time independent spectrum function $A_p(x) = A_{\omega,\boldsymbol{p}}(t,\boldsymbol{x}) = A_{\omega,\boldsymbol{p}}$, the above equation becomes

$$A_{\omega,\boldsymbol{p}} = 2\pi\delta(\omega - \epsilon_{\boldsymbol{p}}) \tag{3.137}$$

This is suitable for quasiparticles that have a long quasiparticle life time $1/\tau_{\text{qp}} \ll 1$, as we discussed before. These kinds of quasiparticles are usually well defined near a sharp fermi surface at low temperature.[14] Note the delta function is the Fourier space form of a free particle time evolution $\sim e^{-\mathrm{i}\epsilon_{\boldsymbol{p}}t}$. Now with the above equation the self-energy $\Sigma^{>}$ can be written as

$$\Sigma^{>}_p = -\mathrm{i}U_0^2 \int_{p_1p_2p_3} (2\pi)^d \delta^d_{p,p_1+p_2-p_3}(1-n_{p_1})n_{p_3}(1-n_{p_2})(2\pi)^3\delta_{\omega_1-\epsilon_{\boldsymbol{p}_1}}\delta_{\omega_2-\epsilon_{\boldsymbol{p}_2}}\delta_{\omega_3-\epsilon_{\boldsymbol{p}_3}} \tag{3.138}$$

We can now perform the integrals for the frequency deltas by using $\int_\omega 2\pi\delta(\omega) = \int \frac{\mathrm{d}\omega}{2\pi}2\pi\delta(\omega) = 1$, and assume an energy dependent only distribution $n_p = n_{\omega,\boldsymbol{p}} \approx n_\omega$, one has

$$\Sigma^{>}_{\omega,\boldsymbol{p}} = -\mathrm{i}\int \mathrm{dPS}\,|\mathcal{T}|^2(1-n_{\epsilon_{\boldsymbol{p}_1}})n_{\epsilon_{\boldsymbol{p}_3}}(1-n_{\epsilon_{\boldsymbol{p}_2}}) \tag{3.139}$$

Here we used the fermion-fermion scattering amplitude $\mathcal{T}$ and the differential phase space dPS, which are defined as

$$\begin{cases} \mathcal{T} = U_0 \\ \mathrm{dPS} = \frac{\mathrm{d}^{d-1}p_1}{(2\pi)^{d-1}}\frac{\mathrm{d}^{d-1}p_2}{(2\pi)^{d-1}}\frac{\mathrm{d}^{d-1}p_3}{(2\pi)^{d-1}}(2\pi)^d\delta^{d-1}_{\boldsymbol{p},\boldsymbol{p}_1+\boldsymbol{p}_2-\boldsymbol{p}_3}\delta_{\epsilon_{\boldsymbol{p}},\epsilon_{\boldsymbol{p}_1}+\epsilon_{\boldsymbol{p}_2}-\epsilon_{\boldsymbol{p}_3}} \end{cases} \tag{3.140}$$

If we consider only the energy dependencies of the distributions, i.e., $n_p = n_{\omega,\boldsymbol{p}} \approx n_\omega$, The $\Sigma^{<}$ becomes

$$\Sigma^{<}_{\epsilon_{\boldsymbol{p}}} = +\mathrm{i}\int \mathrm{dPS}\,|\mathcal{T}|^2 n_{\epsilon_{\boldsymbol{p}_1}}(1-n_{\epsilon_{\boldsymbol{p}_3}})n_{\epsilon_{\boldsymbol{p}_2}} \tag{3.141}$$

Note that the overall sign is different from $G^{>}$. Use the identities $\Sigma^K = \Sigma^{<} + \Sigma^{>}$, $\Sigma^R - \Sigma^A = \Sigma^{>} - \Sigma^{<}$,

[14] As in the Landau Fermi liquid.

and $h = (2n-1)$, the collision integral $I_{\rm qp}(x,p) = \mathrm{i}\Sigma^K(x,p) - h(x,p)\Gamma(x,p)$ can be computed as

$$\begin{aligned} -2I_{\rm qp}(t,\epsilon_{\boldsymbol{p}}) = I_{\rm col} &= \mathrm{i}\Sigma^K - h\Gamma = \mathrm{i}(\Sigma^> + \Sigma^<) - \mathrm{i}(1-2n)(\Sigma^> - \Sigma^<) \\ &= 2\int \mathrm{dPS}\,|\mathcal{T}|^2\left\{n(1-n_1)(1-n_2)n_3 - (1-n)n_1n_2(1-n_3)\right\} \\ &= 2\int \mathrm{dPS}\,|\mathcal{T}|^2\left\{\mathcal{N}_{\rm out}(t,\epsilon_{\boldsymbol{p}}) - \mathcal{N}_{\rm in}(t,\epsilon_{\boldsymbol{p}})\right\} \end{aligned} \tag{3.142}$$

Note that $I_{\rm col}$, and thus $I_{\rm qp}$ here is with translational invariance, and is independent of the averaged position $x \equiv x_{\rm av}$, namely $I_{\rm col}(x,p) = I_{\rm col}(t,p)$. The fermionic quasi-particle collision integral $I_{\rm qp}$ is thus in a well-known form, and it can be found in [25, 29]. We can find the following properties of the final quantum Boltzmann equation and its collision integral. The evolution equation is $\hat{\mathrm{d}}_t[n(t)] \sim I_{\rm qp}[n(t)]$. The $\mathcal{N}_{\rm out}$ may be written into $\mathcal{N}_{\rm out} = n/\tau$, where the τ plays the role of the half life time of the momentum $\boldsymbol{p}$ particle. The quasi-particle collision integral has an "in" and "out" form, or a "gain" and "loss" form. This is expected since the self-energy diagram considered here is closed related the quasi-particle collision or relaxation rate. Whenever a quasi-particle or a quasi-hole with momentum $\boldsymbol{p}$ is scattered, it "decays" into in other momenta through a $2 \to 2$ scattering process [59, 94]. This process is inelastic in the sense that the incident particle's momentum is changed after the scattering process. It can be seen from the (3.139) and (3.139), or diagrammatically by applying the Cutkosky cut rules [28, 34], the field theoretical diagrammatical version of the optical theorem. One can check that the collision integral is nullified by Fermi-Dirac[15] distribution $n = n_{\rm FD}$. This provides the stability of the fermionic quasiparticle equilibrium.

To reach a simpler equation where the "in" and "out" structures are clear, we can again assume the quasiparticle weight $\tilde{Z} = 1$. And further we can assume that there is no external potential, i.e. $\hat{\mathrm{d}}_t = \partial_t$. Then the kinetic equation can be written into

$$-2\partial_t n(t) = \partial_t[1-n(t)] - \partial_t n(t) = 2\int \mathrm{dPS}\,|\mathcal{T}|^2\left\{\mathcal{N}_{\rm out}(t,\epsilon_{\boldsymbol{p}}) - \mathcal{N}_{\rm in}(t,\epsilon_{\boldsymbol{p}})\right\} - 1 \tag{3.143}$$

Again $h = 1-2n$ is used.

Note here we did not consider other scattering process, for instance, the ones that change the particle number, e.g., $1 \to 2$, $2 \to 1$, $2 \to 3$, $\ldots$, $i \to j$. They can appear in a full treatment of the kinetic equations [33].

3.7 Fluctuation dissipation theorem and KMS boundary condition

In this section, we review some consequences of the so-called Kubo-Martin-Schwinger conditions, which can be regarded as criteria of the equilibrium. This section follows the [95, 96], and reviews [83, 88].

The thermal equilibrium states are important stable states of many-body systems in the thermodynamic limit, which are believed to be related to the ergodicity and the detail balance. For quantum many-body systems, there are many puzzles about how quantum many-body systems evolve and provide observables that are thermal. Especially when we consider the deterministic nature of the

[15] Bose-Einstein distribution in the bosonic case. In the collision integral, it is needed to replace $n \to -n$ to reach a bosonic version quasi-particle collision integral.

unitary evolution of the many-body wave function in closed quantum systems, the thermalization becomes microscopically a "surprise". Besides those conceptual difficulties, a theoretical way to define the thermal equilibrium can be reached through the symmetries of the fields on the CTP. This symmetry is usually called the Kubo-Martin-Schwinger (KMS) condition. The result of this symmetry on 2-point functions is the fluctuation-dissipation theorem (FDT).

To see how KMS and FDT arise from the equilibrium, let us start with the thermal density matrix

$$\rho_0 = \frac{1}{Z_0} e^{-\beta_0 H} \tag{3.144}$$

This is a thermal mixed state density matrix which has the distribution depending on the states' eigen energies which are multiplied by a single parameter, the inverse temperature[16] $\beta_0 = 1/T_0$. The system has a time-independent Schrodinger picture Hamiltonian H, which implies that the system is time translational invariant. The Z_0 is a normalization factor.

We first review the consequence of the thermal density matrix for the two-point functions. Following [83] we consider the thermal density matrix $\rho_0 = \frac{1}{Z_0} e^{-\beta_0 H}$. We start at the partition function level, recall that

$$e^{\mathrm{i}W[J_+,J_-]} = \mathrm{Tr}\left[\left(T e^{-\mathrm{i}\int_t J_+(t)\hat{\phi}_+(t)}\right)\frac{1}{Z_0}e^{-\beta_0 H}\left(\overline{T} e^{\mathrm{i}\int_t J_-(t)\hat{\phi}_-(t)}\right)\right] \tag{3.145}$$

$$= \frac{1}{Z_0}\mathrm{Tr}\left[\left(T e^{-\mathrm{i}\int_t J_+(t)\hat{\phi}_+(t)}\right) e^{-\alpha H} e^{+\alpha H} e^{-\beta_0 H}\left(\overline{T} e^{\mathrm{i}\int_t J_-(t)\hat{\phi}_-(t)}\right) e^{(-\alpha+\beta_0)H} e^{-(-\alpha+\beta_0)H}\right] \tag{3.146}$$

$$= \frac{1}{Z_0}\mathrm{Tr}\left[e^{-\beta_0 H} e^{\alpha H}\left(T e^{-\mathrm{i}\int_t J_+(t)\hat{\phi}_+(t)}\right) e^{-\alpha H} e^{-(\beta_0-\alpha)H}\left(\overline{T} e^{\mathrm{i}\int_t J_-(t)\hat{\phi}_-(t)}\right) e^{(\beta_0-\alpha)H}\right] \tag{3.147}$$

where at the third line the cyclic rule of the trace is applied. Now we can use the identity for the time translation $e^{\mathrm{i}\theta H}\hat{\phi}(t)e^{-\mathrm{i}\theta H} = \hat{\phi}(t+\theta)$ and reach

$$e^{\mathrm{i}W[J_+,J_-]} = \mathrm{Tr}\left[\left(\overline{T} e^{\mathrm{i}\int_t J_-(t)\hat{\phi}_-(t+\mathrm{i}(\beta_0-\alpha))}\right)\frac{1}{Z_0}e^{-\beta_0 H}\left(T e^{-\mathrm{i}\int_t J_+(t)\hat{\phi}_+(t-\mathrm{i}\alpha)}\right)\right] \tag{3.148}$$

Here again the cyclic rule is applied. Compare with (3.145), one can see that the right hand side is in a partition function form, however the position T and the $\overline{T}$ terms are switched. Formally we can write

$$e^{\mathrm{i}W[J_+,J_-]} = e^{\mathrm{i}W_{\mathsf{T}}[J_-(t-\mathrm{i}(\beta_0-\alpha)),J_+(t+\mathrm{i}\alpha)]} \tag{3.149}$$

Where the time variables are redefined to move the constant shifts to the sources $J_\pm$. The W_{T} is the notation for the T and $\overline{T}$ switched functional [95].

We can then match[17] the second functional derivatives of the (3.145) and the (3.148). Let $\hat{\phi} = \varphi$, where φ is a real bosonic scalar field.

$$\mathrm{Tr}_{\rho_0}[\varphi_-(t)\varphi_+(t')] = \mathrm{Tr}_{\rho_0}[\varphi_+(t'-\mathrm{i}\alpha)\varphi_-(t+\mathrm{i}(\beta_0-\alpha))] \tag{3.150}$$

[16] Set the Boltzmann constant $k_{\mathrm{B}} = 1$.

[17] Or equivalently we can expand them to $W \sim \sum_{mn} W^{(m,n)}(J_+)^m(J_-)^n$.

If the time reversal symmetry $\varphi(t) = \varphi(-t)$ is assumed, it can be written as

$$\mathrm{Tr}_{\rho_0}[\varphi_-(t)\varphi_+(t')] = \mathrm{Tr}_{\rho_0}[\varphi_+(-t' + \mathrm{i}\alpha)\varphi_-(-t - \mathrm{i}(\beta_0 - \alpha))] \tag{3.151}$$

And if we assume the space and time translational invariance of the system, and do Fourier transforms, one can find

$$+ e^{-\beta_0\omega} D^>(\omega, \boldsymbol{p}) = D^<(\omega, \boldsymbol{p}) \tag{3.152}$$

This is a well-known relation [81, 97]. Equivalently, it is the fluctuation dissipation theorem (FDT)

$$D^K = (1 + 2n_{\mathrm{BE}})(D^R - D^A) \tag{3.153}$$

where $n_{\mathrm{BE}}(\omega) = 1/(e^{\beta_0\omega} - 1)$ is the Bose-Einstein distribution. For fermions, we have an additional minus sign, and the periodic condition becomes anti-periodic.

$$G^K = (1 - 2n_{\mathrm{FD}})(G^R - G^A) \tag{3.154}$$

We can see that the thermal density matrix gives us exact relations between G^K and G^R where the equilibrium distribution function pops out. This looks like a symmetry, and indeed it can be written into a symmetry of the fields.

Now back to the equation (3.148), generally one cannot just replace W_{T} by W and find a symmetry from (3.148). With a thermal density matrix, we can define a discrete symmetry transforms that contains time-reversal symmetry that transform $W[J_+, J_-]$ to $W[\tilde{J}_+, \tilde{J}_-]$

$$W[J_+, J_-] = W[\mathsf{K}_\alpha J_+, \mathsf{K}_\alpha J_-] \tag{3.155}$$

We will not derive this, but instead directly define K, see, for instance, Ref. [95] for derivations. The definition of the K_α is as follows. Consider an imaginary time translation which is followed by a time-reversal transform

$$\Theta \mathrm{T}_{\mathrm{i}\alpha} \tag{3.156}$$

where Θ is the discrete symmetry of the system that contains the time reversal. For instance the ones in CPT discrete transformations that including the time-reversal T. We can choose $\Theta = \mathsf{T}, \mathsf{PT}, \mathsf{CT}, \mathsf{CPT}$. And the imaginary time translation is defined as

$$\mathrm{T}_{\mathrm{i}\alpha}\phi(t, \boldsymbol{x}) = \phi(t + \mathrm{i}\alpha, \boldsymbol{x}) \tag{3.157}$$

And the transform K_α is defined as the $\Theta\mathrm{T}$ combinations [83]

$$\tilde{\phi}_+ = \mathsf{K}_\alpha\phi_+ = \Theta\mathrm{T}_{-\mathrm{i}\alpha}\phi_+ \tag{3.158}$$

$$\tilde{\phi}_- = \mathsf{K}_\alpha\phi_+ = \Theta\mathrm{T}_{\mathrm{i}(\beta_0-\alpha)}\phi_- \tag{3.159}$$

The tilde fields are the transformed fields under K_α. Note the K_α transform the $+$ and $-$ fields differently. Choosing $\Theta = \mathsf{T}$, and ϕ a real bosonic field. With those definitions we can find

$$\begin{aligned}\tilde{\phi}_+ &= \mathsf{K}_\alpha\phi_+ = \mathsf{T}\,\mathrm{T}_{-\mathrm{i}\alpha}\phi_+ = \mathsf{T}\phi_+(t - \mathrm{i}\alpha, \boldsymbol{x}) \\ &= \phi_+(-t + \mathrm{i}\alpha, \boldsymbol{x})\end{aligned} \tag{3.160}$$

Here $\phi^* = \phi$ for real fields is understood. One can verify that $K_\alpha K_\alpha \phi = \phi$. Note that here for simplicity, we consider the +1 sign for the time reversal. Here used $\mathsf{T}\phi_s(t+\mathrm{i}\alpha, \boldsymbol{x}) = \phi_s^*(-t-\mathrm{i}\alpha, \boldsymbol{x})$.[18] Note that the imaginary shift is sign flipped as well. Now, we have

$$\tilde{\phi}_+(x) = \phi_+(-t+\mathrm{i}\alpha, \boldsymbol{x}) \tag{3.161}$$

$$\tilde{\phi}_-(x) = \phi_-\left(-t-\mathrm{i}\left(\beta_0-\alpha\right), \boldsymbol{x}\right) \tag{3.162}$$

Here, $\alpha \in [0, \beta_0]$ can be arbitrarily chosen. For instance, if the $\alpha = \beta_0/2$, then

$$\tilde{\phi}_s = \phi_s(-t + s\frac{\mathrm{i}\beta_0}{2}, \boldsymbol{x}) \tag{3.163}$$

where $s \in \{+,-\}$.

The $W[J_+, J_-] = W[\mathsf{K}_\alpha J_+, \mathsf{K}_\alpha J_-] = W[\tilde{J}_+, \tilde{J}_-]$ can be used as a symmetry to construct and constrain effective field theories [83] with the action I_{EFT}, schematically $e^{\mathrm{i}W} = \int_\Lambda \mathrm{d}[\chi_1, \chi_2] e^{\mathrm{i}I_{\mathrm{EFT}}[\chi_1, J_1, \chi_2, J_2, \rho_0]}$, where Λ is the UV cutoff that specifies the smallest scale that the effective theory is describing, χ are the effective degrees of freedom that are still fluctuating. The ρ_0 is again a initial density matrix. This kind of effective theory is used for constructing hydrodynamics equations [83, 95] from the action principle and deriving the local second law [98] of the macroscopic system in a local equilibrium.

3.8 Dynamical renormalization group

The renormalization group method can be applied to Keldysh actions, where the +/− flow of the dynamical fields should be considered [99–101]. From the Keldysh functional integral, we know that the action can be written as

$$S = S_+[\varphi_+, \psi_+, \bar{\psi}_+] - S_-[\varphi_-, \psi_-, \bar{\psi}_-] \tag{3.164}$$

Now, as an example, we can consider Yukawa coupling terms on the CTP

$$g^+(k)\varphi_+\bar{\psi}_+\psi_+ + g^-(k)\varphi_-\bar{\psi}_-\psi_- \tag{3.165}$$

where k is the RG scale. At the initial scale $k = \Lambda_0$, that is, microscopically, we can assume that we have

$$g^+(\Lambda_0) = g^-(\Lambda_0) \tag{3.166}$$

When we do the coarse-graining and lower the scale, the coupling g^+ and g^- at a given scale can be different

$$g^+(k) \neq g^-(k) \tag{3.167}$$

Because those couplings can have their own flows. Schematically we can write down

$$\partial_k g^+(k) = \beta^+(g^+(k), g^-(k), \ldots), \quad \partial_k g^-(k) = \beta^-(g^+(k), g^-(k), \ldots) \tag{3.168}$$

In practice these coupled equations can result in new (meta)-stable phases that are transient but long-lived, and they are sometimes called non-equilibrium fixed points. Perturbatively the usually

[18] Here we follow [83]. This definition is different from [96], where $\mathsf{T}\phi_s(t, \mathbf{x}) = \phi^*_{-s}(-t, \mathbf{x})$, $s = \pm$ labels the contour.

Feynman diagram technique can be applied [102]. For recent studies, see [99, 103] in the time-space. And for Floquet frequency space see [100, 101]. The detailed treatment is beyond the scope of our discussion.

3.9 Other contour settings

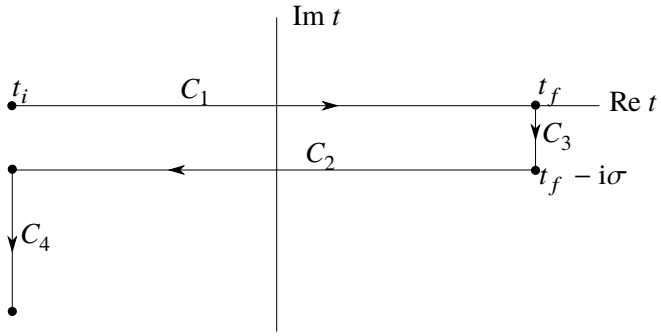

Figure 3.2: At initial time, if the system is at the equilibrium, a Matsubara branch can be added to take into account the initial correlations.

We end this chapter with some discussions of other contour settings. We consider two representative settings.

As th first example, we consider a frequently mentioned contour setting [81, 104], which is shown in the Fig. 3.2. The action on this contour is

$$S = \int_C dtL(t) = \int_{t_\mathrm{i}}^{t_\mathrm{f}} dtL_1(t) - i\int_0^{\sigma} d\tau L_2\left(t_\mathrm{f} - i\tau\right) - \int_{t_\mathrm{i}}^{t_\mathrm{f}} dtL_3(t - i\sigma) - i\int_{\sigma}^{\beta} d\tau L_4\left(t_\mathrm{i} - i\tau\right) \tag{3.169}$$

where L is the Lagrangian, and 1, 2, 3, and 4 correspond to the contour C_1 ,C_2, C_3, and C_4. This contour is intensively used for the Kadanoff-Baym equation and its applications in dynamical mean field theory [3], especially for the "quench" setup.

For the second example, we consider the out-of-time-order correlator (OTOC). Quantum information scrambling [105] can be measured by the commutator square

$$C(t) = \langle [W(t), V]^\dagger [W(t), V] \rangle \tag{3.170}$$

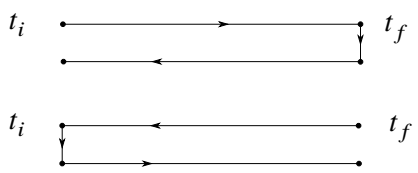

Figure 3.3: (upper) Forward time evolution. (lower) Backward time evolution. Not the "backward" does not mean the backward contour line, but the evolution direction compare with the usual CTP.

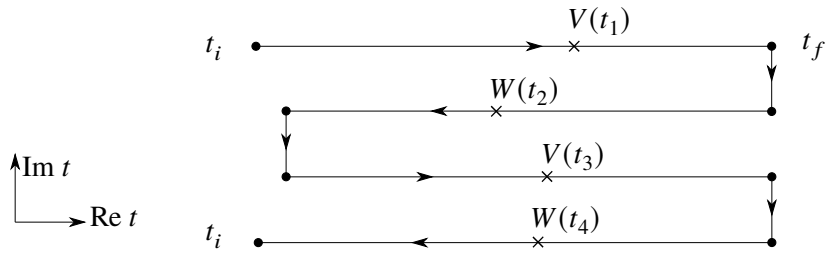

Figure 3.4: The contour for the out-of-time-order correlator (OTOC), here it reads $\langle V(t_4)W(t_3)V(t_2)W(t_1)\rangle$, the operators are insert on different contour pieces. It need to evolve the system both forward and backward in time.

where V is a time-independent reference operator and $W(t)$ is a time-dependent operator that at the initial time is local in a small area of the space and commutes with V, $[W(0), V] = 0$. The $C(t)$ can then be computed from another quantity $\mathcal{F}(t)$ through

$$C(t) = 2 - 2\,\mathrm{Re}[\langle W(t)VW(t)V\rangle] = 2 - 2\mathrm{Re}\,\mathcal{F}(t) \tag{3.171}$$

where

$$\mathcal{F}(t) \equiv \langle W(t)VW(t)V\rangle \tag{3.172}$$

The $\mathcal{F}$ is a special case of the so-called out-of-time order correlator [83] $\mathcal{F}(t_4, t_3, t_2, t_1)$

$$\mathcal{F}(t_4, t_3, t_2, t_1) \equiv \mathrm{Tr}[\rho_0 V(t_4)W(t_3)V(t_2)W(t_1)] \equiv \langle V(t_4)W(t_3)V(t_2)W(t_1)\rangle \tag{3.173}$$

The $\mathcal{F}$ can be represented on a Schwinger-Keldysh like contour. The contour setting shown in Fig. 3.4, with $t_3 = t_1$ and V time independent. There are different ways to compute the OTOC explicitly, one of them is to use Keldysh perturbation theory. In the solid state physics context, an example is [106]. The short time [105] behavior of $\mathcal{F}(t)$ is $\mathcal{F}(t) \sim 1 - \varepsilon e^{\lambda_L t}$ and λ_L is usually regarded as the quantum analog of the Lyapunov exponent, a constant that characterize to the chaotic behavior. This quantity has been intensively studied in recent years, especially for the Sachdev-Ye-Kitaev model [107].

3.10 Summary

We briefly reviewed the Keldysh method in this chapter. The Keldysh method unifies the equilibrium and non-equilibrium physics through an additional degree of freedom. The Keldysh method allows direct usages and extensions of existing field theoretical methods. The diagrammatics in the Keldysh method includes additional tensor vertex structures, and we show how to use them by examples. We also used the Dyson equations to show how to derive the Kadanoff-Baym equations and the kinetic equations.

We can summarize this chapter in the following graph.

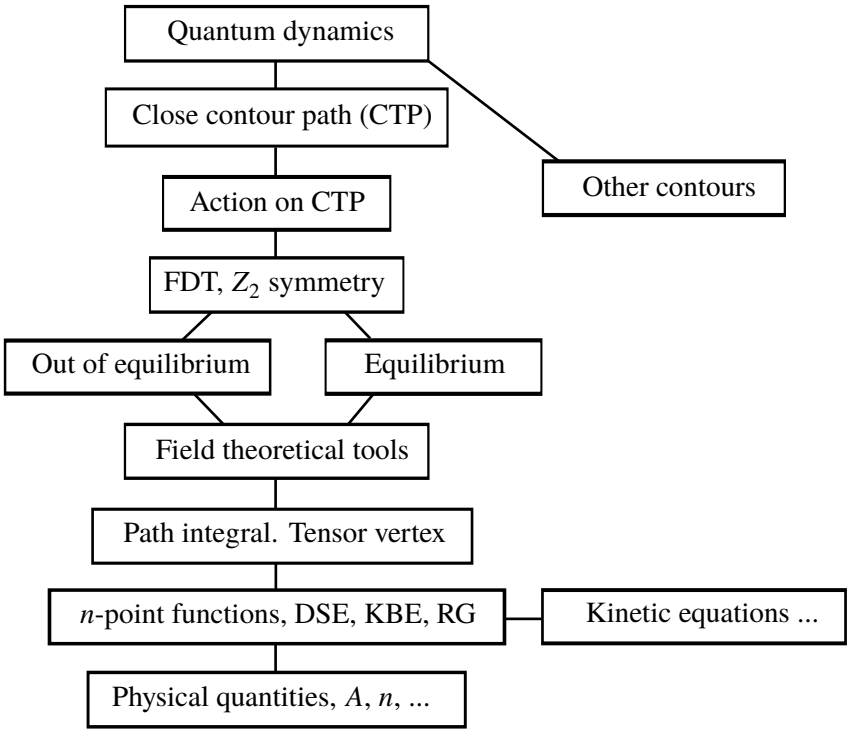

Figure 3.5

CHAPTER 4

Topological matter

4.1 Introduction

There is no doubt that topological matter is now one of the central themes of condensed matter physics. Although the first milestone of it was during the 1980s when the integer quantum Hall effect IQHE and fractional quantum Hall effects FQHE were discovered, its range of application is mostly extended in the past one or two decades, especially by the topological insulator TI, a bulk insulator that has edge states counting by the topological invariant. Pioneered by the early works, e.g., the works of Su, Schrieffer, and Heeger [108], of Simenoff [109, 110], and of Haldane [111], the topological insulator was first purposed by Kane and Mele [112]. The first solid-state experiment that realized the quantum spin Hall effect QSHE through (Hg, Cd)Te quantum wells is in 2007 [113, 114]. And the first topological insulator observed in lab is Bi_xSb_{1-x} [114, 115] in 2008.

A topological insulator (TI) is an insulator in the bulk that has conducting edge states on the boundary. On the other hand, if there are band touching points (or band touching lines), there are topological phenomena as well and may be different from the topological insulators. Especially in $d_s = 3$ they are called [116] Weyl semi-metal, Dirac semi-metal, line nodal semi-metal and so on. They are called semi-metals since they are not insulating everywhere in the bulk by a sizable gap, but have some band crossing. Actually, those kinds of topological phases can be understood by using almost the same reasoning as that for the topological insulators.

Topological aspects and corresponding geometric aspects are intensively studied in recent years in solid-state physics, atomic physics and quantum information/computation communities. I will not try to summarize all these large amount of results. Here, by using topological insulators, quantum Hall effects as examples, I review several ideas that are simple and important for understanding topological matters. Many good textbooks, lecture notes, and research papers are available. For instance, a well-known book of topology and geometry for physicists [117]. Textbooks in condensed matter physics [24, 118]. A simple and mathematically clear review of the topological insulator can be found in [119], and in [120, 121]. Some great lecture notes can be found in [122]. Explanations about the Altland-Zirnbauer class for topological insulators and superconductors are in the article [123].

There are also many good review papers about the concept of topological order can be found in [124]. The definition of the name "topological order" is ambiguous in many literature, thus quite confusing. Here I usually avoid to directly use this word. The detailed discussions about the topological order in the sense of the Ref. [124] are beyond the scope of this thesis, however I will give a short discussion

in 4.7, where the topological insulators belong to the symmetry protected topological (SPT) phases, which are without the intrinsic topological order, but have some non-trivial topological properties protected by symmetries.

One objective of this chapter is to discuss the periodically driven extension of the topological insulator, the Floquet topological insulators, or even the Floquet topological matters in general. Since the periodically driven systems are usually out of equilibrium, one may wonder why we spend quite some time on topological systems in equilibrium, and zero temperature. The reason is simply that the stories for the Floquet topological matters will not be so different from their equilibrium cousins. Despite of the similarities, still many novel properties can be found in the Floquet topological matters.

Though many features of the Floquet TI can be understood by applying the methods used in the equilibrium systems, a new generation of topological matters are also founded. It is called the "intrinsic dynamical" or "anomalous" Floquet topological phases [13, 125], which is a result of the non-trivial winding (from the micro-motion) induced by the periodically driving. There are also discussions such as the heating problem and the many-body dynamics in the individual Floquet part of this thesis, which I will not repeat them in this part.

This part of the thesis is organized as follows. First I introduce an old and simple example for topology in Section. 4.2. Then in Section. 4.3, several mathematical definitions are introduced for later definitions of topological invariants, and for calculational conveniences. Moreover, effective field theories built by topological terms will be used to present the general structure of the response of TI regardless the microscopic details. The connection between quantum anomalies and topological matters are also briefly discussed. In Section. 4.4 I list the discrete symmetry used frequently for classifying topological systems. Then in Section. 4.5 a recent development of the Floquet topological insulators is reviewed. Since the topological invariant is not always analytically reachable, we review several well-known numerical techniques in Section. 4.6 with some examples.

4.2 Topology and monopoles

In order to understand how the topology takes part in, let us first discuss the magnetic monopole purposed by Dirac [126] in the 1930s, and then the further studies from Wu and Yang [117]. These examples will help us to define useful mathematical concepts such as the fibre bundles and character classes.

One can see that many concepts in this section are universal and in some sense intuitive. The reason might be that, roughly speaking, the topological insulator with Berry phases can be regarded as a parameter space gauge theory, e.g., a $U(1)$ gauge theory, or the “electrodynamics”.

4.2.1 Dirac monopole

Dirac considered [117, 126] a magnetic monopole[1] located at $r = 0$

$$\nabla \cdot \boldsymbol{B} = 4\pi g \delta^3(\boldsymbol{r}) \tag{4.1}$$

with the magnetic field strength

$$\boldsymbol{B} = g\boldsymbol{r}/r^3 \tag{4.2}$$

[1] Let’s assume the magnetic monopole once exists.

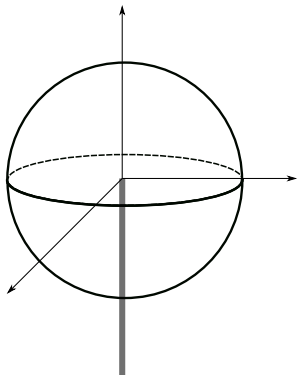

Figure 4.1: The Dirac string

One can then try to write down the vector gauge potential $\boldsymbol{A} = (A_x, A_y, A_z)$ satisfying

$$\boldsymbol{\nabla} \times \boldsymbol{A} = g\boldsymbol{r}/r^3 + \cdots \tag{4.3}$$

For instance, one may try to define

$$\boldsymbol{A}_{\mathrm{N1}} = \left(\frac{-gy}{r(r+z)}, \frac{gx}{r(r+z)}, 0\right) \tag{4.4}$$

or to define

$$\boldsymbol{A}_{\mathrm{S1}} = \left(\frac{gy}{r(r-z)}, \frac{-gx}{r(r-z)}, 0\right) \tag{4.5}$$

and so on. However, a string of singularity is inevitably introduced whenever one attempts to define a smooth vector potential $\boldsymbol{A}$ globally. This string, as the obstruction to make a global smooth vector potential impossible, is called Dirac string given by the "$\cdots$" in (4.3). This obstruction is there whenever a monopole is present inside the volume we care about.

4.2.2 Wu-Yang monopole and fibre bundle

Wu and Yang [127] in the 1970s found another description for the Dirac monopole by using fibre bundle. Since, as Dirac observed, the string of singularities is always presented, to define a smooth gauge potential globally is then an impossible mission. On the other hand, one can try to define a transition function t_{NS} between two different gauge potentials. A global description can be reached by patching the local smooth potentials, the ways of patching are depending on topological properties.

Define the gauge potential for the upper hemisphere U_{N} of the surface $S^2 = \mathbb{R}^3 - \{0\}$, named A_{N}, and that for lower hemisphere U_{S}, named A^S. They are the local section of the connection ω, reads

$$U_{\mathrm{N}} = \{(\theta, \phi) \mid 0 \leq \theta \leq \pi/2 + \varepsilon, 0 \leq \phi < 2\pi\} \tag{4.6}$$

$$U_{\mathrm{S}} = \{(\theta, \phi) \mid \pi/2 - \varepsilon \leq \theta \leq \pi, 0 \leq \phi < 2\pi\} \tag{4.7}$$

$$\sigma^*_{\mathrm{N/S}}\omega = A_{\mathrm{N/S}} \tag{4.8}$$

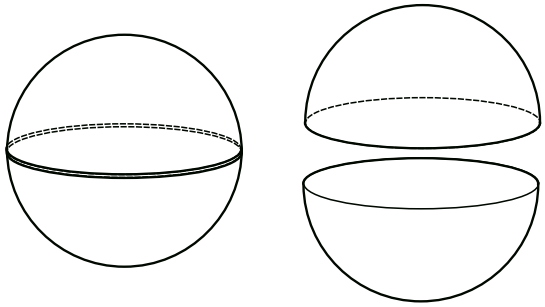

Figure 4.2: Wu-Yang's magnetic monopole gauge potential setup. (Left) Note the two S^1 on the boundary of the two covers, U_N and U_S. (Right) The U_N and U_S.

ω is the connection 1-form. σ_i^* is the local pullback section. Wu and Yang's choices are

$$A_{\mathrm{N}} = \mathrm{i}g(1-\cos\theta)\mathrm{d}\phi, \quad A_{\mathrm{S}} = -\mathrm{i}g(1+\cos\theta)\mathrm{d}\phi \tag{4.9}$$

with the transition function t_{NS} on the boundary of two local sections, the equator. The transition function maps the manifold of equator, i.e. a circle S^1, to the structure group $U(1)$, $\varphi : S^1 \to U(1)$

$$t_{\mathrm{NS}}(\phi) = \exp[\mathrm{i}\varphi(\phi)] \tag{4.10}$$

and by definition $\mathrm{d}\varphi = -\mathrm{i}\left(A_{\mathrm{N}} - A_{\mathrm{S}}\right) = 2g\mathrm{d}\phi$ the transition between A_{N} and A_{S} is

$$A_{\mathrm{N}} = t_{\mathrm{NS}}^{-1}A_{\mathrm{S}}t_{\mathrm{NS}} + t_{\mathrm{NS}}^{-1}\mathrm{d}t_{\mathrm{NS}} = A_{\mathrm{S}} + \mathrm{i}\mathrm{d}\varphi \tag{4.11}$$

the total flux Φ though the 2-sphere S^2 then can be computed by using the patches (local sections) and the Stokes theorem

$$\begin{aligned}\Phi = \int_{S^2}\mathbf{B}\cdot\mathrm{d}\mathbf{S} &= \int_{U_{\mathrm{N}}}F_{\mathrm{N}} + \int_{U_{\mathrm{S}}}F_{\mathrm{S}} = \int_{U_{\mathrm{N}}}\mathrm{d}A_{\mathrm{N}} + \int_{U_{\mathrm{S}}}\mathrm{d}A_{\mathrm{S}} \\ &= \int_{\partial U_{\mathrm{N}}}A_{\mathrm{N}} + \int_{\partial U_{\mathrm{S}}}A_{\mathrm{S}} = \int_{S^1}A_{\mathrm{N}} - \int_{S^1}A_{\mathrm{S}} \\ &= \int_{S^1}\mathrm{i}\mathrm{d}\varphi = 2g\int_0^{2\pi}\mathrm{d}\phi = 4\pi g\end{aligned} \tag{4.12}$$

where $F = \mathrm{d}A$ is understood. The Stokes theorem is used at the second line, it transfers the integration to a line integral along the equator. Note that here we can define a winding number

$$\nu = \frac{\Phi}{2\pi} = 2g \in \mathbb{Z} \tag{4.13}$$

which can be regarded as a topological invariant.

4.2.3 Fibre bundle

The mathematical concept of the fibre bundle is frequently used to describe gauge theory and topological systems. Following [117] I summarize this concept briefly here. A differentiable fibre bundle [117, 119] (E, π, M, F, G) has the following ingredients. (I also mark that which part it corresponds to Wu and Yang's interpretation of the Dirac magnetic monopole.)

Total space E A differentiable manifold, the point on it called u. As the name it suggests, it contains other spaces we will consider. Especially if the bundle is trivial $E = M \times F$.

Base space M A differentiable manifold, with point p on it. Intuitively it is where the fibre sit, or where the "roots" of fibres are. It is covered by a set of open covering $\{U_i\}$, with $U_i \bigcap U_j \neq \emptyset$ and $M = \bigcup_i U_i$. In Wu-Yang monopole, $\{U_i\} = \{U_{\mathrm{N}}, U_{\mathrm{S}}\}$. The base space of Wu-Yang monopole is $E = S^2$.

Projection π A surjection $E \xrightarrow{\pi} M$.

(Typical) fibre F A differentiable manifold. The fibre of Wu-Yang monopole is $F = U(1) = S^1$.

Local trivialization ϕ_i A map $E \supset \pi(U_i) \xrightarrow{\phi_i^{-1}} U_i \times F$. The local trivialization in Wu-Yang monopole is $\phi_{\mathrm{N}}^{-1}(u) = (p, e^{\mathrm{i}\alpha_{\mathrm{N}}})$ and $\phi_{\mathrm{S}}^{-1}(u) = (p, e^{\mathrm{i}\alpha_{\mathrm{S}}})$.

Transition function t_{ij} A map $U_j \times F \xrightarrow{t_{ij}} U_i \times F$, $t_{ij} \equiv \phi_{i,p}^{-1} \circ \phi_{j,p}$ The transition function in Wu-Yang monopole is t_{NS} and t_{SN}.

Structure group G A group act on fibre F on the left. The structure group of Wu-Yang monopole is $G = U(1) = S^1$.

Additionally, we also have several useful definitions.

(Cross) section σ and local section σ_i A map $M \xrightarrow{\sigma} E$. It is the inverse of the projection $\pi \circ \sigma = \mathrm{Id}_M$. The local section is defined as $U_i \xrightarrow{\sigma_i} E$.

Pullback section σ^* A map $\omega \xrightarrow{\sigma^*} A_i$ that map the connection in the total space E to local connection of the local trivialization $\phi_i(\pi(U_i))$.

Principal bundle $P(M, G)$ A fibre bundle with $F = G$, i.e., its fibre is the structure group. Thus, it is usually denoted as $P(M, G) \equiv ((E, \pi, M, F, G))$ by its base manifold and structure group, also called G bundle over M. Wu-Yang monopole is then a principal bundle $P(S^2, U(1))$.

For describing the gauge theory, we still need the differential structure, for doing calculus on the manifold. Here I focus on the definition of the connection on principal bundle.

Connection ω and local connection A_i $\omega \in \mathfrak{g} \otimes T^*P$, $A_i \equiv \sigma_i^* \omega \in \mathfrak{g} \otimes \Omega^1(U_i)$. $\mathfrak{g}$ is the Lie algebra of Lie group G. And $\Omega^1(M) = T^*M$ is the set of 1-form, also called the dual vector or the cotangent space of M. The Wu-Yang monopole have local connection A_{N} and A_{S}, the gauge potentials.

From the above, one can then summarize that the principal bundle is a natural language for the Dirac magnetic monopole as Wu and Yang analyzed. Further, not a surprise, it turns out to be a useful language for gauge theories and some specific condensed matter systems which have gauge structures, e.g., anomalies in field theory, quantum Hall effects, and topological insulators in solid-state systems.

4.2.4 Berry connection

As introduced by Berry [128], a quantum mechanical system with adiabatic time evolution can acquire a connection (vector potential) called Berry connection, which has components

$$A_i^n(\boldsymbol{\lambda}) \equiv \langle n(\boldsymbol{\lambda}) | \partial_{\lambda^i} | n(\boldsymbol{\lambda}) \rangle \tag{4.14}$$

where $|n(\boldsymbol{\lambda}(t))\rangle$ is the instantaneous eigenstate of the system Hamiltonian depending on a set of parameters $\boldsymbol{\lambda} = (\lambda_1, \cdots, \lambda_i, \cdots)$. The original Berry phase is a $U(1)$ phase $e^{-\mathrm{i}\gamma_B}$, that means the eigenstates are non-degenerate.

The above Berry phase can be regarded as an abelian gauge structure. The non-abelian generalization is pointed out by Wilczek and Zee [129]. Consider that $|m\rangle$ and $|n\rangle$ are in a degenerate subspace

$$A_i^{mn}(\boldsymbol{\lambda}) \equiv \langle m(\boldsymbol{\lambda}) | \partial_{\lambda^i} | n(\boldsymbol{\lambda}) \rangle \tag{4.15}$$

The connection with the above matrix components is called Berry-Wilczek-Zee connection [130], or non-Abelian Berry connection.

One can see that the Berry phase structure of the two-level quantum mechanical system [117, 120] with the Hamiltonian

$$H(\boldsymbol{h}(\boldsymbol{\lambda})) = \boldsymbol{h}(\boldsymbol{\lambda}) \cdot \boldsymbol{\sigma} \tag{4.16}$$

is identical to the Wu-Yang monopole, that is, $P(S^2, U(1))$. This gauge structure is helpful to understand the topological (Chern) insulators.

Also by identifying the Berry connection with the $U(1)$ gauge field and thus the 1-forms in the Dirac monopole, one can find that if a monopole is set inside the considered sphere, it is impossible to define a global smooth eigenstate since the $A_i(\boldsymbol{\lambda})$ will divergent

$$A_i \to \infty \tag{4.17}$$

on the Dirac string. This monopole is, for a two-band model represented by the case

$$\boldsymbol{h} = 0 \tag{4.18}$$

that is where the gap closes, since the gap size is $2\|\boldsymbol{h}\|$.

4.3 Characteristic classes and topological terms

4.3.1 Basic definitions

Here I define some useful mathematical, mostly differential geometrical, concepts by following [117]. They will make the structure of this chapter more transparent and make the equations shorter.

Wedge product, exterior product Wedge product gives anti-symmetrized tensor product

$$\mathrm{d}x^\mu \wedge \mathrm{d}x^\nu = \mathrm{d}x^\mu \otimes \mathrm{d}x^\nu - \mathrm{d}x^\nu \otimes \mathrm{d}x^\mu \tag{4.19}$$

where $\otimes$ is the tensor product. In general

$$\mathrm{d}x^{\mu_1} \wedge \mathrm{d}x^{\mu_2} \wedge \ldots \wedge \mathrm{d}x^{\mu_n} = \sum_{P\in S_n} \mathrm{sgn}(P)\mathrm{d}x^{\mu_{P(1)}} \wedge \mathrm{d}x^{\mu_{P(2)}} \wedge \ldots \wedge \mathrm{d}x^{\mu_{P(n)}} \tag{4.20}$$

$\mathrm{sgn}(P)$ is "+" for even permutations and "−" for odd ones, S_n is the symmetric group of order n, which contents the operations to symmetrize the tensor indices, $P \in S_n$.

Levi-Civita symbol the Levi-Civita symbol is defined as $\varepsilon^{P(1)P(2)P(3)\ldots P(n)} = \mathrm{sgn}(P)$ for $P \in S_n$. If $n = 2$, we have $\varepsilon^{12} = -\varepsilon^{21}$. One may use it to anti-symmetrize the tensor. For example we have

$$\mathrm{d}x^\mu \wedge \mathrm{d}x^\nu = \varepsilon_{\mu\nu}\mathrm{d}x^\mu \otimes \mathrm{d}x^\nu \tag{4.21}$$

Differential form differential n-form ω is a totally anti-symmetric $(0, n)$ tensor

$$\omega = \frac{1}{n!}\omega_{\mu_1\mu_2\cdots\mu_n}\mathrm{d}x^{\mu_1} \wedge \mathrm{d}x^{\mu_2} \wedge \cdots \wedge \mathrm{d}x^{\mu_n} \tag{4.22}$$

the set of n-form on manifold M is denoted as $\Omega^n(M)$, at point $p \in M$ it is denoted by $\Omega^n_p(M)$.

The product $\wedge : \Omega^q_p(M) \times \Omega^r_p(M) \to \Omega^{q+r}_p(M)$ of a q-form ω and a r-form ξ

$$\omega \wedge \xi = (-1)^{qr}\xi \wedge \omega \tag{4.23}$$

as a trivial extension. Where the product is associated

$$(\omega \wedge \xi) \wedge \eta = \omega \wedge (\xi \wedge \eta) \tag{4.24}$$

For a q-form ξ, q odd

$$\xi \wedge \xi = 0 \tag{4.25}$$

An example would be $F \wedge F$

$$F \wedge F = (\frac{1}{2!}F_{\mu\nu}\mathrm{d}x^\mu \wedge \mathrm{d}x^\nu) \wedge (\frac{1}{2!}F_{\rho\sigma}\mathrm{d}x^\rho \wedge \mathrm{d}x^\sigma) \tag{4.26}$$

$$= \frac{1}{4}F_{\mu\nu}F_{\rho\sigma}\mathrm{d}x^\mu \wedge \mathrm{d}x^\nu \wedge \mathrm{d}x^\rho \wedge \mathrm{d}x^\sigma \tag{4.27}$$

which is closed related to $d = 4$ case of θ-term which reads $\mathcal{L}_\theta = \frac{e^2}{32\pi^2}\varepsilon^{\alpha\beta\mu\nu}F^{a\mu\nu}F^a_{\mu\nu}$ [34, 131], and the Chern character that will be introduced later.

Volume form The volume element of a dimension m orientable manifold M equips metric g is a differential m-form call volume form Ω_M, it is defined as

$$\Omega_M \equiv \sqrt{|g|}\,\mathrm{d}x^1 \wedge \mathrm{d}x^2 \wedge \ldots \wedge \mathrm{d}x^m \tag{4.28}$$

the norm $|g|$ is defined by the determinant $\det(g)$, and usually it is normalized to $\det(g) = 1$.

Exterior derivatives Exterior derivative d_n or simply d act on a n-form maps a n-form to a $(n+1)$-form

$$\mathrm{d}\omega = \frac{1}{n!}\left(\frac{\partial}{\partial x^\nu}\omega_{\mu_1\ldots\mu_n}\right)\mathrm{d}x^\nu \wedge \mathrm{d}x^{\mu_1} \wedge \ldots \wedge \mathrm{d}x^{\mu_n} \tag{4.29}$$

It has an important property $\mathrm{d}^2 = 0$ that is

$$\mathrm{d}^2\omega = \mathrm{d}(\mathrm{d}\omega) = 0 \tag{4.30}$$

which is reminiscent of the boundary operation of the (co-)homology group. For instance, the derivative of the connection 1-form $A = A_\mu \mathrm{d}x^\mu$ for $U(1)$ theory is

$$\mathrm{d}A = \mathrm{d}(A_\mu \mathrm{d}x^\mu) = \frac{1}{1!}\frac{\partial A_\mu}{\partial x^\nu}\mathrm{d}x^\nu \wedge \mathrm{d}x^\mu = \frac{1}{2}(\partial_\nu A_\mu + \partial_\nu A_\mu)\mathrm{d}x^\nu \wedge \mathrm{d}x^\mu \tag{4.31}$$

$$= \frac{1}{2}(\partial_\nu A_\mu \mathrm{d}x^\nu \wedge \mathrm{d}x^\mu + \partial_\mu A_\nu \mathrm{d}x^\mu \wedge \mathrm{d}x^\nu) \tag{4.32}$$

$$= \frac{1}{2}(\partial_\nu A_\mu \mathrm{d}x^\nu \wedge \mathrm{d}x^\mu - \partial_\mu A_\nu \mathrm{d}x^\nu \wedge \mathrm{d}x^\mu) \tag{4.33}$$

$$= \frac{1}{2}F_{\nu\mu}\mathrm{d}x^\nu \wedge \mathrm{d}x^\mu = F \tag{4.34}$$

where $F_{\nu\mu} = \partial_\nu A_\mu - \partial_\mu A_\nu$ as the usual field strength.

For q-form ω and r-from ξ, $\mathrm{d}(\xi \wedge \omega) = (\mathrm{d}\xi) \wedge \omega + (-1)^q \xi \wedge (\mathrm{d}\omega)$.

Stokes theorem The Stokes theorem is

$$\int_{\partial M} \omega = \int_M \mathrm{d}\omega \tag{4.35}$$

where M is a differentiable manifold and ∂M is its boundary. ω and $\mathrm{d}\omega$ are differential forms with compatible dimensions respectively, since the exterior derivative maps a m-form to a $(m+1)$-from, thus $1 + \dim\omega = \dim\mathrm{d}\omega$.

Differential map and pullback of manifolds Here I define the differential map and pullback of the manifolds. A smooth map between two manifolds $f : M \to N$ induces differential map f_* between

the tangent vector space T_pM and $T_{f(p)}N$ of M and N at point p

$$f_* : T_pM \to T_{f(p)}N \tag{4.36}$$

the reverse of the differential map is called pullback f^*

$$f^* : T^*_{f(p)}N \to T^*_pM \tag{4.37}$$

where the $T^*_{f(p)}N$ and T^*_pM are the cotangent vector space, or the dual vector space.

Hodge star The Hodge star for a 2-form on a $m = 4$ dimensional manifold with a flat metric read

$$\star\,(\mathrm{d}x^\mu \wedge \mathrm{d}x^\nu) = \frac{1}{2}\varepsilon^{\mu\nu\rho\sigma}\mathrm{d}x_\rho \wedge \mathrm{d}x_\sigma \tag{4.38}$$

A frequently encountered example is the curvature 2-form, with field strength $F_{\mu\nu}(x)$

$$\star\,(F_{\mu\nu}\mathrm{d}x^\mu \wedge \mathrm{d}x^\nu) = F_{\mu\nu} \star\,(\mathrm{d}x^\mu \wedge \mathrm{d}x^\nu) = \frac{1}{2}F_{\mu\nu}\varepsilon^{\mu\nu\rho\sigma}\mathrm{d}x_\rho \wedge \mathrm{d}x_\sigma \tag{4.39}$$

The general definition is for a m-dimensional manifold M

$$\star\,(\mathrm{d}x^{\mu_1} \wedge \cdots \wedge \mathrm{d}x^{\mu_n}) = \frac{\sqrt{|g|}}{(m-n)!}\varepsilon^{\mu_1\cdots\mu_n}{}_{\nu_{n+1}\cdots\nu_m}\mathrm{d}x^{\nu_{n+1}} \wedge \cdots \wedge \mathrm{d}x^{\nu_m} \tag{4.40}$$

For Lorentzian metric

$$\star\star\omega = (-1)^{n(m-n)}\omega \tag{4.41}$$

and for Euclidean metric

$$\star\star\omega = (-1)^{1+n(m-n)}\omega \tag{4.42}$$

Last but not the least, the Hodge star of the identity 1 is the volume form

$$\star\, 1 = \Omega_M \tag{4.43}$$

If a differential form has its Hodge star equal to itself, it is self-dual.

One can define the inner product of differential forms through the Hodge star

$$(\omega, \xi) = \int \omega \wedge \star\xi \tag{4.44}$$

The Maxwell equation can be written [117] compactly by differential forms and the Hodge star, $\mathrm{d} \star F = \star J$.

Bianchi identity

$$\mathrm{D}F \equiv \mathrm{d}F + A \wedge F - F \wedge A = \mathrm{d}F + [A, F] = 0 \tag{4.45}$$

The above definitions are mostly sufficient for later discussions of the topological insulator. In the next section, we will define the characteristic classes, which will be used to define some topological invariants.

4.3.2 Characteristic classes

With the definitions of the previous section, we can list the definitions of Chern characters and Chern-Simons form for Chern characters here. More details can be found in the book [117]. Those characters are closely related to the topological invariant in physics context. In this section, I also use the shorthand notation

$$(F)^j \equiv \wedge_j F = F \wedge \cdots \wedge F \tag{4.46}$$

Chern character

The Chern character can be defined by combining curvature two-form (or one may call it field strength two-form)

$$\mathrm{ch}(F) \equiv \mathrm{tr} \exp\left(\frac{\mathrm{i}F}{2\pi}\right) = \sum_{j=1} \frac{1}{j!} \mathrm{tr}\left(\frac{\mathrm{i}F}{2\pi}\right)^j \tag{4.47}$$

Where the j-th Chern character

$$\mathrm{ch}_j(F) \equiv \frac{1}{j!} \mathrm{tr}\left(\frac{\mathrm{i}F}{2\pi}\right)^j \tag{4.48}$$

The manifold dimension $\dim M = d$, and for $j > d/2$ the $\mathrm{ch}_j(F)$ vanishes. Let us see two examples up to $j = 2$. First, $j = 1$ is a 2-form

$$\mathrm{ch}_1(F) = \frac{\mathrm{i}}{2\pi} \mathrm{tr}\, F \tag{4.49}$$

and $j = 2$ is a four-form is

$$\mathrm{ch}_2(F) = \frac{1}{2}\left(\frac{\mathrm{i}}{2\pi}\right)^2 \mathrm{tr}\, F^2 \tag{4.50}$$

Chern-Simons form of Chern character

Chern-Simons form of Chern character is defined as [117]

$$Q_{2j-1}(A, F) = \frac{1}{(j-1)!}\left(\frac{\mathrm{i}}{2\pi}\right)^j \int_0^1 \mathrm{d}t\, \mathrm{str}\left(A, F_t^{j-1}\right) \tag{4.51}$$

where $F \equiv \mathrm{d}A$ and

$$F_t = t\mathrm{d}A + t^2 A^2 = tF + \left(t^2 - t\right) A^2 \tag{4.52}$$

The symmetrized trace str is defined as

$$\mathrm{str}\left(A_1, A_2, \ldots, A_r\right) \equiv \frac{1}{n!} \sum_P \mathrm{tr}\left(A_{P(1)}, A_{P(2)}, \ldots, A_{P(n)}\right) \tag{4.53}$$

where $P(n)$ is permutations of the indices. For instance

$$\mathrm{str}\left(A_1, A_2\right) = \frac{1}{2} \sum_P \mathrm{tr}\left(A_{P(1)}, A_{P(2)}\right) = \frac{1}{2} \mathrm{tr}\left(A_1 A_2 + A_2 A_1\right) \tag{4.54}$$

Note that the wedges are suppressed. Then the Chern-Simons form can be written as

$$Q_{2j-1}(A,F) = \frac{1}{(j-1)!}\left(\frac{\mathrm{i}}{2\pi}\right)^j \int_0^1 \mathrm{d}t\ \mathrm{tr}\left(AF_t^{j-1}\right) \tag{4.55}$$

by using the anti-symmetric nature of the wedge product.

Usually, it is sufficient to know up to 5-form corresponds to 5-dimensional space(-time), and they all have some applications in physics or physical models. The Chern-Simons 1-form is

$$Q_1(A,F) = \frac{\mathrm{i}}{2\pi}\int_0^1 \mathrm{d}t\ \mathrm{tr}\, A = \frac{\mathrm{i}}{2\pi}\mathrm{tr}\, A \tag{4.56}$$

the Chern-Simons 3-form is

$$Q_3(A,F) = \left(\frac{\mathrm{i}}{2\pi}\right)^2 \int_0^1 \mathrm{d}t\ \mathrm{str}\left(A, t\mathrm{d}A + t^2A^2\right) = \frac{1}{2}\left(\frac{\mathrm{i}}{2\pi}\right)^2 \mathrm{tr}\left(A\mathrm{d}A + \frac{2}{3}A^3\right) \tag{4.57}$$

For the case curvature two form $F = \mathrm{d}A = 0$ we have

$$Q_3(A,0) = \frac{1}{2}\left(\frac{\mathrm{i}}{2\pi}\right)^2 \mathrm{tr}\int_0^1 \mathrm{d}t A t^2 A^2 = \frac{-1}{24\pi}\mathrm{tr}\, A^3 \tag{4.58}$$

In some context, the local 3-form $K \equiv \mathrm{tr}(A\mathrm{d}A + \frac{2}{3}A^3)$ is called Chern-Simons form, and $\mathrm{tr}\, F^2 = \mathrm{d}K$, this is the same as the simple identity $\mathrm{ch}_2(F) = \mathrm{d}Q_3(A,F)$, the only difference is the normalization.

As the last example, the Chern-Simons 5-form is

$$Q_5(A,F) = \frac{1}{2}\left(\frac{\mathrm{i}}{2\pi}\right)^3 \int_0^1 \mathrm{d}t\ \mathrm{str}\left(A, \left(t\mathrm{d}A + t^2A^2\right)^2\right) = \frac{1}{6}\left(\frac{\mathrm{i}}{2\pi}\right)^3 \mathrm{tr}\left(A(\mathrm{d}A)^2 + \frac{3}{2}A^3\mathrm{d}A + \frac{3}{5}A^5\right) \tag{4.59}$$

in many applications up to 5-form is enough since the space-time dimension is usually $d \leq 4$ and for the case $d = 4$ the space-time manifold can be thought as the boundary of a $d = 5$ manifold, e.g. in the dimensional reduction.

4.3.3 Degree of map

The degree of a map is a homotopic invariant, thus a topological invariant. It uses

$$\pi_d(S^d) = \mathbb{Z} \tag{4.60}$$

where π_d is the d dimensional homotopy group, S^d is the d-sphere.

Here I follow [119, 132]. Let M to be an orientable $(n-1)$-dimensional closed manifold and P be the punctured space $P = \mathbb{R}^n - \{0\}$, i.e., a one point removed Euclidean space. Define a projection π'_N

$$\pi'_N : \left(\mathbb{R}^n - \{0\}\right) \to S^{n-1}, \qquad y \mapsto \tfrac{y}{\|y\|} \tag{4.61}$$

where the unit sphere $S^{n-1} = \{z, |r = \sum_i z_i^2 = 1\}$. And define the map

$$f : M \to P, \tag{4.62}$$

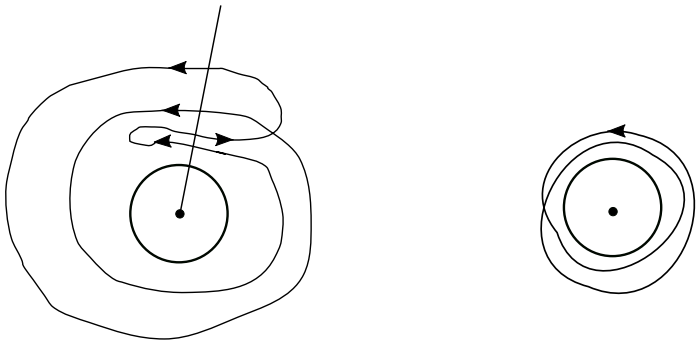

Figure 4.3: Degree of map for the case deg = 2 and $n = 2$. Note that the surface, or a closed line here, $N = f(M)$ can intersect itself in the punctured space $P = \mathbb{R}^n - \{0\}$. (Left) A ray from the origin of P is drawn and it intersects with the surface N. Depending on wether the line is come from the right or the left to the intersection, "+1" or "−1" is marked. The winding number is equal to sum up the +1 and −1. (Right) the winding when map to S^l, $l = 1$ here.

and $f(M)$ is immersed into P, i.e. $f(M)$ can intersect itself. Obviously

$$M \xrightarrow{f} P \xrightarrow{\pi'_N} S^{n-1} \tag{4.63}$$

One can then define the product of the maps g which maps M to the $(n-1)$ sphere

$$g : M \xrightarrow{g=\pi'_N \circ f} S^{n-1} \tag{4.64}$$

Since $f(M)$ can be regarded as a hyper-surface in $N = \mathbb{R}^n - \{0\}$, we can then ask how many times it (net) encloses the origin 0. This is counted by the degree of map g, or the winding number. The degree of map $\deg(g)$ is defined as [132]

$$\deg(g) \equiv \frac{1}{\mathrm{A}_{n-1}} \int_M f^* \tau = \frac{1}{\mathrm{A}_{n-1}} \int_{f_* M} \tau \tag{4.65}$$

where A_{n-1} is the area of the unit sphere of $(n-1)$ dimension. The f^* is the pullback of f. The f_* is the differential map, the inverse of f^*. The $(n-1)$-form τ is defined as $\pi'^* \sigma$ where the sphere area of S^{n-1} can be computed in $\mathbb{R}^n$ by integrate over σ

$$\mathrm{A}_{n-1} = \int_{\mathbf{S}^{n-1}} \sigma = \int_{\mathbf{S}^{n-1}} \star(r dr) \tag{4.66}$$

in above $\star$ is the Hodge star and $r\mathrm{d}r \equiv \sum_i y_i \mathrm{d}y_i$. One can proof that [132]

$$\tau \equiv \pi^* \sigma = \frac{\sigma}{r^n} = \frac{1}{r^n} \star (r dr) = \frac{1}{\|r\|^n} \sum_{i=1}^{n} (-1)^{i-1} y_i \mathrm{d}y_1 \mathrm{d}y_2 \cdots \widehat{\mathrm{d}y_j} \cdots \mathrm{d}y_n \tag{4.67}$$

here $\widehat{\mathrm{d}y_j}$ means $\mathrm{d}y_j$ is omitted, also the wedge symbols are suppressed. Now we can compute the

degree in the punctured space $P = \mathbb{R}^n - \{0\}$

$$\deg(g) = \frac{1}{\mathrm{A}_{n-1}} \int_{f_* M} \frac{1}{\|r\|^n} \star (r dr) \tag{4.68}$$

$$= \frac{1}{\mathrm{A}_{n-1}} \int_{f(M)} \frac{1}{\|y\|^n} \sum_{i=1}^{n} (-1)^{i-1} y_i \mathrm{d}y_1 \mathrm{d}y_2 \cdots \widehat{\mathrm{d}y_j} \cdots \mathrm{d}y_n \tag{4.69}$$

Since the map π_N is fixed, it is also convenient to define

$$\deg(f) \equiv \deg(g) \tag{4.70}$$

Example: $n = 3$

Recall that for Euclidean space the dimension n unit ball have the volume V_n and its boundary is S^{n-1} has the area A_n, they have the relation $n\mathrm{V}_n = \mathrm{A}_{n-1}$. The explicit form of V_n and A_n read

$$\mathrm{V}_n = \frac{\pi^{n/2}}{\Gamma\left(\frac{n}{2}+1\right)}, \qquad \mathrm{A}_n = \frac{2\pi^{\frac{n+1}{2}}}{\Gamma\left(\frac{n+1}{2}\right)} \tag{4.71}$$

Γ is the gamma function. Thus for $n = 3$ the area of S^2 is $\mathrm{A}_2 = 4\pi$, then

$$\deg(f) = \frac{1}{4\pi} \int_{f(M)} \frac{1}{2} \epsilon^{ijk} \frac{y_i}{\|y\|^3} \mathrm{d}y_j \wedge \mathrm{d}y_k \tag{4.72}$$

Recall that the magnetic monopole has the magnetic field strength $\boldsymbol{B} = \boldsymbol{r}/r^3$, which we have encountered when discussing the Dirac monopole. The degree can be regarded as the total magnetic flux that goes through the surface $N = f(M)$.

Now I make some contact with the lattice Hamiltonian. Let us consider a map

$$\boldsymbol{h} : T^2 \to \mathbb{R}^n - \{0\}, \qquad \boldsymbol{k} \mapsto \boldsymbol{h}(\boldsymbol{k}) \tag{4.73}$$

here $\boldsymbol{k} = (k_x, k_y)$. The $\boldsymbol{h}$ maps the $d_s = 2$ Brillouin zone torus to the punctured space. And in $d_s = 2$ generally a 2 by 2 lattice Hamiltonian with periodic boundary conditions can be written as

$$H(\boldsymbol{k}) = h_0(\boldsymbol{k})\mathbb{1} + \boldsymbol{h}(\boldsymbol{k}) \cdot \boldsymbol{\sigma} \tag{4.74}$$

where $\boldsymbol{\sigma} = (\sigma_x, \sigma_y, \sigma_z)^\intercal$, and $\mathbb{1}$ is the identity matrix. Here I set $h_0 = 0$ without loss of generality. It is clear that this setup is corresponding to above discussion with $f = \boldsymbol{h}$. The equation (4.72) becomes

$$\deg(\boldsymbol{h}) = \frac{1}{2\pi \mathrm{i}} \int_{\mathrm{BZ}} F \tag{4.75}$$

The definition of F absorbed a factor of $\mathrm{i}/2$ which is merely a convention, i.e.

$$F \equiv \frac{\mathrm{i}}{4} \epsilon^{ijk} \frac{y_i}{\|y\|^3} \mathrm{d}y_j \wedge \mathrm{d}y_k = \frac{\mathrm{i}}{2} \frac{\boldsymbol{h}}{\|h\|^3} \cdot \left(\frac{\partial \boldsymbol{h}}{\partial k_x} \times \frac{\partial \boldsymbol{h}}{\partial k_y} \right) \mathrm{d}k_x \wedge \mathrm{d}k_y \tag{4.76}$$

Now we find that there are two equivalent way [119], through the degree or through the bundle map, to compute the first Chern number Ch_1 for a 2 by 2 Hamiltonian on $d_s = 2$ lattice with periodic boundary condition [119]

$$\mathrm{Ch}_1 = \deg(\boldsymbol{h}) = \frac{1}{2\pi \mathrm{i}} \int_{\mathrm{BZ}} F = \frac{1}{2\pi \mathrm{i}} \int_{\partial \boldsymbol{h}^{-1}(U_{\mathrm{N}})} \mathrm{d} \log \left(t_{\mathrm{NS}} \circ \boldsymbol{h} \right) \tag{4.77}$$

here the integration of the Chern character 2-form is denoted by Ch_1.

4.3.4 Topological terms

Frequently in literatures people can find the name "topological terms". Usually it means the building blocks of a topological field theory, or terms related to the topological properties of the action. The topological part S_{top} in the action $S = S_1 + S_{\mathrm{top}}$ is an integral of topological terms. Here we follow the naming convention in the textbook of Altland and Simons [118] to call them θ-terms, Wess-Zumino terms, and Chern-Simons terms. However, the detailed notations used here may slightly different from the Ref. [118].

The map $\phi : M \to N$ from the base manifold M to the target space N induces the pullback ϕ^*

$$\begin{aligned} \phi^* : T^*_{\phi(x)}(N) &\to T^*_x(M) \\ \omega &\mapsto \phi^*(\omega) \equiv \omega \circ \phi_* \end{aligned} \tag{4.78}$$

Here I choose the partition function convention

$$Z = \int \mathrm{d}[\phi] e^{\mathrm{i}S[\phi]} = \int \mathrm{d}[\phi] e^{\mathrm{i}\int_t L[\phi]} \tag{4.79}$$

which may gives a $-\mathrm{i}$ factor difference when compared with the imaginary time convention.

Theta term

For $\phi : M \to N$ with the base manifold M and the target manifold N have the same dimension $\dim M = \dim N$

$$S_{\mathrm{top}} = S_{\mathrm{theta}}[\phi] = \int_M \theta \phi^* \Omega_N \tag{4.80}$$

where Ω_N is the volume form of N and ϕ^* is the pullback, θ is a function of space-time. The integration is simple to carry out

$$S_{\mathrm{theta}}[\phi] = \int_M \theta \phi^* \Omega_N = \int_N \theta \Omega_N = \theta \times (\text{integer}) \tag{4.81}$$

where the last equality assumed θ is a constant, although it can depend on space-time coordinates.

An example is that in dimension $d = 4$, the θ-term Lagrangian density [34, 131] is

$$S_{\mathrm{theta}} = -\int \frac{\theta e^2}{8\pi^2} \operatorname{tr} F \wedge F = -\int \mathrm{d}^4 x \mathcal{L}_\theta = -\int \mathrm{d}^4 x \frac{\theta e^2}{32\pi^2} \varepsilon^{\mu\nu\rho\sigma} F_{\mu\nu} F_{\rho\sigma} \tag{4.82}$$

Note the same indices summed, and we used $\frac{-1}{8\pi^2}\operatorname{tr} F\wedge F=\frac{-1}{32\pi^2}\varepsilon^{\mu\nu\rho\sigma}\operatorname{tr}\left(F_{\mu\nu}F_{\rho\sigma}\right)$. This is corresponds to the chiral anomaly[2] and the axion[3] physics for the CP violation problem. In condensed matter contexts, this term gives the magnetoelectric effect in the $d_s=3$ topological insulator [133] or Weyl semimetal [116] which can be understood by applying the axion electrodynamics [134–136]. To see this we use the electrodynamics conventions of the $U(1)$ gauge field and rewrite

$$\mathcal{L}_\theta=\frac{\theta e^2}{32\pi^2}\varepsilon^{\mu\nu\rho\sigma}F_{\mu\nu}F_{\rho\sigma}=\frac{\theta e^2}{4\pi^2}\boldsymbol{E}\cdot\boldsymbol{B}=\frac{\theta e^2}{2\pi h}\boldsymbol{E}\cdot\boldsymbol{B} \tag{4.83}$$

where $e=\hbar=h/2\pi=1$ are restored. Note that θ is only defined module of 2π. And if require time-reversal, $\theta=0,\pi \mod 2\pi$. If one define $\tilde{F}^{\mu\nu}\equiv\varepsilon^{\mu\nu\rho\sigma}F_{\rho\sigma}$, the $\mathcal{L}_\theta=\frac{\theta e^2}{16\pi^2}F_{\mu\nu}\tilde{F}^{\mu\nu}$.

In general the θ-term can be written [123] as

$$S_\theta=\int_M\theta\,\mathrm{ch}_n(F) \tag{4.84}$$

Here, in general, one can assume θ has space-time dependencies.

Wess-Zumino term

Another important topological term is the Wess-Zumino (WZ) term. Compare with the θ-term, the WZ-term has base manifold 1 dimension lower than the target manifold, $\dim M=\dim N-1$. The Wess-Zumino term can be the map between the base and target manifold $\tilde{\phi}:U=S^{d+1}_{\text{north}}\to N=S^{d+1}$, $\tilde{\phi}$ is the dimensionally extension of the map $\phi:M=S^d\to\Gamma_{\text{north}}\subset S^{d+1}=N$ and we require

$$\phi(x)=\tilde{\phi}(x),\qquad\text{if}\quad x\in\Gamma_{\text{north}} \tag{4.85}$$

with $\Gamma_{\text{north}}=\partial U$ is the equator with the corresponding orientation. One can regard that the WZ-term is living on the boundary of the target manifold

$$S_{\text{top}}=S_{\text{WZ}}[\phi]=w\int_{U=S^{d+1}_{\text{north}}}\tilde{\phi}^*\Omega_N \tag{4.86}$$

one can proof the $S_{\text{WZ}}[\phi]$ is invariant under the continuous deformation of ϕ.

Now we derive the form of WZ-term on the base manifold M, first write the $d+1$ volume form of the target manifold N into a exterior derivative of a d-form by $\Omega_N=\mathrm{d}K_{\text{north}}$

$$S_{\text{WZ}}[\phi]=w\int_{U=S^{d+1}_{\text{north}}}\tilde{\phi}^*\mathrm{d}K_{\text{north}}=\mathrm{i}w\int_U\mathrm{d}\left(\tilde{\phi}^*K_{\text{north}}\right)=\mathrm{i}w\int_{\partial U}\tilde{\phi}^*K_{\text{north}} \tag{4.87}$$

$$=w\int_{\Gamma_{\text{north}}}\tilde{\phi}^*K_{\text{north}}=w\int_{M=S^d}\phi^*K_{\text{north}} \tag{4.88}$$

[2] Or axial anomaly, or abelian anomaly, or Adler–Bell–Jackiw anomaly.

[3] The name is from a brand of laundry detergent, made by Frank Wilczek

On the second line above, we used the condition (4.85). We find that the WZ-term can be written as

$$S_{\mathrm{WZ}}[\phi] = w \int_M \phi^* K_{\mathrm{north}} \tag{4.89}$$

Here the coefficient w should follow a quantization condition. This can be seen by considering the alternative gauge choice which one choose the WZ term to be living on the boundary of the $U = S^{d+1}_{\mathrm{south}}$, and gives the action S'_{WZ}. Now subtract the "north" and "south" actions, one has

$$S_{\mathrm{WZ}}[\phi] - S'_{\mathrm{WZ}}[\phi] = w \int_{S^{d+1}_{\mathrm{S}}} \tilde{\phi}^* \omega + w \int_{S^{d+1}_{\mathrm{N}}} \tilde{\phi}^* \omega = w \int_{S^{d+1}} \tilde{\phi}^* \omega = w \times (\text{integer}) \tag{4.90}$$

Since the exponential of the action $e^{-\mathrm{i}S}$ should be gauge invariant, $e^S - e^{S'} =$, the difference between these actions can be integer times 2π, which requires

$$w = 2\pi k, \quad k \in \mathbb{Z} \tag{4.91}$$

An important example of the WZ-term is the Wess-Zumino-Witten WZW term[4], which is introduce by Witten to the non-linear sigma model [137, 138] in $d = 2$ spacetime dimension and where he found a non-abelian bosonization relation. The setting of the WZW-term is $\phi : M = S^2 \to \Gamma \subset S^2 = N$, $g \in \mathrm{U}(n)$, $U(n)$ is the n-th unitary group. Thus, g in the given basis is a matrix. The WZW action is then

$$S_{\mathrm{WZW}}[g] = \frac{1}{8\pi} \int_{S^2} \mathrm{d}^2 x \, \mathrm{tr} \left(\partial_\mu g \partial_\mu g^{-1} \right) + \Gamma_{\mathrm{WZW}}[g] \tag{4.92}$$

Where the topological WZW-term is

$$\Gamma_{\mathrm{WZW}}[g] = -\frac{i}{12\pi} \int_{B^3} \mathrm{d}^3 x \varepsilon^{ijk} \, \mathrm{tr} \left(g^{-1} \partial_i g \, g^{-1} \partial_j g \, g^{-1} \partial_k g \right) \tag{4.93}$$

Here the matrix multiplications are implied.

Chern-Simons term

The last topological term will be discussed here is the Chern-Simons [139] term. In condensed matter physics, it is especially important for describing integer and fractional Hall effects in space-time dimension $d = 2 + 1$. It is defined as

$$S_{\mathrm{CS}}[A] = \frac{1}{4\pi} \int_{M_3} \mathrm{d}^3 x \varepsilon^{\mu\nu\sigma} A_\mu \partial_\nu A_\sigma \tag{4.94}$$

note that here I add the prefactor [122] $\frac{1}{\mathrm{Area}[S^2]} = \frac{1}{4\pi}$ which makes the integration to be 2π on $M_3 = S^2 \times S^1$

$$S_{\mathrm{CS}}[A] = \frac{1}{4\pi} \int_{M_3} A \wedge \mathrm{d}A \tag{4.95}$$

The S_{CS} and the CS-term has the following properties:

[4] Or Wess-Zumino-Novikov-Witten term.

1. It is not gauge invariant by itself, but gauge invariant on the exponential, and by modules of 2π.
2. It breaks the time-reversal symmetry and parity symmetry.
3. The gauge invariance allows to multiply any integer to the Chern-Simons term.
4. It gives only constraints to the equation of motions. The pure CS action has its Hamiltonian equals to zero [27]. There is no dynamics from merely CS term. The CS term only provide topological data.

We can see that the topological action with CS-term can be written as

$$S_{\text{top}} = kS_{\text{CS}} \tag{4.96}$$

k is an integer to ensure the gauge invariance of $\exp kS_{\text{CS}}$, k is also called the level of the Chern-Simons action.

Last but not the least, although in quantum Hall physics the term in (4.94) is frequently used, the topological action with the full Chern-Simons term in $d = 3$ is

$$S'_{\text{top}} = \frac{k}{4\pi}\int_M \text{tr}\left(A\text{d}A + \frac{2}{3}A^3\right) = k\int_M Q_3(A,F) \tag{4.97}$$

This is also what we saw in (4.57). There are relations between the CS wave functions in $d = 3$ and WZW correlation functions in $d = 2$ are usually called CS/WZW correspondence. This "bulk/boundary" correspondence can be regarded as a specific example of the holographic principle, one may consult the original references, e.g. [140, 141], and other literatures and lecture notes [142]. More recent version of this type of correspondence is the so-called AdS/CFT [143].

4.3.5 Effective field theory with topology

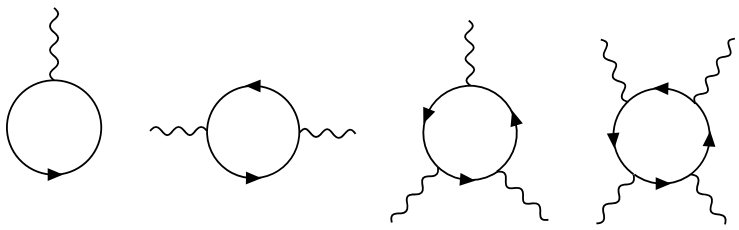

Figure 4.4: One loop diagrams corresponding to C_n. From the left to the right for space-time dimension $d = 1, 3, 5, 7$ respectively. The n is equal to $(d-1)/2$. See also [134, 144].

Consider [142] the Dirac fermions couple to a background $U(1)$ abelian[5] gauge field A, expand the fermionic determinant perturbatively or use Schwinger's proper-time method. The one fermion loop

[5] For A non-abelian the result [142] is

$$S^{\text{CS}}_{\text{eff}} = \frac{N_f}{2}\frac{1}{4\pi}\frac{m}{|m|}\int \text{d}^3x\epsilon^{\mu\nu\rho}(A_\mu\partial_\nu A_\rho + \frac{2}{3}A_\mu A_\nu A_\rho) \tag{4.98}$$

effective action for N_f mass m fermion flavors of Dirac fermion is

$$S_{\text{eff}}(A,m) = N_f \,\mathrm{i}\log\det(\mathrm{i}\partial\!\!\!/ + A\!\!\!/ + m) \tag{4.99}$$

Here $A\!\!\!/ = \gamma^\mu A^\mu$. The γ matrices for three dimension should be used. Expand around A and take the long wave-length $p \to 0$ and large mass $m \to \infty$ limit at zero-temperature, in $d = 2+1$ one have

$$S_{\text{eff}}^{\text{CS}} = \frac{N_f}{2}\frac{1}{4\pi}\frac{m}{|m|}\int \mathrm{d}^3x\epsilon^{\mu\nu\rho}A_\mu\partial_\nu A_\rho \tag{4.100}$$

One can see that this is a pure topological action which is metric independent, and itself has no dynamics. In many quantum systems with topological nature, the effective field theory at IR has the action contains only topological terms[6] just like the above action. These actions can give the topological response of a class of topological insulators [24, 134, 145, 146].

Couple the lattice fermion with an external gauge field A_μ, the effective theory can be also obtain by gradient expanding about the A_μ effective action. The effective action S_{eff} is obtained by integrating out fermion. For instance starting from the partition function [120] of the single particle lattice Hamiltonian[7]

$$e^{\mathrm{i}S_{\text{eff}}} = \int \mathrm{d}[\psi,\psi^\dagger]\exp\mathrm{i}\int \mathrm{d}t\left[\sum_m \psi^\dagger_{m\alpha}\left(i\partial_t\right)\psi_{m\alpha} - H[A]\right] \tag{4.101}$$

$$= \det\left[\left(i\partial_t - A_{0m}\right)\delta^{a\beta}_{mn} - H^{a\beta}_{mn}e^{iA_{mn}}\right] \tag{4.102}$$

Here m,n are lattice indices and α,β are sublattice indices. The A^0_m and A_{mn} are external lattice gauge potentials which should be distinguished with the Berry connection. One can find that the action S_{eff} for IR physics is a topological action proportional to the Chern-Simons action

$$S_{\text{eff}} = \mathrm{C}_n S_{\text{CS}} \tag{4.103}$$

Here C_n is an integer number called the n-th Chern number. The details of the derivation which used gradient expansions can be found in the master thesis of Vaeyrynen [147] for topological insulator, or in an relatively old article of Volovik [148] which is done in the context of He^3 superfluid. More generally the symmetry considerations can also lead to a topological action [122]. Here I focus on the structure that those effective actions imply, by using the known results and skip most of the detail derivations.

The S_{CS} action [144] in odd space-time dimension $d = 2n+1$ is

$$S_{\text{CS}} = \frac{1}{\mathrm{A}_{2n}}\Gamma^{(d=2n+1)}_{\text{CS}} = \frac{1}{\mathrm{A}_{2n}}\varepsilon_{\alpha_1\ldots\alpha_{2n+1}}\int \mathrm{d}^{2n+1}xA_{\alpha_1}\partial_{\alpha_2}A_{\alpha_3}\ldots\partial_{\alpha_{2n}}A_{\alpha_{2n+1}} \tag{4.104}$$

Where A_{2n} is the area of S^{2n}. The prefactor k is computed by the Feynman diagram [144] with $n+1$

[6] As a topological field theory.

[7] Surely the effective field theory is not restricted to the quadratic case.

external photon legs

$$\begin{aligned} \mathrm{C}_n = \mathrm{A}_{2n} \frac{\mathrm{i}\varepsilon_{\alpha_1\beta_1\ldots\alpha_n\beta_n\alpha_{n+1}}}{(n+1)(2n+1)!} \left(\frac{\partial}{\partial\left(q_1\right)_{\beta_1}}\right)\cdots\left(\frac{\partial}{\partial\left(q_n\right)_{\beta_n}}\right) \\ \times \int_{\mathrm{BZ}} \frac{d^{2n+1}p}{(2\pi)^{2n+1}} \operatorname{tr}\left[G(p)\Lambda_{\alpha_1}\left(p, p-q_1\right) G\left(p-q_1\right)\ldots\Lambda_{\alpha_{n+1}}\left(p+q_{n+1}, p\right)\right]\Big|_{q_1=0} \end{aligned} \tag{4.105}$$

Further the Wald identity [28] from the gauge invariance (charge conservation) gives the relation between photon-electron vertex Λ_μ and the fermion propagator G, it reads

$$\Lambda_\mu(p,p) = -\mathrm{i}\frac{\partial}{\partial p_\mu} G^{-1}(p) \tag{4.106}$$

where p is the four-momentum vector. Then the prefactor C_n can be written into the from for dimension $d = 2n+1$

$$\mathrm{C}_n = \frac{(-\mathrm{i})^n \varepsilon_{\mu_1\ldots\mu_{2n+1}}}{(n+1)(2n+1)!} \int \frac{\mathrm{d}^{2n+1}p}{(2\pi)^{2n+1}} \operatorname{tr}\left\{\left[G(p)\partial_{\mu_1} G(p)^{-1}\right]\ldots\left[G(p)\partial_{\mu_{2n+1}} G(p)^{-1}\right]\right\} \tag{4.107}$$

The $d = 2+1$ case of the above equation is interesting and very relevant to condensed matter physics. For topological insulator[134, 145, 149] in $d = 2+1$, we have a Chern-Simons term with prefactor C_1, the first Chern number [134], it reads

$$S_{\mathrm{eff}} = \frac{\mathrm{C}_1}{4\pi} \int dt \int d^2x A_\mu \varepsilon^{\mu\nu\tau}\partial_\nu A_\tau \equiv \int dt \int d^2x \mathcal{L}_{\mathrm{eff}} \tag{4.108}$$

where the $\mathcal{L}_{\mathrm{eff}}$ is Lagrangian density. From this Lagrangian density the current vector [150] can be computed by functional derivative from the $\mathcal{L}_{\mathrm{eff}}[A]$

$$J_\mu(\mathbf{x}) = \frac{\delta\mathcal{L}_{\mathrm{eff}}}{\delta A_\mu(\mathbf{x})} = \frac{\mathrm{C}_1}{2\pi}\varepsilon^{\mu\nu\tau}\partial_\nu A_\tau \tag{4.109}$$

Then the IQHE phenomena are reproduced through this procedure. Recall that

$$F_{\mu\nu} = \partial_\mu A_\nu - \partial_\nu A_\mu \tag{4.110}$$

and $E^i \equiv F^{0i}$, $B_i \equiv \varepsilon_{ijk}\partial_j A_k$ for $i, j, k \neq 0$. One has the spatial current

$$J_i = \frac{\delta\mathcal{L}_{\mathrm{eff}}}{\delta A_i} = \frac{\mathrm{C}_1}{2\pi}(\varepsilon^{i0j}\partial_0 A_j + \varepsilon^{ij0}\partial_j A_0) \tag{4.111}$$

$$J_i = \frac{\mathrm{C}_1}{2\pi}\varepsilon^{ij}E_j \tag{4.112}$$

and the time component of the current is

$$J_0 = \frac{\delta \mathcal{L}_{\text{eff}}}{\delta A_0} = \frac{\mathrm{C}_1}{2\pi}\varepsilon^{0ij}\partial_i A_j = \frac{\mathrm{C}_1}{2\pi}\varepsilon^{ij}\partial_i A_j \tag{4.113}$$

$$J_0 = \frac{\mathrm{C}_1}{2\pi}B \tag{4.114}$$

where $B = B_z$ is point out of the $d_s = 2$ plane, as in the standard Hall effect setup. The conductance tensor [151] σ is defined as

$$J_i = \sigma_{ij}E_j \tag{4.115}$$

then the Hall conductance is that observed in IQHE

$$\sigma_{\mathrm{H}} \equiv \sigma_{xy} = \frac{J_x}{E_y} = \frac{\mathrm{C}_1}{2\pi} = \frac{e^2}{2\pi\hbar}\mathrm{C}_1 = \frac{e}{\Phi_0}\mathrm{C}_1 \tag{4.116}$$

during the last two equal signs, the $e^2/\hbar$ is resumed and the definition of the flux quantum $\Phi_0 = 2\pi\hbar/e$ is used.

Simplified form in non-interacting case

In the context of single-particle lattice Hamiltonian, the case $n = 1$ and $n = 2$ can be simplified into the form

$$\mathrm{C}_1 = \frac{1}{2\pi}\int \mathrm{d}^2 k F_{xy}(\boldsymbol{k}) \tag{4.117}$$

and

$$\mathrm{C}_2 = \frac{1}{32\pi^2}\int \mathrm{d}^4 k \epsilon^{ijk\ell}\,\mathrm{tr}\left[F_{ij}F_{k\ell}\right] = \frac{1}{16\pi^2}\,\mathrm{tr}\int_{M_4} F\wedge F \tag{4.118}$$

These equations can be reached by deforming the original Hamiltonian to the flat band Hamiltonian and uses several projector identities and integrate out the frequency integral. See Ref. [120] or [134] for details. Note that when considering lattice models, the included Berry vector potential is only for the occupied bands.

4.3.6 Interacting topological insulator with Green's functions

From the above discussion, we found that the topological invariant can be also defined for interacting systems. This has been purposed by many authors, for instance, Volovik [152] suggests that for the Fermi liquids one may use the equation (4.107) to compute the topological invariant. The discussions of how to compute the topological invariants for interacting systems can be found in references [153–156] and the references therein, as well as [120, 134, 145]. Let's write down one candidate of the topological invariant for the $d = 2 + 1$ dimensional interacting quantum anomalous Hall (QAH) insulator [154]

$$\mathrm{C}_1 = \frac{\pi}{3}\int \frac{d^3k}{(2\pi)^3}\,\mathrm{tr}\left[\epsilon^{\mu\nu\rho}G\partial_\mu G^{-1}G\partial_\nu G^{-1}G\partial_\rho G^{-1}\right] \tag{4.119}$$

We can see that there is a additional frequency integral, which makes the computation heavier than that for the free Hamiltonian. However, if we have a good approximation of the interacting single particle Green's function $G(k^\mu) \equiv G(\omega, \boldsymbol{k})$ the above invariant is still practically useful.

It is interesting that people further observed [155] that it is possible to evaluate the above formula at zero frequency $\omega \equiv k_0 = 0$ when computing the topological invariants and analogy with the simplification from (4.119) to (4.117), a similar simplification can be taken for the usual topological insulators. Then the frequency integral in 4.119 is avoided.

The topological Hamiltonian is defined as

$$H_{\text{top}}(\boldsymbol{k}) \equiv -G^{-1}(\omega = 0, \boldsymbol{k}) = H_0(\boldsymbol{k}) + \Sigma(0, \boldsymbol{k}) \tag{4.120}$$

Where self-energy[8] $\Sigma(\omega, \boldsymbol{k})$ is corresponding to the interacting Hamiltonian $\hat{H}(\boldsymbol{k}) = \hat{H}_0(\boldsymbol{k}) + \hat{H}_{\text{int}}$. And $\hat{H}_0 \equiv c^\dagger_\alpha(\boldsymbol{k}) H_{\alpha\beta}(\boldsymbol{k}) c_\beta(\boldsymbol{k})$, same indices are summed. The H_{top} is a good object for computing the topological invariant rather than the effective Hamiltonian which is defined as $H_{\text{eff}}(\omega, \boldsymbol{k}) \equiv H_0(\boldsymbol{k}) + \Sigma(\omega, \boldsymbol{k})$. In Ref. [155] Wang and Yan show that the H_{eff} gives a wrong value for the topological invariant of a anomalous quantum Hall model[9], and the H_{top} gives the correct one, although the effective Hamiltonian result is which one may first expect to be correct in a self-consistent quasi-particle picture. The reason is that the topological Hamiltonian correctly take the zero modes' or the edge states' information that are all contained in $G^{-1}(\omega = 0, \boldsymbol{k})$.

The topological invariants can be then computed by modifying the non-interacting invariants through a straightforward substitution, mainly by replacing the non-interacting eigenstates by the eigenstates of H_{top}. The eigenstates $|\alpha(\omega = 0, \boldsymbol{k})\rangle$ of H_{top}

$$G^{-1}(\omega = 0, \boldsymbol{k}) \, |\alpha(\omega = 0, \boldsymbol{k})\rangle = \mu_\alpha(\omega = 0, \boldsymbol{k}) \, |\alpha(\omega = 0, \boldsymbol{k})\rangle \tag{4.121}$$

One still need, in analogy with the occupied band, to define the 'R-zero' as the eigenstate $|\alpha(\omega = 0, \boldsymbol{k})\rangle$ with the eigenvalue $\mu_\alpha(\omega = 0, \boldsymbol{k}) > 0$. These R-zeros span the R-space. Then define the Berry vector potential, or Berry connection

$$\mathcal{A}_i \equiv \mathrm{i} \sum_{\alpha \in \text{R}-\text{space}} \langle \alpha(\omega = 0, \boldsymbol{k}) | \partial_{k_i} | \alpha(\omega = 0, \boldsymbol{k}) \rangle \tag{4.122}$$

then the corresponding field strength is $\mathcal{F}_{ij} \equiv \partial_{k_i} \mathcal{A}_j - \partial_{k_j} \mathcal{A}_i$, the first Chern number is then looks identical to the non-interacting case (4.117), and reads

$$\mathrm{C}_1 = \frac{1}{2\pi} \int \mathrm{d}^2 k \, \mathcal{F}_{xy}(\boldsymbol{k}) \tag{4.123}$$

4.3.7 Dimensional reduction

For topological insulators, Qi, Hughes, and Zhang [24, 134, 145] used a dimensional reduction (Kaluza-Klein) fashion to treat the $d-1$ dimensional time reversal topological insulators as the reduction of the d dimensional charge pump. This procedure is closed related to the Laughlin's argument in the IQHE.

[8] The $\Sigma(\omega, \boldsymbol{k})$ can be computed by a self-consistent method first, though for H_{top} only the $\omega = 0$ part is used.

[9] The Qi-Wu-Zhang model.

Here I follow [24, 134] to briefly discuss how it works. Here we consider a compact Euclidean time $x^0 \in S^1$. For more details see [24, 134, 145], as well as [123].

The example is the case with charge conjugate symmetry C and no others, it is in the Altland-Zirnbauer classes[10] with Cartan label "D". The dimensional ladders are

$$d = 2 + 1 \;\rightarrow\; d = 1 + 1 \tag{4.124}$$

$$\mathbb{Z} \qquad \rightarrow \qquad \mathbb{Z}_2 \tag{4.125}$$

For 2 + 1 dimension, the gapped fermion effective action reads

$$S_{2+1}[A] = \frac{\mathrm{C}_1}{4\pi} \int_{S^1\times S^1\times S^1} \mathrm{d}t\mathrm{d}k^1\mathrm{d}k^2 \epsilon_{\mu\nu\lambda} A^\mu \partial^\nu A^\lambda \tag{4.126}$$

where A^μ is the Berry connection, and C_1 is the first Chern number. Note the superscripts are indices (not powers). Write one of the k directions, say the direction "x^2" into $\Phi(x) = \oint_{S^1} \mathrm{d}x^2 A^2$ gives

$$S_{1+1}[A] = \frac{\mathrm{C}_1}{2\pi} \int_{S^1\times S^1} \mathrm{d}t\mathrm{d}k^1 \Phi(x) \epsilon_{\mu\nu} \partial^\mu A^\nu \tag{4.127}$$

Then we try to restrict the $\Phi(x)$ by the charge conjugate symmetry.

$$\Phi(t, k^1) = \sum_{E_\alpha(k)<0} \oint_{S^1} \mathrm{d}k^2 A^2 = \sum_{E_\alpha(k)<0} \oint_{S^1} \mathrm{d}x^2 \left\langle t, k^1, k^2, \alpha \right| \partial_{x^2} \left| t, k^1, k^2, \alpha \right\rangle \tag{4.128}$$

Where α labels energy eigenstates, i.e., energy bands. The occupied bands are the ones $E_\alpha(k) < 0$, the fermi surface is $E = 0$, and there a gap is assumed. Now apply the charge conjugate which gives

$$|t, k^1, k^2\rangle \rightarrow |t, 2\pi - k^1, -k^2, \alpha\rangle^* \tag{4.129}$$

and

$$E_\alpha(\boldsymbol{k}) \rightarrow -E_\alpha(-\boldsymbol{k}) \tag{4.130}$$

Note the charge conjugate symmetry gives that if E is an eigen energy of the Hamiltonian, then $-E$ is an eigen energy as well. Thus we have

$$\Phi(t, k^1) = \sum_{-E_\alpha(2\pi-k^1,-k^2)>0} \oint_{S^1} \mathrm{d}k^2 \left\langle t, 2\pi - k^1, -k^2 \right|^* \partial_{k^2} \left| k^0, 2\pi - k^1, -k^2 \right\rangle^* = -\Phi(t, 2\pi - k^1) \tag{4.131}$$

where we did $-k^2 \rightarrow k^2$ and used $\partial_{-k} = -\partial_k$. Note $\Phi(t, k^1) = \Phi(t, 2\pi + k^1)$. The integration $\oint_{S^1} \mathrm{d}k^2 \ldots$ can be regarded as a charge pump, namely a Thouless pump. The $\Phi(t, k^1)$ has the physical meaning of the electron polarization, that is the electron displacement, which should only defined mod 2π because of the lattice periodicity. Thus, the following relation is also defined up to 2π

$$\Phi(t, k^1) + \Phi(t, 2\pi - k^1) = 0 \bmod 2\pi \tag{4.132}$$

[10] They will be introduced in the next few sections

and for $k^1 = 0$ or $k^1 = \pi$ we can solve[11]

$$\Phi = 0 \text{ or } \pi \tag{4.133}$$

We assumed $\Phi(t, k^1)$ is a continuous function, other values of Φ will break the charge conjugate symmetry or the continuity of the $\Phi(x)$. The $\{0, \pi\}$ gives a $\mathbb{Z}_2$ classification, where the topological invariant only have two possible values. Here a gauge choice that gives smooth connection A^2 is assumed, a discussion independent of the gauge choice can be found in [134].

We can see that this method can derive a sequence of decedents of a high dimensional topological insulator. This idea can be also applied to reach a complete classification of the non-interacting topological insulators and superconductors [123].

4.4 Discrete symmetries

Discrete symmetries [34, 122, 123] play important rules in the classification of topological insulators. Here I review the discrete symmetries in different space-time dimensions in position space and momentum space. It is instructive to apply the symmetry operation to the Dirac fermion that fulfills the Clifford algebra. The corresponding operation in matrix form of a chosen representation is also presented.

Analogy to the continuous (e.g. Lorentz) transformation $\mathsf{U}(\Lambda)^{-1}\psi(x)\mathsf{U}(\Lambda) = D(\Lambda)\psi(\Lambda^{-1}x)$. The discrete parity transformation P is

$$\mathsf{P}\psi(x) = \mathsf{U}_{\mathcal{P}}^{-1}\psi(x)\mathsf{U}_{\mathcal{P}} = D_{\mathcal{P}}\psi(\mathcal{P}x) \tag{4.134}$$

define the unitary transformation $\mathsf{U}_{\mathcal{P}}$ on field operator $\psi(x)$, the resulting effect is equivalent to multiply a rotation [12] matrix $D_{\mathcal{P}}$ and perform the parity transformation $\mathcal{P}$ to the spacetime coordinate x. Note that $D_{\mathcal{P}}^2 = \pm 1$ is allowed. Similarly, we can define other discrete transformations.

The spatial reflection R_i for i-th spatial direction

$$\mathsf{R}_i\psi(x) = \mathsf{U}_{\mathcal{R}_i}^{-1}\psi(x)\mathsf{U}_{\mathcal{R}_i} = D_{\mathcal{R}_i}\psi(\mathcal{R}_i x) \tag{4.135}$$

The time reversal transformation T with $D(\mathcal{T})^2 = \pm 1$

$$\mathsf{T}\psi(x) = \mathsf{U}_{\mathcal{T}}^{-1}\psi(x)\mathsf{U}_{\mathcal{T}} = D_{\mathcal{T}}\psi(\mathcal{T}x) \tag{4.136}$$

Where $\mathcal{T}x = (-t, x_i)$.

The Z_2 transformation Z_2

$$\mathsf{Z}_2\psi(x) = \mathsf{U}_{\mathcal{Z}}^{-1}\psi(x)\mathsf{U}_{\mathcal{Z}} = D_{\mathcal{Z}}\mathcal{Z}[\psi](x) = -\psi(x) \tag{4.137}$$

Note the $\mathcal{Z}$ is acting on ψ.

Charge conjugate C

$$\mathsf{C}\psi(x) = \mathsf{U}_{C}^{-1}\psi(x)\mathsf{U}_{C} = D_{C}C[\psi](x) \tag{4.138}$$

[11] The mod 2π here allows the appearance of the value 2π, which correspond to a complete pump.

[12] D for Drehung, I thank Lu Yu to point out this to me.

note here the previous coordinate transformation is now act on the operator in a functional like way $C[\psi]$ as the Z_2 case. One possible choice of charge conjugate is $\mathsf{C}\psi(x) = \psi^\dagger(x)$ which is sometimes called particle-hole symmetry.

Chiral transformation S or the sublattice transformation

$$\mathsf{S}\psi(x) = \mathsf{U}_{\mathcal{S}}^{-1}\psi(x)\mathsf{U}_{\mathcal{S}} = D_{\mathcal{S}}\psi(\mathcal{S}x) \tag{4.139}$$

which is the product of the charge conjugate and time reversal $\mathsf{S} = \mathsf{T}\cdot\mathsf{C}$.

All above transformations play some rules in the topological insulators.

The above definitions are general and abstract. We can write down the transforms in a more specific way with matrices. For instance [122], in $d = 2+1$ the time reversal can take the form

$$\mathsf{T}\psi(t,\boldsymbol{x}) = \pm\sigma_1\psi(-t,x_1,x_2) \tag{4.140}$$

and the parity

$$\mathsf{P}\psi(t,x_1,x_2) = \sigma_2\psi(t,-x_1,-x_2) \tag{4.141}$$

the reflection of the first spatial coordinate

$$\mathsf{R}_1\psi(t,x_1,x_2) = \sigma_2\psi(t,-x_1,x_2) \tag{4.142}$$

For topological insulators with a time-independent Hamiltonian. It is usually more direct to use the symmetry transformation on the Hamiltonian matrices. Define $\mathcal{K}$ as the conjugate operation $\mathcal{K}A\mathcal{K}^{-1} = A^*$, the standard form of those transformations are [157] summarize in Table. 4.1.

For lattice Hamiltonians, the particle-hole symmetry (PHS), time-reversal symmetry (TRS) and chiral symmetry (CS) symmetries can be identified by applying symmetry transforms, for instance, for the particle-hole symmetry PHS (or charge conjugating CC), we have

$$D_C \equiv \mathcal{K}C \tag{4.143}$$
$$D_C H(x) D_C^{-1} = H(Cx) \tag{4.144}$$
$$CH(\boldsymbol{k})C^{-1} = -H^*(-\boldsymbol{k}) \tag{4.145}$$

where the criterion is the second or the third line, i.e., if the Hamiltonian fulfills the identity (4.144) or equivalently (4.145) it has PHS. Note we still have two possibilities $\mathsf{C}^2 = \pm 1$, $D_C^* D_C = \pm\mathbb{1}$.

We can also write down the transform for the time reversal symmetry TRS

$$D_{\mathcal{T}} \equiv \mathcal{K}\theta \tag{4.146}$$
$$D_{\mathcal{T}} H(x) D_{\mathcal{T}}^{-1} = H(\mathcal{T}x) \tag{4.147}$$
$$\theta H(\boldsymbol{k})\theta^{-1} = H^*(-\boldsymbol{k}) \tag{4.148}$$

with $D_{\mathcal{T}}^* D_{\mathcal{T}} = \pm\mathbb{1}$.

Cartan Label	Symmetry Operator
BDI, D, DIII	$C = \sigma_1 \otimes \mathbb{1}$
CII, C, CI	$C = i\sigma_2 \otimes \mathbb{1}$
AI, BDI, CI	$\theta = \mathbb{1}$
AII, CII, DIII	$\theta = \mathbb{1} \otimes i\sigma_2$
AIII	$D_{\mathcal{S}} = \sigma_3 \otimes \mathbb{1}$

Table 4.1: The standard transformation matrices. Here $\mathbb{1}$ is the identity matrix with compatible dimension to ensure the total matrix have the correct dimension. From [157].

For the chiral symmetry CS, it is

$$D_{\mathcal{S}} = C\theta \tag{4.149}$$

$$D_{\mathcal{S}} H(x) D_{\mathcal{S}}^{-1} = H(\mathcal{S}x) \tag{4.150}$$

$$D_{\mathcal{S}} H(\boldsymbol{k}) D_{\mathcal{S}}^{-1} = -H(\boldsymbol{k}) \tag{4.151}$$

However if the Hamiltonian has the CS, it has $\mathsf{C}^2 = \pm 1$, $D_{\mathcal{S}}^* D_{\mathcal{S}} = \mathbb{1}$ in contrast to the PHS and TRS. Matrices C, θ and $D_{\mathcal{S}}$ are defined in the Table. 4.1.

4.4.1 Ten-fold way for non-interacting topological insulators

The classification of the non-interacting topological insulators is first done by Kitaev in the Ref. [158], through K-theory. Then Ryu, Schnyder, Furusaki and Ludwig in Ref. [123] used the dimensional reduction in the same spirit of Ref. [134] to clarify the dimensional hierarchy of the 10 symmetry classes of the topological insulators, usually this method is called tenfold way, the classes are called Altland-Zirnbauer classes, since those classed were point in the work early by Alexander Altland and Martin Zirnbauer in 1997 [159]. Although we will not review the long and detailed treatments of the tenfold way here, we list the classification result and it will provide a clear overview of the relations between the topological insulators and their symmetries, as well as the corresponding geometry and topology.

Consider a single particle Hamiltonian

$$\hat{H} = \psi_i^\dagger H_{ij} \psi_j \tag{4.152}$$

where the Hamiltonian matrix H_{ij} can be classified as in the random matrix theory [159], the Altland-Zirnbauer AZ class, by its symmetries. The specific discrete symmetry will point us to a topological invariant that its value can characterize the topological phase of the system. The possible values are Z, $2Z$ and Z_2 for topological insulators. In the papers [123, 158] the discrete symmetries used are time reversal T, charge conjugate C and chiral symmetry S. They provide a periodic table of topological insulators and topological superconductors without particle-particle interactions, i.e. within the one-particle Hamiltonian.

Now we convince ourselves that there are 10, rather than other number of classes. Since we can have $\mathsf{T}^2 = \pm 1$, plus the case without it, there are 3 possibilities. W can also have C since $\mathsf{C}^2 = \pm 1$, there are again 3 possibilities. The chiral symmetry only have two possibilities $\mathsf{S}^2 = 1$ and without it.

Cartan label	T	C	S	$d_s = 0$	1	2	3	4	5	6	7
A	0	0	0	$\mathbb{Z}$	0	$\mathbb{Z}$	0	$\mathbb{Z}$	0	$\mathbb{Z}$	0
AIII	0	0	1	0	$\mathbb{Z}$	0	$\mathbb{Z}$	0	$\mathbb{Z}$	0	$\mathbb{Z}$
AI	+1	0	0	$\mathbb{Z}$	0	0	0	$2\mathbb{Z}$	0	$\mathbb{Z}_2$	$\mathbb{Z}_2$
BDI	+1	+1	1	$\mathbb{Z}_2$	$\mathbb{Z}$	0	0	0	$2\mathbb{Z}$	0	$\mathbb{Z}_2$
D	0	+1	0	$\mathbb{Z}_2$	$\mathbb{Z}_2$	$\mathbb{Z}$	0	0	0	$2\mathbb{Z}$	0
DIII	-1	+1	1	0	$\mathbb{Z}_2$	$\mathbb{Z}_2$	$\mathbb{Z}$	0	0	0	$2\mathbb{Z}$
AII	-1	0	0	$2\mathbb{Z}$	0	$\mathbb{Z}_2$	$\mathbb{Z}_2$	$\mathbb{Z}$	0	0	0
CII	-1	-1	1	0	$2\mathbb{Z}$	0	$\mathbb{Z}_2$	$\mathbb{Z}_2$	$\mathbb{Z}$	0	0
C	0	-1	0	0	0	$2\mathbb{Z}$	0	$\mathbb{Z}_2$	$\mathbb{Z}_2$	$\mathbb{Z}$	0
CI	+1	-1	1	0	0	0	$2\mathbb{Z}$	0	$\mathbb{Z}_2$	$\mathbb{Z}_2$	$\mathbb{Z}$

Table 4.2: Periodic table classification, also called Altland-Zirnbauer classes. T is the time-reversal symmetry, C is the charge-conjugate symmetry, and S is the chiral symmetry. From [123].

The "10" is then a simple counting of numbers, it stands for

$$3 \times 3 - 1 + 2 = 10 \tag{4.153}$$

where "3×3" is counting combinations of T and C. And there is only one of the cases which the chiral symmetry is not fixed by T and C, that is when T and C are not the symmetry of the Hamiltonian but their product S is. This gives us the "$-1 + 2$".

The elements in the periodic table can be related by a dimensional ladder [117, 123]. One well-known example of this kind of dimensional ladder is that in the gauge theory the $d = 4$ spacetime dimension abelian anomaly is equivalent to $d = 3$ parity anomaly and to $d = 2$ non-abelian anomaly, see for instance the Ref. [117].

Let us summarize some of the properties of the AZ classes:

1. There are two subsets, complex and real classes.
2. Only real cases have $\mathbb{Z}_2$ (and $2\mathbb{Z}$).
3. For real classes Z have two decedents, 2Z do not have decedents within the same class.
4. Bott periodicity holds. The table has a dimensional periodicity 8 for real classes. For complex classes it repeats with period 2.

There is a closed relation between the classification of the topological insulators and that of the Anderson localization, where one can see in Table. 4.3. The classification seems can be done by using the K-theory, as it was done originally by Kitaev in the Ref. [158]. The corresponding classifying spaces and the K groups are listed in Table. 4.4.

4.5 Floquet topological matters

The Floquet story of the topological matter is closed to the previous discussions. The topological invariants and Hamiltonians usually have there direct generalizations in the Floquet picture. Beside

Cartan label	T	C	S	$\exp\{itH\}$ for Hamiltonian H	G/H (ferm. NLσM)
A (unitary)	0	0	0	$\mathrm{U}(N)$	$\mathrm{U}(2n)/\mathrm{U}(n)\times\mathrm{U}(n)$
AIII (ch. unit.)	0	0	1	$\mathrm{U}(N+M)/\mathrm{U}(N)\times\mathrm{U}(M)$	$\mathrm{U}(n)$
AI (orthogonal)	+1	0	0	$\mathrm{U}(N)/\mathrm{O}(N)$	$\mathrm{Sp}(2n)/\mathrm{Sp}(n)\times\mathrm{Sp}(n)$
BDI (ch. orth.)	+1	+1	1	$\mathrm{O}(N+M)/\mathrm{O}(N)\times\mathrm{O}(M)$	$\mathrm{U}(2n)/\mathrm{Sp}(2n)$
D(BdG)	0	+1	0	$\mathrm{SO}(2N)$	$\mathrm{O}(2n)/\mathrm{U}(n)$
DIII(BdG)	-1	+1	1	$\mathrm{SO}(2N)/\mathrm{U}(N)$	$\mathrm{O}(2n)$
AII (symplectic)	-1	0	0	$\mathrm{U}(2N)/\mathrm{Sp}(2N)$	$\mathrm{O}(2n)/\mathrm{O}(n)\times\mathrm{O}(n)$
CII (ch. sympl.)	-1	-1	1	$\mathrm{Sp}(N+M)/\mathrm{Sp}(N)\times\mathrm{Sp}(M)$	$\mathrm{U}(2n)/\mathrm{O}(2n)$
C(BdG)	0	-1	0	$\mathrm{Sp}(2N)$	$\mathrm{Sp}(2n)/\mathrm{U}(n)$
CI(BdG)	+1	-1	1	$\mathrm{Sp}(2N)/\mathrm{U}(N)$	$\mathrm{Sp}(2n)$

Table 4.3: Cartan labels and groups of the tenfold way. The T means preserving the time-reversal symmetry, C the charge conjugation, and S the chiral symmetry. Note that in the last column H means a group, not the Hamiltonian, and the cosets G/H correspond to target spaces of the long-wavelength Anderson localization in given symmetries. From [123].

Cartan label	Time evolution operator $\exp\{itH\}$	Fermionic replica NLσM target space	Classifying space for K-theory
A	$\mathrm{U}(N)\times\mathrm{U}(N)/\mathrm{U}(N)$	$\mathrm{U}(2n)/\mathrm{U}(n)\times\mathrm{U}(n)$	$C_0:\mathrm{U}(N+M)/\mathrm{U}(N)\times\mathrm{U}(M)$
AIII	$\mathrm{U}(N+M)/\mathrm{U}(N)\times\mathrm{U}(M)$	$\mathrm{U}(n)\times\mathrm{U}(n)/\mathrm{U}(n)$	$C_1:\mathrm{U}(N)\times\mathrm{U}(N)/\mathrm{U}(N)$
AI	$\mathrm{U}(N)/\mathrm{O}(N)$	$\mathrm{Sp}(2n)/\mathrm{Sp}(n)\times\mathrm{Sp}(n)$	$R_0:\mathrm{O}(N+M)/\mathrm{O}(N)\times\mathrm{O}(M)$
BDI	$\mathrm{O}(N+M)/\mathrm{O}(N)\times\mathrm{O}(M)$	$\mathrm{U}(2n)/\mathrm{Sp}(2n)$	$R_1:\mathrm{O}(N)\times\mathrm{O}(N)/\mathrm{O}(N)$
D	$\mathrm{O}(N)\times\mathrm{O}(N)/\mathrm{O}(N)$	$\mathrm{O}(2n)/\mathrm{U}(n)$	$R_2:\mathrm{O}(2N)/\mathrm{U}(N)$
DIII	$\mathrm{SO}(2N)/\mathrm{U}(N)$	$\mathrm{O}(n)\times\mathrm{O}(n)/\mathrm{O}(n)$	$R_3:\mathrm{U}(2N)/\mathrm{Sp}(2N)$
AII	$\mathrm{U}(2N)/\mathrm{Sp}(2N)$	$\mathrm{O}(2n)/\mathrm{O}(n)\times\mathrm{O}(n)$	$R_4:\mathrm{Sp}(N+M)/\mathrm{Sp}(N)\times\mathrm{Sp}(M)$
CII	$\mathrm{Sp}(N+M)/\mathrm{Sp}(N)\times\mathrm{Sp}(M)$	$\mathrm{U}(n)/\mathrm{O}(n)$	$R_5:\mathrm{Sp}(N)\times\mathrm{Sp}(N)/\mathrm{Sp}(N)$
C	$\mathrm{Sp}(2N)\times\mathrm{Sp}(2N)/\mathrm{Sp}(2N)$	$\mathrm{Sp}(2n)/\mathrm{U}(n)$	$R_6:\mathrm{Sp}(2N)/\mathrm{U}(N)$
CI	$\mathrm{Sp}(2N)/\mathrm{U}(N)$	$\mathrm{Sp}(2n)\times\mathrm{Sp}(2n)/\mathrm{Sp}(2n)$	$R_7:\mathrm{U}(N)/\mathrm{O}(N)$

Table 4.4: Cartan labeled tenfold classes with the space of the time evolution operator, the target space. From [123].

those similarity, there are also new properties that the Floquet topological systems have, the so-called "anomalous" Floquet topological phases.

For Floquet systems we have a time-dependent Hamiltonian with period T

$$H(t) = H(t+T) \tag{4.154}$$

and unitary evolution operator

$$U(t_1, t_0) = \hat{T} \exp\left\{-\mathrm{i}\int_{t_0}^{t_1} H(s)\mathrm{d}s\right\} \tag{4.155}$$

We can choose to set $t_0 = 0$ and define

$$U(t) = \hat{T} \exp\left\{-\mathrm{i}\int_{0}^{t} H(s)\mathrm{d}s\right\} \tag{4.156}$$

The eigenvalues of $H(t)$ now becomes t-dependent and usually is not the most convenient quantity to consider with. One can define the eigenvalue of the unitary operator for one period as

$$U(T)\left|\psi_\alpha\right\rangle = e^{-\mathrm{i}\epsilon_\alpha T}\left|\psi_\alpha\right\rangle \tag{4.157}$$

where ϵ_α is called the quasi-energy of Floquet state $|\psi_\alpha\rangle$. I will discuss more details about the Floquet theory and the quasi-energy in the separated Floquet chapter later. One important property of the quasi-energy is that, it is periodic

$$e^{-\mathrm{i}\epsilon_\alpha T} = \exp\left\{-\mathrm{i}\left(\epsilon_\alpha + \frac{2\pi}{T}\right)T\right\} \rightarrow \epsilon_\alpha = \epsilon_\alpha + \frac{2\pi}{T} \tag{4.158}$$

We can also define the rescaled quasi-energy as

$$\varepsilon = \epsilon T \tag{4.159}$$

which gives a dimensionless version of the quasi-energy.

4.5.1 Floquet topological insulator

Let us first consider a direct application of our knowledge of topological insulators to the Floquet cases. As we see from $H(t,k)$, an additional compact direction S^1 is added to the original manifold M, usually $M = \mathrm{BZ}$ where BZ is the Brillouin zone torus. This can be regarded as a Hamiltonian [14, 157] on

$$S^1 \times \mathrm{BZ} \tag{4.160}$$

This additional S^1 gives new possibilities to the topological invariants. See Fig. 4.5.

4.5.2 Classification of the Floquet topological insulator

The classification of non-interacting topological insulators, in the sense of the tenfold way, is done around 2016, there are many papers contributed to this problem, see [157, 160–162].

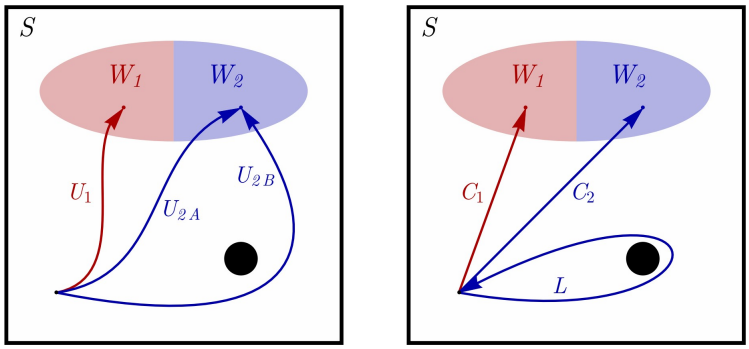

Figure 4.5: (Left) Obstruction of the Floquet unitaries can be regarded in a usual way that a obstruction (black dot) is present and two parameter path of unitary operators, say evolution unitary, U_{2A} and U_{2B} are homotopically distinct since one cannot continuously deform one to another. The obstruction, the black point can be think to be also presented in the time evolution space, that a winding can occur because of the Floquet driving. (Right) Deformed path show that U_{2A} and U_{2B} are different up to a winding L. From [14].

To classify the (non-interacting) Floquet topological system through their discrete symmetries, we need similar but slightly different definitions of the symmetry criteria. By following Ref. [14, 157] we can write down symmetry operations for $H(t)$ and the $U(t)$ as:

The particle-hole[13] symmetry (PHS),

$$\begin{cases} D_C \equiv \mathcal{K}C \\ D_C H(x) D_C^{-1} = H(Cx) \\ CH(x)C^{-1} = -H^*(-\boldsymbol{k},t) \end{cases} \tag{4.161}$$

$$D_C H(\boldsymbol{k},t) D_C^{-1} = -H(-\boldsymbol{k},t) \rightarrow D_C U(\boldsymbol{k},t) D_C^{-1} = U(-\boldsymbol{k},t) \tag{4.162}$$

The time reversal symmetry (TRS)

$$\begin{cases} D_{\mathcal{T}} \equiv \mathcal{K}\theta \\ D_{\mathcal{T}} H(x) D_{\mathcal{T}}^{-1} = H(\mathcal{T}x) \\ \theta H(\boldsymbol{k},t)\theta^{-1} = H^*(-\boldsymbol{k},T-t) \end{cases} \tag{4.163}$$

$$D_{\mathcal{T}} H(\boldsymbol{k},t) D_{\mathcal{T}}^{-1} = H(-\boldsymbol{k},T-t) \rightarrow D_{\mathcal{T}} U(\boldsymbol{k},t) D_{\mathcal{T}}^{-1} = U(-\boldsymbol{k},T-t)U^\dagger(-\boldsymbol{k},T) \tag{4.164}$$

The chiral symmetry (CS)

$$\begin{cases} D_{\mathcal{S}} = C\theta \\ D_{\mathcal{S}} H(x) D_{\mathcal{S}}^{-1} = H(\mathcal{S}x) \\ D_{\mathcal{S}} H(\boldsymbol{k},t) D_{\mathcal{S}}^{-1} = -H(\boldsymbol{k},T-t) \end{cases} \tag{4.165}$$

$$D_{\mathcal{S}} H(\boldsymbol{k},t) D_{\mathcal{S}}^{-1} = -H(\boldsymbol{k},T-t) \rightarrow D_{\mathcal{S}} U(\boldsymbol{k},t) D_{\mathcal{S}}^{-1} = U(\boldsymbol{k},T-t)U^\dagger(\boldsymbol{k},T) \tag{4.166}$$

[13] Or charge conjugation

The matrices θ, $D_{\mathcal{S}}$ and C are defined in Table. 4.1. Note that when the time-reversal operation participates, we have $T \to T - t$ for the periodically driven Hamiltonian.

Now the Floquet version of tenfold way can be derived [157, 162]. For instance in the Ref. [157], Roy and Harper used the Hermitian unitary, which takes the form

$$H_U(\boldsymbol{k}, t) = \begin{pmatrix} 0 & U(\boldsymbol{k}, t) \\ U^\dagger(\boldsymbol{k}, t) & 0 \end{pmatrix} \tag{4.167}$$

And then apply the K-theory to classify the Floquet topological insulators. One can see that the objects that are used for classification is the Floquet unitaries rather than the Hamiltonian. In Ref. [162], Yao, Yan and Wang used the dimensional reduction to do the classification, especially the explicit topological invariants can be found therein. The resulting table is shown in Table. 4.5. One can see from the table that the Floquet topological insulators can have more possible values available for their topological invariants than the topological insulators without drive. Let us focus on a class which has the particle-hole symmetry or chiral symmetry, say the class AIII [161], one can see that there is a pair of invariants $\mathbb{Z}^2$ labeling the topological phase according to Table. 4.5, we can name it

$$\nu = (\nu_0, \nu_\pi) \tag{4.168}$$

This can be understood [161] by noticing that the chiral symmetry maps the quasi-energy $\epsilon \to -\epsilon$, which means if the system has the chiral symmetry[14] the symmetry operation maps $\epsilon T = 0 \to \epsilon T = 0$ and $\epsilon T = \pi \to \epsilon T = -\pi = \pi$, where I used the ϵT is defined mod 2π. Now suppose the bulk unitary have the quasi-energy with gaps around 0 and π. Then the in gap states at $0, \pi$ are protected by this symmetry. The pair of the invariants ν is exactly counting the numbers of the 0-modes and the π-modes. The Floquet topological insulators with $\nu_\pi \neq 0$ is called anomalous, since it is a new phase without a equilibrium counterpart, and it also means the time evolution unitary cannot be written simply as the exponential of the H^{eff}.

4.5.3 Anomalous Floquet topological phase

In the previous sections, the possibilities of the additional topological invariants that is introduced by the periodic drive were briefly discussed. However specific examples are missing. In this section I will first define one of the simplest topological invariants which can capture the ν_π appeared in equation (4.168), by following the work of Rudner, Lindner, Berg, and Levin [125]. We start with the winding number [14, 123, 125, 165] of $S^1 \times \text{BZ} = S^1 \times (S^1 \times S^1) \to U(N)$, which is defined as

$$w[V] = \frac{1}{16\pi^2} \int dt dk_x dk_y \, \text{tr}\left(V^{-1}\partial_t V \left[U^{-1}\partial_{k_x} V, V^{-1}\partial_{k_y} V\right]\right) \tag{4.169}$$

where $[A, B]$ is the commutator, and the $V(t, k_x, k_y)$ should be periodic for all its arguments. Since the Floquet unitary $U(t)$ can be decomposed as $U(t) = V(t)e^{\mathrm{i}H^{\text{eff}}t}$ with fix branch cut convention of the H^{eff}

$$H^{\text{eff}}_\varepsilon(k) = \frac{\mathrm{i}}{T} \log_{-\varepsilon} U(T, k) \tag{4.170}$$

[14] The PHS works similarly, see [163] for some discussions.

Cartan label	T	C	S	$d_s = 0$	1	2	3	4	5	6	7
A	0	0	0	$\mathbb{Z}^{\times N}$	$\emptyset$	$\mathbb{Z}^{\times N}$	$\emptyset$	$\mathbb{Z}^{\times N}$	$\emptyset$	$\mathbb{Z}^{\times N}$	$\emptyset$
AIII	0	0	1	$\emptyset$	$\mathbb{Z}^{\times 2}$	$\emptyset$	$\mathbb{Z}^{\times 2}$	$\emptyset$	$\mathbb{Z}^{\times 2}$	$\emptyset$	$\mathbb{Z}^{\times 2}$
AI	+1	0	0	$\mathbb{Z}^{\times N}$	$\emptyset$	$\emptyset$	$\emptyset$	$\mathbb{Z}^{\times N}$	$\emptyset$	$\mathbb{Z}_2^{\times N}$	$\mathbb{Z}_2^{\times N}$
BDI	+1	+1	1	$\mathbb{Z}_2^{\times 2}$	$\mathbb{Z}^{\times 2}$	$\emptyset$	$\emptyset$	$\emptyset$	$\mathbb{Z}^{\times 2}$	$\emptyset$	$\mathbb{Z}_2^{\times 2}$
D	0	+1	0	$\mathbb{Z}_2^{\times 2}$	$\mathbb{Z}_2^{\times 2}$	$\mathbb{Z}^{\times 2}$	$\emptyset$	$\emptyset$	$\emptyset$	$\mathbb{Z}^{\times 2}$	$\emptyset$
DIII	-1	+1	1	$\emptyset$	$\mathbb{Z}_2^{\times 2}$	$\mathbb{Z}_2^{\times 2}$	$\mathbb{Z}^{\times 2}$	$\emptyset$	$\emptyset$	$\emptyset$	$\mathbb{Z}^{\times 2}$
AII	-1	0	0	$\mathbb{Z}^{\times N}$	$\emptyset$	$\mathbb{Z}_2^{\times N}$	$\mathbb{Z}_2^{\times N}$	$\mathbb{Z}^{\times N}$	$\emptyset$	$\emptyset$	$\emptyset$
CII	-1	-1	1	$\emptyset$	$\mathbb{Z}^{\times 2}$	$\emptyset$	$\mathbb{Z}_2^{\times 2}$	$\mathbb{Z}_2^{\times 2}$	$\mathbb{Z}^{\times 2}$	$\emptyset$	$\emptyset$
C	0	-1	0	$\emptyset$	$\emptyset$	$\mathbb{Z}^{\times 2}$	$\emptyset$	$\mathbb{Z}_2^{\times 2}$	$\mathbb{Z}_2^{\times 2}$	$\mathbb{Z}^{\times 2}$	$\emptyset$
CI	+1	-1	1	$\emptyset$	$\emptyset$	$\emptyset$	$\mathbb{Z}^{\times 2}$	$\emptyset$	$\mathbb{Z}_2^{\times 2}$	$\mathbb{Z}_2^{\times 2}$	$\mathbb{Z}^{\times 2}$

Table 4.5: Floquet tenfold way. From [14, 164]. The possible values ν becomes ν^{n_p}, $n_p = \{1, 2\}$ for with PHS or CS, and ν^{n_p}, $N \in \mathbb{Z}$ otherwise. For instance for class A, $\nu = \mathbb{Z} \to \nu^N = \mathbb{Z}^N$.

where $\varepsilon = \epsilon T$. A periodic V in time t can be deformed from the Floquet unitary through a one parameter family U_s by $U_0 = U$, $U_1 = V_\epsilon$. The homotopy theorem guarantees the topological information is preserved during the deformation. The proper deformed unitary[15] for computing the winding number can be then defined as

$$V_\varepsilon(t, k) = U(t, k)\mathrm{e}^{\mathrm{i}tH_\varepsilon^{\mathrm{eff}}(k)} \tag{4.172}$$

with the branch cut convention [161]

$$\log_{-\varepsilon}\left(\mathrm{e}^{\mathrm{i}\varphi}\right) = \mathrm{i}\varphi \quad \text{for} \quad -\varepsilon - 2\pi < \varphi < -\varepsilon \tag{4.173}$$

The winding number around the rescaled quasi-energy ε is now reached by sending (4.172) to (4.171), that is

$$\begin{aligned} w\left[V_\varepsilon\right] &= \text{Winding number at } \varepsilon \\ &= \frac{1}{16\pi^2}\int dt dk_x dk_y \,\mathrm{tr}\left(V_\varepsilon^{-1}\partial_t V_\varepsilon\left[V_\varepsilon^{-1}\partial_{k_x}V_\varepsilon, V_\varepsilon^{-1}\partial_{k_y}V_\varepsilon\right]\right) \\ &= \text{The number of edge states at one edge} \end{aligned} \tag{4.174}$$

this is "roughly" the degree of map V_ε, and it also takes the form $\int Q(V^{-1}\mathrm{d}V, 0)$, with $Q(A, F)$ the Chern-Simons form.

[15] Originally in Ref. [125] it is defined as

$$U_\varepsilon(\boldsymbol{k}, t) = \begin{cases} U(\boldsymbol{k}, 2t) & \text{if } 0 \le t \le T/2 \\ V_\varepsilon(\boldsymbol{k}, 2T - 2t) & \text{if } T/2 \le t \le T \end{cases} \tag{4.171}$$

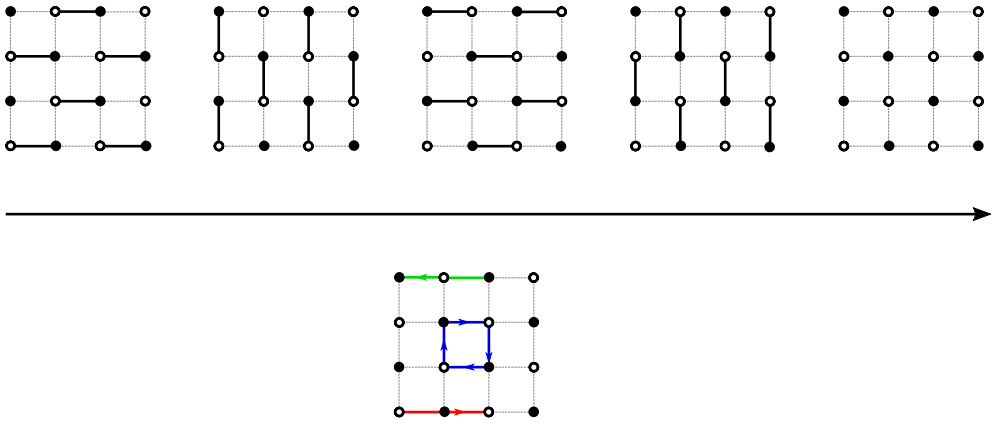

Figure 4.6: The RLBL model [125]. Empty sites are A sites and black sites are B sites. (Upper panel) Snap shot for each $T/5$ in one period, tick line means a non-zero hopping. The arrow means the time direction. (Lower panel) The motion of the particles, green for the upper edge, blue for the in bulk, red for the lower edge. One can see that the edge state is only possible with drive.

One can also [125] show that the Chern number of the quasi-energy window $\varepsilon \in [\varepsilon', \varepsilon]$ is

$$w\left[V_{\varepsilon'}\right] - w\left[V_{\varepsilon}\right] = \mathrm{C}_{\varepsilon\varepsilon'} \tag{4.175}$$

which are the difference between the winding number at the quasi-energies ε and ε'.

4.5.4 Rudner-Lindner-Berg-Levin model

The anomalous Floquet topological phase can be understood better through exampels. Here we reproduce a lattice realization from the Ref. [125]. In [125] Rudner, Lindner, Berg and Levin introduced nowadays called Rudner-Lindner-Berg-Levin RLBL model, named by the authors. The RLBL is a two dimensional, $d_s = 2$, model on a square lattice. The Hamiltonian of the RLBL model is [125]

$$\begin{aligned} \hat{H}(t) &= \sum_{\boldsymbol{k}} \begin{pmatrix} c^{\dagger}_{\boldsymbol{k},A} & c^{\dagger}_{\boldsymbol{k},B} \end{pmatrix} H(\boldsymbol{k},t) \begin{pmatrix} c_{\boldsymbol{k},A} \\ c_{\boldsymbol{k},B} \end{pmatrix} \\ H(\boldsymbol{k},t) &= -\sum_{n=1}^{4} J_n(t) \left(e^{i\mathbf{b}_n\cdot\boldsymbol{k}}\sigma^{+} + e^{-i\mathbf{b}_n\cdot\boldsymbol{k}}\sigma^{-} \right) + \delta_{AB}\sigma_z \end{aligned} \tag{4.176}$$

where $\sigma^{\pm} = \left(\sigma_x \pm i\sigma_y\right)/2$, and the reciprocal vector $\mathbf{b}_1 = -\mathbf{b}_3 = (a, 0)$ and $\mathbf{b}_2 = -\mathbf{b}_4 = (0, a)$. Here we set the lattice constant $a = 1$. The c and $c^{\dagger}$ are the creation and annihilation operators. The time

dependent hopping takes the simple form

$$\begin{cases} J_1(t) = J & \text{if} \quad 0T/5 \le t < 1T/5, \quad J_{i\neq 1} = 0 \\ J_2(t) = J & \text{if} \quad 1T/5 \le t < 2T/5, \quad J_{i\neq 2} = 0 \\ J_3(t) = J & \text{if} \quad 2T/5 \le t < 3T/5, \quad J_{i\neq 3} = 0 \\ J_4(t) = J & \text{if} \quad 3T/5 \le t < 4T/5, \quad J_{i\neq 4} = 0 \\ \text{No hopping} & \text{if} \quad 4T/5 \le t < 5T/5 \end{cases} \tag{4.177}$$

See also the Fig. 4.6 where a cartoon is presented. The above model is the original version of the RLBL model, and the last $1/5$ period is without hopping.

In Fig. 4.7 we present the resulting quasi-energy spectra of the RLBL model for different parameters. Where we can see there are three cases $w = (0, 0)$, $w = (0, 1)$ and $w = (1, 1)$ and

$$w \equiv \left(w\left[V_{\varepsilon=0}\right], w\left[V_{\varepsilon=\pi}\right]\right) \tag{4.178}$$

One can check numerically the direct computation from the (4.174) also gives the same result.

4.6 Examples and numerical methods to compute topological invariants

In many applications of the topological insulator, one will need some efficient numerical methods to determine values of the topological invariants. Here we briefly review several representative method for the topological insulators and Floquet topological insulators. The computation is typically done numerically, by no means that analytical calculations are impossible.

Since the Floquet topological insulator can be regarded as a special generalization of the topological insulator in equilibrium, and the topological invariants of them have similar forms, it is not a surprise that the sets of tools for computing the invariants in both cases are almost identical. I will summarize some of them in the following sections.

4.6.1 Direct methods

One of the most direct methods to compute the topological invariants is to perform the multi-dimensional integral over the closed manifold in the momentum space. Numerically, this is usually performed by finite difference and numerical integration by applying Riemannian sum or other integration methods. For instance the Thouless-Kohmoto-Nightingale-den Nijs (TKNN) invariant [166] for $\mathbb{Z}$ classes is a $d_s = 2$ integration with the Chern character (the field strength) on S^2, denote the resulting number as Ch_1 the first Chern number.

$$\mathrm{Ch}_1 = \int_{k_x, k_y \in T^2} F_{xy}(k_x, k_y) \tag{4.179}$$

In some highly symmetric model, the topological invariant can be computed in an economical way. For instance, if the model has time-reversal invariance and reflection symmetries, the $\mathbb{Z}_2$ invariant of it can be counted [167] at the time-reversal-invariant-momentums (TRIM).

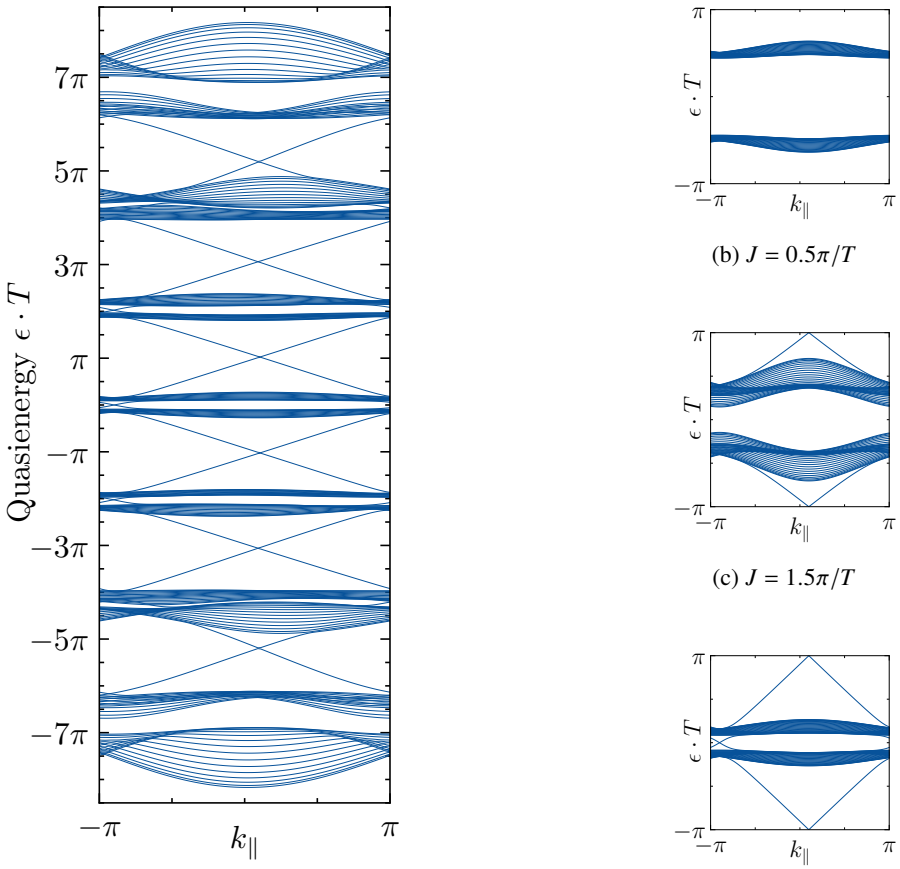

(a) $J = 2.5\pi/T$

(b) $J = 0.5\pi/T$

(c) $J = 1.5\pi/T$

(d) $J = 2.5\pi/T$

Figure 4.7: RLBL model for $\delta_{AB} = 0.5\pi/T$, T is the time period, as in [125]. (Left) Extended zone spectra. (Right) Diagonalize the $U(T, \boldsymbol{k})$.

Band inversion

The band inversion is also an efficient way to identify the topological invariant, at least qualitatively. Suppose one has a two-band model and one knows the band shape of the upper E_u and lower E_d band without coupling between them, i.e, the off-diagonal matrix element switch off. Then if we switch on the off-diagonal matrix elements with not too large values, the band shapes will not change dramatically. If the bands without coupling are overlapped with each other some gaps will be opened at the crossing points of E_u and E_d, and these are also where the edge states cross appears for a open boundary condition.

Edge states

The bulk-boundary correspondence state that the bulk topological invariant is counting the number of the edge states at the boundary. Clear discussions can be found in the Fruchart and Carpentier's review [119] on p.16 with massive Dirac equations in $d_s = 2$, or in the book of Fradkin [24].

For Floquet systems we have already presented an example in the previous section by using the

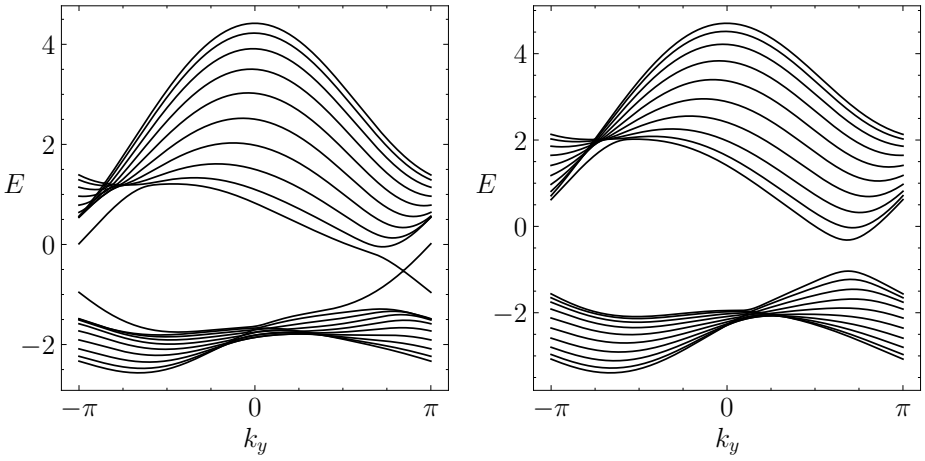

Figure 4.8: Haldane model [111] with cylindrical geometry. The open boundary condition is taken on x direction.

RLBL model as an example.

4.6.2 Fukui-Hatsugai-Suzuki method

Around 2005, Fukui, Hatsugai and Suzuki [168] purposed an efficient numerical algorithm[16] to compute the equation (4.179), the Thouless-Kohmoto-Nightingale-Nijs (TKNN) invariant. This method is now widely used and called Fukui-Hatsugai-Suzuki (FHS) method. In Fig. 4.9 one can see that the first Chern number computed from FHS method for the middle band $\mathrm{Ch}_1 = -2.0000000565$ where the known analytical result is $\mathrm{Ch}_1 = -2$. It returns the integer numbers for a high accuracy to 10^{-7} from a relative coarse 9×27 momentum grid, a single computation at most takes several seconds.

The key part of the FHS method is that to compute the field strength by link variables. Suppose the n-th eigenstate of the Hamiltonian is $|n\rangle$, the link variable is

$$U_\mu(\boldsymbol{k}) \equiv \frac{1}{\mathcal{N}_\mu(\boldsymbol{k})} \langle n(\boldsymbol{k}) | n(\boldsymbol{k} + \hat{e}_\mu) \rangle \tag{4.180}$$

with $\mathcal{N}_\mu(\boldsymbol{k}) \equiv |\langle n(\boldsymbol{k}) | n(\boldsymbol{k} + \hat{e}_\mu)\rangle|$. The $\boldsymbol{k} = (k_{x,i}, k_{y,j})$ is on a two dimensional grid, $i, j \in \mathbb{Z}$ and $i \in [1, N_x]$, $j \in [1, N_y]$. The $\hat{e}_\mu$ is the unit vector on μ direction, $\hat{e}_\mu \equiv L_\mu / N_\mu$, L_μ is the length of the Brillouin zone along μ direction. The field strength, or the Berry curvature F is computed by a Wilson loop

$$F_{xy}(\boldsymbol{k}) \equiv \ln U_1(\boldsymbol{k}) U_2(\boldsymbol{k} + \hat{e}_x) [U_1(\boldsymbol{k} + \hat{e}_y)]^{-1} [U_2(\boldsymbol{k})]^{-1} \tag{4.181}$$

The F should have the its value $-\pi < \frac{1}{\mathrm{i}} F_{xy}(\boldsymbol{k}) \leq \pi$. After we know the field, the first Chern number

[16] From the reference cited there in [168], it seems that they used some techniques from the lattice gauge theory.

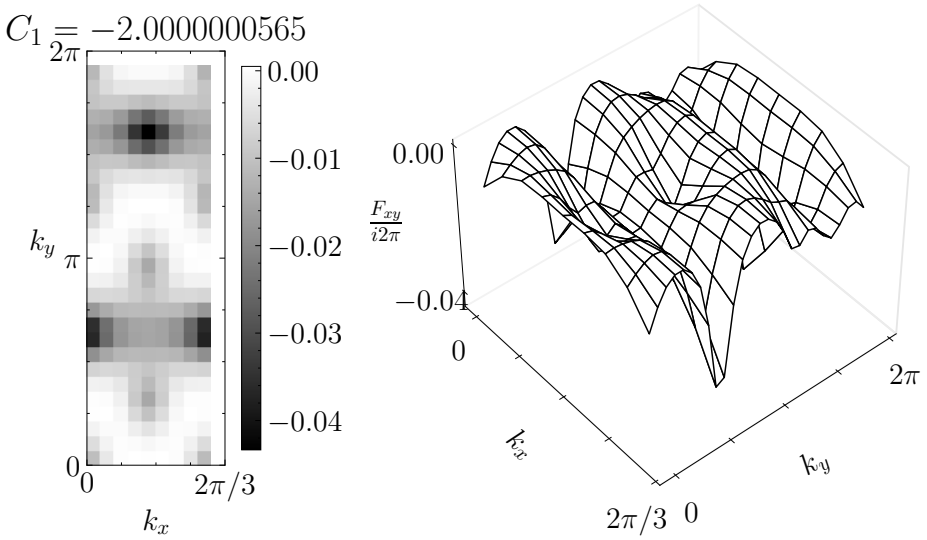

(a) (b)

Figure 4.9: The plots reproduced the setup in the original reference [168] of the Fukui-Hatsugai-Suzuki method. Here the setup is spinless fermions under an external magnetic field, the Hamiltonian is $H = -t\sum_{\langle i,j\rangle} c_i^\dagger e^{i\theta_{i,j}} c_j$, with the flux per plaquette $\phi = \sum_\square \theta_{i,j}/(2\pi) = 1/3$. The $C_1 = \mathrm{Ch}_1$ is the TKNN invariant (first Chern number) of the middle band of the three-band system. Note that due to the magnetic field the Brillouin zone interval changed, since now the Hamiltonian has the periodicity $H(k_x, k_y) = H(k_x + 2\pi/3, k_y) = H(k_x, k_y + 2\pi)$.

of the n-th band can be computed through summation

$$\mathrm{Ch}_{1,n} \equiv \frac{1}{2\pi \mathrm{i}} \sum_{\boldsymbol{k}} F_{xy}(\boldsymbol{k}) \tag{4.182}$$

Note that here the sum $\sum_{\boldsymbol{k}} F(\boldsymbol{k}) \equiv \sum_{i,j} F(k_{x,i}, k_{y,j})$ is without the normalization.

Clearly, the FHS method is applicable to the Floquet topological insulator with periodic boundary condition, i.e., in pure momentum space. One of the application can be found in [169], where they find the Chern invariant/number C_1 of the lower Floquet band in the first Floquet-Brillouin zone can get larger integer numbers when decreasing the driven frequency. This is a result of the periodicity of the quasi-energy that multiple band inversions can contribute. The detail phase diagram marked by different Chern numbers is complicated and available in [169].

4.6.3 Wannier center charge pump method

In 2011 [170], Yu, Qi, Bernevig, Fang, and Dai purposed a version of Wannier center charge pump which provides an intuitive and computational feasible way to compute the $\mathbb{Z}_2$ invariant, for example in the quantum spin Hall effect (QSHE). This method returns charge pump trajectories which are parametrized by k_y, and the topological invariant can be read off from the winding of the trajectories. An introduction can be also found in [171].

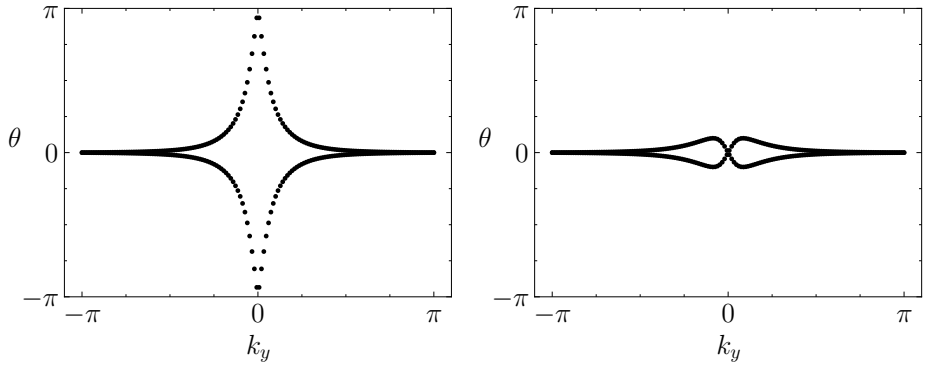

Figure 4.10: The $\mathbb{Z}_2$ Wannier-center charge pump for BHZ model, actually only the part $k_y \in [-\pi, 0]$ is needed for identifying the topological invariant.

The recipe of this method is again simple. Since the discrete non-abelian Berry curvature is

$$F^{mn}_{i,i+1}\left(k_y\right) = \left\langle m, k_{x,i}, k_y \mid n, k_{x,i+1}, k_y \right\rangle \tag{4.183}$$

The $U(2N)$ Wilson loop is $D(k_y) = P\exp\left\{-\mathrm{i}\int_{C_{k_y}} A(\boldsymbol{k})\mathrm{d}k\right\}$, where P is the path ordering, C is the integration contour. Then the D can be obtained through

$$D\left(k_y\right) = F_{0,1}F_{1,2}F_{2,3}\cdots F_{N_x-2,N_x-1}F_{N_x-1,0} \tag{4.184}$$

The Wilson loop has $2N$ eigenvalues which are complex numbers with the angular form

$$\lambda^D_m(k_y) = \left|\lambda^D_m\right| e^{\mathrm{i}\theta^D_m(k_y)}, \quad m = 1, 2, \ldots, 2N \tag{4.185}$$

The Wannier center is then the phase of those eigenvalues

$$\theta^D_m(k_y) = \mathrm{Im}\left[\log \lambda^D_m(k_y)\right] \tag{4.186}$$

In Fig. 4.10 we reproduced the result of [170] for the Bernevig-Hughes-Zhang (BHZ) model. We can see that the topological nontrivial phase has a non-zero winding, since we cannot find a horizontal line without a intersection with the charge pump line. Note the horizontal line should be on the available discrete grid points.

This method is applicable to many studies of topological insulators, see e.g [130]. For the Floquet case, the charge pump method is considered in [172] recently.

4.6.4 Other methods

There are other methods to compute the topological invariants. For instance, the phase band method [160, 173] for the Floquet topological phase. The curvature renormalization group [174], for

Floquet setup, see [175, 176].

4.7 Symmetry protected topological order and intrinsic topological order

Let us end this chapter by some discussions about the definition of the topological order.

Nowadays, popular definitions of the topological order are usually based on the works of Alexei Kitaev [177], or Xiao-Gang Wen [178]. The ideas behind the topological order exists before their works and can be traced back to the early study of the quantum Hall effects, and even earlier in the studies of gauge theories. Roughly speaking, the integer quantum Hall effect (IQHE) and the fractional quantum Hall effect (FQHE) correspond to two different classes, the symmetry-protected topological (SPT) order [179] and intrinsic topological order (ITO). Many of recent studies [177, 180, 181] use category theory and group cohomology, projective symmetry groups, and parton constructions which are surely beyond the scope of our discussion. For topological orders, some recent reviews may be found in [124, 182, 183].

Note the definition of the topological order varies by context and authors. From the field theory point of view [178], one definition is that the topological order exists for a system if the low energy, long wavelength, effective theory of the system is a topological field theory, e.g., a Chern-Simons theory.

From the quantum information point of view [183–186], the considering state[17] of the system with non-trivial SPT are short-range entangled and can be transformed to a product state with finite steps of local[18] unitary transformations without closing the energy gap, however these steps will break at least one of the symmetries of the system. The states with ITO are long-range entangled and any finite steps of local unitary transformations can not continuously, without closing the energy gap, transform it into a product state. Note [183] that if the thermodynamic limit is needed, we assume it is taken first, before any unitary transformation. Further, if ITO is protected by symmetries, they are called symmetry enriched topological order (SET).

With those definitions, for lattice models, the topological insulators (which can have particle-particle interactions) belong to SPT. The toric code [187] belongs to ITO. The ITO usually cannot be described by a band theory picture, and the ground state degeneracy is only depending on the topology.

The SPT and ITO are also both interesting when we study strongly correlated systems. Especially for ITO where the experiment realizations and observations are still limited. The newly developed techniques of the non-equilibrium quantum many-body system may help us to find some way to probe and analyze those phases.

[17] Usually it is the many-body ground state.

[18] Here local means in a finite and small region.

4.8 Summary

In this chapter we reviewed the concepts and formalism of the topological systems. Especially the topological insulator and its required mathematical back ground. We first introduced the geometric and topological aspects of the simple gauge theory through standard examples, the magnetic monopoles. Then we reviewed briefly the effective topological field theory, as long as its application for understanding topological insulators. Several lattice model both for static topological insulator and its generalization, namely the (anomalous) Floquet topological insulator is reviewed as examples. We summarized them by the known ten-fold way and Floquet ten-fold way from discrete symmetries. We also reviewed several numerical method. In the end we discussed briefly the topological order.

Let us also summarize this chapter by the following graph Fig. 4.11.

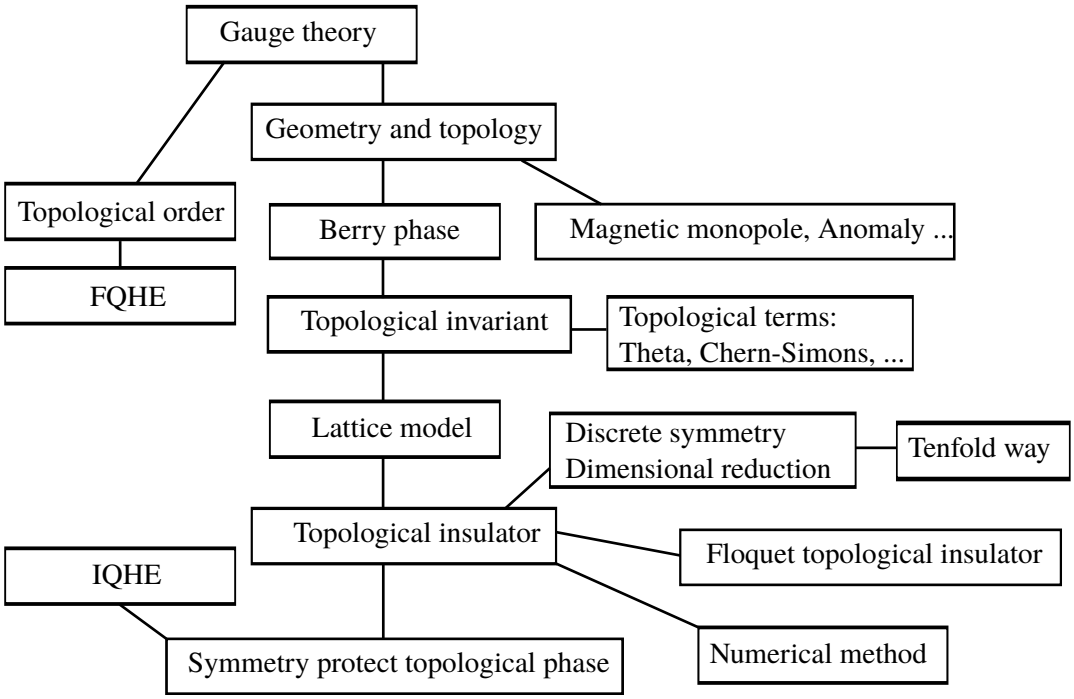

Figure 4.11: A short summary of topological matter.

CHAPTER 5

Periodic driving: Floquet theory

In this chapter, we will introduce the basic concepts of the Floquet system [3, 13–15], which treats the light field semi-classically. By discussing a quantum photon model, we discuss the power and limitations of the Floquet picture. Then we discuss the Floquet theorem, Floquet Green's functions and their properties.

5.1 Semi-classical approximation of the light coupled to a two-level atom

In this chapter we will consider Hamiltonian with time periodic parameters

$$H(t) = H(t+T) \tag{5.1}$$

Where T is the time period, t is the time. People may wonder that how the time-dependent Hamiltonian $H(t) = H(t+T)$ can occur? In this section, I follow [188] to show how can a time-periodic Hamiltonian arise from the semi-classical description of matter coupled to photons. This can be seen from a two-level atom couples to a single photon mode with the Hamiltonian [188]

$$H = \Omega a^\dagger a + \frac{A}{2}\frac{1}{\sqrt{N_{\text{ph}}}}\left(a^\dagger + a\right)\sigma^x + \Delta\sigma^z \tag{5.2}$$

where $a^\dagger$ and a are creation and annihilation operators of photons with energy Ω. A is the coupling constant between light and matter. N_{ph} is the average photon number. The σ matrices are the pauli matrices represent the atomic states. The Δ is the level spacing of the atom.

Recall that we can write[1]

$$Z = \int \mathrm{d}[a^\dagger, a] \exp\left\{\mathrm{i}\int \mathrm{d}t a^\dagger(\mathrm{i}\partial_t - \Omega)a - \frac{A}{2}\frac{1}{\sqrt{N_{\text{ph}}}}\left(a^\dagger + a\right)\sigma^x - \Delta\sigma^z\right\} \tag{5.3}$$

The semi-classical model can be derived by integrating out the photon fields and taking the saddle

[1] I used the same notation for the operator and its coherent state expectation value.

point approximation, the result gives a effective Hamiltonian with periodically modulating parameters

$$H_{\rm sc}(t) = A\cos(\Omega t)\sigma^x + \Delta\sigma^z \tag{5.4}$$

The applicability and applicable regimes of $H_{\rm sc}$ can be check by the exact diagonalization[2]. Use the initial states and measure observable for H and $H_{\rm sc}$ by

$$|\psi_{\rm init}\rangle = |{\rm coh}(N_{\rm ph})\rangle \otimes |\downarrow\rangle\,, \qquad \langle\hat{O}(t)\rangle = \langle\psi_{\rm init}|e^{{\rm i}Ht}\hat{O}e^{-{\rm i}Ht}|\psi_{\rm init}\rangle \tag{5.5}$$

$$|\psi_{\rm sc,init}\rangle = |\downarrow\rangle\,, \qquad \langle\hat{O}(t)\rangle = \langle\psi_{\rm sc,init}|e^{{\rm i}\int H_{\rm sc}(t){\rm d}t}\hat{O}e^{-{\rm i}\int H_{\rm sc}(t){\rm d}t}|\psi_{\rm sc,init}\rangle \tag{5.6}$$

where $|\downarrow\rangle = (0,1)^\intercal$ is the lower atomic state. The photon coherent state is defined as [189]

$$|{\rm coh}(N_{\rm ph})\rangle = e^{-N_{\rm ph}/2}\sum_{n=0}^{\infty}\frac{(N_{\rm ph})^{n/2}}{\sqrt{n!}}|n\rangle \tag{5.7}$$

and $|n\rangle$ is the n-photon Fock state, $N_{\rm ph}$ is the mean photon number $\langle{\rm coh}(N_{\rm ph})|a^\dagger a|{\rm coh}(N_{\rm ph})\rangle = N_{\rm ph}$. The distribution of the photon number is the Poisson distribution and the annihilation operators have the eigenvalues $a\,|{\rm coh}(N_{\rm ph})\rangle = \sqrt{N_{\rm ph}}$, actually the coherent state will have a classical limit when take $N_{\rm ph}\to\infty$.

In Fig. 5.1, I used the package Quspin to produce four plots where one can see that in the uppermost plots the expectation value of the atomic operator $\langle\sigma^x\rangle_{\rm sc}(t)$ from semi-classical Hamiltonian is mostly agreed with that from the quantum Hamiltonian $\langle\sigma^x\rangle(t)$, one can see when the photon number is lower or the coupling strength A is larger, or the driving frequency is lower (closer to the resonance frequency $\Delta = 2$). The results from the semi-classical Hamiltonian (5.4) show more deviation from that of quantum photons (5.2). This is expected since the semi-classical limit works well for large mode occupation number where the fluctuation is suppressed as $1/\sqrt{N_{\rm ph}}$. And near the resonance or at strong coupling, the photon number fluctuations affect the dynamics of the atomic states more pronounced.

The model such as Eq. 5.2 is surely not the only possibility of reaching Eq. 5.4, but it is still one of the possible microscopic origins and it is relevant in the quantum optics context where laser lights, as coherent photon sources, are used.

Some recent theoretical discussions of Floquet (classical, large photon number) for deep quantum regime (cavity, small photon number) can be found in [190], and [191]. Further, as phonon, photon can also induce an effective particle-particle interaction that can support superconductivity [192].

[2] See also the Quspin document https://scipost.org/SciPostPhys.2.1.003/pdf, in the section 2.4 there. We are also following it here.

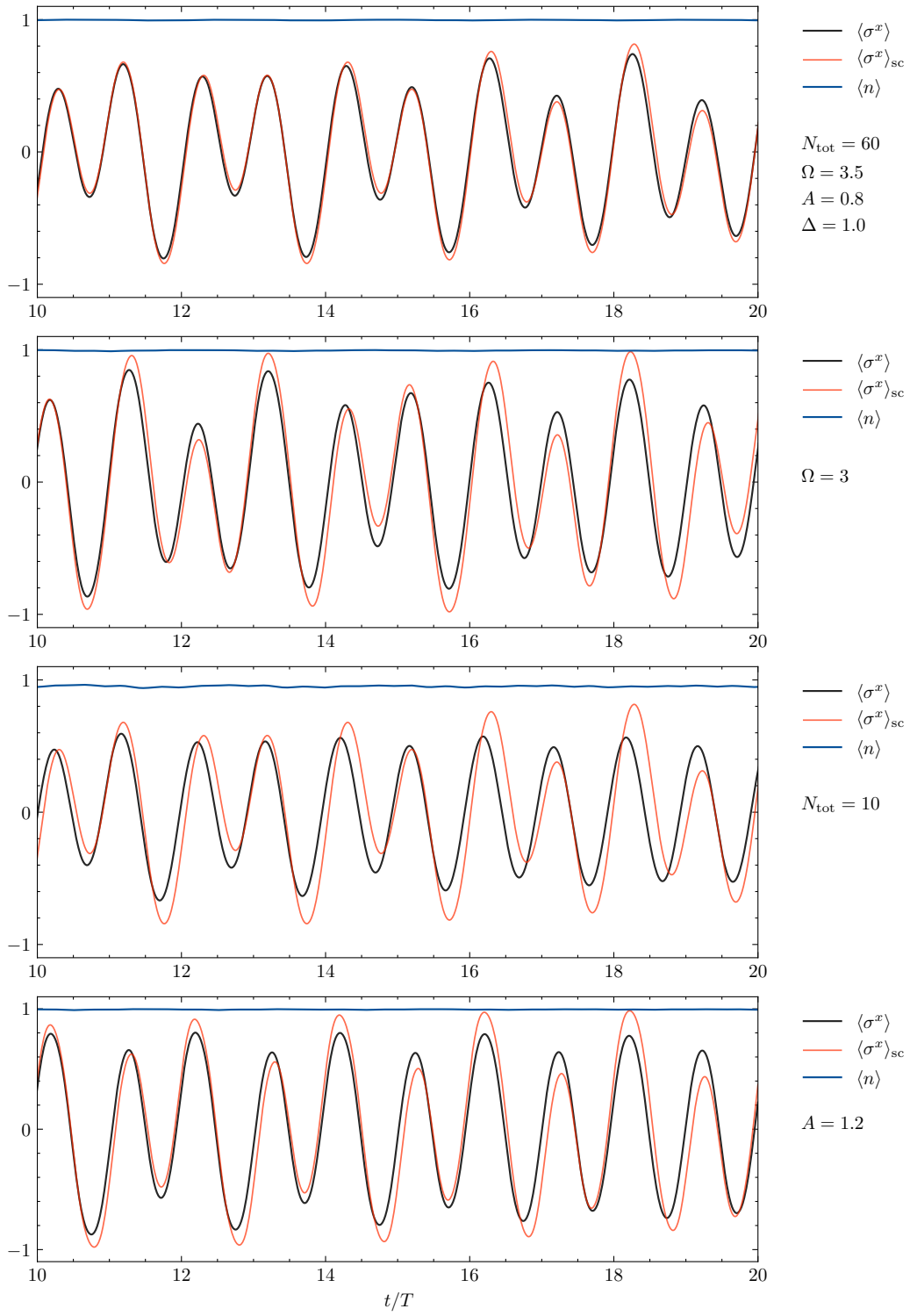

Figure 5.1: Exact diagonalization vs Floquet (semi-classical) approximation for Hamiltonian (5.2) and 5.4. Used Quspin. The $n = a^\dagger a$. The $N_{\rm tot}$ is the maximum photon occupation. $N_{\rm tot} = 2N_{\rm ph}$ where $N_{\rm ph}$ is the average photon number in the initial photon coherent state. The x axis is the time t in unit of the time period $T \equiv 2\pi/\Omega$. Plotted results after 10 periods. Used Quspin.

5.2 Floquet theorem

In this section, we review the use of the Floquet theorem, in the context of quantum mechanical systems.

The Floquet theorem [3] states that if we have the Schrödinger equation with a time periodic Hamiltonian

$$\mathrm{i}\frac{\mathrm{d}}{\mathrm{d}t}\Psi(t) = H(t)\Psi(t), \quad H(t) = H(t+T) \tag{5.8}$$

then we can prove that the time evolution operator $U(t,t_0)$, with $\Psi(t) = U(t,t_0)\Psi(t_0)$, has the property

$$U(t+T,t_0+T) = U(t,t_0) \tag{5.9}$$

and the unitary can be written as

$$U(t,t_0) = P(t,t_0)e^{-\mathrm{i}Qt} \equiv P(t,t_0)e^{-\mathrm{i}H_{\mathrm{eff}}t} \tag{5.10}$$

where P is periodic in time for all of its variables

$$P(t,t_0) = P(t+T,t_0), \quad P(t,t_0) = U(t,t_0)e^{\mathrm{i}H_{\mathrm{eff}}t} \tag{5.11}$$

The P is sometimes called micro-motion operator. The $H_{\mathrm{eff}} \equiv Q$ is a Hermitian matrix called (stroboscopic) Floquet effective Hamiltonian.

We can find that the eigenstates of the time evolution operator over one full period have the following form

$$U(t+T,t_0)\Psi_\alpha(t) = e^{-\mathrm{i}\epsilon_\alpha T}\Psi_\alpha(t), \quad \Psi_\alpha(t) = e^{-\mathrm{i}\epsilon_\alpha t}u_\alpha(t) \tag{5.12}$$

where $u_\alpha(t) = u_\alpha(t+T)$ is a periodic function of t, is called micro-motion of the Floquet state. The real number ϵ_α is called quasienergy which is unique up to integer multiples of $\Omega = 2\pi/T$, and $\Psi_\alpha(t)$ is called Floquet state which is for the quasienergies ϵ_α.

Derive the Floquet theorem

We can justify the (5.10), (5.9) and (5.12) as follows. First we can write out a general form of $U(t,t_0)$ as

$$U(t,t_0) = \hat{T}\exp\left\{-\mathrm{i}\int_{t_0}^{t}\mathrm{d}sH(s)\right\}, \quad U(t+T,t_0+T) = \hat{T}\exp\left\{-\mathrm{i}\int_{t_0+T}^{t+T}\mathrm{d}sH(s)\right\} \tag{5.13}$$

Since $H(t) = H(t+T)$, we have the integral $\int_{t_0+T}^{t+T}\mathrm{d}sH(s) = \int_{t_0}^{t}\mathrm{d}(\tau+T)H(\tau+T) = \int_{t_0}^{t}\mathrm{d}\tau H(\tau)$, which implies $U(t+T,t_0+T) = U(t,t_0)$, see also Eq. 5.9.

Now consider the unitary for one time period T, we can separate the time-periodic part and the non-time-periodic part of the time evolution operator,

$$U(t+T,t_0) = \underbrace{U(t+T,t_0+T)}_{=U(t,t_0)}U(t_0+T,t_0) \tag{5.14}$$

where $U(t_0+T,t_0)$ is frequently called Floquet operator. We can always write the U in terms of a

Hermitian operator $Q(t_0)$ since $U(t_0+T,t_0)$ is unitary, which will give us

$$e^{-\mathrm{i}Q(t_0)T} = U(t_0+T,t_0) \tag{5.15}$$

With the above definitions. The unitary U then can be written as

$$U(t+T,t_0) = U(t,t_0)e^{-\mathrm{i}Q(t_0)T} \tag{5.16}$$

Multiply on right by $e^{\mathrm{i}Q(t_0)(t+T)}$ we have

$$U(t+T,t_0)e^{\mathrm{i}Q(t_0)(t+T)} = U(t,t_0)e^{-\mathrm{i}Q(t_0)T}e^{\mathrm{i}Q(t_0)(t+T)} = U(t,t_0)e^{\mathrm{i}Q(t_0)t} \tag{5.17}$$

This allows us to define a T-periodic operator named $P(t,t_0) \equiv U(t,t_0)e^{\mathrm{i}Q(t_0)t}$,

$$P(t+T,t_0) \equiv U(t+T,t_0)e^{\mathrm{i}Q(t_0)(t+T)} = U(t,t_0)e^{\mathrm{i}Q(t_0)t} = P(t,t_0) \tag{5.18}$$

this actually is what we saw in Eq. 5.10. Now we know that If $\Psi(t)$ is a solution of the Schrödinger equation, then it can be written in terms of a Hermitian operator $Q(t_0)$ and a unitary time-periodic operator $P(t,t_0)$:

$$\Psi(t) = U(t,t_0)\Psi(t_0) = P(t,t_0)e^{-\mathrm{i}Q(t_0)t}\Psi(t_0) \tag{5.19}$$

One can let the initial state $\Psi(t_0)$ to be an eigenstate of $Q(t_0)$, which can be denoted by $\Psi_\alpha(t_0)$ with eigenvalue ϵ_α. This means $Q(t_0)\Psi_\alpha(t_0) = \epsilon_\alpha\Psi_\alpha(t_0)$ and $e^{-\mathrm{i}Q(t_0)t}\Psi_\alpha(t_0) = e^{-\mathrm{i}\epsilon_\alpha t}\Psi_\alpha(t_0)$. We then have

$$\Psi_\alpha(t) = e^{-\mathrm{i}\epsilon_\alpha t}\underbrace{P(t,t_0)\Psi_\alpha(t_0)}_{\equiv u_\alpha(t)} \tag{5.20}$$

One can see that $u_\alpha(t)$ is a periodic function satisfies $u_\alpha(t+T) = u_\alpha(t)$ and this is the reason that people call it micro-motion of the Floquet state. This is exactly the Eq. 5.12. And the quasienergies ϵ_α do not depend on t_0, which allows us to drop the t_0 in $Q(t_0)$.

Note that the above discussions suggest that the $U(t,t_0)$ can be also written in the form [15]

$$U\left(t,t_0\right) \equiv U_F(t)\exp\left\{-\mathrm{i}\left(t-t_0\right)H_F\right\}U_F^\dagger\left(t_0\right) \tag{5.21}$$

where $U_F(t+T) = U_F(t)$ is the micro-motion that is closely related to $P(t,t_0)$, up to a unitary transform. H_F is called effective Hamiltonian. The micro-motion can be written into

$$U_F(t) = e^{-\mathrm{i}K(t)} \tag{5.22}$$

and $K(t)$ is called kick operator [15, 17].

For systems with more than a single level, it is quite rare for people to find analytical expressions for the quasi-energies and Floquet states. However, in some driven two-level systems, the quasi-energy and the time-dependent states can be reached analytically, I will review one of these examples in Section. 5.4. Those analytical results will also show the complexity of the Floquet systems.

Although the analytical solutions for the Floquet eigenvalue problems are rare, there are many efficient numerical methods available, which can help us to understand complex Floquet systems. We discuss two representative methods here in the following sections.

Compute the Floquet states by using Floquet matrix

To determine ϵ_α, we can Fourier expand (mode expand) the $u(t)$ as $u_\alpha(t)$ as $u_\alpha(t) = \sum_n e^{-in\Omega t} u_\alpha^n$, $\Omega = 2\pi/T$, where u_α^n is called the nth Floquet mode of the Floquet state. Then we have

$$\sum_n (H_{mn} - n\Omega\delta_{mn}) u_\alpha^n = \epsilon_\alpha u_\alpha^m \tag{5.23}$$

where

$$H_{mn} \equiv \frac{1}{T}\int_0^T \mathrm{d}t e^{i(m-n)\Omega t} H(t) \tag{5.24}$$

is called Floquet matrix of the Hamiltonian. We can see the quasienergies ϵ_α are the eigenvalues of the infinite-dimensional Floquet matrix $H_{mn} - n\Omega\delta_{mn}$. Note that we can clear see if ϵ_α is an eigenvalue of $H_{mn} - n\Omega\delta_{mn}$, the same holds of $\epsilon + n\Omega$, for arbitrary integer n. To avoid the redundancies of ϵ_α, we may impose a condition for the quasienergies that $-\Omega/2 \leq \epsilon_\alpha < \Omega/2$. By using the Floquet theorem, the time-dependent ordinary differential equations have been transformed into a time-independent eigenvalue problem, which can be solved by simple linear algebra (if one truncates the matrix size).

Compute the Floquet states by using $U(t_0 + T, t_0)$

Another way to compute the Floquet states and quasienergies is to diagonalize the evolution operator for one full period $U(t_0 + T, t_0)$, or equivalently the Floquet effective Hamiltonian[3]

$$H_F = \mathrm{i}\frac{1}{T}\log U(t_0 + T, t_0) \tag{5.25}$$

The eigenstates of the H_{eff}, or equivalently the eigenstates of $U(t_0 + T, t_0)$, are then the Floquet eigenstates $\Psi_\alpha(t_0)$ and we can evolve these states to get in $\Psi_\alpha(t)$ by using (5.20), or we can just use the evolution unitary to envolve $\Psi_\alpha(t_0)$.

Compute the Floquet states by perturbation theories

With the Floquet matrix and quasi-energies, it becomes obvious that the standard perturbation theory techniques can be applied to the periodically driving cases. The popular methods includes Magnus expansions [15], high-frequency expansions [17], the Brillouin-Wigner perturbation theory [169], the adiabatic perturbation theory [193, 194]. Those methods work in a certain parameter region and can be regarded as approximations of the full Floquet matrix.

5.2.1 Floquet Engineering

The periodic drive can considerably change the behaviours of the quantum systems. Where effectively the physical quantities or model parameters like hoppings of the lattice models, band structures, as well as topological properties can be changed in a way where systems without drive can hardly reach. These kinds of manipulations of quantum systems are usually called Floquet engineering [6, 13, 15].

[3] The branch cut of the logarithm may need to be specified in practices

5.3 Heating of periodically driven many-body systems

5.3.1 Heating of Floquet systems

Continously driving systems may introduce heating effects, where the system absorbs energy from the external field/bath and becomes less ordered. In Floquet systems the heating problem is usually unfavourable, since people are interested in the exotic phase and orders with some special occupations of the states. If a system is uniformly occupied, or at "infinite temperature", those exotic phases or orders would be washed out.

General periodically driven systems without any local conserved quantities will likely to end up with infinite temperature $T = \infty$, which is homogeneous with maximum thermodynamic entropy following the volume law. The infinite temperature states are usally featureless. The infinite temperature fate of the Floquet systems can be understood as a result of the Floquet version of the eigenstate thermalization hypothesis (ETH), which may be called Floquet-ETH. For systems with conserved quantities, the infinite temperature can be reached for each sector (of conserved quantity). Note since the ETH is not strictly proofed, the Floquet-ETH is also still a hypothesis, although people verified it in many systems numerically and experimentally [18, 195].

Now we follow [18] to see how the Floquet-ETH happens. We assume the system is prepared at the state $|\chi(t+nT)\rangle = \sum_\alpha c_\alpha \exp(-\mathrm{i}\epsilon_\alpha nT)|\psi_\alpha(t)\rangle$, $|psi_\alpha(t)\rangle$ which is the manybody Floquet eigenstate. The late time density matrix can be written as

$$\langle O\rangle = \langle\chi(t+nT)|O|\chi(t+nT)\rangle = \sum_\alpha \sum_\beta c^*_\alpha c_\beta \mathrm{e}^{-i(\epsilon_\alpha-\epsilon_\beta)nT} \left\langle\psi_\beta(t)|O|\psi_\alpha(t)\right\rangle \tag{5.26}$$

Here the late time means n large, where the Riemann-Lebesgue lemma implies the self-diagonalize of the density matrix, and only $\epsilon_\alpha = \epsilon_\beta$ elements are left non-zero. Mark βs that fulfill the relation $\epsilon_\alpha = \epsilon_\beta$ by $\beta(\alpha)$, then for $n \to \infty$

$$\rho \sim \sum_\alpha \sum_{\beta(\alpha)} \mathrm{e}^{inT\left(\epsilon_\alpha-\epsilon_{\beta(\alpha)}\right)} c^*_\alpha c_{\beta(\alpha)} \left|\psi_\alpha(t)\right\rangle \left\langle\psi_{\beta(\alpha)}(t)\right| \tag{5.27}$$

This is called [18] the quasi-diagonal ensemble. On can see from the above equation that, late time density matrix can be rather featureless since the quasienergies are only conserved up to integer multiples of Ω. This implies a infinite temperature final state.

5.3.2 Possible solutions of the heating problem

As we see from the previous discussions, the Floquet version of eigenstate thermalization (ETH) states that for a closed system the infinite late time states of the system will be at infinite temperature and have the maximum entropy. The thermalization will then wash out many features produced by the periodic drive. For instance, for topological systems such as topological insulators, a well defined and sharp enough Fermi surface inside the bulk spectrum gap is usually required. Then if we require a similar setup in the Floquet driven topological insulator, this kind of occupation seems hard to reach, since the system heats up and the initial filling conditions are destroyed.

To deal with the heating problem, there are at least two possible ways. The first one is that we can find a system with some interesting properties even at the temperature $T_0 \to \infty$. The second way is

that to keep the system away from heating, at least for a long enough time compare to the drive period.

There are three approaches purposed in the literature to avoid heating, or at least partially prevent the system to be heated up for a longer time. They are prethermalization, many-body localization and cooling. [14]

Prethermalization

Prethermalization or prethermal state is a long live meta stable state that a system can reach. Although for late times the system may eventually thermalized, at a time window we can still have some interesting physics. For prethermalization, an estimation of thermalization time for both with and without driving can be found in Ref. [196], and it provides a theorem that may be called Abanin-De Roeck-Ho-Huveneers (ADHH) theorem by the names of the authors. The central result of ADHH can be summarized as follows. For a certain type of short-range Hermitian operator G, we can split it to the form

$$G \equiv \nu N + Y \tag{5.28}$$

Clearly, G can have different meanings, such as Hamiltonian or other Hermitian operators. In the driven case G is the generator in the extended Hilbert (Floquet) space, roughly it is $G = \mathrm{i}\partial_t - H(t)$, in the non-driven case G is the total Hamiltonian. N and Y are the sums of local short-range operators, and the terms are commuting with their summation partners. Note, although in Ref. [196] the operator N should be strictly local, i.e., act on a single site, in Ref. [197] the condition is relaxed to the finite range.

Now in Floquet case, one can choose $\nu = 2\pi/T = \Omega$, which is the driving frequency, $H(t+T) = H(t)$. And $Y = H(t) = D + V(t)$ where D is the time average $(1/T)\int_0^T H(t)$ and $V(t) = H(t) - D$, N is then the rest part in the extended Hilbert space $\nu N = G - Y$ which is closed related to the time derivative. In non-driven case, the ν can be the Hubbard interaction $\nu = U$ in Fermi-Hubbard model [196], then $G = UN + Y$,$Y = H_0$ is the non-interacting part of the total Hamiltonian and N is the Hubbard interaction. Other way around, ν can be the hopping strength for the Majorana chain [197].

From this point of view, in Ref. [196] it is suggested that the thermalization time can be exponentially long if we have the separation of scales which means

$$\nu/J_0 \gg 1 \tag{5.29}$$

Here $J_0 \sim \|Y\|$ is a local energy scale. For example, for Fermi-Hubbard model without driving the J_0 can be the hopping amplitude J_{hop}. In the driving case, the above condition implies a high drive frequency, where "high" means to compare with other local scales of the systems. The thermalization rate $1/\tau_*$ is thus exponentially small [196]

$$\tau_* \sim \exp\left\{c\frac{\nu/J_0}{[1+\log(\nu/J_0)]^3}\right\} \tag{5.30}$$

Here τ_* is the thermalization time which characterizes the time that system needed to be thermalized, c is a constant. The scale separation can let the model follow approximate conservation laws and against fast thermalization. Further discussions about the almost conserved quantities and their rules in protecting edge zero modes in the non-driving case can be found in Ref. [197]. The Ref. [197] discussed the Majorana zero modes of the Kitaev chain, which is important for topological quantum

computing. In Ref. [197], the Majorana zero modes are protected by the quasi-conserving quantities generated by the scale separation. They are then free of "quasiparticle poisoning", the annihilation of the zero modes caused by the bulk quasiparticles.

There are many works that studied the prethermalization of the Floquet systems. For instance, in [198] the many-body prethermalized Thouless pump is studied by exact diagonalizations. The resonantly driven Hubbard model is studied in [199] by using dynamical mean-field theory (DMFT) with non-crossing approximation (NCA) as an impurity solver in the time space. The Ref. [199] gives a resonant example of prethermalization with low drive frequency, where the drive frequency is comparable to the bandwidth, and the system is in the Mott insulator phase. An effective non-interacting Hamiltonian is also suggested in [199] to explain the long lifetime of the quasi-steady state.

Manybody localizations

The long prethermalization time from the scale separations suggest that the novel phenomenons in Floquet systems can be long live if the driven frequency is high enough. There are also other possibilities to keep the system from completely heating up for a long time. On of them is the manybody localization.

The manybody localization [195] (MBL) can protect manybody localized systems form thermalizing by long quantum memories. The thermalization can be understood in a quantum information manner that the initial local quantum information is “diffusing” to the larger area and then are locally lost. The MBL states effectively have local qubits that are approximate integral of motions where the quantum memory can be preserved locally, namely they are not thermalizable.

For manybody localization, there are some good reviews [195, 200]. Good discussions can be found in [18] where the Floquet-ETH and Floquet-MBL phases are discussed. And especially in [18] a “spatio-temporally ordered” phase they called π spin glass (πSG) as an example for the possibility of Floquet-MBL phase which is unique in the driven systems.

Remarkably there are cold atom experiments that realized the MBL Floquet states [201–204], they are also called “Floquet time-crystal” [205] or discrete time-crystal. The π spin glass [206] is recently realized by Google Quantum AI and their collaborators.

Cooling

To avoid heating, one can also couple the system to an external bath, where the heat in the system can be transported to the bath. External baths are common in solid-state systems and has been studied in many references [3]. The external bath can help the system to stay at a finite effective temperature. In general, any open driven quantum system [101] has the potential to be stabilized by its external bath.

Few quantum photons

As we have seen in the previous sections, the Floquet systems can be regarded as a large photon number semi-classical approximation of a quantum light-matter coupled system. The heating problem then can be regarded as the consequence of absorbing a lot of photons. It is then natural to think that if the total photon number is limited to a small number, the heating problem may be avoided. Still a question will be if the interesting properties of the Floquet systems can be kept with such a low number of photons. Some recent studies of cavity quantum electrodynamics setup show that it can be, see for instance [190].

Infinite temperature density matrix

There are other possibilities, where the infinite temperature will still give non-trivial properties. For instance for the systems with the generalized Gibbs ensemble (GGE). Some discussions about GGE can be found in [207], where the density matrix has the form

$$\rho \sim \mathrm{e}^{-\Sigma_\alpha \lambda_\alpha I_\alpha} \tag{5.31}$$

Where the α marks conserving sectors that the system can be decomposed to. The GGE will give disconnected sectors of the system, that can be individually at infinite time. For applications to Floquet systems one may see [87].

5.4 Analytical solution of a simple driven two-level system: RPL

As we discussed at the begining of this chapter, we will review some analytical results for the Floquet systems that can help us to see the complexity of Floquet systems. In this section, I follow the paper by Schmidt, Schnack, and Holthaus [208]. In the Ref. [208] they computed the analytical solutions of the rabi problem with linear polarized driving (RPL), which is a good example. One small technical difference here is that we use Mathematica, which allows one to calculate the solution in the most straightforward way by using the built-in functions of the Mathematica. This makes the reproducing work much simpler.

There are many works on the analytic solutions of driven two-level systems, e.g. see [208–216]. Where in many of them the Schrödinger equation of driven single particle two level systems are rewritten into confluent Heun equations, which has the general solutions named Heun functions [217–220]. Here we will also use this kind of method.

Following [208], we consider the linear polarization Rabi problem (RPL), the Hamiltonian[4] is

$$H(\tau) = \frac{1}{2}\begin{pmatrix} f\sin\tau & \Delta \\ \Delta & -f\sin\tau \end{pmatrix} = \frac{1}{2}\Delta\sigma^x + \frac{1}{2}f\sin\tau\sigma^z \tag{5.32}$$

where $\tau = \Omega t$ is the dimensionless time. One can to scale $\tau \to \tau/\Omega$, $f \to f\Omega$ and $\Delta \to \Delta\Omega$ to recover the dimension of time $[t]$, which has the inverse dimension of energy $[E]^{-1}$. The σ^x and σ^z are Pauli matrices and the f and Δ are real number parameters.

The Schrödinger equation of the dimensionless time is

$$\mathrm{i}\frac{\mathrm{d}\psi(\tau)}{\mathrm{d}\tau} = H(\tau)\psi(\tau) \tag{5.33}$$

here $\psi = (\psi_1, \psi_2)^T$. One can see that for the Hamiltonian (5.32) there are symmetries for the unitaries

$$\widetilde{\mathcal{T}}: \quad U(\pi+\tau,\pi) = \mathcal{T}U(\tau,0)\mathcal{T}, \quad \mathcal{T} = \sigma^x \tag{5.34}$$

and

$$\widetilde{C}: \quad U(\pi-\tau,\pi) = U^*(\tau,0) \tag{5.35}$$

[4] This model can be regarded as the same model as the Eq. 5.4, since a unitary transformation can exchange the position of the Pauli matrices.

as U^* is the complex conjugate of U. The above symmetry implies

$$U(2\pi,\pi) = \mathcal{T}U(\pi,0)\mathcal{T} \tag{5.36}$$
$$U(0,\pi) = U^*(\pi,0) \tag{5.37}$$
$$U(\pi,0) = U\left(\frac{\pi}{2},0\right)^{\intercal} U\left(\frac{\pi}{2},0\right) \tag{5.38}$$

$$U(2\pi,0) = \begin{pmatrix} \psi_1(2\pi) & -\psi_2^*(2\pi) \\ \psi_2(2\pi) & \psi_1^*(2\pi) \end{pmatrix} = \begin{pmatrix} 1-2r_0^2 & 2ir\sqrt{1-r_0^2}e^{-i\alpha_0} \\ 2ir_0\sqrt{1-r_0^2}e^{i\alpha_0} & 1-2r_0^2 \end{pmatrix} \tag{5.39}$$

where the explicit form of r_0 and α_0 will be defined later through Heun functions.

In above (5.33) are two coupled first-order ordinary differential equation. By substituting one to another, it is possible to eliminate $\psi_2(\tau)$ (or $\psi_1(\tau)$) and the resulting equation of ψ_1 (ψ_2) is now second order. Then we can apply suitable variable transformations where the above equations can be written into a confluent Heun equation

$$\frac{\mathrm{d}^2y}{\mathrm{d}z^2} + \left(\frac{\gamma}{z} + \frac{\delta}{z-1} + \epsilon\right)\frac{\mathrm{d}y}{\mathrm{d}z} + \frac{(\alpha z - q)}{(z-1)z}y = 0 \tag{5.40}$$

We can see that at $z = 1$ the equation is singular. The above equation confluent Heun equation is solved by the confluent Heun functions[5], just like the hypergeometric functions which solves hypergeometric differential equation. The Heun function HeunC(z) have 5 parameters and can be written as

$$\mathrm{HeunC}(q,\alpha,\gamma,\delta,\epsilon,z) \tag{5.41}$$

For $\psi_1(\tau)$ with the Hamiltonian (5.32), the suitable transformations are

$$z(\tau) = \sin^2\frac{\tau}{2}, \qquad y_1(z) = e^{-\mathrm{i}fz(\tau)}\psi_1(\tau) \tag{5.42}$$

and the corresponding solution $y_1(z)$ is

$$y_1(z) = \mathrm{HeunC}\left(q = \frac{1}{4}\left(\Delta^2 + 4if\right), \alpha = 2\mathrm{i}f, \gamma = \frac{1}{2}, \delta = \frac{1}{2}, \epsilon = 2if, z\right) \tag{5.43}$$

For $\psi_2(\tau)$ the transformations are

$$z(\tau) = \sin^2\frac{\tau}{2}, \qquad y_2(\tau) = \left(\frac{1}{-\mathrm{i}v\sqrt{z(\tau)}}e^{\mathrm{i}fz(\tau)}\psi_2(\tau)\right)^* \tag{5.44}$$

the solution $y_2(z)$ is

$$y_2(z) = \mathrm{HeunC}\left(q = \frac{1}{4}\left(8\mathrm{i}f + \Delta^2 - 1\right), \alpha = 3\mathrm{i}f, \gamma = \frac{3}{2}, \delta = \frac{1}{2}, \epsilon = 2\mathrm{i}f, z\right) \tag{5.45}$$

[5] Here I use the name in Mathematica, i.e. HeunC it is available since version 12.0.

Now we are ready to compute quasienergies. We can define two constants for convenience [208]

$$\begin{aligned} r_0 &= -\sqrt{2}\Delta\,\mathrm{Re}\left(e^{\mathrm{i}f}\,y_1(z)y_2(z)\right)\Big|_{z=\frac{1}{2}} \\ \alpha_0 &= \arg\left(e^{\mathrm{i}f}\,y_1^2(z) - \tfrac{\Delta^2}{2}e^{-\mathrm{i}f}\,(y_2^2(z))^*\right)\Big|_{z=\frac{1}{2}} \end{aligned} \tag{5.46}$$

The dimensionless quasienergy ϵ/Ω is then directly related to r_0 by [208]

$$\pm\frac{\epsilon(f,\Delta)}{\Omega} = \mp\frac{1}{\pi}\arcsin\left(-r_0\right) \tag{5.47}$$

See also Fig. 5.2. The α_0 will be used to calculate the wave function.

To get the wave-function $\psi(\tau)$, we can first define its components into real and imaginary parts as follows

$$\psi(\tau) = \begin{pmatrix}\psi_1(\tau)\\ \psi_2(\tau)\end{pmatrix} = \begin{pmatrix}u_1(\tau)+\mathrm{i}v_1(\tau)\\ u_2(\tau)+\mathrm{i}v_2(\tau)\end{pmatrix} \tag{5.48}$$

It is obvious that the $\psi_{1/2}$ can be computed from $y_{1/2}$ immediately through

$$\psi_1(\tau) = e^{\mathrm{i}f\,z}y_1(\tau), \qquad \psi_2(\tau) = -\mathrm{i}\Delta\sqrt{z}e^{-\mathrm{i}f\,z}y_2^*(\tau) \tag{5.49}$$

However we will face a problem when $y(z)$ pass the singular point $z = 1$ (or $\tau = \pi$). To deal with the singular points, one can use the solutions in the first quarter, i.e. in $[0, \pi/2)$, to recover the whole period $[0, 2\pi)$ by applying symmetry identities (5.36), see also Fig. 5.4. In below, from (5.50) to (5.53), I list the relations between the $\psi(\tau)$ when $\tau \in [0, \pi/2)$ and ψ when τ in other intervals belongs to $[0, 2\pi)$ provided in [208].

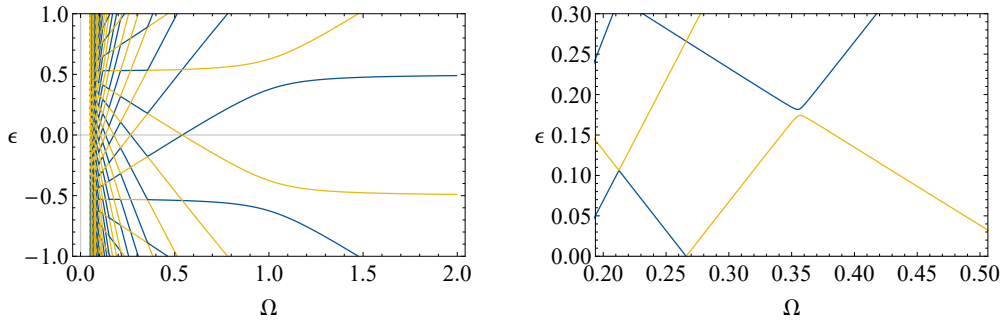

Figure 5.2: Quasi-energies ϵ vs Ω with the amplitude $F = f\Omega = 1/2$ and the Larmor frequency $\Omega_0 = \Delta\Omega = 1$. Start from $\Omega = 0.05$ to avoid extremely low driven frequency. Included up to ± 20 side bands to reach low driven frequencies. (left) The quasienergies ϵ vs Ω. (right) One can see that there are small avoided crossing between Floquet side bands.

Here I list the definition of u_1, u_2 and v_1, v_2, following [208] In the interval $\tau \in [0, \pi/2)$ one has

$$u_1 = \mathrm{Re}\,\psi_1(\tau), \quad v_1 = \mathrm{Im}\,\psi_1(\tau), \quad u_2 = \mathrm{Re}\,\psi_2(\tau), \quad v_2 = \mathrm{Im}\,\psi_2(\tau) \tag{5.50}$$

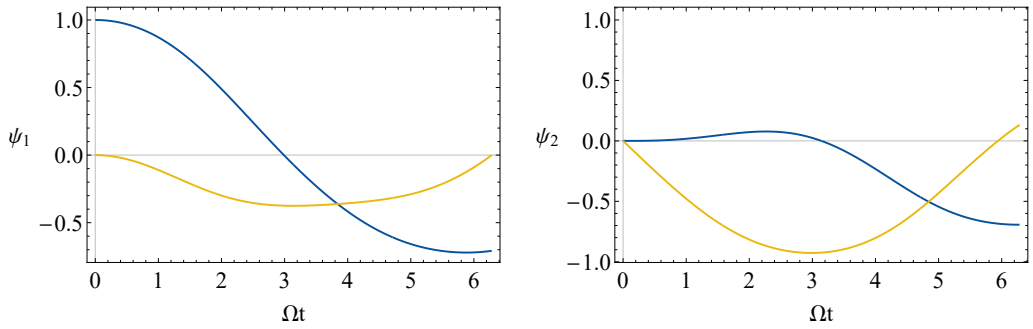

Figure 5.3: Wave-function components $\psi_1(\tau)$ (left) and $\psi_2(\tau)$ (right), with $\tau \equiv \Omega t$. The model parameters are $f = 1/2$ and $\Delta = 1$. The blue (orange) lines are the real (imaginary) parts.

Figure 5.4: RPL two-level state

In the interval $\tau \in [\pi/2, \pi)$ one has

$$\begin{aligned}
u_1(\tau) =& \sqrt{1-r^2}\left(u_1(\pi-\tau)\cos\alpha_0 + v_1(\pi-\tau)\sin\alpha_0\right) + r_0 v_2(\pi-\tau)\\
v_1(\tau) =& \sqrt{1-r_0^2}\left(u_1(\pi-\tau)\sin\alpha_0 - v_1(\pi-\tau)\cos\alpha_0\right) - r_0 u_2(\pi-\tau)\\
u_2(\tau) =& \sqrt{1-r_0^2}\left(u_2(\pi-\tau)\cos\alpha_0 + v_2(\pi-\tau)\sin\alpha_0\right) - r_0 v_1(\pi-\tau)\\
v_2(\tau) =& \sqrt{1-r_0^2}\left(u_2(\pi-\tau)\sin\alpha_0 - v_2(\pi-\tau)\cos\alpha_0\right) + r_0 u_1(\pi-\tau)
\end{aligned} \tag{5.51}$$

In the interval $\tau \in [\pi, 3\pi/2)$ one has

$$\begin{aligned}
u_1(\tau) &= \sqrt{1-r_0^2}\left(u_1(\tau-\pi)\cos\alpha_0 + v_1(\tau-\pi)\sin\alpha_0\right) - r v_2(\tau-\pi)\\
v_1(\tau) &= \sqrt{1-r_0^2}\left(-v_1(\tau-\pi)\cos\alpha_0 + u_1(\tau-\pi)\sin\alpha_0\right) + r_0 u_2(\tau-\pi)\\
u_2(\tau) &= \sqrt{1-r_0^2}\left(-u_2(\tau-\pi)\cos\alpha_0 - v_2(\tau-\pi)\sin\alpha_0\right) - r_0 v_1(\tau-\pi)\\
v_2(\tau) &= \sqrt{1-r_0^2}\left(v_2(\tau-\pi)\cos\alpha_0 - u_2(\tau-\pi)\sin\alpha_0\right) + r_0 u_1(\tau-\pi)
\end{aligned} \tag{5.52}$$

In the interval $\tau \in [3\pi/2, 2\pi)$ one has

$$\begin{aligned}
u_1(\tau) &= \left(1-2r_0^2\right)u_1(2\pi-\tau) + 2r_0\sqrt{1-r_0^2}\left(v_2(2\pi-\tau)\cos\alpha_0 - u_2(2\pi-\tau)\sin\alpha_0\right)\\
v_1(\tau) &= \left(1-2r_0^2\right)v_1(2\pi-\tau) + 2r_0\sqrt{1-r_0^2}\left(u_2(2\pi-\tau)\cos\alpha_0 + v_2(2\pi-\tau)\sin\alpha_0\right)\\
u_2(\tau) &= -\left(1-2r_0^2\right)u_2(2\pi-\tau) + 2r_0\sqrt{1-r_0^2}\left(v_1(2\pi-\tau)\cos\alpha_0 - u_1(2\pi-\tau)\sin\alpha_0\right)\\
v_2(\tau) &= -\left(1-2r_0^2\right)v_2(2\pi-\tau) + 2r_0\sqrt{1-r_0^2}\left(u_1(2\pi-\tau)\cos\alpha_0 + v_1(2\pi-\tau)\sin\alpha_0\right)
\end{aligned} \tag{5.53}$$

We can see that the solutions of a simple driven two-level system, RPL, can be rather complicated. Despite the great value of the analytical solutions, the complications limit their use, if available, in general problems, especially in searching exotic phases. In later sections, I will introduce several numerical or semi-analytical methods which are suitable for driven multi-level quantum systems and the driven quantum lattice models.

5.5 Floquet Green's functions

Here we introduce the so-called Floquet Green's functions [3, 100, 101, 169, 221–224]. We will see that the Floquet Green's functions especially the retarded ones are Green's functions of the Floquet matrix.

5.5.1 Floquet matrix and the extended zone

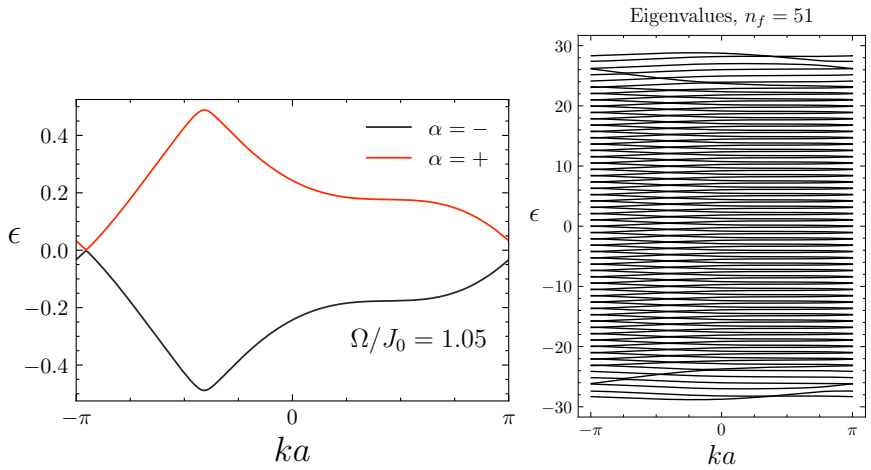

(a) The quasienergies in the FFZ

(b) The eigenvalues of the extended zone Floquet matrix

Figure 5.5: The quasienergies for a Floquet $d_s = 1$ lattice model, the Rice-Mele model with $\Delta_0 = 3.0/J_0$, $J_0 = 1.0$, $\delta_0 = 1.0/J_0$, $\phi = 0$.

We first review the Floquet matrix. The the extended zone Hilbert space [225] is

$$\mathscr{T} \times \mathscr{H} \tag{5.54}$$

with the basis

$$|m\rangle \otimes |i\rangle \tag{5.55}$$

where states $|i\rangle \in \mathscr{H}$ are the states in the original Hilbert space $\mathscr{H}$. $\mathscr{T}$ is the Floquet mode space $|m\rangle \in \mathscr{T}$.

We have seen in the Section. 5.1, one possible microscopic origin of the Floquet matrix (Hamiltonian). The semi-classical approximation works better for higher photon occupation numbers and higher frequency, where the quantum fluctuation from the photon field is getting smaller.

If we treat the photons as external classical field/bath, then the energies of the system have a energy conservation law only up to integer multiple of photon energy $\pm n\Omega$. And the state $|m\rangle \otimes |i\rangle$ can be regarded as m-photon dressed state. Since the photon number is assumed to be very large [225], the m is corresponding to a chosen reference "0". And the Floquet matrix has the general form

$$\mathcal{H}_{mn} = H_{m-n} - \delta_{mn} n\Omega = \begin{pmatrix} \ddots & \ddots & \ddots & \ddots & \ddots \\ \ddots & H_0 + \Omega\mathbb{1} & H_1 & H_2 & \ddots \\ \ddots & H_{-1} & H_0 & H_1 & \ddots \\ \ddots & H_{-2} & H_{-1} & H_0 - \Omega\mathbb{1} & \ddots \\ \ddots & \ddots & \ddots & \ddots & \ddots \end{pmatrix}$$

with the basis

$$|m\rangle \otimes |i\rangle = (\cdots, |\psi_i\rangle \otimes |-1\rangle, |\psi_i\rangle \otimes |0\rangle, |\psi_i\rangle \otimes |+1\rangle, \cdots)^{\mathsf{T}} \tag{5.56}$$

See also (5.23).

A simple example of the time-periodic Hamiltonian would be

$$H(t) = H_0 + H_1 e^{-i\Omega t} + H_{-1} e^{+i\Omega t} = H_0 + \Delta e^{-i\Omega t} + \Delta^\dagger e^{+i\Omega t} \tag{5.57}$$

which can be written into Floquet matrix

$$\begin{pmatrix} \ddots & \ddots & & & \\ \ddots & H_0 - \Omega\mathbb{1} & \Delta & 0 & \\ & \Delta^\dagger & H_0 & \Delta & \\ & 0 & \Delta^\dagger & H_0 + \Omega\mathbb{1} & \ddots \\ & & & \ddots & \ddots \end{pmatrix}$$

5.5.2 Floquet Green's function

In this section, we introduce Floquet representations [3, 221] of the Green's functions. We assume the Green's functions have the symmetry

$$G(t+T, t'+T) = G(t, t') \tag{5.58}$$

This symmetry is true for the Green's functions of the Hamiltonian $H(t) = H(t+T)$ and in a non-equilibrium steady state. I will first derive Floquet representations of Green's functions through the Floquet matrix and Floquet states in the extended zone and then relate them to the time-space Green's functions.

The Floquet representation [3, 221] has a important property that it transforms the following convolution into a matrix product if A and B have the symmetry (5.58). That is

$$[A \circ B]_{mn}(\omega) = [\int_{t'} A(t, t') B(t', t'')]_{mn}(\omega) = A_{mn}(\omega) B_{nl}(\omega) \tag{5.59}$$

This suggests us to define

$$G^R_{mn}(\omega) \equiv \left[\frac{\mathbb{1}}{\omega - \mathcal{H} + \mathrm{i}0^+}\right]_{mn} \tag{5.60}$$

Which is the Floquet representation of $[\mathrm{i}\partial_t - H(t)] \circ G^R(t,t') = \mathbb{1}$. The Floquet matrix $\mathcal{H}$ is defined as

$$\mathcal{H}_{mn} \equiv \int_t (\mathrm{i}\partial_t - H(t)) e^{\mathrm{i}(m-n)\Omega t} \tag{5.61}$$

In this section we always stay in the extended Hilbert space. In the next section, I will show how to get them from the time domain form of the Green's functions.

We can first discuss Floquet systems that have a single level. For a general Floquet matrix of a single level [221], the dimension of the original Hilbert space $\dim \mathscr{H} = 1$. The retarded Green's function in the Floquet representation is[6]

$$\mathcal{H}_{mn}\mathcal{U}_{na} = \epsilon_a \mathcal{U}_{ma} \tag{5.62}$$

and

$$G^R{}_{mn}(\omega) \equiv [(\omega\mathbb{1} - \mathcal{H} + \mathrm{i}0^+)^{-1}]_{nm} = \mathcal{U}_{ma}\frac{\delta^{ab}}{\omega - \epsilon_a + \mathrm{i}0^+}\mathcal{U}^\dagger{}_{bn} \tag{5.63}$$

Note that same indices are summed. We will usually assume the summation of the same indices in most of the time. Clearly the $\mathcal{U}_a{}^m$ is the m-th component of the a-th eigenvector of the Floquet matrix $\mathcal{H}_{mn}$. For the single band (flavor) case the matrix $\mathcal{U}_{ma}$ is a $n_F \times n_F$ square matrix with n_F the dimension of the Floquet space $\mathscr{F}$, which is infinite. The unitary matrix $\mathcal{U} = \{\dots u_a \dots\}$ diagonalizes the Floquet matrix $\mathcal{H}$ and the Green's function matrix $(\omega I - \mathcal{H} + \mathrm{i}0^+)^{-1}$ has the matrix form

$$\mathcal{U}^\dagger \mathcal{H}\mathcal{U} = \mathrm{diag}\{\dots, \epsilon_{a-1}, \epsilon_a, \epsilon_{a+1}, \dots\} \tag{5.64}$$

and

$$\mathcal{U}^\dagger \frac{1}{\omega\mathbb{1} - \mathcal{H} + \mathrm{i}0^+}\mathcal{U} = \mathrm{diag}\left\{\dots, \frac{1}{\omega - \epsilon_a + \mathrm{i}0^+}, \dots\right\} \tag{5.65}$$

Use the identity $G_{m,n}(\omega) = G_{m+l,n+l}(\omega - l\Omega)$ which I will derive in the next section around (5.85), one can see

$$G^R{}_{mn}(\omega) = G_{m+l,n+l}(\omega - l\Omega) = \mathcal{U}_{m+l,a}\frac{\delta^{ab}}{\omega - l\Omega - \epsilon_a + \mathrm{i}0^+}\mathcal{U}^\dagger{}_{b,n+l}, \quad \text{No } l \text{ summation} \tag{5.66}$$

Where $\omega \in (-\infty, +\infty)$. From this identity we can see the redundancies of the above definitions. The redundancies can be eliminate. We can shift ω back to the interval $\omega \in [-\frac{\Omega}{2}, \frac{\Omega}{2}]$ through the above identity and sum them all

$$G^R{}_{mn}(\omega) = \sum_l G_{m+l,n+l}(\omega - l\Omega) = \mathcal{U}_{m+l,a}\frac{\delta^{ab}}{\omega - l\Omega - \epsilon_a + \mathrm{i}0^+}\mathcal{U}^\dagger{}_{b,n+l}, \quad |\omega| \le \frac{\Omega}{2} \tag{5.67}$$

[6] The fraction sandwiched can be also written [3, 221] into a matrix then $G^R = \mathcal{U}Q\mathcal{U}^\dagger$.

Note same indices are summed. We can see that the above definitions have the same information as the (5.63).

For a multi-band lattice system[7] the generalization is simple that for each Floquet index there is a set of quantum number which we absorb them into a single index i. The index i can contain the lattice position, the spin and other internal degrees of freedoms as well as sublattice indices, i.e., $i = (x, \sigma, \ldots)$. The extended Hilbert space is again $\mathscr{H} \times \mathscr{T}$, with the basis $|i\rangle \otimes |m\rangle$. Then for the Floquet matrix $\mathcal{H}_{m\ n}^{\ i\ j}$ we have the Schrödinger equation

$$\mathcal{H}_{m\ n}^{\ i\ j}\mathcal{U}^{n}_{\ ja} = \epsilon_a \mathcal{U}_{m\ a}^{\ i} \tag{5.68}$$

And the retarded Green's function is

$$G^{R}_{m\ n}^{\ i\ j}(\omega) = [\omega\mathbb{1} - \mathcal{H} + \mathrm{i}0^+]^{-1}_{\ m\ n}^{\ i\ j} = \frac{\mathcal{U}^{m+l,j}_{\ \ a}\mathcal{U}^{*l+n,i}_{\ \ a}}{\omega - l\Omega - \epsilon_a + \mathrm{i}0^+} \tag{5.69}$$

Here the matrix u_{mia} is a $n_F \times n_i \times (n_F \times n_i)$ tensor.

One may want to have a more "symmetric" tensor since the linear map corresponds to the $\mathcal{U}$ that maps two indices into one index, i.e., $mi \to a$ rather than $mi \to s\alpha$. We can split the index and write $\mathcal{H}_{mi\,nj}\mathcal{U}_{nj\,s\alpha} = \epsilon_a \mathcal{U}_{ni\,s\alpha}$. The index s is labeling the so-called Floquet Brillouin zones. Since the quasi-energy ϵ_a and $\epsilon_a + s\Omega$ are both the solutions of the same eigen-problem, we can order the quasi-energies in a way that $\epsilon_a + l\Omega = \epsilon_{s\alpha} + l\Omega = \epsilon_\alpha + (s+l)\Omega$, with $\epsilon_\alpha \in [-\frac{\Omega}{2}, \frac{\Omega}{2})$. Many other choices with integer Ω shifts will work equally well, but we will stick to this convention. Further we can use that $\mathcal{U}^{n+l,j}_{\ \ s\alpha} = \mathcal{U}^{n+l+s,j}_{\ \ \ 0\alpha}$, and then rename the dummy index $l + s \to l$, the above equation becomes

$$G^{R}_{m\ n}^{\ i\ j}(\omega) = [\omega\mathbb{1} - \mathcal{H} + \mathrm{i}0^+]^{-1}_{\ m\ n}^{\ i\ j} = \frac{\mathcal{U}^{m+l,i}_{\ \ \ 0\alpha}\mathcal{U}^{*l+n,j}_{\ \ \ 0\alpha}}{\omega - l\Omega - \epsilon_{0\alpha} + \mathrm{i}0^+} \quad |\omega| \le \frac{\Omega}{2} \tag{5.70}$$

This allows us to restrict the $s\alpha$ within $s = 0$, i.e. the first Floquet Brillouin zone, which is usually chosen as $\epsilon_{0\alpha} \in [-\frac{\Omega}{2}, \frac{\Omega}{2})$. The 0α can be abridged to α, this is then the form that appears frequently in many literature.

The (non-interacting) Keldysh Green's function is following the similar procedure, for the case the initial density matrix has the diagonal form[8]

$$\mathrm{Tr}\{\rho\psi_b^\dagger\psi_a\} = \langle\psi_b^\dagger\psi_a\rangle = \langle\psi_a^\dagger\psi_a\rangle\,\delta_{ab} \equiv f_a\delta_{ab} \tag{5.71}$$

Where f_a is defined by $\langle\psi_a^\dagger\psi_a\rangle$. Now we can see the Keldysh Green's function is similar with (5.69), for fermions it reads

$$G^{K}_{minj}(\omega) = -\mathrm{i}\left(1 - 2f_a\right)\delta(\omega - l\Omega - \epsilon_a)\mathcal{U}^{m+l\,i}_{\ \ \ a}\mathcal{U}^{*l+n\,j}_{\ \ \ a} \tag{5.72}$$

The equation (5.69) and (5.72) can define the Floquet non-interacting problem of a closed system for

[7] Here $\mathcal{U}^{m}_{\ a} = \delta^{mn}\mathcal{U}_{am}$. However the ascendence of the index here and later are mainly for reading convenience, and thus they can be safely moved up and down freely.

[8] This density matrix is not entirely general but a good approximation in many applications, especially for the steady states that has a mixed state density matrix that in the late time, which is after a destructive interference of the relative phases. If starting from a pure state that is not a Floquet eigenstate, then some off diagonal terms will enter.

an arbitrary initial condition satisfying (5.71). Frequently we write

$$u^{m\,j}{}_{a} \equiv \mathcal{U}^{m\,j}{}_{a} \tag{5.73}$$

One can check in this case the Green's functions are satisfying the fluctuation-dissipation theorem (FDT) through the distribution factor $1-2f_a$, here we considered the fermionic case. Recall that the retarded Green's function for the Floquet eigenstate $\Psi_a(t)$ is $G_a^R(t,t') = -i\theta(t-t')\Psi_a(t)\otimes\Psi_a^\dagger(t')$, the "$u$" can be reached by

$$u^{n\,j}{}_{a} = \frac{1}{T}\int_0^T \mathrm{d}t\, u^{i}{}_{a}(t)e^{-\mathrm{i}n\Omega t} = \frac{1}{T}\int_0^T \mathrm{d}t\, \Psi^{i}{}_{a}(t)e^{\mathrm{i}\epsilon_a t}e^{-\mathrm{i}n\Omega t} \tag{5.74}$$

where Ψ_a is the wave function of a-th Floquet eigenstate, see also Eq. 5.12.

One can see that (5.69) and (5.72) are very closed to the familiar Lehmann representation of the Green's function, and we may also call them the Floquet Lehmann representations. Although those equations are not always very useful in numerical computations, they still give some physical intuitions, and if the eigenvectors and the eigenvalue can be solved analytically, those representation can provide analytic results.

5.5.3 From time space: Wigner representation and Floquet representation

As we mentioned before, we will show how to connect the time-domain Green's function to Floquet Green's function in this section. And it is also convenient to define the Floquet-Wigner representation of Green's function in the frequency domain, which we will do as well. The Floquet-Wigner representation $\overline{G}_n(\omega)$ of the (2-point) Green's function $G_{ij}(t,t')$ is defined through the Wigner transform, i.e. "center of mass" representation with a following Fourier transform of the time variables of the Green's function[9]

$$\overline{G}_n(\omega) = \int_{-\infty}^{\infty}\mathrm{d}t_\mathrm{r}\frac{1}{T}\int_0^T \mathrm{d}t_\mathrm{a}e^{\mathrm{i}\omega t_\mathrm{r}+\mathrm{i}n\Omega t_\mathrm{a}}G\left(t_\mathrm{a}+t_\mathrm{r}/2, t_\mathrm{a}-t_\mathrm{r}/2\right) \tag{5.75}$$

and

$$G(t,t') = \sum_n\int_{-\infty}^{\infty}\frac{\mathrm{d}\omega}{2\pi}e^{-\mathrm{i}\omega(t-t')-\mathrm{i}n\Omega(t+t')/2}\overline{G}_n(\omega) \tag{5.76}$$

where $T=2\pi/\Omega$ is the time period and $m,n\in\mathbb{Z}$, $\omega\in\mathbb{R}$. In above all the indices and variables other than time were suppressed, $G_{ij}(t,t')\to G(t,t')$. The averaged time t_a and the relative time t_r are defined as

$$t_\mathrm{a}\equiv\frac{t+t'}{2}, t_\mathrm{r}\equiv t-t' \quad\text{and}\quad t=t_\mathrm{a}+\frac{t_\mathrm{r}}{2}, t'=t_\mathrm{a}-\frac{t_\mathrm{r}}{2} \tag{5.77}$$

and the time-domain "center of mass" Green's function is

$$\overline{G}(t_\mathrm{r},t_\mathrm{a}) \equiv G\left(t_\mathrm{a}+t_\mathrm{r}/2, t_\mathrm{a}-t_\mathrm{r}/2\right) \tag{5.78}$$

The Floquet representation can be reached through Floquet-Wigner representation from the following

[9] One may define [101] $\int_\omega = 1/(2\pi)\int_{-\infty}^{\infty}\mathrm{d}\omega$ and $\fint_t = \Omega/(2\pi)\int_0^{2\pi/\Omega}\mathrm{d}t = 1/T\int_0^T\mathrm{d}t$ to shorten the equations.

identity [3, 101]

$$G_{mn}(\omega) = \overline{G}_{m-n}\left(\omega + \frac{m+n}{2}\Omega\right) \tag{5.79}$$

Now use the definition of the Wigner transform, we have

$$G_{mn}(\omega) = \frac{1}{T}\int_0^T \mathrm{d}t_\mathrm{a} e^{\mathrm{i}(m-n)\Omega t_\mathrm{a}} G\left(\omega + \frac{m+n}{2}\Omega, t_\mathrm{a}\right) \tag{5.80}$$

where G_{mn} is called Floquet representation of G. The forward transform from t, t' to ω, m, n is [169]

$$G_{mn}(\omega) = \frac{1}{T}\int_0^T \mathrm{d}t_\mathrm{a} \int_{-\infty}^{\infty} dt_\mathrm{r} e^{\mathrm{i}(\omega+m\Omega)t} G\left(t, t'\right) e^{-\mathrm{i}(\omega+n\Omega)t'} \tag{5.81}$$

and the inverse transform is

$$G\left(t, t'\right) = \sum_{m,n}\int_{-\Omega/2}^{\Omega/2} \frac{\mathrm{d}\omega}{2\pi} e^{-\mathrm{i}(\omega+m\Omega)t} G_{mn}(\omega) e^{\mathrm{i}(\omega+n\Omega)t'} \tag{5.82}$$

where $\Omega = 2\pi/T$. Note the full information of Floquet representation is in

$$\omega \in [-\frac{\Omega}{2}, \frac{\Omega}{2}) \tag{5.83}$$

and other regions of ω can be reconstructed from index shifts. We will see how to do this reconstruction in (5.86).

It is also possible to transfer from the Floquet representation to Floquet-Wigner representation [101] by using

$$\overline{G}_n(\omega) = G_{m+\frac{n}{2},m-\frac{n}{2}}(\omega - m\Omega) \tag{5.84}$$

However, it is not as straightforward as (5.79), since when n is a odd number we need to shift the right hand side ω by a $\frac{1}{2}\Omega$ to get a $\frac{n}{2} + \frac{1}{2}$ to make the index of the Floquet representation integer. The shifts are allowed by the identity of the Floquet representation

$$G_{mn}(\omega) = G_{m+l,n+l}(\omega - l\Omega) \tag{5.85}$$

The Eq. (5.85) is simple to proof, where we can $G(t+T, t'+T) = G(t, t')$ and (5.82) to show

$$[G(t,t')]_{mn}(\omega) = [G(t+lT, t'+lT)]_{mn}(\omega) = G_{m+l,n+l}(\omega - l\Omega) \tag{5.86}$$

Here $[\cdots]_{mn}(\omega)$ means that we are transforming the arguments to the Floquet representation. The relation (5.82) can be used to reconstruct the $G\left(\omega \notin [-\frac{\Omega}{2}, \frac{\Omega}{2})\right)$ from $G\left(\omega \in [-\frac{\Omega}{2}, \frac{\Omega}{2})\right)$.

Note from now on, we will call the Green's functions in Floquet representation "Floquet Green's functions". We will call the Green's functions in Floquet-Wigner representation "Floquet-Wigner Green's functions".

5.5.4 Example: tight-binding model in a DC field

It is instructive to compute some simple Floquet Green's functions. One of the simplest model [3, 226] is the tight-binding single-band lattice electrons couple to direct current (DC) field where the field is introduced through minimal coupling by the Peierls substitution. The Hamiltonian is

$$\hat{H}(t) = \sum_k H(t,k) c_k^\dagger c_k = -\sum_k 2J_0 \cos[k - A(t)] c_k^\dagger c_k \tag{5.87}$$

With the amplitude of the vector potential of the external time-dependent classical DC field

$$A(t) = \Omega t \tag{5.88}$$

Here the coupling constant, the electron charge e is set to $e = 1$ for simplicity, and the lattice constant is set to 1.

We can see that the time evolution unitary of the above Hamiltonian is

$$U(t,0;k) = \hat{T} e^{-\mathrm{i}\int_0^t \mathrm{d}s\, H(s,k)} = e^{-\mathrm{i}\int_0^t \mathrm{d}s\, H(s,k)} = e^{2\mathrm{i}J_0 \sin(k+\Omega t)/\Omega} \equiv \Psi(t,k) \tag{5.89}$$

Where the time-ordering $\hat{T}$ can be dropped for this model since the Hamiltonian for each (t,k) is a scalar. The Floquet index α can be dropped once the First Floquet-Brillouin zone (FBZ) is specified for the same reason. We can see that this model is especially simple since the quasi-energy (in the first Floquet Brillouin zone) is zero

$$\epsilon_{k\alpha} = \frac{1}{T}\mathrm{i}\log U(T,0,k) = \frac{1}{T}\int_0^T \mathrm{d}t\, H(t,k) = 0 \tag{5.90}$$

Thus $u(t,k) = U(t,0;k)$. The extended space micro-motion u^m and its matrix form $\mathcal{U}$ can be obtained by

$$\mathcal{U}_k^{mn} = u_k^{m-n} = \frac{1}{T}\int_0^T \mathrm{d}t\, U(t,0;k) e^{\mathrm{i}0t} e^{-\mathrm{i}(m-n)\Omega t} \tag{5.91}$$

From above, a direct computation gives us

$$\mathcal{U}_k^{mn} = \frac{1}{T}\int_0^T \mathrm{d}t\, e^{-\mathrm{i}\int_0^t \mathrm{d}s\, (-2J_0\cos(k-\Omega t))} e^{-\mathrm{i}(m-n)\Omega t} \tag{5.92}$$

To compute the Fourier modes, we can use the well-known identity (Jacobi-Anger expansion)

$$e^{iz\cos\theta} = \sum_{n=-\infty}^{\infty} i^n \mathcal{J}_n(z) e^{in\theta} \tag{5.93}$$

Where the $\mathcal{J}_n(z)$ is the Bessel function[10] of the first kind. One can directly compute the Fourier transform [3, 226], where

$$\mathcal{U}_k^{mn} = e^{-i(m-n)k - 2i(J_0/\Omega)\sin k} \mathcal{J}_{n-m}\left(2J_0/\Omega\right) \tag{5.94}$$

[10] The BesellJ(n,x)

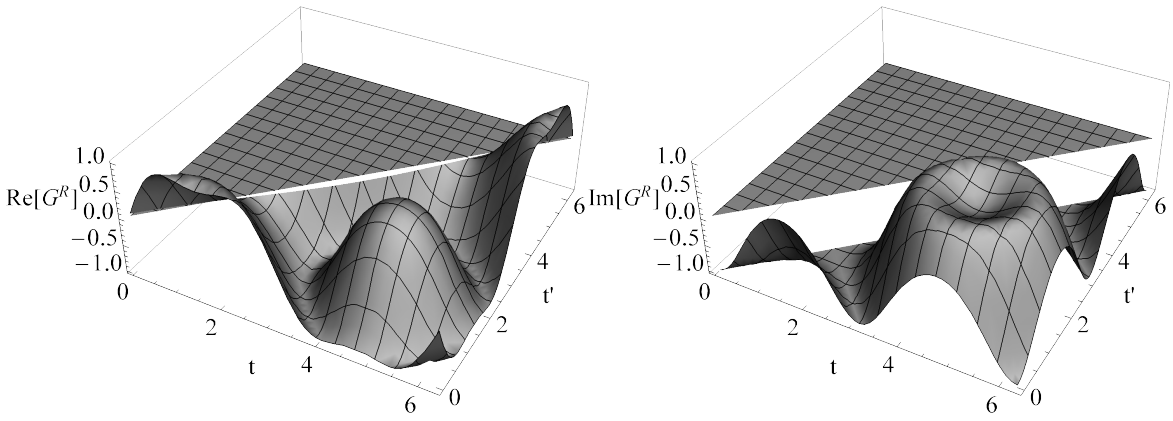

(a) Real part

(b) Imaginary part

Figure 5.6: $G^R(t,t';k=0)$ for the DC Hamiltonian (5.87), with $\Omega = J_0 = 1$, see also (5.95). Where only the first period is plotted, i.e. $t,t' \in [0,T]$, $T = 2\pi/\Omega$ the drive period.

And for $k = 0$ it is especially simple, which is $\mathcal{U}^{mn}_{k=0} = \mathcal{J}_{n-m}(2J_0/\Omega)$.

Now we can write down the retarded Green's function. The retarded Green's function $G^R(t,t') = -\mathrm{i}\theta(t-t')\Psi(t,k)\Psi^\dagger(t',k)$ is

$$G^R(t,t';k) = -\mathrm{i}\theta(t-t')e^{2\mathrm{i}(J_0/\Omega)(\sin(k+\Omega t)-\sin(k+\Omega t'))} \tag{5.95}$$

The symmetry $G(t+T,t'+T) = G(t,t')$ holds trivially. We also plot the $G^R(t,t')$ in Fig. 5.6 for direct references.

Recall the equation (5.70), the Floquet retarded Green's function is

$$G^R_{mn}(\omega,k) = e^{-\mathrm{i}(m-n)k}\sum_l \frac{\mathcal{J}_{m+l}(J_0/\Omega)\mathcal{J}_{l+n}(J_0/\Omega)}{\omega - l\Omega + \mathrm{i}0^+} \tag{5.96}$$

One can see that the relation $G_{m,n}(\omega) = G_{m+l,n+l}(\omega - l\Omega)$ holds and the entire $\omega \in (-\infty,+\infty)$ can be reconstructed from $\omega \in [-\frac{\Omega}{2},\frac{\Omega}{2})$. Where the infinitesimal regulator $\gamma_0 = 0^+$ represents a dissipationless system since the Hamiltonian (5.87) is non-interacting, i.e. the relaxation time $\tau \sim 1/\gamma_0 = \infty$. Since the δ function is very narrow and is not easy to resolve on a plot, we can add a finite constant broadening Γ to it[11]

$$G^R_{mn}(\omega,k) = e^{-\mathrm{i}(m-n)k}\sum_l \frac{\mathcal{J}_{m+l}(J_0/\Omega)\mathcal{J}_{l+n}(J_0/\Omega)}{\omega - l\Omega + \mathrm{i}\Gamma} \tag{5.97}$$

The damping term can be regarded as from coupling the system to an (non-interacting) external bath [3] with flat density of state, with the coupling V and $\Gamma \sim V^2$. The external bath also used later in the chapter for the dynamical mean field theory.

In Fig. 5.7, I plot the Eq. (5.97) and its time space form through analytical formula and the numerical Fourier transform. One can see that the Fourier transform results are agreed with the exact results.

[11] In time domain it is to multiply a small damping term $e^{-\Gamma t}$.

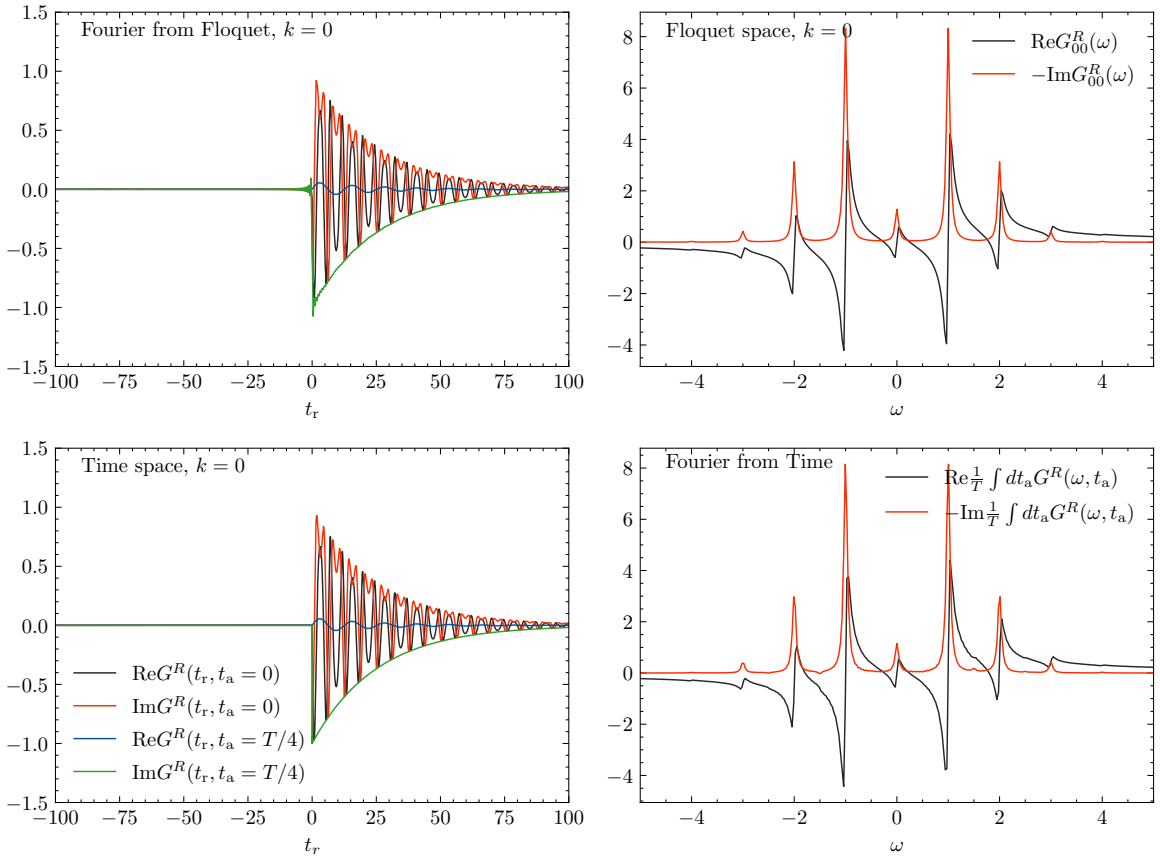

Figure 5.7: The $\overline{G}^R(t_r, t_a)$ and $G^R_{mn}(\omega)$. Used parameters $J_0 = \Omega = 1$, $\Gamma = 0.04$. (Upper Left) $G^R(t_a + t_r/2, t_a - t_r/2)$ Fourier transform from $G^R_{mn}(\omega)$, (Upper right) Eq. 5.97 for $k = 0$, $m = n = 0$. The lower plots, (Lower left) Eq. 5.95 with time "center of mass" $G^R(t_a + t_r/2, t_a - t_r/2)$. (Lower right) Fourier transform from Eq. 5.95, again for $k = m = n = 0$, i.e time averaged over the t_a.

5.5.5 Limitations of the Floquet Green's function method

There are known limitations of the Floquet Green's function method. For instance, in [227], the authors discussed the effect of driving on the phonon bath of the normal static superconductor and compared the solutions from Floquet Green's function and from the time-space direct method by solving the integral-differential Volterra equation. For phonons, the resulting Mathieu equation is unstable near the parametric resonance, where the drive frequency is closed to the internal frequency, and the Fourier transform is ill-defined. This can be one of the general limitations of the Floquet Green's function method, since Floquet Green's functions rely on the discrete Fourier transform and the steady-state assumption.

5.6 Summary

In this chapter we reviewed the Floquet theorem, the Floquet Keldysh Green's functions and Floquet-Wigner representation and Floquet representation for quantum mechanical models through definitions and simple examples. The Floquet Green's functions and Floquet-Wigner Green's function can be compute by starting from the Floquet matrix or from Fourier transfroms of the time space Green's functions that has the Floquet discrete time translational symmetry. All those representations have their own advantages. We also discuss the general heating problem in the periodically driven systems.

Let us summarize this chapter by the following graph.

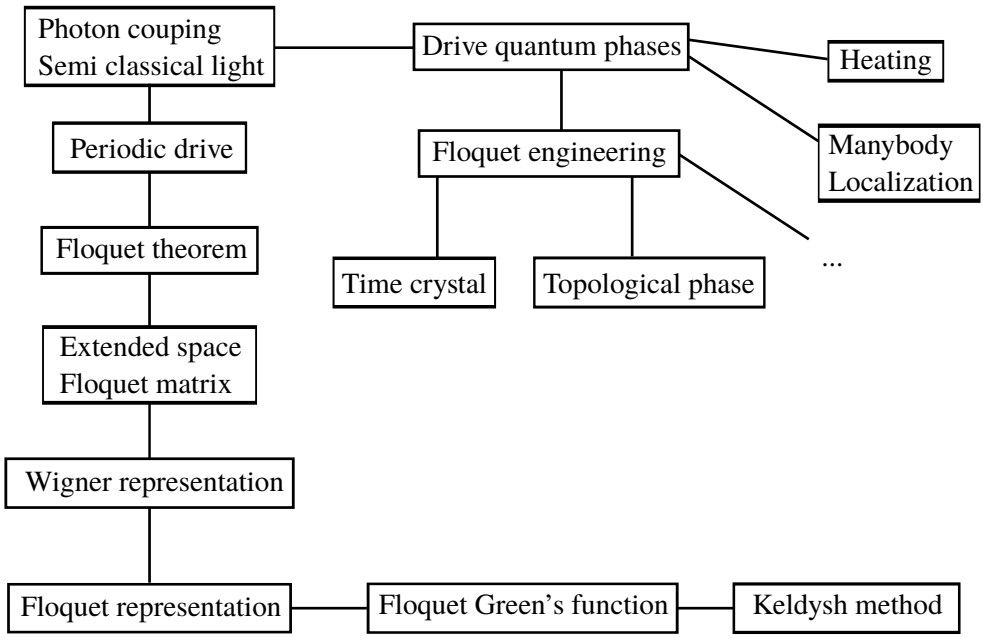

Figure 5.8: Summary of general Floquet theory

CHAPTER 6

Periodically driven systems without interaction: adiabatic and non-adiabatic Thouless pump

In this chapter, we discuss applications of the Floquet theorem, Floquet representation, and Floquet Green's functions to non-interacting problems. We focus on the Thouless pump, a quantized charge pump, and its dissipative extension. The dissipative Thouless pump project is in collaboration with Zlata Fedorova, Prof. Stefan Linden, and Prof. Johann Kroha and published in [228].

6.1 Thouless pump and Rice-Mele model

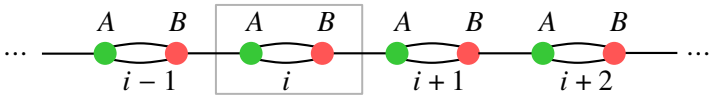

Figure 6.1: Rice-Mele model, which has sublattice A and B.

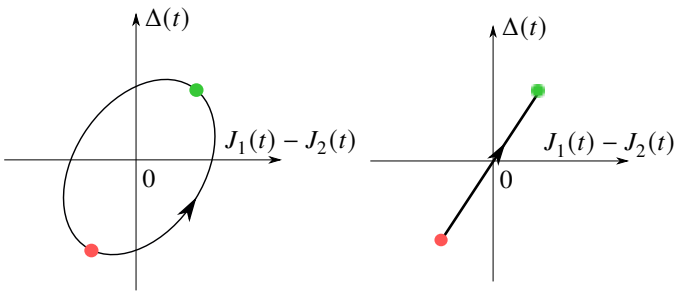

Figure 6.2: Parameter circle, the y-axis is $\Delta(t)$, the x-axis is $J_1(t) - J_2(t)$. The topological phased can be read off from the parameter circle as an alternative of the TKNN invariant of the Thouless pump. (Left pane) A non-zero quantized pump. (Right pane) Pumping charge is zero.

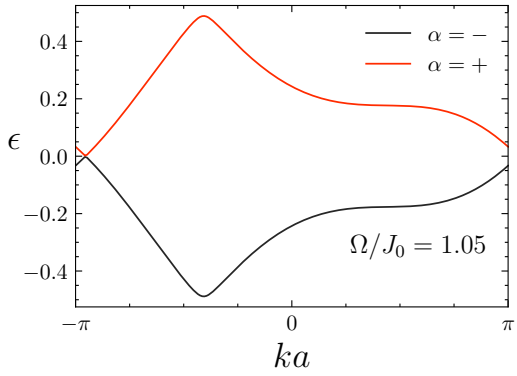

Figure 6.3: The quasienergies in the FFZ. The quasienergies for a Floquet $d_s = 1$ lattice model, the Rice-Mele model with $\Delta_0 = 3.0/J_0$, $J_0 = 1.0$, $\delta_0 = 1.0/J_0$, $\phi = 0$.

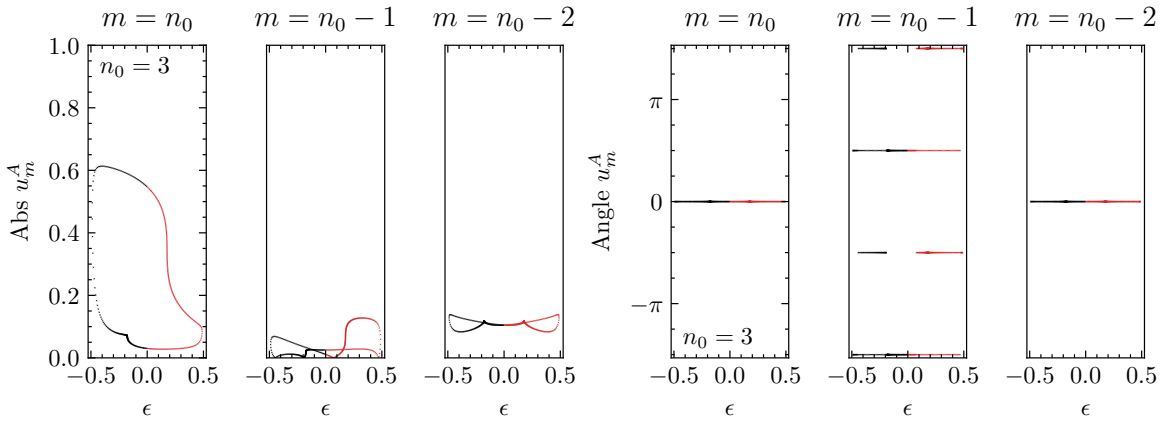

Figure 6.4: For the Rice-Mele model with $\Delta_0 = 3.0/J_0$, $J_0 = 1.0$, $\delta_0 = 1.0/J_0$, $\phi = 0$.

Among the simplest Floquet lattice systems, the Rice-Mele [229] model, as a $d_s = 1$ super-lattice, is intensively studied over the last decades because it can support a quantized charge pump, the Thouless pump. Thouless pump, as first purposed by David Thouless in 1983 [230], is a way to pump integer multiples of the charge for each drive period, and the integer is equal to the Chern number of the Hamiltonian $H(t, k)$, where t is regarded as an additional momentum variable when computing the invariant. This means the pumping charge is proportional to a topological invariant. There are many discussions on Rice-Mele model and its realization in cold-atom systems [231] and condensed matter systems. Here I focus on one of the simplest construction [232–234]. The Rice-Mele model Hamiltonian is

$$\begin{aligned}\hat{H}_{\mathrm{RM}}(t) = &-\sum_{j=1}^{N}\left(J_1(t)\hat{\psi}^{\dagger}_{B,j}\hat{\psi}_{A,j} + J_2(t)\hat{\psi}^{\dagger}_{A,j+1}\hat{\psi}_{B,j} + h.c.\right)\\ &+\sum_{j=1}^{N}\Delta(t)\left(\hat{\psi}^{\dagger}_{A,j}\hat{\psi}_{A,j} - \hat{\psi}^{\dagger}_{B,j}\hat{\psi}_{B,j}\right)\end{aligned} \tag{6.1}$$

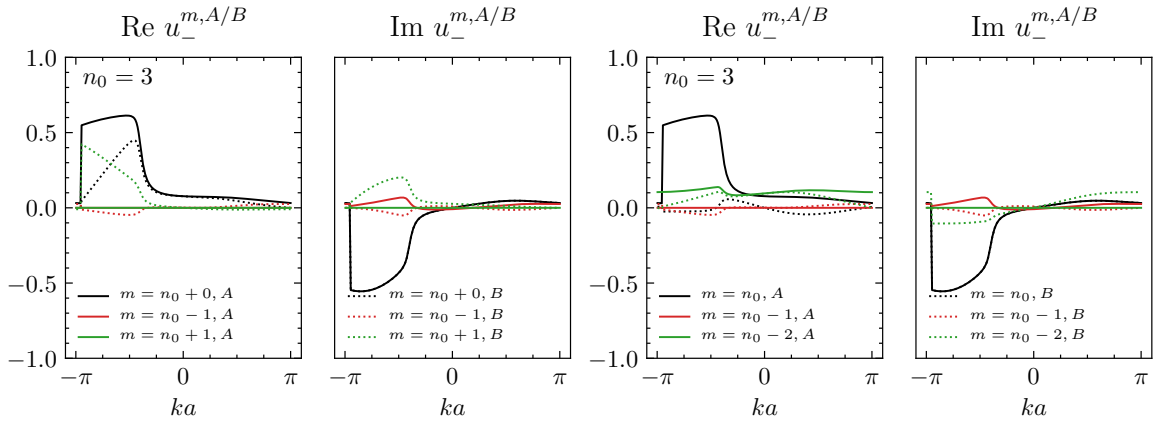

Figure 6.5: For the Rice-Mele model with $\Delta_0 = 3.0/J_0$, $J_0 = 1.0$, $\delta_0 = 1.0/J_0$, $\phi = 0$. Solid lines for "A", dot lines for "B". The discontinuous points are those the spectrum has a crossing.

where the $\hat{\psi}$ and $\hat{\psi}^\dagger$ are the fermionic annihilation and creation operators. For a quantum pump, the time-dependent parameters can be chosen as

$$\begin{cases} J_1(t) = J_0 + \delta_0 \cos(\Omega t) \\ J_2(t) = J_0 - \delta_0 \cos(\Omega t) \\ \Delta(t) = \Delta_0 \sin(\Omega t + \phi) \end{cases} \tag{6.2}$$

I will set $\phi = 0$ except otherwise specified. This gives a phase shift $\pi/2$ between the hopping drive and the on-site potential drive which can be seen by $\sin(x) = \cos(x - \pi/2)$. In momentum space, it has the form

$$H_{\mathrm{RM}}(t,k) = \boldsymbol{d}(t,k) \cdot \boldsymbol{\sigma} \tag{6.3}$$

$$= \begin{pmatrix} \Delta(t) & -J_1(t) - J_2(t)e^{-\mathrm{i}ka} \\ -J_1(t) - J_2(t)e^{+\mathrm{i}ka} & -\Delta(t) \end{pmatrix} \tag{6.4}$$

where the three dimensional vector $\boldsymbol{h}$ has the components

$$\begin{cases} d_1 = -J_1(t) - J_2(t)\cos(ka) \\ d_2 = -J_2(t)\sin(ka) \\ d_3 = \Delta(t) \end{cases} \tag{6.5}$$

One can directly solve the Schrödinger equation $\mathrm{i}\partial_t |\psi(t)\rangle = H(t)|\psi(t)\rangle$ numerically by ODE solvers[1] with low cost, and then measure the current by assuming that before turn on the drive the system is at

[1] For instance, the Runge-Kutta solver, RK45.

the static $\beta = \infty$ ground state. We switch on the drive at $t = t_0 = 0$ where the model is reduced to

$$H_{\mathrm{RM}}(0,k) = \begin{pmatrix} 0 & -J_0 - \delta_0 - (J-\delta_0)e^{-\mathrm{i}ka} \\ -J_0 - \delta_0 - (J-\delta_0)e^{\mathrm{i}ka} & 0 \end{pmatrix} \tag{6.6}$$

It has eigenvalues and eigenvectors at $t_0 = 0$

$$E(t_0,k) = \pm\sqrt{2}\sqrt{(J_0^2-\delta_0^2)\cos(ka) + J_0^2 + \delta_0^2} \tag{6.7}$$

$$\psi(t_0,k) = \frac{1}{\sqrt{C^2(k)+1}}(\mp C(k),1)^{\intercal} \quad \text{and} \quad C(k) = \frac{\sqrt{2}\sqrt{(J_0^2-\delta_0^2)\cos(ka)+J_0^2+\delta_0^2}}{e^{ika}(J_0-\delta_0)+J_0+\delta_0} \tag{6.8}$$

Following [232], we choose a simple parameter setting for a non-zero quantized pump

$$3J_0 = 3\delta_0 = \Delta_0, \quad a = 1.0 \tag{6.9}$$

Under such a setting, $C(k) = 1$, and the initial ground state takes a much simpler form

$$E(t_0,k) = -2J_0, \quad \psi(t_0,k) = \frac{1}{\sqrt{2}}(1,1)^{\intercal} \tag{6.10}$$

The expectation value of the current operator is

$$J_{\mathrm{curr}}(t) = \frac{1}{aN_k}\sum_k \langle\psi(t,k)|\widetilde{J}_{\mathrm{curr}}(t,k)|\psi(t,k)\rangle \tag{6.11}$$

And the charge density pumped in one period is

$$Q_n = \int_{(n-1)T}^{nT} \mathrm{d}t J_{\mathrm{curr}}(t) \tag{6.12}$$

The initial condition and the parameter setting are shown in Fig. 6.6 and Fig. 6.7. We can see that the Q_n are nearly quantized, $Q \sim 0.99$, for $T = 20/J_0$, $\Omega = 2\pi/T = 0.31J_0$.

From Fig. 6.6, we can see that Q_n is very closed to 1 if the drive frequency is low, e.g., the case $\Omega = 0.314J_0$, and decreases if the Ω is increased. This can be seen more clearly in a quasi-energy occupation spectrum, which I will introduce soon in Section. 6.1.2.

6.1.1 Current operator and Floquet Green's function

Here I derive the current operator used in Fig. 6.6 and Fig. 6.7. Note during the derivation of the current operator, we can first transform

$$\psi_{A,k} \to \psi_{A,k}e^{\mathrm{i}ka/2} \tag{6.13}$$

which is a k dependent gauge transform which can be revert later easily and it will not affect the observables of the Rice-Mele model. This is equivalent to insert a virtue flux, see [235] appendix. For

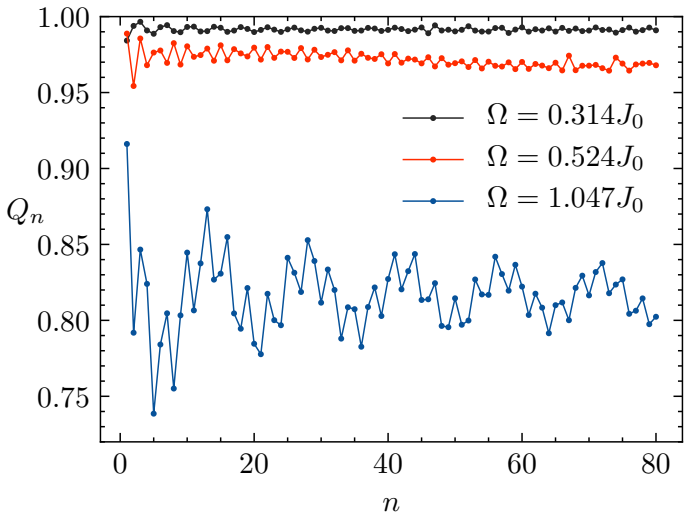

Figure 6.6: Thouless pump for the Rice-Mele model, $3J_0 = 3\delta_0 = \Delta_0$. (Top) The time dependent net current. (Bottom) The net charge pumped for each period. One can see that for this parameter setting the pumped charge is quantized to high accuracy. Used momentum points in the BZ $N_k = 400$, number of the t points used per period is $N_{\text{perperiod}} = 1000$. See also the Ref. [233, 234].

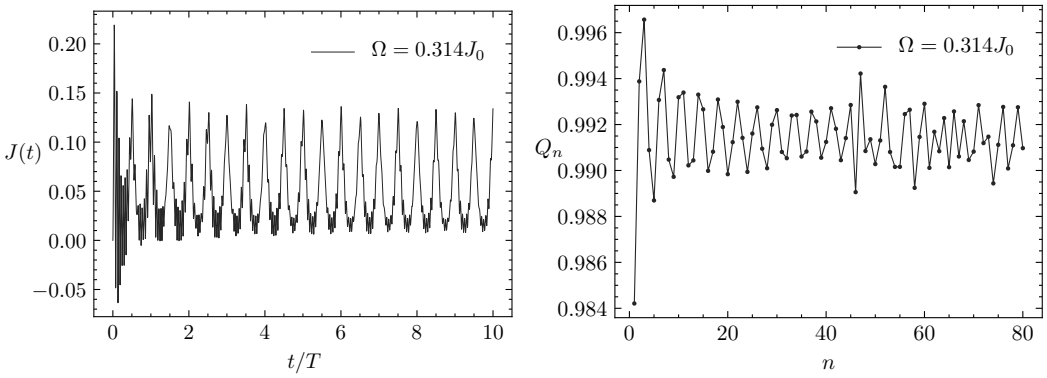

(a) Time dependent current density

(b) Charge density pumped per cycle

Figure 6.7: Thouless pump for the Rice-Mele model with $3J_0 = 3\delta_0 = \Delta_0$. The current becomes steady after a transient dephasing time which is about $2T$. Computed by the current operator. See also the main text.

a dimer model, the current matrix is

$$J_{\text{curr}}(t) = \frac{1}{aN_k}\sum_k \partial_k H_k(t) = \frac{1}{aN_k}\sum_k \begin{pmatrix} 0 & \partial_k J_k \\ \partial_k J_k^* & 0 \end{pmatrix} \tag{6.14}$$

The current operator is thus [235]

$$\hat{J}_{\text{curr}}(t) = \frac{1}{aN_k}\sum_k \left(\partial_k J_k \psi_{kA}^\dagger \psi_{kB} + (\partial_k J_k)^* \psi_{kB}^\dagger \psi_{kA}\right) \tag{6.15}$$

where $J_k^*(t) = J_1(t)e^{-\mathrm{i}ka/2} + J_2(t)e^{+\mathrm{i}ka/2}$ with $J_{1/2} \in \mathbb{R}$ and

$$\partial_k J_k^* = -\mathrm{i}\frac{a}{2}J_1(t)e^{-ika/2} + \mathrm{i}\frac{a}{2}J_2(t)e^{+ika/2} = (\partial_k J_k)^* \tag{6.16}$$

$$\partial_k J_k = +\mathrm{i}\frac{a}{2}J_1(t)e^{+\mathrm{i}ka/2} - \mathrm{i}\frac{a}{2}J_2(t)e^{-\mathrm{i}ka/2} \tag{6.17}$$

Where J_1 and J_2 are defined in the (6.2). Note one can see that generally the current operator for the 1-dimensional bipartite tight binding model will take the form of (6.15).

Transform back $\psi_{A,k} \to \psi_{A,k}e^{-\mathrm{i}ka}$ we have [235]

$$(\partial_k J_k')^* = -\mathrm{i}\frac{a}{2}J_1(t) + \mathrm{i}\frac{a}{2}J_2(t)e^{+\mathrm{i}ka} \tag{6.18}$$

And we can now use $\partial_k J_k'$ to write the current expectation value by using Green's functions. Use the definition $\langle\psi_j^\dagger(t')\psi_i(t)\rangle = \mathrm{i}G_{ij}^<(t,t')$

$$J_{\mathrm{curr}}(t) = \langle\hat{J}_{\mathrm{curr}}(t)\rangle = \frac{1}{aN_k}\sum_k \left(\partial_k J_k' \langle\psi_{kA}^\dagger\psi_{kB}\rangle + (\partial_k J_k')^* \langle\psi_{kB}^\dagger\psi_{kA}\rangle\right) \tag{6.19}$$

$$= \frac{1}{aN_k}\sum_k \left(\partial_k J_k'\mathrm{i}G_{k,BA}^<(t,t) + (\partial_k J_k')^*\mathrm{i}G_{k,AB}^<(t,t)\right) \tag{6.20}$$

For going to the Floquet representation define $\widetilde{J}$ as

$$J_{\mathrm{curr}}(t) = \frac{1}{aN_k}\sum_k \widetilde{J}_{\mathrm{curr}}(t,k) \tag{6.21}$$

We can now use the identity

$$\int_{t\in[0,T]} A(t)B(t,t) = \sum_{mn}\frac{2\pi}{\Omega}\int_{|\omega|\le\Omega/2} A_{mn}B_{nm}(\omega) = \frac{2\pi}{\Omega}\int_{|\omega|\le\Omega/2}\mathrm{Tr}_F[AB](\omega) \tag{6.22}$$

to write the current expectation value by Floquet Green's functions. Here $\int_{|\omega|\le\Omega/2} = \int_{-\Omega/2}^{\Omega/2}\frac{\mathrm{d}\omega}{2\pi}$ and $\int_{t\in[0,T]} = \int_0^T \mathrm{d}t$. The trace is over the Floquet indices $\mathrm{Tr}_F[AB] = \sum_{mn} A_{mn}B_{nm}$. Then the steady state pumping charge per cycle Q_{SS} can be computed by

$$\begin{aligned} Q_{\mathrm{SS}} &= \int_{t\in[0,T]} J_{\mathrm{curr}}(t) \\ &= \frac{\mathrm{i}}{aN_k}\sum_k\sum_{mn}\frac{2\pi}{\Omega}\int_{|\omega|\le\Omega/2}\left([\partial_k J_k']_{mn}[G_{k,BA}^<]_{nm}(\omega) + [(\partial_k J_k')^*]_{mn}[G_{k,AB}^<]_{nm}(\omega)\right) \end{aligned} \tag{6.23}$$

Or in short

$$Q_{\mathrm{SS}} = \frac{\mathrm{i}}{aN_k}\sum_k\frac{2\pi}{\Omega}\int_{|\omega|\le\Omega/2}\mathrm{Tr}_F\left[\partial_k J_k G_{k,BA}^< + (\partial_k J_k)^* G_{k,AB}^<\right](\omega) \tag{6.24}$$

This formula can be used also in interacting systems.

6.1.2 Floquet picture of the Thouless pump

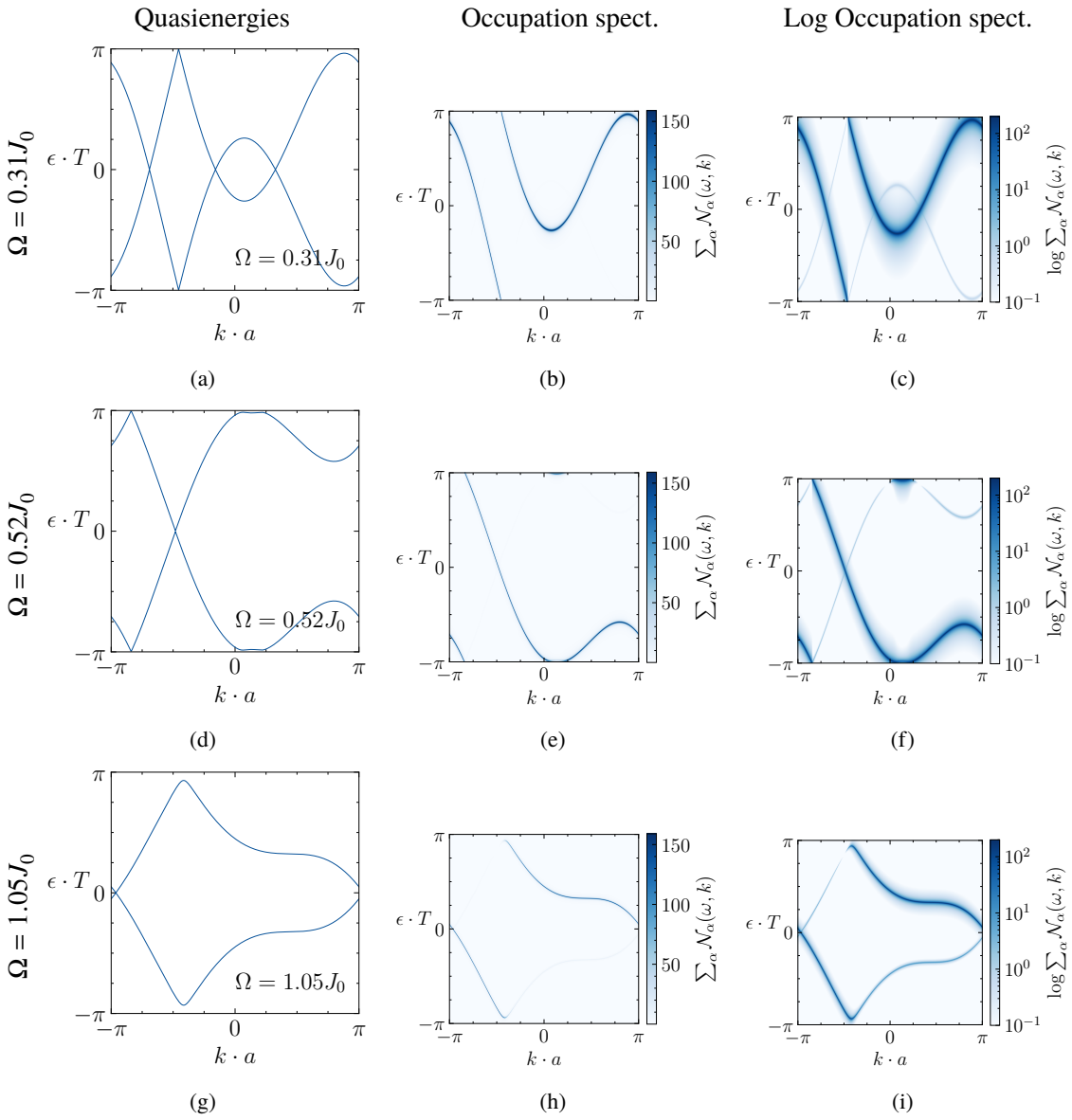

Figure 6.8: The Floquet dispersion (dimensionless, that is $\epsilon \longrightarrow \epsilon T \in [-\pi, \pi]$) and Floquet occupation spectra $\sum_\alpha \mathcal{N}_\alpha(\omega, k)$ for varies drive frequencies. The occupation spectra used the initial condition $\psi(t = 0, k) = (1/\sqrt{2}, 1/\sqrt{2})^\intercal$. (Left column) The quasienergies in the FFZ. (Middle column) The occupation spectra. (Right column) The logarithm scale quasienergy occupation spectra. The first, second and third rows are for $\Omega = 0.31J_0$, $\Omega = 0.52J_0$ and $\Omega = 1.05J_0$ respectively. The charge pumped per cycle is affected by the occupation of the left moving and right moving branches as well as the gap at the $\pm\pi$.

Here I introduce the Floquet picture for the Thouless pump in the Rice-Mele model, see also the

Ref. [232]. Define the Floquet occupation spectrum

$$\mathcal{N}_\alpha(\omega, k) = |\langle\psi_k(0)|\Psi_{k\alpha}(0)\rangle|^2\delta(\omega - \epsilon_\alpha(k)) = n_\alpha(k)\delta(\omega - \epsilon_\alpha(k)) \tag{6.25}$$

where $|\psi_k(0)\rangle$ is the initial time $t = 0$ wave function. The $|\Psi_{k\alpha}(0)\rangle$ are the Floquet eigenstates at $t = 0$ with $\alpha = \pm$. The $\mathcal{N}_{k\alpha}(\omega)$ for drive frequency $\Omega = 0.31J_0, 0.52J_0, 1.05J_0$ are plotted in Fig. 6.8. Here again I use the parameters

$$3J_0 = 3\delta_0 = \Delta_0, \quad J_0 = 1.0, \quad a = 1.0 \tag{6.26}$$

for the Hamiltonian (6.1). The quasienergy and the Floquet states are computed by the extended zone method.

$$\mathcal{H}_F u_\alpha(k) = \epsilon_\alpha(k) u_\alpha(k) \tag{6.27}$$

One can read off from the Fig. 6.6 that for large drive cycles $n \sim 80$

$$\begin{cases} \Omega = 0.31 & Q \approx 0.99 \\ \Omega = 0.52 & Q \approx 0.97 \\ \Omega = 1.05 & Q < 0.85 \end{cases} \tag{6.28}$$

Clearly, the quantization of the charge pump is destroyed by increasing drive frequency Ω. This can be understood easily in a Floquet picture, where we compute the Floquet occupation spectrum (6.25) of the Rice-Mele model. The occupation spectrum shows the occupied part of the Floquet quasienergies for a specific initial condition.

On the left column, the (a), (d), (e), we show the quasienergies of different drive frequencies of the Rice-Mele model. We can clearly see that there are right moving branch and left moving branch, where the right/left is defined by the sign of the slope $\partial\epsilon_k/\partial k$ which is the group velocity.

On the middle column and the right column Fig. 6.8 we show the Floquet occupation spectrum (6.25). From Fig. 6.8 (d-f) one can see that, first, in (d) around $\epsilon = \pm\pi$ and $k = \pi/8$ there is an avoid-crossing band gap opening and the occupation is mixed for left and right moving modes, although the amount is small.

From the Fig. 6.8 (h) and (i), one can see that the counter-propagating branch is occupied even in the non-log figure (h). This kind of occupation is reflected in the drop of the net current.

From the above, we can summarize that the quantization of the pump charge is reached whenever the initial state is (or very closed to) a Floquet eigenstate that has its spectral occupancies winding around the FFZ, integer net winding number. The approximate integral winding is possible as long as the driving frequency is low. The quantized charge pump is then controlled by two factors

1. If the initial state is prepared optimally.

2. If the quasienergy spectral allows full winding through the Floquet-Brillouin zone torus.

The above observations are for the pumped charge $Q_{\rm SS}$ for long time $t = nT$, $n \to \infty$, and can be computed alternatively through [232, 235]

$$Q_{\rm SS} = \sum_\alpha \frac{1}{\Omega}\int_{-\pi/a}^{\pi/a} \mathrm{d}k\, n_\alpha(k)\frac{\partial\epsilon_\alpha(k)}{\partial k} \tag{6.29}$$

one can also pull the T in side the integral to get a equation for the rescaled quasienergy ϵT

$$Q_{\rm SS} = \sum_{\alpha} \frac{1}{2\pi} \int_{-\pi/a}^{\pi/a} \mathrm{d}k \, n_{\alpha}(k) \frac{\partial(\epsilon_{\alpha}(k)T)}{\partial k} \tag{6.30}$$

where m times full winding around the Floquet Brillouin zone will give $Q_{\rm SS} = m$, $m \in \mathbb{Z}$ is a integer.

From an adiabatic perturbation theory computation, see [232, 235], one can find that closed to the adiabatic limit $\Omega \to 0$ ($\Omega \ll J_0$) the non-adiabatic correction is $Q_c = \frac{1}{128}\left(\Omega\Delta_0/J_0^2\right)^2$ for the special setting $\delta_0 = J_0$ applied[2]. For higher frequencies [232, 235] the gaps at $\pm\pi$ grow $\sim \exp(-1/\Omega)$, the occupation dependents on Ω though a function that is not easy to compute, this makes the situation more complicated for intermediate drive frequency $\Omega \sim J_0$. For large enough $\Omega \gg J_0$ one can find the net charge pumped goes to zero by $Q_{\rm SS} \sim \Omega^{-2}$.

We can also see the relationship between $Q_{\rm SS}$ and the Chern number [235]. Use the quasienergy $\epsilon \sim \mathrm{i}\partial_t - H(t)$, one can verify that $Q_{\rm SS} \sim \mathrm{i}\sum_{v\in\text{occupied}} \int_k \int_t \langle \partial_k u_{v,k,t} | \, | \partial_t u_{v,k,t} \rangle - h.c.$ in the adiabatic limit, where $|u_{v,k,t}\rangle$ is the v-th instantaneous eigenstate of the Hamiltonian.

6.2 Fast Thouless pump with dissipation

The adiabatic transport is slow. We know from the previous section that once the drive frequency is increased, the charge pump is getting non-quantized. Actually, the Thouless pump is exactly quantized only when $\Omega \to 0$. A question one may ask: is it possible to have speed and quantization at the same time?

The answer is yes. One possibility is to use dissipations, and with the price that the current is decaying. In this section, we discuss the paper [228], in collaboration with Zlata Fedorova and Prof. Dr. Stefan Linden and Prof. Dr. Johann Kroha from University of Bonn. Topological states for non-Hermitian driven systems are also discussed in [236–238].

6.2.1 The wave-guide experiment

The wave-guide experiment allows us to simulate a quantum mechanical system by the wave-guide arrays where the time direction is mapped to one of the spatial directions of the wave-guides. The resulting equation is exactly the Schrödinger equation. If direction z of the wave-guide is regarded as the time direction, then we can write down the wave-guide equation as

$$\mathrm{i}\frac{\mathrm{d}}{\mathrm{d}z}p(z) = C(z)p(z) \tag{6.31}$$

where $p(z)$ is the wave-guide plasma amplitude, a complex function of z. Indeed the above equation can be mapped to the Schrödinger equation with $\hbar = 1$

$$\mathrm{i}\frac{\mathrm{d}}{\mathrm{d}z}p(z) = C(z)p(z) \to \mathrm{i}\hbar\frac{\mathrm{d}}{\mathrm{d}t}\psi(t) = H(t)\psi(t) \tag{6.32}$$

[2] And generally up to second order in Ω, the non-adiabatic correction [232] is $\frac{\Omega^2\Delta_0^2}{64J_0^4}\left(1+\delta_0^2/J_0^2+\left(1-\delta_0^2/J_0^2\right)\cos(ka)\right)^{-2}$.

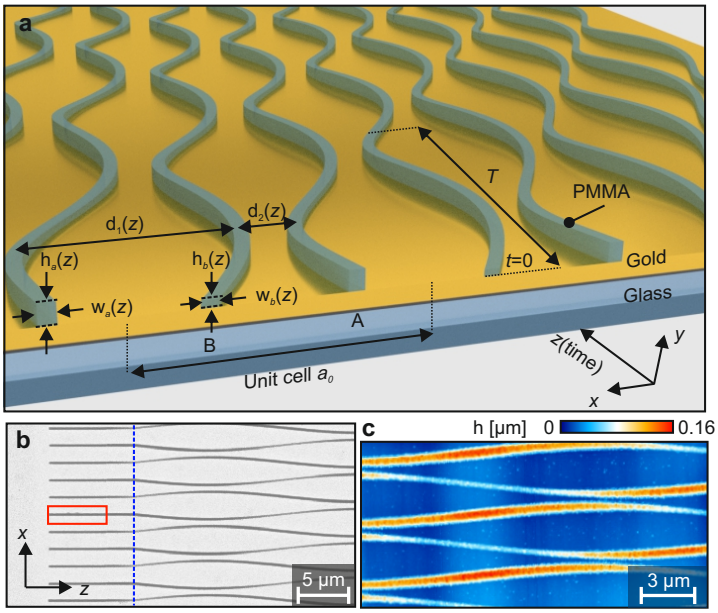

Figure 6.9: (a) The wave-guide height $h_{a/b}(z)$, wave-guide distance $d_{1/2}(z)$ and wave-guide width $w_{a/b}(z)$. (b) View from the top. (c) Atomic force microscopy (AFM) picture. The specific parameters are $J_0 = 0.144\,\mu\text{m}^{-1}$, $u_0 = 1.1J_0$ and $\gamma_0 = 0.8J_0$. The $\Omega = 2\pi/T$ is typically $1.1J_0$. From [228]

Since in this thesis we usually set $\hbar = 1$, the above equation is exactly identical to the Schrödinger equation. We can mimic the single-particle quantum lattice model by the wave-guide array. If the $C(z)$ is z dependent and periodically modulated, the corresponding system is exactly a non-interacting Floquet lattice system.

For simulating the Rice-Mele model, the wave-guide can be organized as in Fig. 6.9. Where the z direction is the "time", and the tight-binding hopping parameters are related to the wave-guide distance $d(z)$. The on-site energy is related to wave-guide height.

More specifically, in the experiments the "on-site energy" has the form $\beta(h) = q_1 + q_2\cos(hq_4) + q_3\sin(hq_4)$. The fitting parameters $q_1 = 7.235$, $q_2 = -0.7062$, $q_3 = -0.2206$, $q_4 = 8.969$, then we can summarize that, for the wave-guide height

$$\Delta\text{h} = 0.053\,\mu\text{m}, \quad \text{h}_0 \approx 0.1\,\mu\text{m} \tag{6.33}$$

and the height depends on z direction

$$\text{h}_{a,b}(z) \approx \text{h}_0 \pm \Delta\text{h} \cdot \sin(2\pi z/P + \Delta\phi) \tag{6.34}$$

and the onsite potential (real part) is

$$u_{a/b}(z) = \beta(h(z)) = q_1 + q_2\cos(h_{a/b}(z)q_4) + q_3\sin(h_{a/b}(z)q_4)$$

with the phase offset $\Delta\phi$. We can write $u_{a/b}(t)$ in an approximate but simpler form

$$u_a(t) = -u_0\cos(\Omega t + \varphi), \quad u_b(t) = u_a(t - T/2) \tag{6.35}$$

where we subtracted a constant is subtracted and renamed the $z \to t$.

The "hopping" $C(d) = p_1 \exp(-p_2 d)$ is related to the wave-guide distance.

$$d_0 = 1.7\,\mu\text{m}, \quad \Delta d = 0.5\,\mu\text{m} \tag{6.36}$$

The fitting parameters are $p_1 = 0.51$, $p_2 = 1.7$ and

$$\mathrm{d}_{1,2}(z) = \mathrm{d}_0 \pm 2\Delta\mathrm{d} \cdot \sin 2\pi z/P \tag{6.37}$$

Thus, the hopping can be written as

$$J_{1/2}(z) = C(d(z)) = p_1 \exp(-p_2 d_{1,2}(z))$$

Again write $z \to t$ and simplify the expression we have

$$J_1(t) = J_0 e^{-\lambda(1-\sin\Omega t)}, \quad J_2(t) = J_1(t - T/2) \tag{6.38}$$

With the above definitions one can write down the position space lattice Hamiltonian. Here we switch to the notations that are commonly used for the lattice tight binding models. See Fig. 6.10, see also [228]

$$\begin{aligned} \hat{H}_{\mathrm{RM}}(t) &= \sum_j \left(J_1(t)\hat{b}_j^\dagger \hat{a}_j + J_2(t)\hat{a}_{j+1}^\dagger \hat{b}_j + \text{h.c.} \right) + \sum_j \left(u_a(t)\hat{a}_j^\dagger \hat{a}_j + u_b(t)\hat{b}_j^\dagger \hat{b}_j \right) \\ \hat{\Gamma}(t) &= \sum_j \left(\gamma_a(t)\hat{a}_j^\dagger \hat{a}_j + \gamma_b(t)\hat{b}_j^\dagger \hat{b}_j \right) \end{aligned} \tag{6.39}$$

We introduced a loss term that makes the Hamiltonian non-Hermitian, with the properties explained in the caption of the Fig. 6.10.

The initial state of the wave-guide experiment is closed but different from the Thouless pump mentioned before. Initially in the experiment a single position space site at $z = 0$ is excited

$$|\psi_{\text{init}}\rangle = |\psi_{i,A}(0)\rangle = 1 \tag{6.40}$$

One can check that this is closed to the initial time $t = 0$ ground state of the fermionic Rice-Mele model.

6.2.2 The non-Hermitian Hamiltonian

Now we can write down the momentum space Hamiltonian for the model Fig. 6.10 of the setup Fig. 6.9. Apply the Fourier transformations $a_i = \sum_k a_k e^{\mathrm{i}kx_{iA}}$ and $b_i = \sum_k b_k e^{\mathrm{i}kx_{iB}}$ to the Hamiltonian (6.39) of the previous section, the tight-binding model is now block diagonal in k-space. The k-th block of the Hamiltonian is

$$H(t,k) = H_{\mathrm{RM}}(t,k) + \mathrm{i}\Gamma(t) \tag{6.41}$$

$$= \begin{pmatrix} u_a(t) & J_k(t) \\ J_k^*(t) & u_b(t) \end{pmatrix} + \mathrm{i} \begin{pmatrix} \gamma_a(t) & 0 \\ 0 & \gamma_b(t) \end{pmatrix}, \tag{6.42}$$

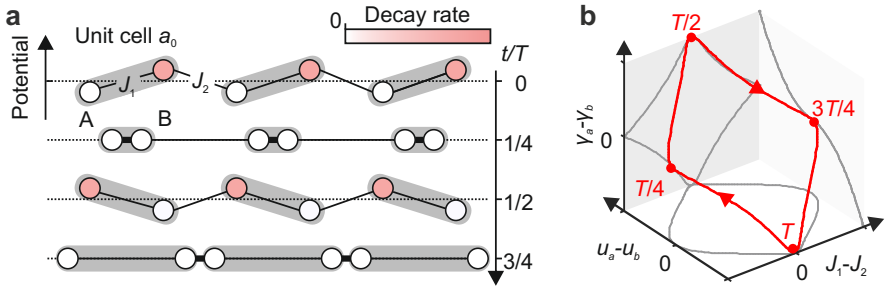

Figure 6.10: The model with driven loss term. The A site has a periodically driven loss γ_a, the B site has a periodically driven loss $\gamma_a(t - T/2)$. In position space that means the loss strength is always low for the initial A site excitation "Input A", and strong for the B case. (Left panel) snapshots of the model for every $T/4$ in one period, the distance and the height of the site represent the hopping strength and the on-site energy strength respectively. Note the lattice is not distorted. (Right panel) the parameter circle with an additional dimension, the loss strength $\gamma_a - \gamma_b$. From [228].

Name	Vlaue	Meaning
J_0	J_0	Hopping strength
u_0	$1.1\,J_0$	On-site energy
Ω	$1.1\,J_0$	Driven frequency
λ	1.75	A dimensionless parameter
φ	0	Phase factor in $u_{a/b}(t)$ and $\gamma_{a/b}(t)$
γ	$0.4\,J_0$	Loss strength

Table 6.1: Typical parameters values. From [228]

where we used $J_k^*(t) = J_1(t)e^{-\mathrm{i}ka/2} + J_2(t)e^{+\mathrm{i}ka/2}$. The $H_{\mathrm{RM}}(k,t)$ and $\Gamma(t)$ are the Hermitian part and loss part of the non-Hermitian Hamiltonian matrix respectively. If we now define $\psi_k = (a_k, b_k)$ then the Hamiltonian operator can be written as $\hat{H}(t) = \sum_k \psi_k^\dagger H_k(t)\psi_k$.

$$\begin{cases} u_a(t) = -u_0\cos(\Omega t + \varphi), & u_b(t) = u_a(t - T/2) \\ J_1(t) = J_0 e^{-\lambda(1-\sin\Omega t)}, & J_2(t) = J_1(t - T/2) \\ \gamma_a(t) = -\gamma_0\Theta\left(u_a(t)\right)\cos(\Omega t + \varphi), & \gamma_b(t) = \gamma_a(t - T/2) \end{cases} \tag{6.43}$$

The typical values of the constants in the above equations are summarized in the Table. 6.1. We can write $H(t,k)$ into Pauli matrices as well, it reads

$$\begin{aligned} \hat{H}_k(t) = &\left(J_1 + J_2\right)\cos\frac{ka_0}{2}\sigma_x + \left(J_1 - J_2\right)\sin\frac{ka_0}{2}\sigma_y \\ &+ \left(u_a - \mathrm{i}\gamma_a\right)\left(1 + \sigma_z\right)/2 + \left(u_b - \mathrm{i}\gamma_b\right)\left(1 - \sigma_z\right)/2 \end{aligned} \tag{6.44}$$

As we know, we can write the $H_{\mathrm{RM}}(k,t)$ into $H_{\mathrm{RM}}(k,t) = (d^0)I + \boldsymbol{d}(t)\cdot\boldsymbol{\sigma} + \cdots$, where $\boldsymbol{\sigma} = (\sigma_1, \sigma_2, \sigma_3)$ are usual Pauli matrices. By noticing $u_a + u_b = 0$ we have $\boldsymbol{d} = (\mathrm{Re}\,J_k^*, \mathrm{Im}\,J_k^*, \frac{1}{2}(u_a - u_b))$. By including the loss term, the instantaneous eigenvalues are $\frac{i\gamma_a + i\gamma_b}{2} \pm \Delta$, where $\Delta =$

$\left(\sqrt{|J_k|^2 + (u_a - u_b + i\gamma_a - i\gamma_b)^2/4}\right)$. The eigenvalue is reduced to $|d|^2$ if one set $\gamma_a = \gamma_b = 0$.

From the instantaneous point of view, we can check the condition of the adiabaticity. Following [193], we focus on the first half of the period. There $\gamma_b = 0$, the adiabatically condition reads $2|\Omega_a(t)| \ll |\Delta(t)|$ here the $\Delta(t)$ gap defined in the instantaneous eigenvalue and $\Omega_a(t) = -\dot{\alpha}/2$. And the α is defined through $\alpha = 2\arctan(J_k/(\Delta_0 - i\gamma_a))$, $\Delta_0 = (u_a - u_b)/2$. The gap varies around for the first half period and for $\gamma_0 = 0$ the instantaneous gap from 0.932 for $(k = -\pi, t = 0.699)$ to 1.154 for $(k = 0, t = 0)$, and the time derivative of the mixture angle can vary considerably, 0 to 10^{15}. For loss strength, γ_0 up to 1 the situation is not changed so much. This indicates that the adiabaticity is not reached for every k point in the first half period and then it won't be reached generally, thus a non-adiabatic treatment, e.g., Floquet theory, is needed.

Since typically $J_0 \sim \Omega \sim u_0$, it is expected that the adiabatic perturbation theory won't work well for low orders of Ω as well as the high-frequency expansion for low orders of Ω^{-1}. For those reasons, we focus on the numerical solutions of the Floquet matrices and the ODE solutions.

The equations of motion of the wave-guide in the k space can be written as

$$i\partial_t \psi_k(t) = H(t,k)\psi_k(t) \tag{6.45}$$

Now our non-Hamiltonian have a discrete time transnational symmetry $H(t) = H(t+T)$, the Floquet theorem applies. As we discussed in the previous chapter, the Floquet theorem [3, 225] states that for a ordinary differential equation $(H(t) - id_t)\psi(t) = 0$ with the time periodicity $H(t) = H(t+T)$, there always exist a set of complete and orthogonal solutions called Floquet states $\Psi_\alpha(t) = e^{-i\epsilon_\alpha t}\phi_\alpha(t)$. The ϵ_α is the quasi-energy just like I discussed in the Floquet theorem section. Further the $\phi_\alpha(t)$ have a periodicity $\phi_\alpha(t) = \phi_\alpha(t+T)$ that allows us to mode expand it to $\phi_\alpha(t) = \sum_m u_\alpha^m e^{-im\Omega t}$. All these Floquet techniques are applicable for an non-Hermitian Hamiltonian, the only difference is that since the Hamiltonian is not self-adjoint $H^\dagger \neq H$, we need to distinguish the left $\langle\psi^L|$ and the right states[3] $|\psi^R\rangle$ where

$$(|\psi^R\rangle)^* = \langle\psi^R| \neq \langle\psi^L| \tag{6.46}$$

With the help of the Floquet theorem and Floquet states, and remind that we can split the $\{\alpha\}$ into $\{k, \alpha\}$ since the Floquet matrix is k-space diagonal, we can rewrite the differential equation

$$\mathcal{H}_k |u_{k\alpha}^R\rangle = \epsilon_{k\alpha} |u_{k\alpha}^R\rangle \quad \text{and} \quad \langle u_{k\alpha}^L| \mathcal{H}_k^\dagger = \langle u_{k\alpha}^L| \epsilon_{k\alpha} \tag{6.47}$$

In the component-wise expression $\sum_n \mathcal{H}_{k,ij}^{mn} u_{k\alpha,j}^n = \epsilon_{k\alpha} u_{k\alpha,i}^m$. Here $i, j \in \{A, B\}$. The static Hamiltonian like matrix $\mathcal{H}$ is called Floquet Hamiltonian, $\mathcal{H}_k^{mn} = H_{k,ij}^{m-n} - n\omega\delta^{mn}\delta_{ij}$. Where $H_{k,ij}^{m-n}$ is obtained by $H_{k,ij}^{m-n} \equiv \frac{1}{T}\int_0^T dt\, e^{i(m-n)\omega t} H_{ij}(t,k)$, T is the time period.

We determine the initial condition [15] of the Floquet problem [174] by inserting the Floquet space projector $\hat{P}_\alpha(t) = |\Psi_\alpha^R(t)\rangle \langle\Psi_\alpha^L(t)|$. The normalization condition is $|\Psi_\alpha^{R/L}(0)\rangle = \frac{|\Psi_\alpha^{R/L}(0)\rangle}{\sqrt{\langle\Psi_\alpha^L(0)|\Psi_\alpha^R(0)\rangle}}$ and the projector is $\hat{P}_\alpha = |\Psi_\alpha^R\rangle \langle\Psi_\alpha^L|$, then we can express the initial state

$$|\psi(0)\rangle = \sum_{k\alpha} \hat{P}_{k\alpha}(0) |\psi(0)\rangle = \sum_{k\alpha} C_{k\alpha} |\Psi_{k\alpha}^R(0)\rangle \tag{6.48}$$

[3] Should not be confused with the "retarded".

with the coefficients $C_{k\alpha} = \langle \Psi^L_{k\alpha}(0)|\psi(0)\rangle$. Here we have already set the initial time $t_0 = 0$ and defined $|\psi(0)\rangle \equiv |\psi_{\text{init}}\rangle$. One can further write arbitrary state into modes $|u^{R,n}_{k\alpha}\rangle$

$$|\psi(t)\rangle = \sum_{k,\alpha,n} C^n_{k\alpha} e^{-\mathrm{i}(\epsilon_{k\alpha}+n\Omega)t} |u^{R,n}_{k\alpha}\rangle, \quad C^n_{k\alpha} = \langle u^{L,n}_{k\alpha} \mid \psi(0)\rangle \tag{6.49}$$

where the $C^n_{k\alpha}$ can be easily computed once the $\langle u^{L,n}_{k\alpha}|$ are computed from the (6.47). The Floquet matrix for the Hermitian part of this model is

$$\mathcal{H}_{mn} = H_{mn} - n\Omega\delta_{m,n} \tag{6.50}$$

and

$$H_{mn} = \begin{pmatrix} \Delta_A^{(m-n)}(z) & J_k^{(m-n)}(z) \\ J_k^{*(m-n)}(z) & \Delta_B^{(m-n)}(z) \end{pmatrix} \tag{6.51}$$

With the components for the hoppings

$$J_k^{(n)} = J_0 e^{-\lambda} I_n(\lambda)((-i)^n e^{+ika_0/2} + e^{-ika_0/2}) \tag{6.52}$$

$$J_k^{*(n)} = J_0 e^{-\lambda} I_n(\lambda)((-i)^n e^{-ika_0/2} + e^{+ika_0/2}) \tag{6.53}$$

Here $I_v(z)$ is the Bessel function of the second kind, it has the relation with the Bessel function of the first kind, $\mathcal{J}_v(x)$ $I_v(z) = \frac{z^v}{(iz)^v}\mathcal{J}_v(iz)$. And a_0 is the lattice constant. And the components for the one-site driving

$$\Delta_a^{(m)} = -\frac{\Delta_0}{2}\delta_{m,1} - \frac{\Delta_0}{2}\delta_{m,-1} \tag{6.54}$$

$$\Delta_b^{(m)} = +\frac{\Delta_0}{2}\delta_{m,1} + \frac{\Delta_0}{2}\delta_{m,-1} \tag{6.55}$$

Use the Floquet matrix, we can compute the Floquet spectra functions.

6.2.3 Observables and spectral quantities

For direct comparisons with the experiment, it is useful to define spectral functions in the extended zone of the Floquet problem, with Floquet mode dependencies. Define $u^{L,nl}_{k\alpha,i} = \langle ki|u^{L,nl}_{k\alpha}\rangle$ and $u^{R,nl}_{k\alpha,i} = \langle ki|u^{R,nl}_{k\alpha}\rangle$, where the momentum-sublattice basis are $|ki\rangle \in \{|k,A\rangle, |k,B\rangle\}$, then one can define a "retarded" Green's function[4]

$$\tilde{G}^{nm}_{k,ij}(E) = \sum_{l,\alpha} \frac{\left(u^{L,nl}_{k\alpha,i}\right)^* u^{R,lm}_{k\alpha,j}}{E - \epsilon_{k\alpha} - l\Omega + \mathrm{i}0} \tag{6.56}$$

[4] The Green's function contains projectors $\sim |u^R\rangle\langle u^L|$

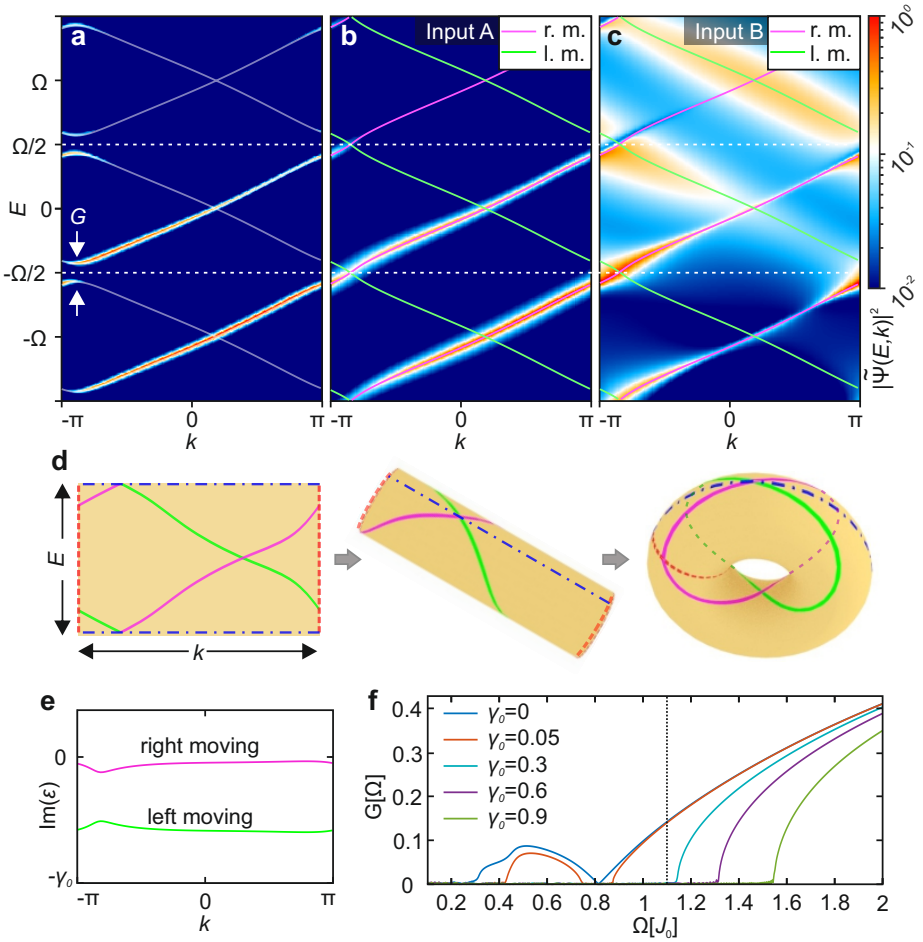

Figure 6.11: (Top) (a) The occupation spectra of the Hermitian, and (b,c) non-Hermitian models. (Middle) (d) The schematic plot of the winding of the Floquet spectra over the Floquet-Bloch Brillouin zone, a torus. (Bottom) (c) The imaginary part of the Hamiltonian, where one can see the left and right moving branches are separated by a gap. (d) The real part gap size G is defined in (a) vs the driving frequency Ω/J_0. (e) Note that the π gap closed in the real part and open in the imaginary part of the quasi-energies for high enough γ_0 which can be interpreted as a topological band structure for the non-Hermitian Hamiltonian. (f) the $\pm\pi$ gap has a finite closed region for finite γ_0 rather than a single closed fine-tuning point when varying Ω/J_0. From [228].

where $u^{nl} \equiv u^{n+l}$. Alternatively, we can define

$$G^{nm}_{k,ij}(E) = \sum_{l,\alpha} \frac{\left(u^{R,nl}_{k\alpha,i}\right)^* u^{R,lm}_{k\alpha,j}}{E - \epsilon_{k\alpha} - l\Omega + \mathrm{i}0} \tag{6.57}$$

Which of the above definitions, (6.56) or (6.57), is better depends on the situation. One can say that the LR projector is more mathematical straightforward. However, it may give a negative result on the physical observables. On the other hand, the RR case has the problem that the inner product is

decaying

$$\langle \Psi^R_{k\alpha}(t) \mid \Psi^R_{k\alpha}(t) \rangle = \mathrm{e}^{-\Gamma_{k\alpha} t} \tag{6.58}$$

Or in another word, $|\Psi^R\rangle$ and $\langle\Psi^R|$ are not orthogonal. This is somehow suitable since the Hamiltonian has a loss term which is purely imaginary. This choice also prevents the computed occupation number to be negative, which happens by using the LR projector.

The (time-averaged) occupation spectrum of G is

$$G^<_{k,ij}(E) \equiv \mathrm{Im}\, G^{00}_{k,ij}(E) \tag{6.59}$$

recall that the $\epsilon_{k\alpha}$ is in general complex, which makes the imaginary part lorentzian with a finite width.

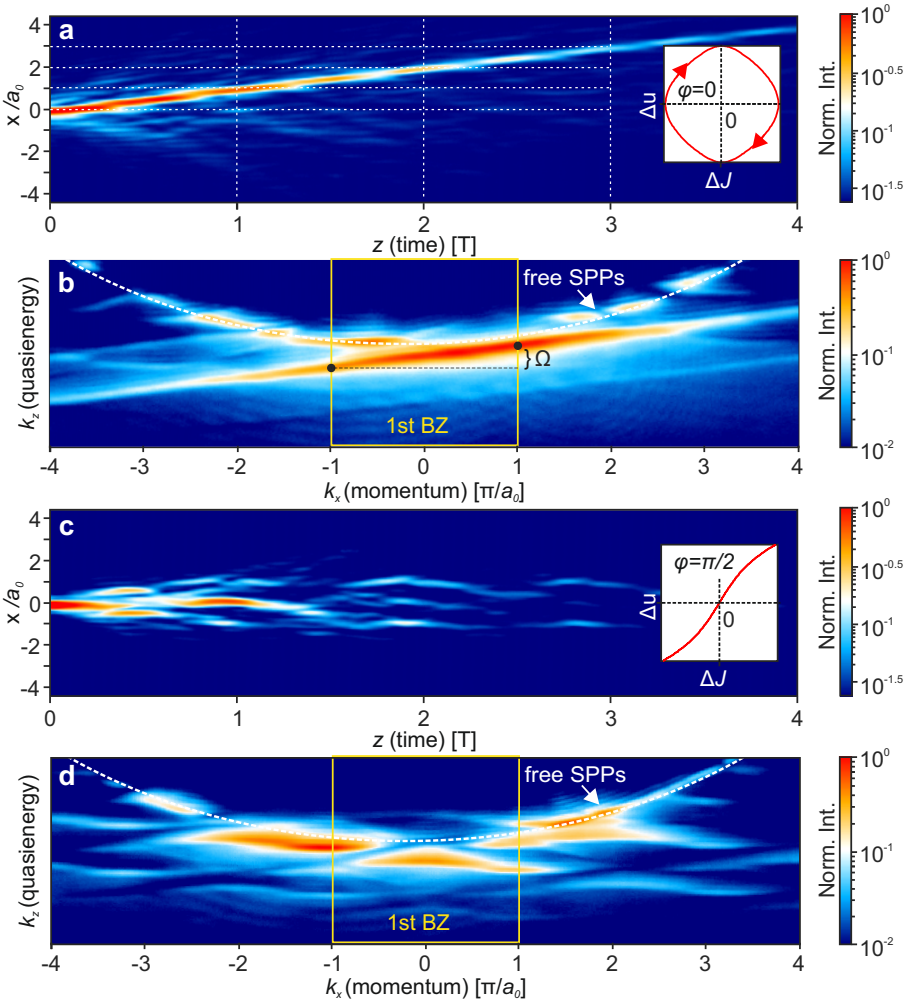

Figure 6.12: $I(E,k)$ measured in the wave-guide experiments. See also the Fig. 6.11. One can see that it have the feature of the Thouless pump that only when the time-reversal symmetry is broken, i.e. $\varphi = 0$, the current is non zero. From [228].

In the experiment (Fig. 6.12) one measures the energy-momentum resolved intensities which are defined as

$$I(E,k) = \left\langle \Psi_k(E) \mid \Psi_k(E) \right\rangle = \sum_{n,m,\alpha\beta} \sum_{l,\gamma} \frac{C^{l*}_{k\beta} C^{l}_{k\alpha} \left(u^{R,nl}_{k\beta\gamma}\right)^* u^{R,lm}_{k,\gamma\alpha}}{\left(E - \varepsilon^*_{k\beta} - l\Omega - i0\right)\left(E - \varepsilon_{k\alpha} - l\Omega + i0\right)} \tag{6.60}$$

If we approximate the initial density matrix that is diagonal for Floquet indices, the above formula can be simplified tod

$$I_\alpha(E,k) = \left\langle \Psi^n_{k\alpha}(E) \mid \Psi^n_{k\alpha}(E) \right\rangle = \sum_{n,m,l,\gamma} C^{l*}_{k\alpha} C^{l}_{k\alpha} \frac{\left(u^{R,nl}_{k\alpha\gamma}\right)^* u^{R,lm}_{k,\gamma\alpha}}{\left|E - \varepsilon_{k\alpha} - l\Omega\right|^2} \tag{6.61}$$

For a single site initial excitation, the only difference between the (6.60) and (6.61) is the denominator modulus squared or not. The $I(E,k)$ is plotted for different losses in the Fig. 6.11. Where one can see that the complete winding is restored by the time-dependent periodic dissipation with enough maximum strength γ_0.

6.2.4 Occupation spectrum

This also allows us to compute the initial occupation $\mathcal{N}$ of the Floquet states $\Psi_{k\alpha}$, just as we discussed before in (6.25), with small modification for the non-Hermitian case

$$\mathcal{N}_i(E) = \sum_{k,\alpha} \mathrm{Im}\left(\frac{1}{\pi} \frac{\Psi^{R,*}_{k\alpha,i}(0)\Psi^{R}_{k\alpha,i}(0)}{E - \epsilon_{k\alpha} + \mathrm{i}0^+}\right) \tag{6.62}$$

here one can see that the $\mathcal{N}_i(E)$ is always positive. Note the drawback for this definition is again that the exact projector is not used and the basis is not orthogonal, although it is positive defined.

The $t_0 = 0$ occupation number spectrum can be computed by the modes $u_{k\alpha}$ directly, for the setup that at $t = 0$ only one site is excited $\Psi_{k\alpha A}(0) = \langle \psi_{kA}(0) | \Psi_{k\alpha}(0) \rangle$ and the occupation spectrum is

$$\begin{aligned} \mathcal{N}_A(E) &= \sum_\alpha \delta(E - \epsilon_{\alpha,k}) |C_{k\alpha}|^2 |\Psi_{k\alpha}(0)|^2 = \sum_\alpha \delta(E - \epsilon_{\alpha,k}) \Psi^*_{k\alpha A}(0) \Psi_{k\alpha A}(0) \\ &= \sum_\alpha \delta(E - \epsilon_{\alpha,k}) (\sum_n u^{n*}_{k\alpha A}) (\sum_m u^{m}_{k\alpha A}) \end{aligned} \tag{6.63}$$

Used only the R (right) states, the $\mathcal{N}_B$ can be computed in the same way.

The $\mathcal{N}_A(E)$ and $\mathcal{N}_B(E)$ for different losses γ_0 are plotted in Fig. 6.13 analog to the standard Rice-Mele model Thouless pump result in the previous sections, see Fig. 6.8. The windings around the FFZ torus are completed for high enough loss, for instance, $\gamma_0/J_0 = 0.4$. The losses for initially excited A or B are different, which can be seen in the model Hamiltonian that the particle (quasi-particle) experiences difference loss when it flies along the high loss route or the low loss route. This is reflected in the Fig. 6.13 as well. For $\gamma_0 = 0$ the A/B the initial choices are identical up to the sign of the slopes. However, when switching on the time-dependent and sub-lattice dependent loss $\gamma_0 \neq 0$, the B initial excitation has a larger spectral broadening and have a mixed left and right moving occupations,

though the spectra have the 0 and $\pm\pi$ gaps are both closed. The A initial excitation gives a complete integer winding and thus a quantized charge pump, with a relatively small spectral broadening. This means a not so short lifetime decaying Thouless pump.

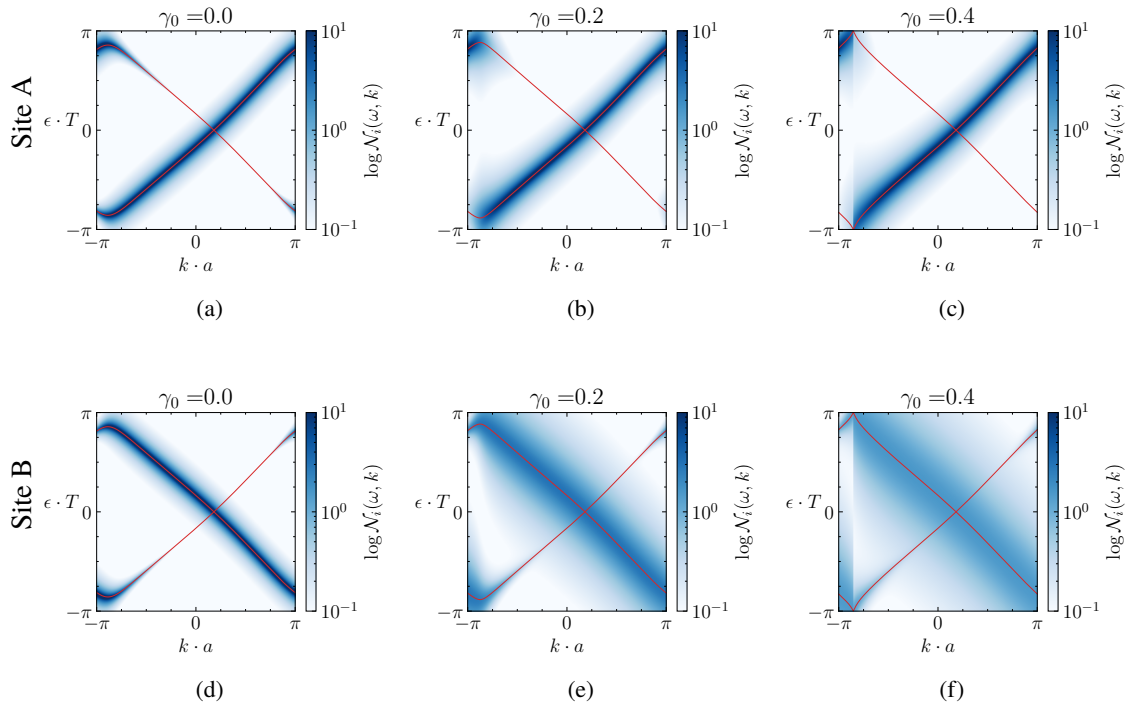

Figure 6.13: (a-c) The $\mathcal{N}_A(E)$ and (d-f) the $\mathcal{N}_B(E)$ for different loss strength, in logarithm scale. See also Eq. (6.63).

6.2.5 Pump charge and current

The current operator [171, 232] can be simply computed from the non-loss part of $H(t)$ which we call it H^h, by $\hat{J}(t) = \frac{1}{Na}\sum_k \partial H_k^h(t)/\partial k$ for the non-Hermitian case as well, the result is

$$\hat{J}(t) = \frac{1}{2N}\sum_k \left[iJ_k(t)b_k^\dagger(t)a_k(t) - \mathrm{i}J_k^*(t)a_k^\dagger(t)b_k(t)\right] \tag{6.64}$$

where $J_k(t) = -J_1(t)e^{-ika/2} + J_2(t)e^{+ika/2}$ with $J_1(t)$, $J_2(t)$ defined in Eq. (6.43). The current expectation value we compute by using the solution $\psi(t)$ of the ordinary differential equation through $a^\dagger(t)\,|0\rangle = \psi_A(t)$, $b^\dagger(t)\,|0\rangle = \psi_B(t)$ and

$$\langle\hat{J}\rangle(t) = \begin{pmatrix}\psi_A^*(t) & \psi_B^*(t)\end{pmatrix}\begin{pmatrix}\hat{J}_{AA}(t) & \hat{J}_{AB}(t)\\ \hat{J}_{BA}(t) & \hat{J}_{BB}(t)\end{pmatrix}\begin{pmatrix}\psi_A(t)\\ \psi_B(t)\end{pmatrix} \tag{6.65}$$

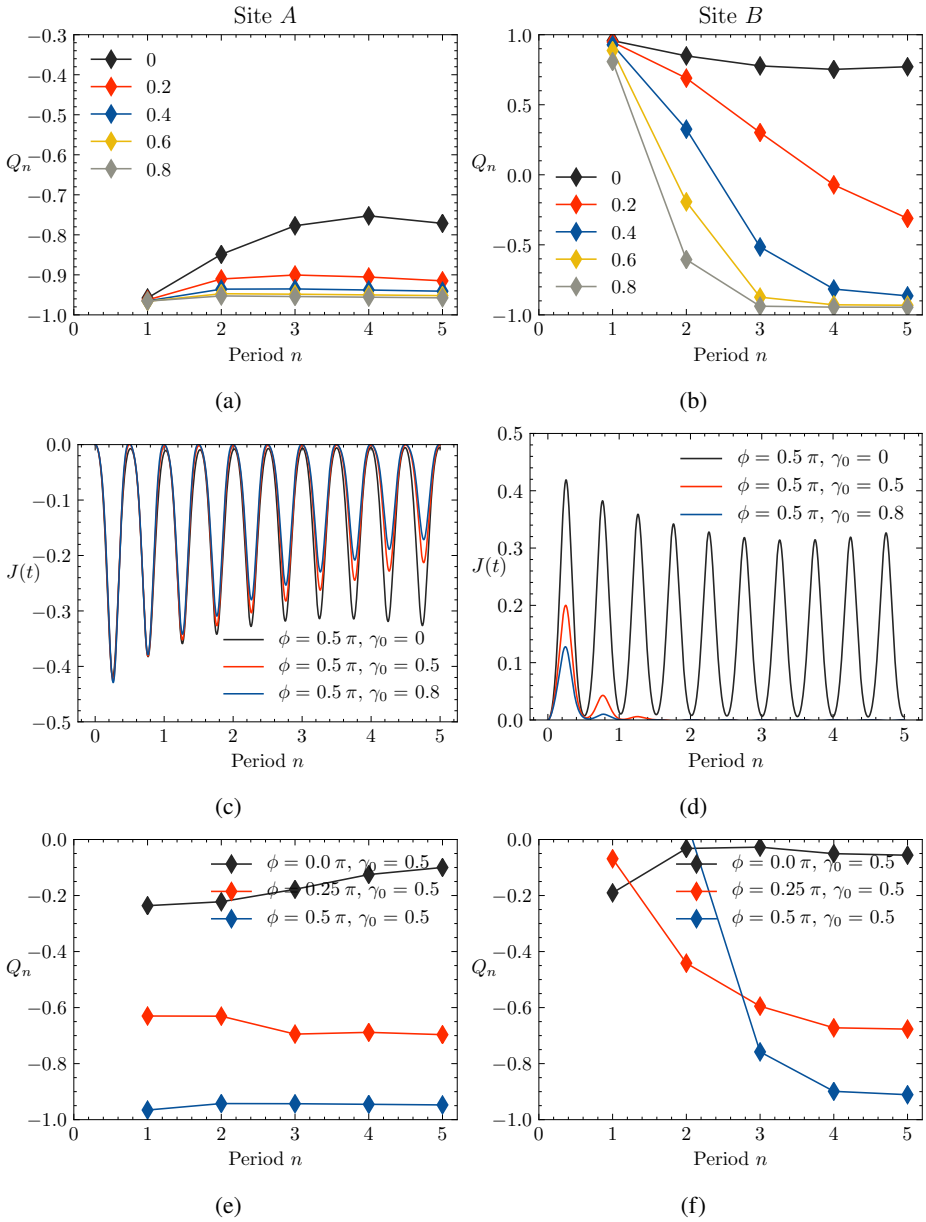

Figure 6.14: Charge pumped per cycle and the time dependent current density computed by directly solving the ODE. The legends in the plots on the first row are for the γ_0.

for the initial condition $\psi_k(t=0) = (1,0)^\intercal$, which corresponds to locally excite a single site in the one dimensional lattice with the spatial dimension $d_s = 1$.

Since the system has a loss term, the wave function is decaying as well as the current expectation value. To get a constant output to help us see the transport behavior better, we normalize the current by $J_{\text{norm}}(t) = \langle \hat{J}(t) \rangle / \sum_i \psi_i^*(t)\psi_i(t)$. For the results obtained by directly solving the time-dependent Schrödinger equation see Fig. 6.14.

Although the numerical result for the Floquet Green's functions will not be presented in this chapter,

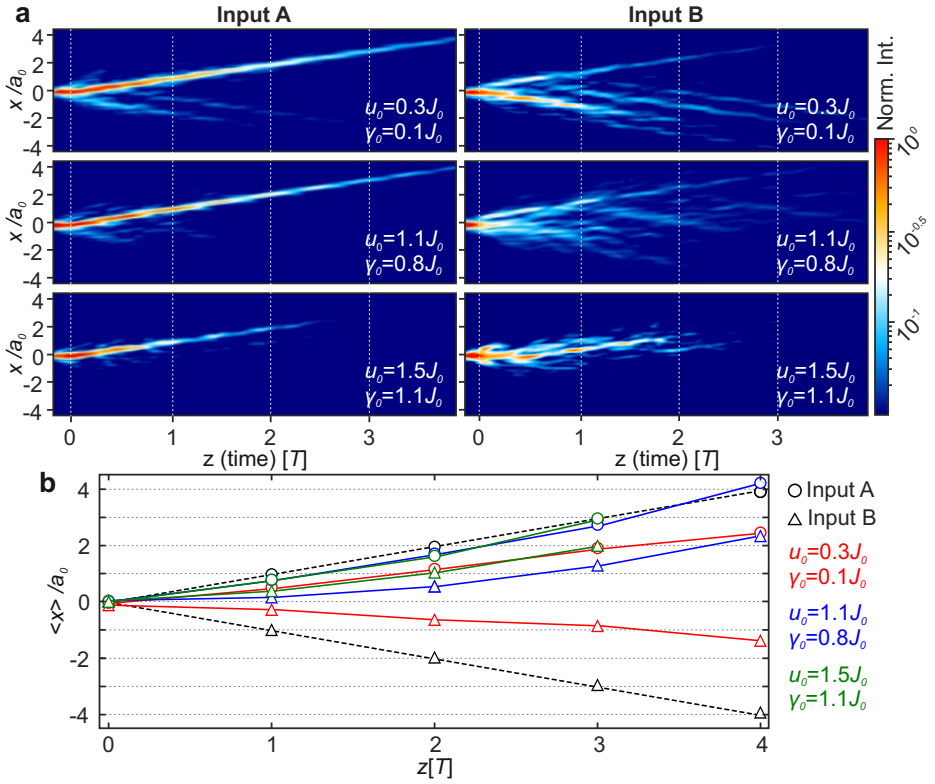

Figure 6.15: (a) The experimental picture. Note that the scale is logarithmic. (b) The center position of the wave packet. From [228].

here I present the discrete Fourier space $J_{k,mn}$ which is especially useful to compute the steady current through the formula $J \sim \mathrm{Tr}[J_k G_k^<]$, where $J_k = J_{k,mn}$ and $G_k^< = G^<_{k,AB}(\omega)$,the trace is taken in the Floquet space and with a integration/summation of the ω and k. For computing the Fourier coefficients. Use the identity of Jacobi-Anger expansion identity

$$e^{iz\cos\theta} = \sum_{n=-\infty}^{\infty} i^n \mathcal{J}_n(z) e^{in\theta} \tag{6.66}$$

where $\mathcal{J}_n(z)$ is the Bessel function of the first kind

$$\mathcal{J}_n(z) = \left(\frac{1}{2}z\right)^n \sum_{k=0}^{\infty} (-1)^k \frac{\left(\frac{1}{4}z^2\right)^k}{k!\Gamma(n+k+1)} \tag{6.67}$$

If let $z = -\mathrm{i}\lambda$ and $\theta = \Omega t$ then

$$e^{\lambda\cos\Omega t} = \sum_{n=-\infty}^{\infty} \mathrm{i}^n \mathcal{J}_n(-\mathrm{i}\lambda) e^{\mathrm{i}n(\Omega t)} \tag{6.68}$$

Use the above expansions, the Fourier coefficients of the hopping are $J_1(t) = J_0 e^{-\lambda} e^{\lambda \sin \Omega t} = \sum_{n=-\infty}^{\infty} J_{1,n} e^{\mathrm{i}n\Omega t}$

$$J_{1,n} = J_0 e^{-\lambda} \mathcal{J}_n(-\mathrm{i}\lambda) = J_0 e^{-\lambda} (-\mathrm{i})^n I_n(\lambda) \tag{6.69}$$

and for $J_2(t)$, and $J_2(t) = J_0 e^{-\lambda} e^{\lambda \cos \Omega t} = \sum_{n=-\infty}^{\infty} J_{2,n} e^{\mathrm{i}n\Omega t}$ one has

$$J_{2,n} = J_0 e^{-\lambda} \mathrm{i}^n \mathcal{J}_n(-\mathrm{i}\lambda) = J_0 e^{-\lambda} I_n(\lambda) \tag{6.70}$$

Then define $A_{mn} = A_{m-n}$, it is straightforward to compute the mode coefficients

$$(\partial_k J_k)_{mn} = \left(+\mathrm{i}\frac{a}{2} J_1(t) e^{+\mathrm{i}ka/2} - \mathrm{i}\frac{a}{2} J_2(t) e^{-\mathrm{i}ka/2} \right)_{mn} \tag{6.71}$$

$$= \frac{\mathrm{i}a}{2} J_0 i^{-n} e^{-\lambda - \frac{1}{2}\mathrm{i}ak} \left(\mathrm{i}^n e^{\mathrm{i}ak} - \mathrm{i}^m \right) \mathcal{J}_{m-n}(-\mathrm{i}\lambda) \tag{6.72}$$

Here we used relation J_n and $(J)_n^*$, i.e., $(J)_n^* = (J_{-n})^*$, and $((\partial_k J_k)^*)_{mn} = ((\partial_k J_k)_{nm})^*$.

6.3 Summary

In this chapter, we discussed the Thouless pump by the Rice-Mele model. Further, we discussed the dissipative non-adiabatic Thouless pumps which are realized in the plasmonic wave-guide experiments. The result shows that the quantized charge pump can be restored by time-dependent stagger onsite losses, where the loss strength is always strong for one species of the site and weak for another. We have done quantitative numerical computations to verify our understanding. Let us summarize this chapter by the following graph.

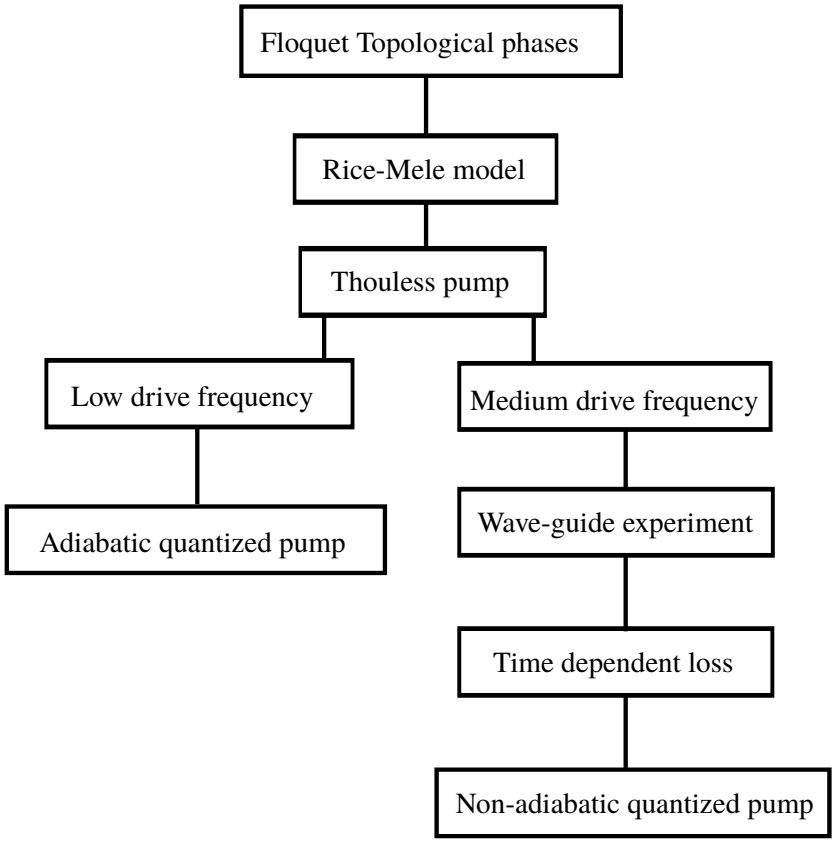

Figure 6.16: Summary of Thouless pumps and non-adiabatic Thouless pumps

CHAPTER 7

Interacting and periodically driven systems: Floquet-Keldysh self-consistent field theory

In this chapter, we review the dynamical mean-field theory (DMFT) and then use its Floquet-Keldysh version to study a Rice-Mele Hubbard model. The Floquet-Keldysh DMFT, as well as the non-equilibrium DMFT, is pioneered by the study of Petra Schmidt and Hartmut Monien [239]. The dynamical mean-field theory is one of the most important and widely used methods for studying strongly correlated systems. Some representative reviews and lecture notes are [240–243]. The diagrammatic extension to nonlocal correlations such as is discussed in [77]. Detail discussions of the non-equilibrium DMFT can be found in [3].

As we have seen in previous chapters the Rice-Mele model and Thouless pump on it give us one of the simplest examples of periodically driven topological phases. The dissipative nonadiabatic Thouless pump introduced in the previous chapter gives us a example that dissipation can be a resource for exotic phenomena, such as topological transport. On the other hand, a natural and intrinsic source of dissipations is the fermion-fermion interaction, e.g. the Hubbard interaction. For the Hubbard interactions, although the interactions are unitary, the dissipation of single-particle quantities exists when we treat the many-body background as an effective bath[1], analogue to the collision integral we have seen in the quantum Boltzmann equation where the single quasiparticles can decay. How can these dissipations apply to transport, and can the drive and interaction introduce new phases? It is also natural to ask if interaction-introduced dissipations are compatible with the Thouless pump? On the other hand, we can find that the Rice-Mele model has a representative band structure and drive frequency dependences. The bandwidth variation of the Rice-Mele model may also help us to understand phenomena in driven topological matters in general, as well as the interplay between the interaction and the drive. In this chapter, we will try to solve the fermionic Rice-Mele-Hubbard model with the Floquet-Keldysh dynamical mean-field theory and try to get qualitative answers to the questions above.

7.1 Hubbard model and conserving approximation

In this section, we review the diagrammatics of the Hubbard model.

[1] Where we integrated out some degrees of freedom of the system.

Recall that the general partition function of a four-fermion a particle-particle interaction can be written as [57], which we discussed in the DSE chapter

$$\exp W[\eta, j] = Z[\eta, j] = \int \mathrm{d}[\hat{\psi}] \exp\left\{\eta_a \hat{\psi}_a + \frac{1}{2} j_{ab} \hat{\psi}_a \hat{\psi}_b - \frac{1}{24} \lambda_{abcd} \hat{\psi}_a \hat{\psi}_b \hat{\psi}_c \hat{\psi}_d\right\} = \int \mathrm{d}[\hat{\psi}] e^{-S} \tag{7.1}$$

Here we use the Euclidean notation for a while. The typical concrete example of the above type model is the Hubbard model, which is a lattice model with spin $\frac{1}{2}$ fermions. Let us define

$$\hat{\psi}_a = \hat{\psi}_{x\alpha} = \left(\psi_{x\uparrow}, \quad \psi_{x\downarrow}, \quad \bar{\psi}_{x\uparrow}, \quad \bar{\psi}_{x\downarrow}\right) \tag{7.2}$$

For simplicity we will drop the "hat" of $\hat{\psi}$ in this section. We will mostly follow [57]. To reach the quartic term of the Hubbard model, choose

$$\lambda_{abcd} = -\epsilon_{\alpha\beta\gamma\delta} U \delta_{xy} \delta_{xz} \delta_{xw} \tag{7.3}$$

where ϵ_{abcd} is the Levi-Civita tensor. The x, y, z, w are space time variables, $\alpha\beta\gamma\delta$ are (super-) field indices. The contraction is straightforward, for clarity, we write out the space-time integrals

$$\begin{aligned} -\frac{1}{24} \lambda_{abcd} \psi_a \psi_b \psi_c \psi_d &= \frac{1}{24} U \int_{xyzw} \epsilon_{\alpha\beta\gamma\delta} \psi_{x\alpha} \psi_{y\beta} \psi_{z\gamma} \psi_{w\delta} \\ &= \frac{1}{24} U \int_x (\psi_{x,1}\psi_{x,2}\psi_{x,3}\psi_{x,4} + 23 \text{ anti-symmetric permutations}) \\ &= \int_\tau U \sum_i \bar{\psi}_{i\uparrow}(\tau)\psi_{i\uparrow}(\tau)\bar{\psi}_{i\downarrow}(\tau)\psi_{i\downarrow}(\tau) \end{aligned} \tag{7.4}$$

where, as we defined, $\psi_{x,1} = \psi_{x\uparrow}$, $\psi_{x,2} = \psi_{x\downarrow}$, $\psi_{x,3} = \bar{\psi}_{x\uparrow}$, and $\psi_{x,4} = \bar{\psi}_{x\downarrow}$. At the last step, we put the spatial coordinates on a lattice and used the lattice position index i.

The quadratic part is chosen as

$$\frac{1}{2} j_{ab} \psi_a \psi_b = \frac{1}{2} \int_{xy} \begin{pmatrix} \psi_{x\uparrow} \\ \psi_{x\downarrow} \\ \bar{\psi}_{x\uparrow} \\ \bar{\psi}_{x\downarrow} \end{pmatrix}^{\mathsf{T}} \begin{pmatrix} 0 & 0 & j_{xy,13} & 0 \\ 0 & 0 & 0 & j_{xy,24} \\ j_{xy,31} & 0 & 0 & 0 \\ 0 & j_{xy,42} & 0 & 0 \end{pmatrix} \begin{pmatrix} \psi_{y\uparrow} \\ \psi_{y\downarrow} \\ \bar{\psi}_{y\uparrow} \\ \bar{\psi}_{y\downarrow} \end{pmatrix} \tag{7.5}$$

Simple to set

$$j_{xy,13} = -j_{xy,31} = j_{xy,24} = -j_{xy,42} = -\delta(\boldsymbol{x} - \boldsymbol{y})\delta(x^0 - y^0)\partial_{x^0} - t\delta(\boldsymbol{x} \pm \boldsymbol{a} - \boldsymbol{y})\delta(x^0 - y^0) \tag{7.6}$$

where $\boldsymbol{a}$ is the unit lattice vector. Here t is the hopping (the tunneling between sites). The notation "t" is standard, though one may need to change it when considering real time formalism to avoid confusions. The above setting gives us

$$\frac{1}{2} j_{ab} \psi_a \psi_b = \int_\tau - \sum_{i\sigma} \bar{\psi}_{i\sigma}(\tau)\partial_\tau \psi_{i\sigma}(\tau) - t \sum_{\langle ij\rangle\sigma} \bar{\psi}_{i\sigma}(\tau)\psi_{j\sigma}(\tau) \tag{7.7}$$

Here $\langle ij \rangle$ means the nearest neighbors on the lattice. And we defined $\tau = x^0$

Consider the paramagnetic case, the Green's function can be written as

$$G_{ab} = \begin{pmatrix} 0 & 0 & G_{xy,\uparrow\uparrow} & 0 \\ 0 & 0 & 0 & G_{xy,\downarrow\downarrow} \\ -G_{yx,\uparrow\uparrow} & 0 & 0 & 0 \\ 0 & -G_{yx,\downarrow\downarrow} & 0 & 0 \end{pmatrix} \tag{7.8}$$

where the off-diagonal terms in spin space are switched off.

Recall that the second order Γ_Φ is

$$\Gamma_2 = \Gamma_1 - \frac{1}{48}\lambda_{atrs}\lambda_{becd}G_{ab}G_{te}G_{rc}G_{sd} \tag{7.9}$$

Perform the contractions give us

$$\Gamma_2 = \Gamma_1 - \frac{1}{2}U^2 G_{xy,\downarrow\downarrow}G_{xy,\uparrow\uparrow}G_{yx,\downarrow\downarrow}G_{yx,\uparrow\uparrow} \tag{7.10}$$

This is clearly 2-particle irreducible (or skeleton). Use 2.114, $\Sigma_{ab} = -\delta\Gamma_\Phi/\delta G_{ba}$. The corresponding U^2 order self-energies are then

$$\Sigma_{2,xy,\uparrow\uparrow} = -\frac{\delta(\Gamma_2 - \Gamma_1)}{\delta G_{yx,\uparrow\uparrow}} = \frac{U^2}{2}G_{xy,\uparrow\uparrow}G_{yx,\downarrow\downarrow}G_{xy,\uparrow\uparrow} \tag{7.11}$$

$$\Sigma_{2,xy,\downarrow\downarrow} = -\frac{\delta(\Gamma_2 - \Gamma_1)}{\delta G_{yx,\downarrow\downarrow}} = \frac{U^2}{2}G_{xy,\downarrow\downarrow}G_{xy,\uparrow\uparrow}G_{yx,\uparrow\uparrow} \tag{7.12}$$

This again defines a self-consistent theory under the conserving approximation.

Use $S = \int_\tau (\sum_{i\sigma} \bar{\psi}_{i\sigma}(\tau)\partial_\tau \psi_{i\sigma}(\tau) - \hat{H})$, we can write down the Hamiltonian of the Hubbard model. For instance, the 1-dimensional Hubbard model with operators can be written as [244]

$$H = -t\sum_{j=1}^{L}\sum_{\sigma=\uparrow,\downarrow}\left(c^\dagger_{j,\sigma}c_{j+1,\sigma} + c^\dagger_{j+1,\sigma}c_{j,\sigma}\right) + U\sum_{j=1}^{L} n_{j\uparrow}n_{j\downarrow} \tag{7.13}$$

where $n = n_{j\sigma} = c^\dagger_{j,\sigma}c_{j,\sigma}$. We replaced $\psi \to c$. The local Hilbert space of site j has the following states

$$|0\rangle, \quad c^\dagger_{j,\uparrow}|0\rangle, \quad c^\dagger_{j,\downarrow}|0\rangle, \quad c^\dagger_{j,\uparrow}c^\dagger_{j,\downarrow}|0\rangle \tag{7.14}$$

The $|0\rangle$ is the empty state where no electron is present.

7.2 Dynamical mean-field theory

7.2.1 Cavity construction

There are several different ways to construct the dynamical mean-field theory. The most popular way is the cavity construction [240, 243]. The cavity construction provides a clear and intuitive picture for

the local approximation of the strongly correlated systems where a local effective bath emergence. It also gives a direct mapping from the lattice model to the quantum impurity model. This mapping allows for practical uses and applications to realistic strongly correlated materials [241].

A dynamical and self-consistent mean-field $\Delta(\omega)$ is bridging a local impurity problem to a lattice problem when we transform the lattice problem to a single site problem embedded in a time-dependent environment. This bridging is conceptually analog to the traditional static mean-field theory, for instance, that for the Ising model.

There are two steps in the construction, the $1/z$ expansion to leading order and matching the Green's functions to close the equations and reach self-consistency. Here the z is the coordination number that is counting the connectivity of the lattice.

The dynamically updating will require the consistency conditions of

1. Local self-energy $\Sigma_{\text{loc}}(\omega)$

2. Dynamical effective bath function, hybridization, $\Delta(\omega)$

Closely following [240], here we do detailed derivations of the cavity construction. Although detail construction is not always important in applications, it still gives us some understandings of this method. We will frequently use the square lattice as an example. In general, at least for the original DMFT, the details of the lattice are less important. The important thing is the validity of the local approximation and a local effective bath, where the effective bath is a dynamical mean-field.

The first step of the DMFT construction is a $1/z$ expansion, here z is the coordination number. The power counting by the coordination number of the lattice model gives the lattice self-energy

$$\Sigma_{ij} \approx \Sigma_{ii}\delta_{ij} = \Sigma_{\text{loc}}\delta_{ij} \tag{7.15}$$

The reason of this approximation can be argued as follows [245]. Consider the d_s spatial dimensional tight binding model, the dispersion reads $\epsilon_{\mathbf{k}} = -2t\sum_{j=1}^{d_s}\cos k_j$, k_j is the quasi-momentum one j-th direction. Consider large spatial dimensions $d_s \to \infty$, the density of states $D(\omega)$, which can be regarded as a probability distribution, trend to a Gaussian distribution because of the central limit theorem

$$D(\omega)|_{d_s\to\infty} = \frac{1}{2\pi}\,A(\omega)|_{d_s\to\infty} = \frac{1}{t\sqrt{2d_s}\sqrt{2\pi}}\exp\left\{-\frac{\omega^2}{(\sqrt{2}t\sqrt{2d_s})^2}\right\} \tag{7.16}$$

If one requires the density of state to keep finite, then the hopping t should scale with the spatial dimension as well. For instance, we can choose

$$t = \frac{t_*}{\sqrt{2d_s}} \tag{7.17}$$

where t_* is an effective hopping that is independent of the spatial dimension. The result is

$$D(\omega)_{d_s\to\infty} = \frac{1}{t^*\sqrt{2\pi}}\exp\left\{-\frac{\omega^2}{(t^*\sqrt{2})^2}\right\} \tag{7.18}$$

Now we can check the local self-energy approximation [3, 240, 241, 246]. The hopping scales like $t = t_*/\sqrt{2d_s} = t_*/\sqrt{z}$, thus we can do a expansion in $1/\sqrt{2d_s}$ as in $1/N$ expansions. Consider the

square lattice, $d_s = 1$, $z = 2$, $d_s = 2$, $z = 4$, and $d_s = 3$, $z = 6$. Thus in d_s spatial dimension, one site on square lattice has $z = 2d_s$ neighbors. Now let us consider the skeleton self-energy. For instance, consider the sunset diagram $\Sigma_{ij}^{\text{sunset}} \sim G_{ij}G_{ij}G_{ji}$ with $|i-j| \leq 1$. It then has each line with non-local contribution scales as $G_{i\neq j} \propto 1/\sqrt{d_s}$ that in total gives $\propto 1/\sqrt{d_s^3}$. Since the self-energy $\Sigma_{ij}^{\text{sunset}}$ can choose j to be $2d_s$ neighbors for a given i, its dimension dependence becomes $\propto 2d_s/\sqrt{d_s^3} = 2/\sqrt{d_s}$. As a result, the nonlocal contribution is $\propto 1/\sqrt{d_s}$ that in $d_s \to \infty$ vanishes. Obviously, the $|i-j| > 1$ contribution vanishes even faster when $d_s \to \infty$. From the above arguments one can understand why "infinite dimension" is widely used in literature. On the other hand, if one can construct a lattice in low spatial dimension but has a large coordination number z, the local approximation should also work well.

Let us summarize the scaling behavior of the hopping. For a general lattice model with the hopping t_{ij}, it should have

$$t_{ij} \sim \left(\frac{1}{\sqrt{d_s}}\right)^{|i-j|} \tag{7.19}$$

and

$$G_{ij} \sim t_{ij} \sim \left(\frac{1}{\sqrt{d_s}}\right)^{|i-j|} \tag{7.20}$$

We also define the symbol $[]_{1/d_s}$ which gives the power of $(1/d_s)^n$

$$a \sim \left(\frac{1}{d_s}\right)^n \to [a]_{1/d_s} = n \tag{7.21}$$

For instance, $[t_{ij}]_{1/d_s} = |i-j|/2$.

Now consider a general lattice partition function

$$Z = \int \prod_{i\sigma} \mathrm{d}[\bar{c}_{i\sigma}, c_{i\sigma}] e^{-S} \tag{7.22}$$

with the action

$$S = \int_\tau \left(\sum_{i\sigma} \bar{c}_{i\sigma}\partial_\tau c_{i\sigma} - \sum_{ij,\sigma} t_{ij}\bar{c}_{i\sigma}c_{j\sigma} - \mu \sum_{i\sigma} \bar{c}_{i\sigma}c_{i\sigma} + U\sum_i n_{i\uparrow}n_{i\downarrow} \right) \tag{7.23}$$

Note here that we use the imaginary time notation and the thermal equilibrium setup, $\int_\tau = \int_0^\beta \mathrm{d}\tau$ to keep the notation close to [240]. As we will see, the DMFT approximate the spatial dependencies. This means, if necessary, the time contour can be changed straightforwardly.

The cavity construction is starting by splitting the action into three parts, they are the cavity site "o", S_o, the action with site o and all bonds to it removed, $S_{(o)}$, and the coupling between the site o and the other sites, S_Δ.

$$S = S_o + S_{(o)} + S_\Delta \tag{7.24}$$

The explicit forms of them are

$$S_{(o)} = \int_\tau \left(\sum_{i\neq o,\sigma} \bar{c}_{i\sigma}(\partial_\tau - \mu) c_{i\sigma} - \sum_{i\neq o, j\neq o,\sigma} t_{ij}\bar{c}_{i\sigma}c_{j\sigma} + U\sum_{i\neq o} n_{i\uparrow}n_{i\downarrow} \right) \tag{7.25}$$

$$S_o = \int_\tau \left(\sum_{\sigma} \bar{c}_{o\sigma}(\partial_\tau - \mu) c_{o\sigma} + U n_{o\uparrow}n_{o\downarrow} \right) \tag{7.26}$$

$$S_\Delta = \int_\tau \left(-\sum_{i\sigma} t_{io}\bar{c}_{i\sigma}c_{o\sigma} - \sum_{j\sigma} t_{oj}\bar{c}_{o\sigma}c_{j\sigma} \right) \tag{7.27}$$

The terms $t_{io}c_{o\sigma}$ and $t_{oj}\bar{c}_{o\sigma}$ can be treated as "external sources" before we take the functional integral of $\bar{c}_{o\sigma}$ and $c_{o\sigma}$ at the last step. To make the notation clear, we define

$$\begin{aligned} \eta_{i\sigma} &\equiv t_{io}c_{o\sigma} \\ \bar{\eta}_{j\sigma} &\equiv t_{oj}\bar{c}_{o\sigma} \end{aligned} \tag{7.28}$$

Note we need to keep in mind that $\bar{\eta}$ and η are depending on $\bar{c}_{o\sigma}$ and $c_{o\sigma}$.

Here we suppress the spin indices since they do not play a role in the power counting of $1/z$ (or $1/d_s$). With the previous definitions, the partition function then can be rewritten as

$$Z = \int \mathrm{d}[\bar{c}_o, c_o] e^{-S_o} \widetilde{Z}[\bar{\eta}, \eta] \tag{7.29}$$

where

$$\begin{aligned} \widetilde{Z}[\bar{\eta},\eta] &= \int \prod_{i\neq o,\sigma} \mathrm{d}[\bar{c}_{i\sigma}, c_{i\sigma}] e^{-S_{(o)}} e^{-S_\Delta} \\ &= \int \prod_{i\neq o,\sigma} \mathrm{d}[\bar{c}_{i\sigma}, c_{i\sigma}] e^{-S_{(o)}} \exp\left\{ \sum_{i\sigma} \bar{c}_{i\sigma}\eta_{i\sigma} + \sum_{j\sigma} \bar{\eta}_{j\sigma}c_{j\sigma} \right\} \end{aligned} \tag{7.30}$$

The $\widetilde{Z}$ can be regarded as a partition function of $S_{(o)}$ with external sources presented. The Schwinger functional of it can be defined as usual

$$e^{\widetilde{W}} = \widetilde{Z} \tag{7.31}$$

Expand the Schwinger functional $\widetilde{W}$, we get a formally exact equation [70]

$$\begin{aligned} \widetilde{W}[\bar{\eta},\eta] &= \sum_{n=1}^{\infty} \widetilde{W}_n \\ &= \sum_{n=1}^{\infty} \frac{(-1)^n}{(n!)^2} \sum_{i_1\cdots j_n} \int \bar{\eta}_{i_1}(\tau_{i_1}) \cdots \bar{\eta}_{i_n}(\tau_{i_n}) \eta_{j_1}(\tau_{j_1}) \cdots \eta_{j_n}(\tau_{j_n}) \widetilde{W}^{(n,n)}_{i_1\cdots j_n}(\tau_{i_1}\cdots\tau_{i_n}, \tau_{j_1}\cdots\tau_{j_n}) \end{aligned} \tag{7.32}$$

Note the $(-1)^n$ is from that we normal ordered Grassmann sources $\bar{\eta}$ and η. Here we neglected constant terms. The $\widetilde{W}^{(n,n)}$ means the result of functional derivative $\widetilde{W}$ functional n-times by $\bar{\eta}$ and then n-times by η.

If we keep only the lowest order of the connectivity, through power counting and comparing, we

have

$$\widetilde{W}[\bar{\eta},\eta] = -\int_{\tau_i\tau_j}\sum_{ij}\bar{\eta}_i(\tau_i)\eta_j(\tau_j)\widetilde{W}^{(1,1)}_{ij}(\tau_i,\tau_j)+\dots \tag{7.33}$$

Here the first term on RHS is of order 0 in $1/d_s$, it is because $t_{ij}\sim(1/\sqrt{d_s})^{|i-j|}$. The "..." terms are higher order in $1/z$ (or $1/d_s$) than the first term and vanishes in the limit $z\to\infty$. This is because the power counting [240] of $1/d_s$ shows that the dimension $[\widetilde{W}_n]_{1/d_s}=n-1$, where $\widetilde{W}=\sum_n\widetilde{W}_n$. Some further discussions can be found in [240].

If we rename the 2-point function $\widetilde{W}^{(1,1)}_{ij}(\tau_i,\tau_j)\to G_{(o),ij}(\tau_i,\tau_j)$, clearly here $G_{(o),ij}$ means the connected (2-point) Green's function with "o" site removed. We keep the spin index suppressed, it reads

$$\widetilde{W}_1[\bar{\eta},\eta] = -\int_{\tau_i\tau_j}\sum_{ij}t_{oi}\bar{c}_o(\tau_i)t_{jo}c_o(\tau_j)G_{(o),ij}(\tau_i,\tau_j) \tag{7.34}$$

where we used the definitions of the η and $\bar{\eta}$. From this expression, it is more clear that it gives $[\widetilde{W}_1]_{1/d_s}=0$. To convince ourselves, one can place i and j as nearest neighbors on the square lattice[2], and j one of the nearest neighbor of the "o"-site. Then the site i is at closest the next nearest neighbor of the "o"-site. We immediately have $t_{oi}\sim(1/\sqrt{d_s})^{|i-i_o|}=(1/\sqrt{d_s})^2$, $t_{jo}\sim(1/\sqrt{d_s})^{|j-i_o|}=(1/\sqrt{d_s})^1$, and $G_{(o),ij}\sim 1/\sqrt{d_s}$. The summations sums d_s possible ways to place i, and the same for j. Thus $\sum_i\sim d_s$, as well as $\sum_j\sim d_s$. Thus $[\widetilde{W}_1]_{1/d_s}=1+1/2+1/2-2=0$.

This means we now have an effective action in the local approximation $S_{\text{eff}}=S_o-\widetilde{W}_1$

$$S_{\text{eff}}=\int_\tau\bar{c}_o(\tau)(\partial_\tau-\mu)c_o(\tau)+\int_{\tau_i\tau_j}\sum_{ij}t_{oi}t_{jo}G_{(o),ij}(\tau_i,\tau_j)\bar{c}_o(\tau_i)c_o(\tau_j)+S_{o,\text{int}} \tag{7.35}$$

In above $S_{o,\text{int}}=\int_\tau Un_{o\uparrow}(\tau)n_{o\downarrow}(\tau)$.

The first two terms in (7.35) are quadratic in c-fields. Consider the time translation invariant case and do the imaginary time Fourier transform to Matsubara frequency. Use $Z_{\text{eff}}=\int D\bar{c}_oDc_oe^{-S_{\text{eff}}}$, one reaches an effective free Green's function which is corresponding to the quadratic part of the S_{eff}

$$\mathscr{G}_0^{-1}\left(\mathrm{i}\omega_n\right)=\mathrm{i}\omega_n+\mu-\sum_{ij}t_{oi}t_{jo}G^{(o)}_{ij}\left(\mathrm{i}\omega_n\right) \tag{7.36}$$

or

$$\mathscr{G}_0^{-1}\left(\mathrm{i}\omega_n\right)=\mathrm{i}\omega_n+\mu-\Delta(\mathrm{i}\omega_n) \tag{7.37}$$

If we define

$$\Delta(\mathrm{i}\omega_n)=\sum_{ij}t_{oi}t_{jo}G^{(o)}_{ij}\left(\mathrm{i}\omega_n\right) \tag{7.38}$$

The $\mathscr{G}_0$ is frequently called Weiss Green's function since it is conceptually very closed to the Weiss mean-field in the usual mean-field theory. Since here $G^{(o)}_{ij}$ is the propagator with the site "o" removed, the propagations that have intermediate steps on the "o" site should be subtracted. This suggests an

[2] The nearest is in the sense of Manhattan distances, i.e. the lines follows the lattice. More concretely one can consider $d_s=2$, for drawing on a paper.

important identity which we will use here without proof

$$G_{ij}^{(o)} = G_{ij} - G_{io}G_{oo}^{-1}G_{oj} \tag{7.39}$$

Note since G_{io} and G_{oj} both contain "o"-site, the double-counting should be canceled by dividing the "o"-site returning propagator.

Now we have

$$\Delta = \sum_{ij} t_{oi}t_{jo}G_{ij}^{(o)} = \sum_{ij} t_{oi}t_{jo}G_{ij} - \sum_{ij} t_{oi}t_{jo}G_{io}G_{oo}^{-1}G_{oj} \tag{7.40}$$

One can then transform the above equation into an equation between the local lattice Green's function and bare effective bath Green's function $\mathcal{G}(\omega)$.

The derivation is as follows. For convenience, define

$$\zeta \equiv \mathrm{i}\omega_n + \mu - \Sigma_{\mathrm{loc}}(\mathrm{i}\omega_n) \tag{7.41}$$

As argued at the beginning of this section, we can assume a local self-energy

$$\Sigma_{ij} \sim \Sigma_{\mathrm{loc}} \tag{7.42}$$

Now we can try to close the self-consistent loop. First we do Fourier transform for lattice indices, use $t_{\boldsymbol{k}} = \sum_{ij} t_{ij} e^{\mathrm{i}\boldsymbol{k}\cdot(\boldsymbol{x}_i - \boldsymbol{x}_j)}$, $\sum_{\boldsymbol{k}} t_{\boldsymbol{k}} = 0$, and the identity for lattice translational invariant quantities $\sum_{i'j'} a_{ii'}b_{i'j'}c_{j'j} = \sum_{\boldsymbol{k}} a_{\boldsymbol{k}}b_{\boldsymbol{k}}c_{\boldsymbol{k}}$, we have

$$\sum_{ij} t_{oi}t_{jo}G_{ij} = \sum_{\boldsymbol{k}} \frac{t_{\boldsymbol{k}}t_{\boldsymbol{k}}}{\mathrm{i}\omega_n + \mu - \Sigma_{\mathrm{loc}}(\mathrm{i}\omega_n) - t_{\boldsymbol{k}}} = \int_\epsilon A_0(\epsilon)\frac{\epsilon^2}{\zeta - \epsilon} \tag{7.43}$$

and

$$\begin{aligned}\sum_{ij} t_{oi}t_{jo}G_{io}G_{oo}^{-1}G_{oj} &= \left(\sum_i t_{oi}G_{io}\right)\left(\sum_j t_{jo}G_{oj}\right)\left(G_{oo}^{-1}\right) \\ &= \left(\sum_{\boldsymbol{k}} t_{\boldsymbol{k}}\frac{1}{\zeta - t_{\boldsymbol{k}}}\right)\left(\sum_{\boldsymbol{k}} t_{\boldsymbol{k}}\frac{1}{\zeta - t_{\boldsymbol{k}}}\right)\left(\sum_{\boldsymbol{k}} \frac{1}{\zeta - t_{\boldsymbol{k}}}\right)^{-1} \\ &= \left(\int_\epsilon A_0(\epsilon)\frac{\epsilon}{\zeta - \epsilon}\right)^2\left(\int_\epsilon A_0(\epsilon)\frac{1}{\zeta - \epsilon}\right)^{-1}\end{aligned} \tag{7.44}$$

For the last equal signs in (7.43) and (7.44) we have used the identity

$$\sum_{\boldsymbol{k}} a(\epsilon_{\boldsymbol{k}}) = \int_\epsilon A_0(\epsilon)a(\epsilon) \tag{7.45}$$

to transfer the momentum sum to an integration[3] over the density of states $D(\omega) = \frac{1}{2\pi}A_0(\omega)$. The $A_0(\omega)$ is defined through $D(\omega)$, where $D(\omega) = \sum_{\boldsymbol{k}} \delta(\omega - t_{\boldsymbol{k}})$. Here $\int_\epsilon = \int_{-\infty}^{\infty} \frac{\mathrm{d}\epsilon}{2\pi}$.

[3] A Hilbert transform.

One can now rewrite the RHS of equation (7.40) and get

$$\Delta = \int_\epsilon A_0(\epsilon)\frac{\epsilon^2}{\zeta-\epsilon} - \left(\int_\epsilon A_0(\epsilon)\frac{\epsilon}{\zeta-\epsilon}\right)^2 \left(\int_\epsilon A_0(\epsilon)\frac{1}{\zeta-\epsilon}\right)^{-1} \tag{7.46}$$

There are two useful identities[4]

$$\int_\epsilon \frac{A_0(\epsilon)\epsilon^2}{\zeta-\epsilon} = \zeta\int_\epsilon \frac{A_0(\epsilon)\epsilon}{\zeta-\epsilon}, \quad \text{and} \quad \int_\epsilon \frac{A_0(\epsilon)\epsilon}{\zeta-\epsilon} = -1 + \zeta\int_\epsilon \frac{A_0(\epsilon)}{\zeta-\epsilon} \tag{7.48}$$

where $\int_\epsilon = \int_{-\infty}^{\infty}\frac{\mathrm{d}\epsilon}{2\pi}$. By using them and perform some algebras, the equation (7.46) becomes

$$\Delta(\mathrm{i}\omega_n) = \zeta - \left(\int_\epsilon \frac{A_0(\epsilon)}{\zeta-\epsilon}\right)^{-1} = \mathrm{i}\omega_n + \mu - \Sigma_{\mathrm{loc}}(\mathrm{i}\omega_n) - G_{oo} \tag{7.49}$$

We can simply call $G_{\mathrm{loc}} = G_{oo}$, then indeed we have

$$\mathscr{G}_0^{-1} = \Sigma_{\mathrm{loc}} + G_{\mathrm{loc}}^{-1} \tag{7.50}$$

where we used the definition $\mathscr{G}_0^{-1} = \mathrm{i}\omega_n + \mu - \Delta(\mathrm{i}\omega_n)$. Now the (7.15) and (7.50) actually close the self-consistent loop.

The above derivations give an intuitive understanding of DMFT. However, one may want a recipe that is simple to use. In the next section, we will discuss a standard way to relate the DMFT to the single impurity Anderson model (SIAM), and perform the DMFT loop.

7.2.2 Single impurity Anderson model and DMFT loop

Here we sketch a standard way to present DMFT as a single impurity Anderson model with dynamical hybridization. Using the arguments in the previous section, we can write the action into a single impurity Anderson model (SIAM), called S_{SIAM}. The bath electron is denoted as c. And the local "impurity" is denoted as d. The action reads

$$S_{\mathrm{SIAM}} = S_c + S_d + S_{cd} \tag{7.51}$$

[4] They can be proven by add and subtract a term, e.g,

$$\int_\epsilon \frac{A_0(\epsilon)\epsilon}{\zeta-\epsilon} = \int_\epsilon \frac{A_0(\epsilon)\epsilon - A_0(\epsilon)\zeta + A_0(\epsilon)\zeta}{\zeta-\epsilon} \tag{7.47}$$

where

$$\begin{aligned} S_d &= \int_t \left(\sum_\sigma d^\dagger_\sigma \left(\mathrm{i}\partial_t - \epsilon_d \right) d_\sigma + U n_{d\uparrow} n_{d\downarrow} \right) \\ S_{cd} &= \int_t \sum_{i\sigma} \left(V_i c^\dagger_{i\sigma} d_\sigma + V_i^* d^\dagger_\sigma c_{i\sigma} \right) \\ S_c &= \int_t \left(\sum_{ij\sigma} c^\dagger_{i\sigma} (\mathrm{i}\partial_t - \widetilde{h}_{ij}) c_{j\sigma} + h.c. \right) \end{aligned} \tag{7.52}$$

where we identified $t_{io} = V_i$, $c_{oo} = d$, and $c_{i\neq o} = c_i$. Note, as a reminder, if one plugs this action into the functional path integral the operators should be convert to Grassmann fields and functionally integrated. And strictly speaking before the translation, the operators in the action should be normal ordered. We can assume we always do this whenever needed. Moreover, we restrict to the single band case here, for multi-band, see for instance the appendix of [247].

Clearly the corresponding Hamiltonian in momentum space reads

$$H_{\mathrm{SIAM}} = H_d + H_c + H_{cd} \tag{7.53}$$

where

$$H_d = \sum_\sigma \epsilon_d d^\dagger_\sigma d_\sigma + U n_{d\uparrow} n_{d\downarrow}, \quad H_c = \sum_{k\sigma} \widetilde{\epsilon}_k c^\dagger_{k\sigma} c_{k\sigma}, \quad H_{cd} = \sum_{k\sigma} \left(V_k c^\dagger_{k\sigma} d_\sigma + V_k^* d^\dagger_\sigma c_{k\sigma} \right) \tag{7.54}$$

Since the SIAM action is quadratic in "c" fields. One can perform a functional version of the Gaussian integral to integrate out the c-electrons and reach

$$S_{\mathrm{eff}} = -\int_{tt'} \sum_\sigma d^\dagger_\sigma(t) G^{-1}_{0d}(t-t') d_\sigma(t') + \int_{tt'} \sum_\sigma d^\dagger_\sigma(t) \Delta(t-t') d_\sigma(t') + U \int_t n_{d\uparrow}(t) n_{d\downarrow}(t) \tag{7.55}$$

Here the so-called hybridization propagator $\Delta(t-t')$ is defined. We used the completing square trick for Grassmann numbers [27]

$$\bar{\psi} K \psi + \bar{\eta}\psi + \bar{\psi}\eta = \left(\bar{\psi} + \bar{\eta} K^{-1} \right) K \left(\psi + K^{-1}\eta \right) - \bar{\eta} K^{-1} \eta \tag{7.56}$$

Although we consider the simplest case where the K, or in this context the $G_c^{-1}(k)$ for S_{eff}, is a scalar function, the K in general can be a matrix, and matrix multiplications are then implied.

The effective action after integration reads

$$S_{\mathrm{eff}} = -\int_{tt'} \sum_\sigma d^\dagger_\sigma(t) \mathscr{G}_0^{-1}(t-t') d_\sigma(t') + U \int_t n_{d\uparrow}(t) n_{d\downarrow}(t) \tag{7.57}$$

In the frequency space, the definition of the $\mathscr{G}_0$ is

$$\mathscr{G}_0^{-1}(\omega) = \omega - \epsilon_d - \Delta(\omega) = G^{-1}_{0d}(\omega) - \Delta(\omega) \tag{7.58}$$

In momentum space

$$\Delta(\omega) = \sum_k |V_k|^2 \widetilde{G}_c(\omega, k) = \sum_k \frac{|V_k|^2}{\omega - \widetilde{\epsilon}_k} \tag{7.59}$$

Here in Δ the $\widetilde{\epsilon}$ (or $\widetilde{G}_{c,k}$) and V_l are parameters, and they should be solved to make the consistency conditions

$$G_{\text{loc}} \stackrel{!}{=} G_{\text{imp}} \quad \text{and} \quad \Sigma_{\text{loc}} \stackrel{!}{=} \Sigma_{\text{imp}} \tag{7.60}$$

Here we defined $G_{\text{imp}} \equiv G_d$ and $\Sigma_{\text{imp}} \equiv \Sigma_d$ to stress they are corresponding to the impurity d.

Note the Σ_{imp} is defined as the self-energy of the d electron with the action S_{eff}, thus

$$\begin{aligned} \Sigma_{\text{imp}}(\omega) &\equiv \mathscr{G}_0^{-1}(\omega) - G_{\text{imp}}^{-1}(\omega) \\ &= [\omega - \epsilon_d - \Delta(\omega)] - G_{\text{imp}}^{-1}(\omega) \\ &= G_{0d}^{-1}(\omega) - \Delta(\omega) - G_{\text{imp}}^{-1}(\omega) \end{aligned} \tag{7.61}$$

To see how to solve the dynamical mean field equations. Let us assume that we can compute $\Sigma_{\text{imp}}(\omega)$ through $\mathscr{G}_0(\omega)$. Starting from a initial guess of the $\Sigma_{\text{imp}}(\omega)$, one can then use the consistency condition

$$\Sigma_{\text{loc}} \stackrel{!}{=} \Sigma_{\text{imp}} \tag{7.62}$$

to compute $G_{\text{loc}}(\omega)$, it reads

$$G_{\text{loc}}^{-1} = \left[\sum_k [G_{0c,k}^{-1} - \Sigma_{\text{loc}}]^{-1}\right]^{-1} = \left[\sum_k [G_{0c,k}^{-1} - \Sigma_{\text{imp}}]^{-1}\right]^{-1} \tag{7.63}$$

Now the $\mathscr{G}_0(\omega)$ can be updated by using the consistency condition

$$G_{\text{imp}} \stackrel{!}{=} G_{\text{loc}} \tag{7.64}$$

which gives

$$\mathscr{G}_0^{-1}(\omega) = G_{\text{imp}}^{-1}(\omega) + \Sigma_{\text{imp}}(\omega) = G_{\text{loc}}^{-1}(\omega) + \Sigma_{\text{imp}}(\omega) \tag{7.65}$$

And the $\mathscr{G}_0^{-1}(\omega)$ can be now used back to update Σ_{imp} which close the loop. The update procedure is repeated will converge to a fixed point solution. This solution is then regarded as the solution of the lattice local self-energy.

In above the Δ is hidden in $\mathscr{G}_0^{-1}$. However we can also compute the hybridization $\Delta(\omega)$ through

$$G_{\text{loc}}^{-1} = \left[\sum_k [G_{0c,k}^{-1} - \Sigma_{\text{loc}}]^{-1}\right]^{-1} = G_{\text{imp}}^{-1} = G_{0d}^{-1} - \Delta - \Sigma_{\text{imp}} \tag{7.66}$$

now use the consistency condition[5] $G_{\text{imp}} = G_{\text{loc}}$, the $\Delta(\omega)$ is then

$$\Delta(\omega) = G^{-1}_{\text{loc}}(\omega) - G^{-1}_{0d}(\omega) + \Sigma_{\text{imp}}(\omega) \tag{7.67}$$

Here the G_{0d} seems to contain a free parameter ϵ_d, it should be chosen as the local potential part of the free local Green's function. For the single-band case, it is trivial and usually zero. One may absorb ϵ_d into the real part of the $\Delta(\omega)$.

As a summary, the DMFT transferred the lattice problem into a single impurity Anderson model with the hybridization function $\Delta(\omega)$, namely a local function depending on the bath density of state, and the bath-impurity coupling V_k. The $\Delta(\omega)$ is self-consistently determined[6]. Then $\Delta(\omega)$ is a dynamical (time-dependent) generalization of the standard Weiss mean-field.

The DMFT loop can be summarized as

$$\xrightarrow[\text{previous iteration}]{\text{Initial guess or}} \Sigma \xrightarrow[(7.66)]{} G_{\text{loc}} \xrightarrow[(7.65)]{} \mathscr{G}_0 \xrightarrow[\text{Impurity solver}]{} \Sigma \xrightarrow[\text{If converged}]{} \text{Result} \tag{7.68}$$

where we suppressed the "imp" and "loc" subscripts of the self-energies.

7.2.3 Special soluble cases

Though the dynamical mean-field approximation greatly simplifies the lattice problem, the analytical solutions are still rarely founded. Here we review some of these special cases that analytical expressions can be written down.

Note for the formula with the Matsubara frequencies $G(\mathrm{i}\omega_n)$ one can use the identity [97]

$$G^R(\omega) = [G(\mathrm{i}\omega_n)]^R = G(\omega + \mathrm{i}0^+) \tag{7.69}$$

which is a substitution $\mathrm{i}\omega_n \to \omega + \mathrm{i}0^+$.

Non-interacting

The first example is the non-interacting case [242] where in Hubbard model

$$U = 0, \quad \Sigma_{\text{imp}} = 0 \tag{7.70}$$

The solutions are rather obvious. In terms of the Matsubara frequencies, they are

$$G_{\text{loc}}(\mathrm{i}\omega_n) = \mathscr{G}_0(\mathrm{i}\omega_n) \tag{7.71}$$

where

$$G_{\text{loc}}(\mathrm{i}\omega_n) = \sum_{\boldsymbol{k}} \frac{1}{\mathrm{i}\omega_n + \mu - \epsilon_d - \epsilon_{\boldsymbol{k}}} \tag{7.72}$$

[5] Note that another possibility [248] to understand the consistency condition is to compute the self-energies from the $V = 0$ functions $G_{..,d}$ and $G_{..,c}$, where $V = 0$ is marked as double dots .. since it is a decoupled setup. And the exact relation $\Sigma_c = V^2 G_{..,d}$ from the Lippmann-Schwinger equation.

[6] Closed related to the coherent potential approximation (CPA) in the context of the disorder systems [249], where an effective media is used.

Atomic limit

In the case where the hopping $t = 0$ the lattice model becomes individual atoms [242], and the kinetic energy is zero, $\epsilon_{\boldsymbol{k}} = 0$, and thus $\Delta = 0$. The Weiss Green's function is

$$\mathscr{G}_0^{-1} = \mathrm{i}\omega_n + \mu - \epsilon_d \tag{7.73}$$

Here μ is the chemical potential. Map to retarded functions simply do $\mathrm{i}\omega_n \to \omega + \mathrm{i}0^+$. The local Green's function is

$$G_{\mathrm{loc}}(\mathrm{i}\omega_n) = \frac{1 - n/2}{\mathrm{i}\omega_n + \widetilde{\mu}} + \frac{n/2}{i\omega_n + \widetilde{\mu} - U} \tag{7.74}$$

and the self-energy is

$$\Sigma_{\mathrm{imp}}(\mathrm{i}\omega_n) = \frac{nU}{2} + \frac{\frac{n}{2}(1 - \frac{n}{2})U^2}{i\omega_n + \widetilde{\mu} - (1 - \frac{n}{2})U} \tag{7.75}$$

where the chemical potential $\widetilde{\mu}$ is using ϵ_d as the reference $\widetilde{\mu} \equiv \mu - \epsilon_d$ and

$$\frac{n}{2} = \frac{e^{\beta\widetilde{\mu}} + e^{\beta(2\tilde{\mu} - U)}}{1 + 2e^{\beta\widetilde{\mu}} + e^{\beta(2\tilde{\mu} - U)}} \tag{7.76}$$

Here $\beta = 1/T$. If we set $\widetilde{\mu} = 0$ then

$$\frac{n}{2} = \frac{1}{3e^{\beta U} + 1} \tag{7.77}$$

If we further take the zero temperature limit $\beta \to \infty$ and choose the attractive case $U < 0$ then $\frac{n}{2} = 1$. This is the full filling case, where $\Sigma = U$ and $G = 1/(\mathrm{i}\omega_n - U)$. The spectrum is a single line at U. For $\widetilde{\mu} = 0$ and $\beta \to \infty$, $U > 0$ one has $n = 0$ that gives $\Sigma = 0$ and $G = 1/(\mathrm{i}\omega_n)$.

Another important case is the half-filling $n = 1$ where

$$G_{\mathrm{loc}}(\mathrm{i}\omega_n) = \frac{1/2}{\mathrm{i}\omega_n + \widetilde{\mu}} + \frac{1/2}{i\omega_n + \widetilde{\mu} - U} \tag{7.78}$$

Falicov-Kimball model

The Falicov-Kimball model is a model which has the form closed to the Hubbard model. However there are also sharp differences which are from the fact that the Falicov-Kimball model only has one kind of mobile electron. One can think Falicov-Kimball model as the Hubbard model with electrons with one kind of spin frozen. This specific structure greatly simplified the dynamics. Here let us consider the minimal Falicov-Kimball model. It has spinless itinerant lattice electron "c" with a single orbital that is coupled to a set of localized spinless electron "f" with a single level. The Hamiltonian reads [221, 246]

$$H_{\mathrm{FK}} = -\sum_{\langle ij \rangle} t c_i^\dagger c_j + U \sum_i c_i^\dagger c_i f_i^\dagger f_i \tag{7.79}$$

The degenerate spin degrees of freedom can be added as well as the coupling to the external magnetic field and the local electron interaction [246]. The DMFT can be exactly solved for the Falicov-Kimball model [250]. A detailed review can be found in [246]. The solution of the local Green's function in

terms of Matsubara frequencies is [246]

$$G_{\mathrm{loc}}(\mathrm{i}\omega_n) = \frac{w_0}{\mathscr{G}_0^{-1}\left(i\omega_n\right)} + \frac{w_1}{\mathscr{G}_0^{-1}\left(i\omega_n\right) - U} \tag{7.80}$$

where $w_1 = 1 - w_0$. The w_1 has the physical meaning of the average density of the f electron. The w_0 and w_1 in general are nonlinear functions of the full local Green's function G and the self-energy Σ. In practice, one can set w_1 to a constant, and solve Σ and G. To solve these nonlinear equations usually a nonlinear solver is required, for instance, the self-consistent loop. Again $\mathscr{G}_0^{-1} = G_{0d}^{-1} - \Delta = G_{\mathrm{loc}}^{-1} + \Sigma_{\mathrm{loc}}$. This solution is closed related to the Hubbard-III approximation [251]. A study of tuning the f electron to a non-zero hopping can be found in [252]. This model has been applied to the Floquet DMFT in the early work of Tsuji, Oka and Aoki [221] and also in [253].

Two-site DMFT

A soluble example is suggested by Potthoff [254], called two-site DMFT. As its name suggests, the DMFT here is an impurity site that couples with a single bath site.

In this setting, however, the self-consistent condition $G_{\mathrm{imp}} \stackrel{!}{=} G$ should be modified. The two consistent conditions are now $n_{\mathrm{imp}} \stackrel{!}{=} n$ and $V^2 \stackrel{!}{=} zM_2^{(0)}$. Where $n = \left\langle n_{i\uparrow}\right\rangle + \left\langle n_{i\downarrow}\right\rangle$, and $n_{\mathrm{imp}} \equiv 2n_d$, and $M_2^{(0)} = \sum_{j\neq i} t_{ij}^2 = \int dx x^2 \rho_0(x)$. Here z is the quasi-particle weight. The hybridization reads

$$\Delta(\omega) = \frac{V^2}{\omega + \mu - \epsilon_c} \tag{7.81}$$

where the ϵ_c is the energy of the single bath site.

For half-filling, analytical solution [254] can be reached. Consider the Bathe lattice in infinite dimension, i.e., semi-circular spectral function

$$A_0(\omega) = \frac{1}{t_*^2}\sqrt{4t_*^2 - \omega^2} \tag{7.82}$$

For half-filling $\mu = U/2$ and $n = \left\langle n_{i\uparrow}\right\rangle + \left\langle n_{i\downarrow}\right\rangle = 1$, the self-energy is

$$\Sigma(\omega) = \frac{U}{2} + \frac{U^2}{8}\left(\frac{1}{\omega - 3V} + \frac{1}{\omega + 3V}\right) \tag{7.83}$$

For the semicircular case $M_2^{(0)} = \sum_{j\neq i} t_{ij}^2 = 1$, the critical interaction strength is

$$U_{\mathrm{c}} = 6\sqrt{M_2^{(0)}} = 6 \tag{7.84}$$

The two site DMFT self-consistent condition gives

$$V = \sqrt{M_2^{(0)} - \frac{U^2}{36}} \tag{7.85}$$

This allows us to compute the interacting local spectral function without iteration, it reads

$$A(\omega) = A_0(\omega + \mu - \Sigma(\omega)) \tag{7.86}$$

One can verify that the Mott transition happens when the interaction across the critical strength U_c. The quasi-particle peak is present in the metallic phase, agree with the three peak structure of the Hubbard model.[7] The quasi-particle weight z is

$$z = 1 - \frac{U^2}{U_c^2} \tag{7.87}$$

Away from half-filling, it may need to be treated numerically. The $n \neq 1$ results can also be found in the reference [254].

7.3 Non-equilibrium DMFT

It is now straightforward to change the time integration to contour time integration

$$S_{\text{eff}} = -\int_{C(t,t')} \sum_\sigma d_\sigma^\dagger(t) G_{0d}^{-1}(t,t') d_\sigma(t') + \int_{C(t,t')} \sum_\sigma d_\sigma^\dagger(t) \Delta(t,t') d_\sigma(t') + U \int_{C(t)} n_\uparrow(t) n_\downarrow(t) \tag{7.88}$$

With this effective impurity action, one can derive a set of equations for $G^{R/A/K}$ and thus the DMFT for non-equilibrium systems [3]. From the discussions of the previous Keldysh chapter, we know that the double contour gives an additional degree of freedom which can be regarded as the evolution of distributions. Here the effective bath can have a dynamically updating distribution function as well, which is on its Keldysh component. One can map the contour time integral to a real-time integral with tensor vertices in the same manner as we did in the Keldysh chapter.

Another way to derive [3, 243] the DMFT on the contour time path may be starting from the local "Phi"-functional from $\Gamma_\Phi = \sum_i \Gamma_{\Phi,ii}[G]$.

7.4 Impurity solvers

7.4.1 Solvers

The impurity solvers that are available for non-equilibrium DMFT (at least before 2014) are reviewed in [3]. Here we briefly discuss some of them, both in and out of equilibrium.

Iterating perturbation theory (IPT) and its extensions IPT is a weak coupling solver [240]. The simplest version of the IPT is to use the 2nd order diagram from the Luttinger-Ward functional, without self-consistent loops. The 2nd order version gives an interpolation between the non-interacting case $U \to 0$ and the atomic limit $U \to \infty$ and thus very successful to capture the Mott physics qualitatively in equilibrium.

[7] This is more closed to Fermi-liquid and different from the Falicov-Kimball model, where the quasi-particle peak is absent.

Non-crossing approximation (NCA) and its extensions Non-crossing approximation (NCA) is a strong coupling solver with the slave-boson technique. The standard NCA is non-perturbative in Kondo energy (temperature). It correctly captures the atomic limit and the Kondo resonance. However, it has some disadvantages that it does not give the correct infrared exponents, this can be cured by further resummation [255]. The standard NCA has the strict $Q = 1$ constraint has the causality problem since it can exceed the unitary limit [241]. This problem may be fixed through a soften constraint, $Q = \sum_n a_n^\dagger a_n = q_0 N$.

Monte Carlo solvers Several Monte Carlo methods for quantum many-body systems are available. For the quantum impurity problem, the continuous-time Monte Carlo (CT-QMC) is usually the choice [20], where a diagrammatic expansion is used for Monte Carlo sampling. It is called "continous time" since time discretizations, which are error-producing, can be avoided. The CT-QMC has several versions, by using the hybridization expansion, CT-HYB, by using interaction expansion, CT-INT, and, by using the Hirsh-Fye method, where the Hubbard-Stratonovich auxiliary fields are used for sampling, CT-AUX. In non-equilibrium situations, there are extensions of those methods. However, the computational cost is usually larger where the sign problem also becomes serious in many systems. Those issues are expected from the complexity of the real-time dynamics.

Numerical renormalization group (NRG) The numerical renormalization group is a Wilsonian renormalization group method that can be traced back to Wilson's original papers [65] on RG of the Kondo model. It is very accurate and in many cases as the standard to compare with.

Exact diagonalization (ED) The Anderson impurity model can be exactly diagonalized, the major bottleneck is again the exponentially increasing Hilbert space.

Tensor network solvers The tensor network methods, e.g., density matrix renormalization group (DMRG) can be applied to the quantum impurity model and can be treated as impurity solvers [256]. They can be also combined with "auxiliary master equation", see for instance [257].

Numerical packages for DMFT There are many good open-source packages, for examples:

- In equilibrium: Triqs [258], ALPS [259]
- Out of equilibrium: Nessi [260]

where the impurity solvers are usually provided.

7.4.2 Example: Real-time iterated perturbation solver in equilibrium

The result is shown in Fig. 7.1, which follows the reference [261] and the package[8]. Recall the simplest Hubbard model

$$H = -\sum_\sigma t_{\langle ij\rangle} c_{i\sigma}^\dagger c_{j\sigma} - U c_{i\uparrow}^\dagger c_{i\downarrow}^\dagger c_{i\uparrow} c_{i\downarrow} \tag{7.89}$$

[8] See https://github.com/Titan-C/pydmft from Óscar Nájera

With $U > 0$ the repulsive interaction. Here $c^\dagger_{i\downarrow} c^\dagger_{i\uparrow} c_{i\downarrow} c_{i\uparrow} = -n_{i\uparrow} n_{i\downarrow}$, and $n_{i\sigma} = c^\dagger_{i\sigma} c_{i\sigma}$. The iterated impurity solver is to replace lattice Green's function by the Weiss Green's function in the skeleton self-energies, i.e., the self-energy from the Γ_Φ of the 2-PI effective action.

$$G \to \mathscr{G}_0, \quad \Gamma_\Phi[G] \to \Gamma_\Phi[\mathscr{G}_0] \tag{7.90}$$

As an example, we consider a very simple and important case [240], the Hubbard model on the Bethe lattice with $z \to \infty$, with time translational invariant, i.e., with a time-independent Hamiltonian, and at half-filling. We consider the paramagnetic case

$$\mathscr{G}_{0,\sigma} = \mathscr{G}_{0,\bar{\sigma}} \tag{7.91}$$

Rather than use Matsubara Green's function, here we use the real time Keldysh Green's functions. However we will fix the distribution to equilibrium distribution function at the half-filling $\mu = 0$

$$n(\epsilon) = n_{\mathrm{F}}(\epsilon) = \frac{1}{e^{\beta\epsilon} + 1} \tag{7.92}$$

This means that we do not evolve the distribution part and the Green's functions always fulfill FDT. For later usage we note that

$$n_{\mathrm{F}}(\epsilon) = 1 - n_{\mathrm{F}}(-\epsilon) \tag{7.93}$$

which can be verified directly. Further, since we have particle-hole symmetry here, the Weiss Green's function gives a spectral function with the following symmetry property

$$A_0(\omega) = A_0(-\omega) \tag{7.94}$$

As usual, we used the definition

$$A_0(\omega) = \mathrm{i}(\mathscr{G}_0^R(\omega) - \mathscr{G}_0^A(\omega)) = -2\mathrm{Im}\, \mathscr{G}_0^R(\omega) \tag{7.95}$$

with the normalization condition $\int_\omega A(\omega) = \int \frac{\mathrm{d}\omega}{2\pi} A(\omega) = 1$.

From the causal structure of the frequency space Green's functions we have

$$2\mathrm{i}\mathrm{Im}\, \Sigma^R(\omega) = \Sigma^>(\omega) - \Sigma^<(\omega) \tag{7.96}$$

Thus if we can compute $\Sigma^{</>}$ we can then compute $\mathrm{Im}\, \Sigma^R(\omega)$. The first-order correction is a Hartree term which at half-filling is a shift of the chemical potential and can be absorb into the definition, thus we neglect it here. As discussed before the skeleton diagrams for the second order, U^2, are

$$\begin{aligned} \Sigma^> &= U^2 [\mathscr{G}_0^>(\epsilon)] \circ [\mathscr{G}_0^>(\epsilon)] \circ [\mathscr{G}_0^<(-\epsilon)] \\ \Sigma^< &= U^2 [\mathscr{G}_0^<(\epsilon)] \circ [\mathscr{G}_0^<(\epsilon)] \circ [\mathscr{G}_0^>(-\epsilon)] \end{aligned} \tag{7.97}$$

where we used the paramagnetic condition $\mathscr{G}_{0,\sigma} = \mathscr{G}_{0,\bar{\sigma}}$ which gives a factor of 2, and drop the spin indices. The "$\circ$" means convolution, here for frequency space it is defined as

$$a \circ b = \int_{\omega'} a(\omega') b(\omega - \omega') = \int \frac{\mathrm{d}\omega'}{2\pi} a(\omega') b(\omega - \omega') \tag{7.98}$$

We can now use the FDT for fermion Green's function

$$\begin{aligned}\mathscr{G}_0^<(\omega) &= \mathrm{i}A_0(\omega)n_\mathrm{F}(\omega) \equiv \mathrm{i}A_+(\omega)\\ \mathscr{G}_0^>(\omega) &= -\mathrm{i}A_0(\omega)(1-n_\mathrm{F}(\omega)) \equiv -\mathrm{i}A_-(\omega)\end{aligned} \tag{7.99}$$

where we defined short-hand notations $A_\pm$. Use $A_0(-\omega) = A_0(\omega)$ and $n_\mathrm{F}(\omega) = 1 - n_\mathrm{F}(-\omega)$, we get the identity

$$A_+(\omega) = A_-(-\omega) \tag{7.100}$$

or equivalently $\mathscr{G}_0^<(\omega) = -\mathscr{G}_0^>(-\omega)$.

Now the lesser self-energy can be written as

$$\begin{aligned}\Sigma^<(\omega) &= U^2(-\mathrm{i}^3)[A_+(\epsilon)\circ A_+(\epsilon)\circ A_-(-\epsilon)](\omega)\\ &= \mathrm{i}U^2[A_+(\epsilon)\circ A_+(\epsilon)\circ A_+(\epsilon)](\omega) \equiv \mathrm{i}2\pi U^2 A_{+++}(\omega)\end{aligned} \tag{7.101}$$

where we defined $2\pi A_{+++} = [A_+(\epsilon)\circ A_+(\epsilon)\circ A_+(\epsilon)](\omega)$, and used $A_+(\epsilon) = A_-(-\epsilon)$. Similarly, we can derive

$$\Sigma^>(\omega) = -\mathrm{i}2\pi U^2 A_{+++}(-\omega) \tag{7.102}$$

Use $2\mathrm{i}\mathrm{Im}\,\Sigma^R = \Sigma^R - \Sigma^A = \Sigma^> - \Sigma^<$, the imaginary part of the retarded self-energy in frequency space is[9]

$$\mathrm{i}\mathrm{Im}\,\Sigma^R(\omega) = -\mathrm{i}\pi U^2(A_{+++}(-\omega) + A_{+++}(\omega)) \tag{7.104}$$

Since $\Sigma^R(\omega)$ is an analytical retarded function, the real part of $\Sigma^R(\omega)$ can be computed by using the Kramers-Krönig relation. For a retarded function, the real part is the Hilbert transform of "-1" times its imaginary part

$$\mathrm{Re}\,\Sigma^R(\omega) = \mathrm{p.v.}\int \frac{\mathrm{d}\omega'}{\pi}\frac{-\mathrm{Im}\,\Sigma^R(\omega')}{\omega-\omega'} \tag{7.105}$$

Here p.v. $\int$ means the Cauchy's principal value integral. We can define

$$\mathrm{H}[A](x) \equiv \mathrm{p.v.}\int_{-\infty}^{+\infty}\frac{\mathrm{d}\epsilon}{\pi}\frac{A(\epsilon)}{x-\epsilon} \tag{7.106}$$

then $\mathrm{Re}\,\Sigma^R(\omega) = \mathrm{H}[-\mathrm{Im}\,\Sigma^R]$.

Now consider properties of the Bethe lattice [240, 262, 263] in $z\to\infty$, the density of states are now semi-circular

$$\frac{1}{2\pi}A_{0,\mathrm{Bethe}}(\epsilon) = \frac{1}{2\pi t_*^2}\sqrt{4t_*^2-\epsilon^2} \tag{7.107}$$

Note that $2t_*$ is the semi circle radius, t_* is the effective hopping amplitude of the Bethe lattice[10].

[9] For numerics, one may need to write out the integral

$$A_{+++}(\omega) = 2\pi\left(\frac{1}{2\pi}\right)^3\int_{-\Lambda}^{\Lambda}\mathrm{d}\omega'\int_{-\Lambda}^{\Lambda}\mathrm{d}\omega''A_+(\omega')A_+(\omega'')A_+(\omega'+\omega''-\omega) \tag{7.103}$$

where Λ is a UV cut-off which should be much larger than the non-interacting half-bandwidth $\Lambda \gg D$.

[10] The the lattice dimension [263] d_l can be defined as $\lim_{n\to\infty}(\ln c_n)/\ln n = d_l$, where $c_n = 1 + m_1 + m_2 + \ldots + m_n$ as the total number of sites that can be reached by n steps. Bethe lattice is special that it has $d_l = \infty$, even when it connectivity z

The semi-circular density of state gives a simple relation[11] between the local Green's function and the hybridization

$$\Delta(\omega) = t_*^2 G_{\rm loc}(\omega) \tag{7.108}$$

The computation of the local Green's function from its self-energy and density of states are also simplified by noticing the Hilbert transform [240]

$$\mathrm{H}\left[\frac{1}{2}A_{0,\mathrm{Bethe}}\right](\zeta) = \frac{1}{2t_*^2}\left(\zeta - s\sqrt{\zeta^2 - 4t_*^2}\right) \tag{7.109}$$

The H[...] means the Hilbert transform of ... as we defined.

We now have DMFT equations

$$\mathscr{G}_0^R(\omega) = \frac{1}{\omega + \mathrm{i}0^+ - \Delta(\omega)} = \frac{1}{\omega + \mathrm{i}0^+ - t_*^2 G_{\rm loc}^R(\omega)} \tag{7.110}$$

$$G_{\rm loc}^R(\omega) = \mathrm{H}\left[\frac{1}{2}A_{0,\mathrm{Bethe}}\right](\zeta)\Big|_{\zeta=\omega-\Sigma^R(\omega)} \tag{7.111}$$

and the DMFT loop

$$\Sigma^R \xrightarrow[(7.111)]{} G_{\rm loc}^R \xrightarrow[(7.110)]{} \mathscr{G}_0^R \xrightarrow[(7.104),(7.105)]{} \Sigma^R \tag{7.112}$$

After converged, the local spectral function is computed from

$$A_{\rm loc}(\omega) = -2\mathrm{Im}\, G_{\rm loc}^R(\omega) \tag{7.113}$$

See Fig. 7.1 for plots, where we choose $t_* = 0.5D$, and $D = 1.0$ is the energy unit as well as the half-bandwidth.

7.5 Floquet DMFT

The Floquet-Keldysh DMFT is pioneered in the work [239], and later it has been applied in many systems [3]. The Dyson equations (or Dyson-Schwinger equations) are general and exact quantum relations for correlation functions. On the contour time path (CTP) These equations have a formal structure that is almost identical to their equilibrium counterparts. The major difference is that the statistical and spectral components are not related by the Fluctuation-Dissipation theorem (FDT), but remains two degrees of freedom on top of all the detailed structure of the models. For the basis of $\psi_{1/2}$ and for two-point function, the Dyson equation is

$$G^{-1}(t_1, t_2) = G_0^{-1}(t_1, t_2) - \Sigma(t_1, t_2) \tag{7.114}$$

and can be derived from (2.113) by setting $J_2 = 0$. Here all indices other than time are suppressed. The above equation in a Floquet representation becomes matrix equations

$$G_{mn}^{-1}(\omega) = G_{0,mn}^{-1}(\omega) - \Sigma_{mn}(\omega) \tag{7.115}$$

is finite. This can be intuitively understood since it is a tree without cycle.

[11] See, e.g., Ref. [240], Appendix.A.3.

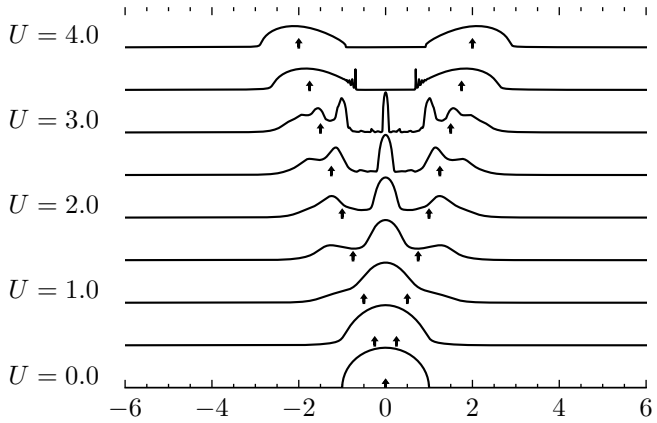

Figure 7.1: The x axis is ω/D. The real time equilibrium DMFT for Hubbard model with iterated perturbation solver with $\beta = 1/T = 1000$ at half-filling. The non-interacting density of states is chosen as semi-circular with the half-bandwidth $D = 1.0$. The frequency is restricted to $\omega \in [-6, 6]$, with $2^{16} = 65536$ points. The spectral function $A_{\text{loc}}(\omega) = -2\text{Im}\, G^R_{\text{loc}}(\omega)$ for $U = 0$ to $U = 4$ with the step 0.5 are shown. The semi-circular is corresponding to the Bethe lattice (the interior part of a Cayley tree [263])) at infinite dimension. The $\pm U/2$ are marked with arrows. One can see a phase transition from metallic phase to Mott insulator phase, the metal to insulator transition (MIT). In between a quasi-particle peak located at $\omega = 0$ is clear visible.

here we used the identity to convert the convolution to discrete sums for Floquet Green's functions. $[A * B](t_1, t_2) = \sum_l A_{ml}(\omega) B_{ln}(\omega)$. More details can be found in the work of Tsuji, Oka, and Aoki [221]. Usually, solving matrix equations are much simpler than integral equations. However, here it seems the exact matrix size is infinity. One then has to truncate the matrix for practical computations. Fortunately, the needed matrix size will remain relatively small, especially for relatively high driven frequencies. This can be seen by looking at the Floquet band structures. Since the index m is corresponding to the m-th photon level, and the transition from 0-th photon level will need a m-photon process that has the probability is decreasing rapidly for large $|m|$.

7.5.1 Self-consistent loop

The DMFT procedure is summarized in the following in Fig. 7.2

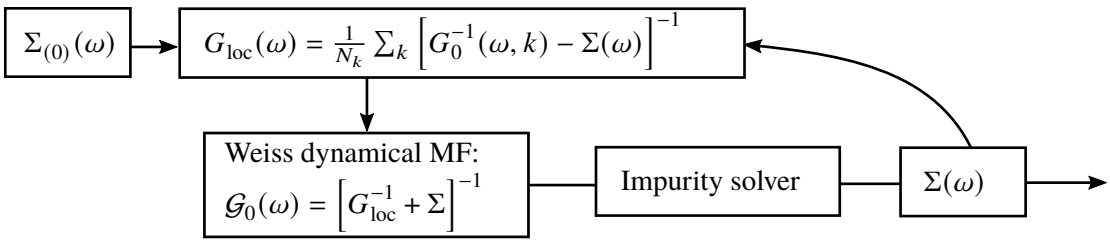

Figure 7.2: The DMFT loop applies to Floquet DMFT as well. All self-energies and Green's functions should be understood in Keldysh and Floquet space, so do the inversions.

In the Floquet-Bloch space, the self-energy of the lattice model and the impurity model have the relation

$$\Sigma = \Sigma[\mathscr{G}_0]_{mn}(\omega) \tag{7.116}$$

where the self-energy is computed as $\Sigma[\mathscr{G}_0]$ and has a flat k dependence, $\Sigma[\dots]$ represents the self-energy functional. Using (7.116) the Dyson equation for lattice Green's function G given by (7.115) becomes

$$G^{-1}_{mn}(\omega, k) = G^{-1}_{0,mn}(\omega, k) - \Sigma[\mathscr{G}_0]_{mn}(\omega) \tag{7.117}$$

Note that here the lattice Green's functions for different k have the same self-energy. Now, define the local lattice Green's function

$$G_{\mathrm{loc},mn}(\omega) = \frac{1}{N_k}\sum_k G_{mn}(\omega, k) \tag{7.118}$$

Where we have set the lattice constant $a = 1$. Since the hybridization between the impurity and the bath is a dynamical Weiss mean-field and should be treated self-consistently, the impurity Green's function then should satisfy

$$\mathscr{G}^{-1}_{0,mn} = G^{-1}_{\mathrm{loc},mn} + (\Sigma[\mathscr{G}_0])_{mn} \tag{7.119}$$

Now starting from an initial guess of $\Sigma[G] = \Sigma[\mathscr{G}_0]$, one can evaluate the self-consistent loop by repeating (7.117) to (7.119) till reaches the convergence. The difference between the results of the n-th iteration $\Sigma_{[n]}$ and the $(n-1)$-th iteration $\Sigma_{[n-1]}$ should be small, that is

$$\| \Sigma_{[n]} - \Sigma_{[n-1]} \| < \text{tolerance} \tag{7.120}$$

7.5.2 Self-energy and diagrammatics

As we discussed before the iterative perturbation theory to second order in U will require two skeleton diagrams that the full propagators $G_{mn}(\omega)$ are replaced by the Weiss Green's function $\mathscr{G}_{0,mn}(\omega)$. The frequency convolutions of the self-energy can be evaluated by multi-dimensional Fourier transform. Combine the knowledge of the Keldysh tensor vertex, the Floquet representation, and the real time DMFT with IPT, we can write down the diagrams as follows

$$\Sigma^{il}_1(t_1, t_2) = -\mathrm{i}U_0 \nu_{ijkl} G^{jk}(t_1, t_1)\delta_{jk}\delta(t_1 - t_2) \tag{7.121}$$

$$\Sigma^{ll'}_2(t_1, t_2) = U_0^2 G^{ii'}(t_1, t_2)\nu_{ijkl} G^{jj'}(t_1, t_2) G^{k'k}(t_2, t_1)\nu_{i'j'k'l'} \tag{7.122}$$

The tensor vertex is defined as before around (3.79)

$$\gamma^{(4)}_{ijkl} = \frac{1}{2}U_0\left(\tau^0 \otimes \tau^1 + \tau^1 \otimes \tau^0\right)_{ijkl} = U_0 \nu_{ijkl} \tag{7.123}$$

where the $\gamma^{(4)}$ is the bare 4-vertex with Keldysh indices, and ν_{ijkl} is the tensor without interaction strength multiplied. The U_0 is Hubbard interaction.

Again τ^i are the Pauli matrices that are for Keldysh space. The form of this vertex can be verified by contracting the tensor vertex for Yukawa interaction [29], as we have done before for the general cases in the Keldysh chapter, by setting the boson propagator $D(x, y) = \tau_0$, or directly from the bare

action of functional derivatives. These we have been discussed in the Keldysh chapter, see (3.79). The first-order term, (7.121), is a Hartree term. Perform the tensor contraction, the result is $\Sigma_1^K = 0$ and

$$\Sigma_1^R(t_1,t_2) = -\mathrm{i}U_0 G^K(t_1,t_1)\delta(t_1-t_2) = \Sigma_1^A(t_1,t_2) \tag{7.124}$$

We can reach the above result by direct tensor contraction. Another way to see this is to use Feynman rules, see for instance [224].

Note that a proper causal structure should be preserved if one transform to Floquet (frequency) space.

$$\Sigma^R_{1,mn}(\omega) = -\mathrm{i}U_0 \int_{\omega'} \sum_{n'} G^K_{m-n+n',n'}(\omega') e^{a'0^+} \tag{7.125}$$

For Σ_2, (7.122), again perform the contractions, but in the $+/-$ basis. The second-order term are

$$\Sigma_2^> = U_0^2 G^>(t_1,t_2)G^>(t_1,t_2)G^<(t_2,t_1) \tag{7.126}$$

$$\Sigma_2^< = U_0^2 G^<(t_1,t_2)G^<(t_1,t_2)G^>(t_2,t_1) \tag{7.127}$$

The above equations can be written down immediately, by marking the two vertices on the diagram by $+/-$ and $-/+$. Remind that

$$G^{</>} = F \mp \frac{1}{2}\mathrm{i}A = \frac{1}{2}(G^K \pm (G^R - G^A)) \tag{7.128}$$

The Floquet representation of the second-order contribution $[\Sigma_2(t_1,t_2)]_{mn}$ can be derived, suppressing variables and indices other than time we have, with contour indices suppressed

$$\begin{aligned}[\Sigma_2(t_1,t_2)]_{mm'} &= U_0^2[G(t_1,t_2)G(t_1,t_2)G(t_2,t_1)]_{mm'}(\omega) \\ &= U_0^2 \sum_{s,n,s',n'} \int_{\omega'\omega''} G_{ss'}(\omega')G_{nn'}(\omega'')G_{s'+n'-m',s+n-m}(\omega'+\omega''-\omega)\end{aligned} \tag{7.129}$$

with the Floquet representation. For practical computations, the Wigner representation [3, 223, 239, 264] is useful, under it the Σ_2 has the form

$$[\overline{\Sigma}_2]_m(\omega) = U_0^2 \sum_{s,n} \int_{\omega',\omega''} \overline{G}_s(\omega')\overline{G}_n(\omega'')\overline{G}_{-s-n+m}(\omega'+\omega''-\omega) \tag{7.130}$$

The Wigner and Floquet representation can be transformed to each other through (5.84)

$$\overline{G}_n(\omega) = G_{m+\frac{n}{2},m-\frac{n}{2}}(\omega - m\Omega) \tag{7.131}$$

or (5.79)

$$G_{mn}(\omega) = \overline{G}_{m-n}\left(\omega + \frac{m+n}{2}\Omega\right) \tag{7.132}$$

and usually with the aid of (5.85). We discussed them before in the Floquet chapter. Note that we can reconstruct $\overline{G}_n(\omega)$ by

$$G_{mn}(\omega) \quad \omega \in [-\Omega/2, \Omega/2) \tag{7.133}$$

In practical numerical computations, the maximal absolute value $|m|$ and $|n|$, thus their difference

$|m-n|$, are up to a truncation, where the $\overline{G}_{m-n}$ has smaller and smaller available energy window for higher harmonics $|m-n|$ if it is reconstructed from G_{mn}. Since the amplitude of higher harmonics decays rapidly, we can usually pad the higher harmonics to match the length 0-th of the harmonics.

We then can compute the Dyson equation of G^R, G^A and G^K. The Keldysh part of the self-energy Σ^K can be obtained from $\Sigma^>$ and $\Sigma^<$ directly through

$$\Sigma^K_{mn}(\omega) = [\Sigma^> + \Sigma^<]_{mn}(\omega) \tag{7.134}$$

and

$$\mathrm{iIm}\,\Sigma^R_{mn}(\omega) = [\Sigma^> - \Sigma^<]_{mn}(\omega) \tag{7.135}$$

Note that the Keldysh self-energy and the Keldysh part of the Dyson equation will give a self-consistent solution of the distributions or occupations, where if we restore the spatial dependence and make the semi-classical quasiparticle approximation, then we can find a quantum Boltzmann equation [223]. The advanced self-energy can be computed from the retarded one using the general relation

$$\Sigma^A_{mn}(\omega) = [(\Sigma^R)^\dagger]_{mn}(\omega) = [\Sigma^R_{nm}(\omega)]^* \tag{7.136}$$

Here the Hermitian conjugation is acting on all indices, including the Floquet indices m, n.

For a system with sublattice (flavor, orbital, etc.) structure we can write

$$\Sigma_{xy|\eta\rho|\sigma\sigma} = -\frac{\delta\Gamma_\Phi}{\delta G_{yx|\rho\eta|\sigma\sigma}} = \frac{24}{48}U^2 G_{xy|\eta\rho|\bar\sigma\bar\sigma} G_{yx|\rho\eta|\bar\sigma\bar\sigma} G_{xy|\eta\rho|\sigma\sigma}, \quad \text{no sum} \tag{7.137}$$

If we write out the sublattice indices, assume they are A and B for simplicity, then the self-energies are

$$\begin{aligned}
\Sigma_{xy|\mathrm{AA}|\sigma\sigma} &= \frac{1}{2}U_0^2 G_{xy|\mathrm{AA}|\bar\sigma\bar\sigma} G_{yx|\mathrm{AA}|\bar\sigma\bar\sigma} G_{xy|\mathrm{AA}|\sigma\sigma}, \quad \text{no sum} \\
\Sigma_{xy|\mathrm{AB}|\sigma\sigma} &= \frac{1}{2}U_0^2 G_{xy|\mathrm{AB}|\bar\sigma\bar\sigma} G_{yx|\mathrm{BA}|\bar\sigma\bar\sigma} G_{xy|\mathrm{AB}|\sigma\sigma}, \quad \text{no sum} \\
\Sigma_{xy|\mathrm{BA}|\sigma\sigma} &= \frac{1}{2}U_0^2 G_{xy|\mathrm{BA}|\bar\sigma\bar\sigma} G_{yx|\mathrm{AB}|\bar\sigma\bar\sigma} G_{xy|\mathrm{BA}|\sigma\sigma}, \quad \text{no sum} \\
\Sigma_{xy|\mathrm{BB}|\sigma\sigma} &= \frac{1}{2}U_0^2 G_{xy|\mathrm{BB}|\bar\sigma\bar\sigma} G_{yx|\mathrm{BB}|\bar\sigma\bar\sigma} G_{xy|\mathrm{BB}|\sigma\sigma}, \quad \text{no sum}
\end{aligned} \tag{7.138}$$

Note here no summation (integration) for same indices. If we neglect the spatial dependence of G and apply the Keldysh vertex, the result in time space is

$$\Sigma^{ll'}_{\eta\rho|\sigma\sigma} = -\frac{\delta\Gamma_\Phi}{\delta G^{ji}_{\rho\eta|\sigma\sigma}} = \frac{1}{2}U_0^2 G^{ii'}_{\eta\rho|\bar\sigma\bar\sigma} v_{ijkl} G^{jj'}_{\rho\eta|\bar\sigma\bar\sigma} G^{k'k}_{\eta\rho|\sigma\sigma} v_{i'j'k'l'}, \quad \text{no sum for } \sigma, \bar\sigma, \rho, \eta \tag{7.139}$$

Here we suppressed the time variables which follows the order of the Keldysh indices on superscript. One can see that the time space structure is unchanged, so do the procedures needed to transform to Floquet space, and the identities for real time Green's functions. Although lengthy but straight forward we can write done the full expression by using (7.130) in frequency space and in Wigner

representation

$$\left[\overline{\Sigma}^{ll'}_{\eta\rho|\sigma\sigma}\right]_{\omega,m} = \frac{1}{2}U_0^2 \left[\overline{G}^{ii'}_{\eta\rho|\bar{\sigma}\bar{\sigma}}\right]_{\omega'|s} \nu_{ijkl} \left[\overline{G}^{jj'}_{\rho\eta|\bar{\sigma}\bar{\sigma}}\right]_{\omega''|n} \left[\overline{G}^{k'k}_{\eta\rho|\sigma\sigma}\right]_{\omega'+\omega''-\omega|-s-n+m} \nu_{i'j'k'l'} \tag{7.140}$$

where the same indices are summed or integrated except $\sigma, \bar{\sigma}, \rho, \eta$.

Now for IPT solver of DMFT we do

$$G \to \mathscr{G}_0 \tag{7.141}$$

to reach the lowest order IPT.

To make contact with the standard DMFT construction, we can use that in time space the hybridization function $\Delta = G_{0d}^{-1} - \mathscr{G}_0^{-1}$ is

$$\Delta_{\eta\rho|\sigma\sigma'}(t_1, t_2) = \begin{pmatrix} \Delta_{\mathrm{AA}|\sigma\sigma'} & \Delta_{\mathrm{AB}|\sigma\sigma'} \\ \Delta_{\mathrm{BA}|\sigma\sigma'} & \Delta_{\mathrm{BB}|\sigma\sigma'} \end{pmatrix} (t_1, t_2) \tag{7.142}$$

In the single impurity Anderson model picture, it can be regarded as

$$\Delta_{\eta\rho|\sigma\sigma'}(t_1, t_2) = \sum_k V^\dagger_{k\eta\sigma}(t_1) G_{c,k|\eta\rho|\sigma\sigma'}(t_1, t_2) V_{k\rho\sigma'}(t_2), \quad \text{no same index sum} \tag{7.143}$$

where G_c is the conduction electron bath Green's function.

7.5.3 Couple to bath

To allow a steady-state solution, the diven system is usually connected to a bath, which can absorb the heat generated by the drive. We consider here the fermionic bath [3, 169, 221, 265]

$$H = H_{\mathrm{sys}} + H_{\mathrm{mix}} + H_{\mathrm{bath}} \tag{7.144}$$

where $H_{\mathrm{mix}} = \sum_{i,p} V_p \left(c_i^\dagger b_{i,p} + b_{i,p}^\dagger c_i\right)$, and $\Sigma_{\mathrm{bath}}\left(t, t'\right) = \sum_p V_p G_{\mathrm{bath},p}\left(t, t'\right) V_p$, in Keldysh space the bath self-energy reads

$$\Sigma_{\mathrm{bath}} = \begin{pmatrix} \Sigma^R_{\mathrm{bath}}(\omega) & \Sigma^K_{\mathrm{bath}}(\omega) \\ 0 & \Sigma^A_{\mathrm{bath}}(\omega) \end{pmatrix} = \begin{pmatrix} -i\Gamma & -2i\Gamma h(\omega) \\ 0 & i\Gamma \end{pmatrix} \tag{7.145}$$

Here the bath is at equilibrium with temperature $\beta = 1/T$, so that the $h(\omega)$ reads

$$h(\omega) = \tanh(\beta\omega/2) \tag{7.146}$$

For the system-bath hybridization we neglect the frequency dependence, i.e.

$$\Gamma(\omega) = \sum_p \pi V_p^2 \delta\left(\omega + \mu_b - \epsilon_{b,p}\right) \sim \Gamma \tag{7.147}$$

This is reasonable for a featureless bath that has a wide bandwidth, for instance a tight-binding free fermion bath. In general, the frequency dependence may play a rule, e.g., for the topological property [13].

Now we apply the Floquet DMFT to the Rice-Mele Hubbard model

7.5.4 Floquet DMFT for Rice-Mele model

The Hamiltonian of the Rice-Mele Fermi Hubbard model is

$$H(t) = H_{\mathrm{RM}}(t) + H_{\mathrm{int}} \tag{7.148}$$

Where the H_{RM} is same to the H_{RM} in (6.1), however here we make some changes of the notations for clarity

$$\begin{aligned} H_{\mathrm{RM}}(t) = &-\sum_{i=1}^{N}\left(J_+(t)c^\dagger_{i+1|\mathrm{B}}c_{i\mathrm{A}} + J_-(t)c^\dagger_{i+1|\mathrm{A}}c_{i\mathrm{B}} + h.c.\right) \\ &+\sum_{i=1}^{N} V(t)\left(c^\dagger_{i\mathrm{A}}c_{i\mathrm{A}} - c^\dagger_{i\mathrm{B}}c_{i\mathrm{B}}\right) \end{aligned} \tag{7.149}$$

where

$$\begin{cases} J_+(t) = J_0 + J_1\cos(\Omega t) \\ J_-(t) = J_0 - J_1\cos(\Omega t) \\ V(t) = V_0 + V_1\sin(\Omega t + \phi) \end{cases} \tag{7.150}$$

And

$$H_{\mathrm{int}} = -U\sum_{i=1}^{N} c^\dagger_{i\mathrm{A}\uparrow}c^\dagger_{i\mathrm{A}\downarrow}c_{i\mathrm{A}\uparrow}c_{\mathrm{A},i\downarrow} - U\sum_{i=1}^{N} c^\dagger_{i\mathrm{B}\uparrow}c^\dagger_{i\mathrm{B}\downarrow}c_{i\mathrm{B}\uparrow}c_{i\mathrm{B}\downarrow} \tag{7.151}$$

The non-interacting part in Floquet space can be written into a block matrix with a tight binding model style,

$$\mathcal{H} = H_{m-n} - \Omega\delta_{mn} = \begin{pmatrix} \ddots & \ddots & & & \\ \ddots & \boldsymbol{H}_0 - \Omega\mathbb{1} & \boldsymbol{H}_{-1} & \boldsymbol{0} & \\ & \boldsymbol{H}^\dagger_{-1} & \boldsymbol{H}_0 & \boldsymbol{H}_{-1} & \\ & \boldsymbol{0} & \boldsymbol{H}^\dagger_{-1} & \boldsymbol{H}_0 + \Omega\mathbb{1} & \ddots \\ & & & \ddots & \ddots \end{pmatrix}$$

Where[12]

$$\boldsymbol{H}_0 = \begin{pmatrix} V_0 & J_0^k \\ J_0^k & -V_0 \end{pmatrix}, \quad \boldsymbol{H}_{-1} = \frac{1}{2}\begin{pmatrix} V_1 & -J_1^{k,\phi} \\ J_1^{k,\phi} & -V_1 \end{pmatrix}$$

We set $\phi = 0$ and define

$$J_0^k \equiv -J_0(1 + \cos(ka_0) - \mathrm{i}\sin(ka_0)), \quad J_1^k \equiv \mathrm{i}J_1(-1 + \cos(ka_0) - \mathrm{i}\sin(ka_0)) \tag{7.152}$$

[12] Note here the $J_{0/1}$ are hopping parameters.

See also the (6.3). Now

$$H_{m-n}(k) = \begin{pmatrix} \ddots & \ddots & \ddots & \ddots & & & & \\ \ddots & V_0 & J_0^k & V_1/2 & -J_1^k/2 & & 0 & \\ \ddots & J_0^k & -V_0 & J_1^k/2 & -V_1/2 & & & \\ \ddots & V_1/2 & J_1^{*k}/2 & V_0 & J_0^k & V_1/2 & -J_1^k/2 & \\ & -J_1^{*k}/2 & -V_1/2 & J_0^k & -V_0 & J_1^k/2 & -V_1/2 & \ddots \\ & & & V_1/2 & J_1^{*k}/2 & V_0 & J_0^k & \ddots \\ & 0 & & -J_1^{*k}/2 & -V_1/2 & J_0^k & -V_0 & \ddots \\ & & & & \ddots & \ddots & \ddots & \ddots \end{pmatrix} \tag{7.153}$$

The basis is $|k\rangle \otimes |m\rangle \otimes |\eta\rangle$. Note $J_1^{*k} \equiv (J_1^k)^*$.

We will consider the paramagnetic case for simplicity, where

$$G_{\ldots|\sigma\sigma} = G_{\ldots|\bar{\sigma}\bar{\sigma}} \tag{7.154}$$

Where $\bar{\sigma}$ is $-\sigma$. And the Green's functions are spin diagonal

$$G_{\ldots|\sigma\sigma'} = G_{\ldots|\sigma\sigma}\delta_{\sigma\sigma'} \tag{7.155}$$

Moreover we will consider the self-energy that is strictly local in space, that means

$$\Sigma_{\ldots|\mathrm{AB}} = \Sigma_{\ldots|\mathrm{BA}} = 0 \tag{7.156}$$

Since Hartree terms give an energy shift we can absorb it into energy definition as a shift of the bath chemical potential, and we absorb it into the energy definition. Note in the presented model the symmetry $\Sigma_{\mathrm{AA}} = \Sigma_{\mathrm{BB}}$ is fulfilled very well in most of the cases during the iteration, one can see this from the figures of the next section.

7.6 Numerical results

In the numerical computations, we always choose the static hopping as the energy unit

$$J_0 = 1.0 \tag{7.157}$$

and fix the model parameters as

$$V_0 = 0, \quad V_1 = 1.0J_0, \quad J_1 = 1.0J_0 \tag{7.158}$$

This simple parameter setting allows the Rice-Mele model to have an adiabatic quantized Thouless pump phase, which is a semiconductor in low drive frequencies. For high drive frequencies it will crossover to a metallic phase. This allows us to study the interplay between the semiconductor to

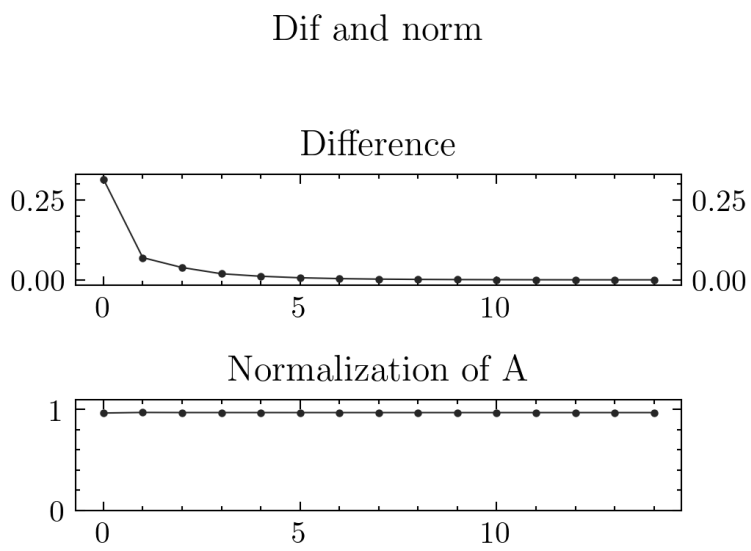

Figure 7.3: Typical "dif" and "norm" during the self-consistent loop of the numerical computation. (Upper) The integrated absolute value of the difference of adjacent time averaged Floquet Wigner retarded self-energy's zeroth component $\int_\omega |[\overline{\Sigma}^R_{0|\mathrm{AA}}]_{n+1}(\omega) - [\overline{\Sigma}^R_{0|\mathrm{AA}}]_n(\omega)|$. (Lower) the normalization $\int_\omega A(\omega)$ of the spectral function $A(\omega) \equiv -2\mathrm{Im}\, \overline{G}^R_{0|\mathrm{AA}}$.

metal crossover and the metal to Mott insulator transition.

The lattice constant is always set to unity

$$a_0 = 1.0 \tag{7.159}$$

We choose J_0 as the energy unit, that means

$$\omega = \omega/J_0, \quad \Omega = \Omega/J_0 \tag{7.160}$$

We consider half-filling free fermion thermal external bath (7.145) with the parameters

$$\beta = 20J_0, \quad \Gamma = 0.1/J_0 \tag{7.161}$$

Here $\beta = 20$ ($T = 0.05J_0$) is a low enough temperature for Mott physics, but high enough to avoid very sharp spectral features which usually make the converge harder. $\Gamma = 0.1J_0$ for non-interacting problem without external bath the dissipation is approaching zero, the external thermal bath gives a finite dissipation even for non-interacting case which allows us to invert the Floquet Dyson equation stably. Here we choose $\Gamma = 0.1J_0$ which is small enough for a near quantization of non-interacting Thouless pump for very low drive frequencies. For a high interaction strength, the dissipation of the interaction, the imaginary part of the retarded self-energy, is usually much greater than $0.1J_0$, and the results are expected to be not sensitive to this choice.

For very low drive frequency, the required Floquet matrix will be very large and hard to solve. Here we choose the lowest drive frequency to be $\Omega = 1.0$ where the Floquet matrix size still not too large.

For the Ω scan we choose the total Floquet matrix size $2 * n_f \times 2 * n_f$ as a function of Ω

$$n_f(\Omega) = 2\left\lceil \frac{a}{2\Omega} \right\rceil + 1 + b \tag{7.162}$$

where $\lceil x \rceil$ means ceil x to next integer. We choose $a = 11$ and $b = 4$ to make n_f an odd number, which is required. Since for low Ω we have small Floquet Brillouin zone, the number of points per Floquet Brillouin zone N_ω can be chosen lower to keep ω mesh density, here we choose

$$N_\omega(\Omega) = 2\left\lceil \frac{1}{2}\Omega \times 2^8 \right\rceil \tag{7.163}$$

This ensures N_ω is an even number. Although the $N_\omega(\Omega)$ will not keep the mesh number density per energy N_ω/Ω unchanged, it still gives a less varying mesh number density.

The convolutions of the self-energies are evaluated by using Fast Fourier Transform (FFT).

7.6.1 Density plot for time-averaged spectral functions

In Fig. 7.4 we can see how the $A_{\text{tav.}}(\omega) \equiv -2\text{Im}\overline{G}^{R}_{0|\text{AA}}(\omega)$ changes with two relatively small interaction.

On the top panel of Fig. 7.4, we show $U = 1.10$ case. On the left hand side of the top panel, we show a density plot for $A_{\text{tav.}}(\omega)$, and one the right hand side we show for $\Omega = 1.00, 4.56, 8.11, 11.67$, the momentum dependent spectral function $A_{\text{tav.}}(\omega, k) \equiv -2\text{Im}\,\overline{G}^{R}_{0|\text{AA}}(\omega, k)$ where $\overline{G}(\omega, k)$ is obtained from the non-interacting Green's function can the local self-energy $\Sigma(\omega)$ computed from the Floquet-DMFT. The $U = 1.10$ is actually very similar to the non-interacting case. For $\Omega < 2$, there are two bands. From the $A_{\text{tav.}}(\omega, k)$ for $\Omega = 1.0$ one can see the two bands actually have their finer structure, where each of them split into three small bands, which can be understood as the overlap of the time-independent bands and the Floquet bands. It is worth noticing that this finer structure is not so clear in the density plot because of the color code range we choose. For the slightly high drive frequencies $\Omega \sim 1.5$ to $\Omega \sim 4.0$, there are two "eye" structures, indicating the avoided crossing of the center Floquet band and the Floquet side bands, where a gap is generated. This can be best seen from the momentum dependent spectral function on the right-hand side, where $\Omega = 4.56$ is roughly a band touching fine tuning point, where one can imagine that for lower Ω the Floquet side bands get closer to the center bands in the $\omega \in [-\Omega/2, \Omega/2)$, and level repulsion occurs.

On the lower panel of Fig. 7.4, we can see the case for $U = 3.10$. For this not so strong interaction, the bands are smeared out because of the imaginary part of the self-energy. Or one can say that the finite interaction makes incoherence, and the single-particle picture becomes less valid. However, one can still see the density of states looks qualitatively unchanged. From the momentum dependent $A_{\text{tav.}}(\omega, k)$ one can further verify this statement.

On the top panel of Fig. 7.5 we increase U to $U = 5.10$, at this interaction strength, the $A_{\text{tav.}}(\omega, k)$ becomes less structured in the range of $\Omega \sim 1.5$ to $\Omega \sim 6.0$, although two Hubbard band like peak indeed appears, the $\omega \in [-U/2, U/2]$ gives a rather flat shape, there is no clear quasi-particle peak. For higher drive frequency $\Omega > 7.5$, the the quasi-particle peak reappears with two forming Hubbard bands. For low $\Omega \sim 1.0$, one can still see the Rice-Mele two-band structure.

In the lower panel of Fig. 7.5, we increase U to $U = 7.10$. For low Ω where $\Omega \in [1.0, 2.5]$ there is a crossover, that the center peak disappears, and the two upper Hubbard bands and two lower Hubbard bands merge to one upper and one lower band. Here, a clear structure is established that one can clearly see two Hubbard bands even for intermediate drive frequencies $\Omega \sim 2.5$ to $\Omega \sim 7.5$. However, the center quasi-particle peak is highly suppressed from $\Omega \sim 1.5$ to $\Omega \sim 7.5$, and then appears. The revival of this peak can be explained further by looking at the occupation spectrum and we will discuss later. There is a new feature at $\Omega \sim 2.5$ to $\Omega \sim 7.5$ that two $\omega = \Omega/2$ peak bridges the Hubbard band to the center quasi-particle peak, this can be related to the avoid crossing of the center Floquet bands and the side bands at the Floquet Brillouin zone boundary, where one can compare with Fig. 7.4 that they are at $\omega = \Omega/2$ as well.

We show time-averaged density of states $A_{\text{tav.}} = -2\text{Im}\,\overline{G}^{R}_{0|AA}(\omega)$, and the effective distribution $n_{\text{dist}} = \text{Im}\,\overline{G}^{<}_{0|\text{AA}}(\omega)/-2\text{Im}\,\overline{G}^{R}_{0|\text{AA}}(\omega)$ and occupation spectrum $\text{Im}\,\overline{G}^{<}_{0|AA}(\omega)$ in Fig. 7.6. From the middle column, we can read the effective distribution for different interaction strengths $U = 1.10, 3.10, 5.10, 7.10, 9.10$ from the top to the bottom. The n_{dist} is an analog to the familiar Fermi-Dirac distribution, and the shape of it can be seen as a modification of the Fermi-Dirac distribution. The most obvious difference is that the n_{dist} has a Floquet side band structure, that the excitation to $+\Omega$ is visible at a platform around $\omega = \Omega$ line. And around $\omega = -\Omega$ a square slot, or a valley is there. By

increasing the U, those platforms and valleys doubled because of the Hubbard band structure, we can see lower Hubbard bands (LHB) and upper Hubbard bands (UHB) clearly. An important feature of the low temperature Fermi-Dirac distribution is that it has a stage around $\omega = 0$. The Fermi-liquid theory gives that for even large interaction strength the stage in the distribution remains finite, where the discontinuous part is proportional to the quasi-particle weight that corresponds to the spectral weight of the center quasiparticle peak. From the Fig. 7.6 we can see that this stage is suppressed at intermediate drive frequency, for instance $\Omega \sim 5.0$ when $U = 9.10$. One can expect that the quasiparticle peak is then destroyed. By looking at n_{dist} figures, one can see that the interaction gives a "heating" effect to the distribution function, that effectively the temperature T_{eff} around $\omega = 0$, if we regard it as an approximate Fermi-Dirac distribution there, will be increased because of the decreasing slope of the distribution function. This heating effect may also explain the strong suppression of the center quasiparticle peak.[13]

Another thing about Fig. 7.6 is the $\omega = \Omega/2$ line that bridges the Hubbard bands, LHB and UHB, and the quasiparticle peak that reappeared at high drive frequencies. They can be best seen at the spectral function plots of $U = 9.10$, however from the distribution plot we can hardly distinguish them from the background.

[13] There is actually an issue with one dimension system, that the Landau Fermi-liquid is not exactly valid even for relatively weak interaction, and one dimensional systems are usually Luttinger liquid. Thus the quasiparticle situation maybe different. Our treatment cannot be accurate for the one-dimensional systems. However, we can regard this computation as a study of two band driven Hubbard model where local correlation is dominated and with one-dimensional density of state as the input.

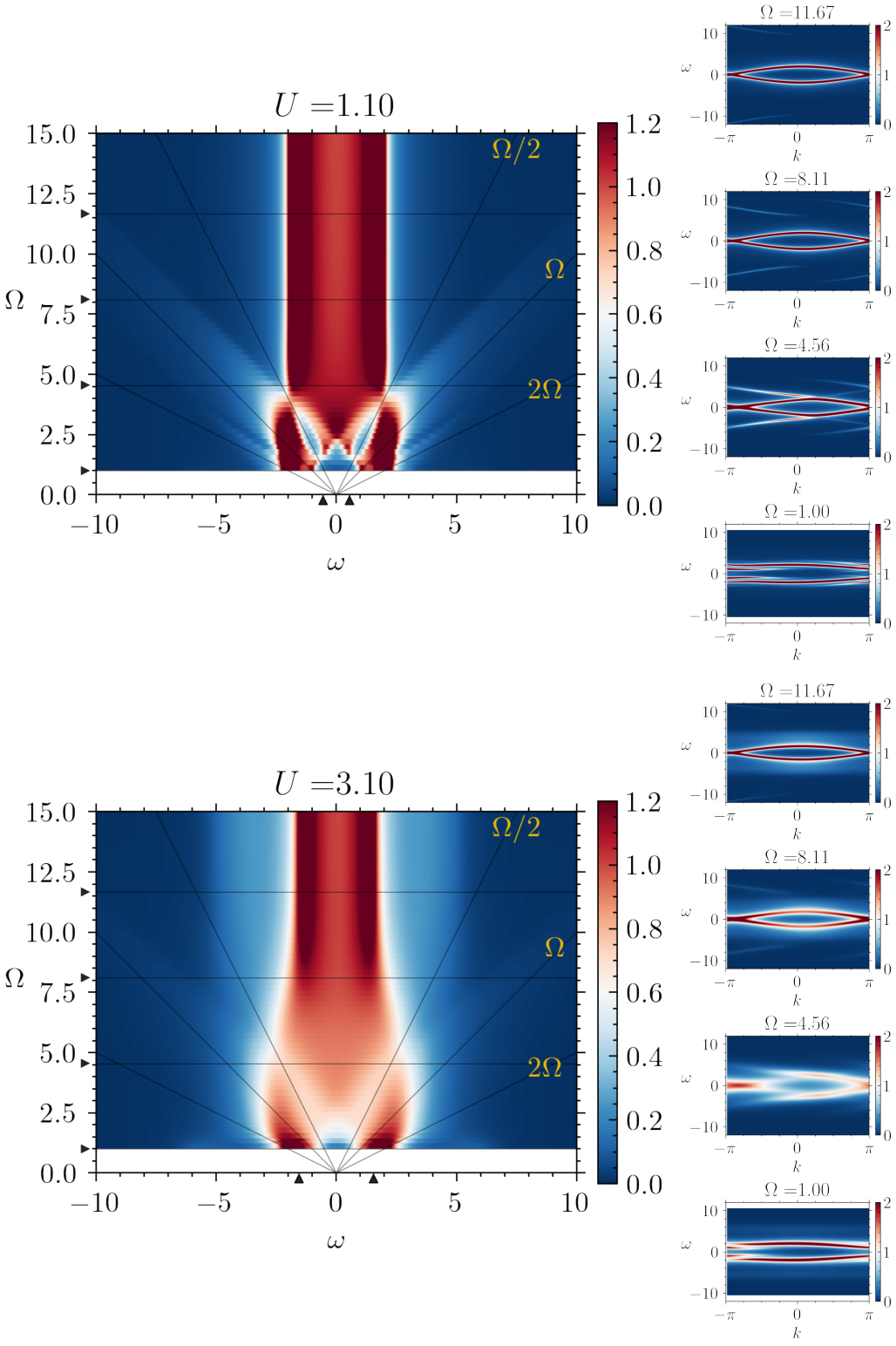

Figure 7.4: (Left) $-2\mathrm{Im}\,\overline{G}^{R}_{0|AA}(\omega)$ for different Ω, (Right) The k dependent spectral function $-2\mathrm{Im}\,\overline{G}^{R}_{0|AA}(\omega, k)$. The position of Ω in the 4 right plots are marked by small triangles near the Ω ticks of the left plot.

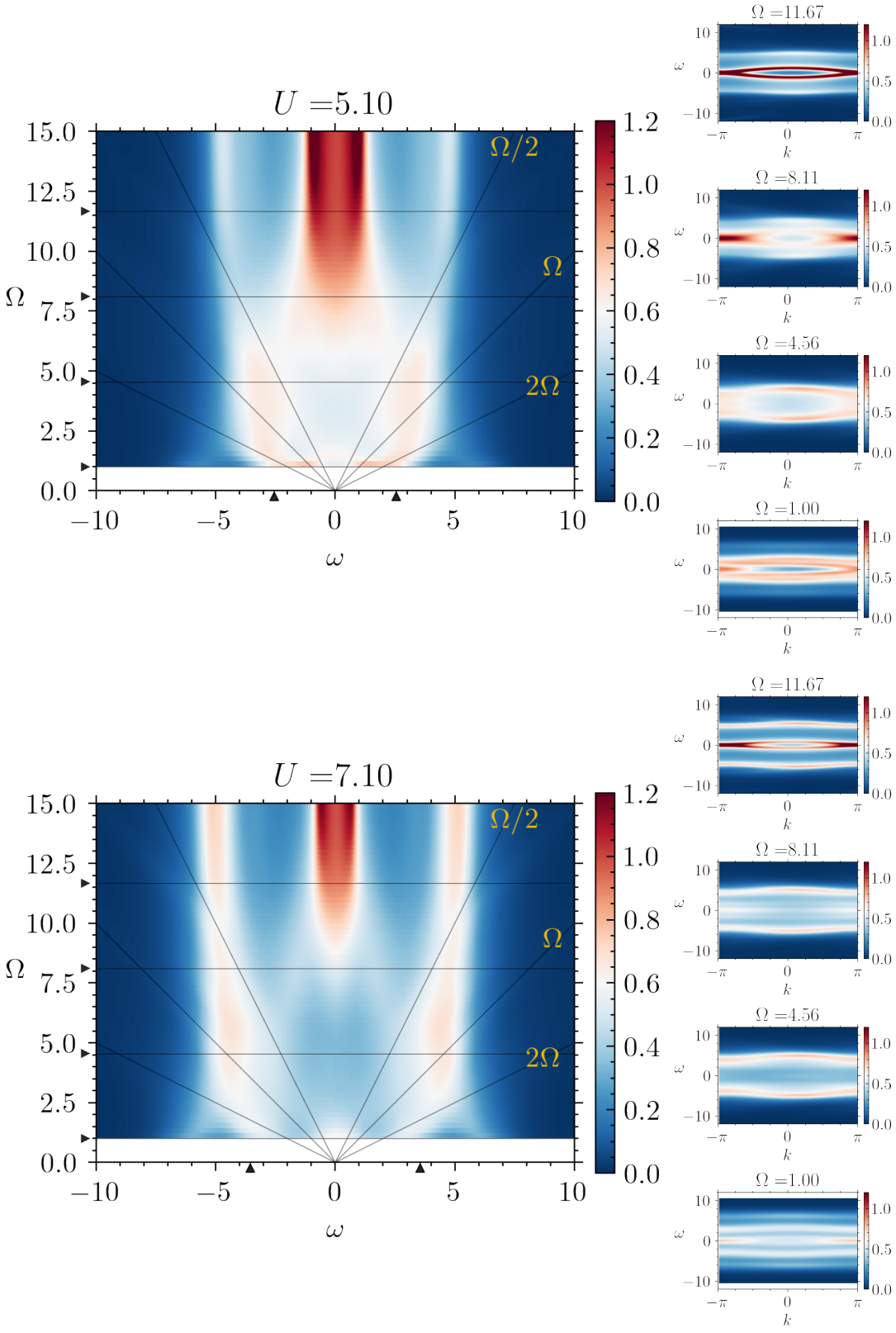

Figure 7.5: (Left) $-2\mathrm{Im}\,\overline{G}^{R}_{0|AA}(\omega)$ for different Ω, (Right) $G^{R}_{00|AA}(\omega,k)$. The position of Ω in the right plots are marked by small triangles.

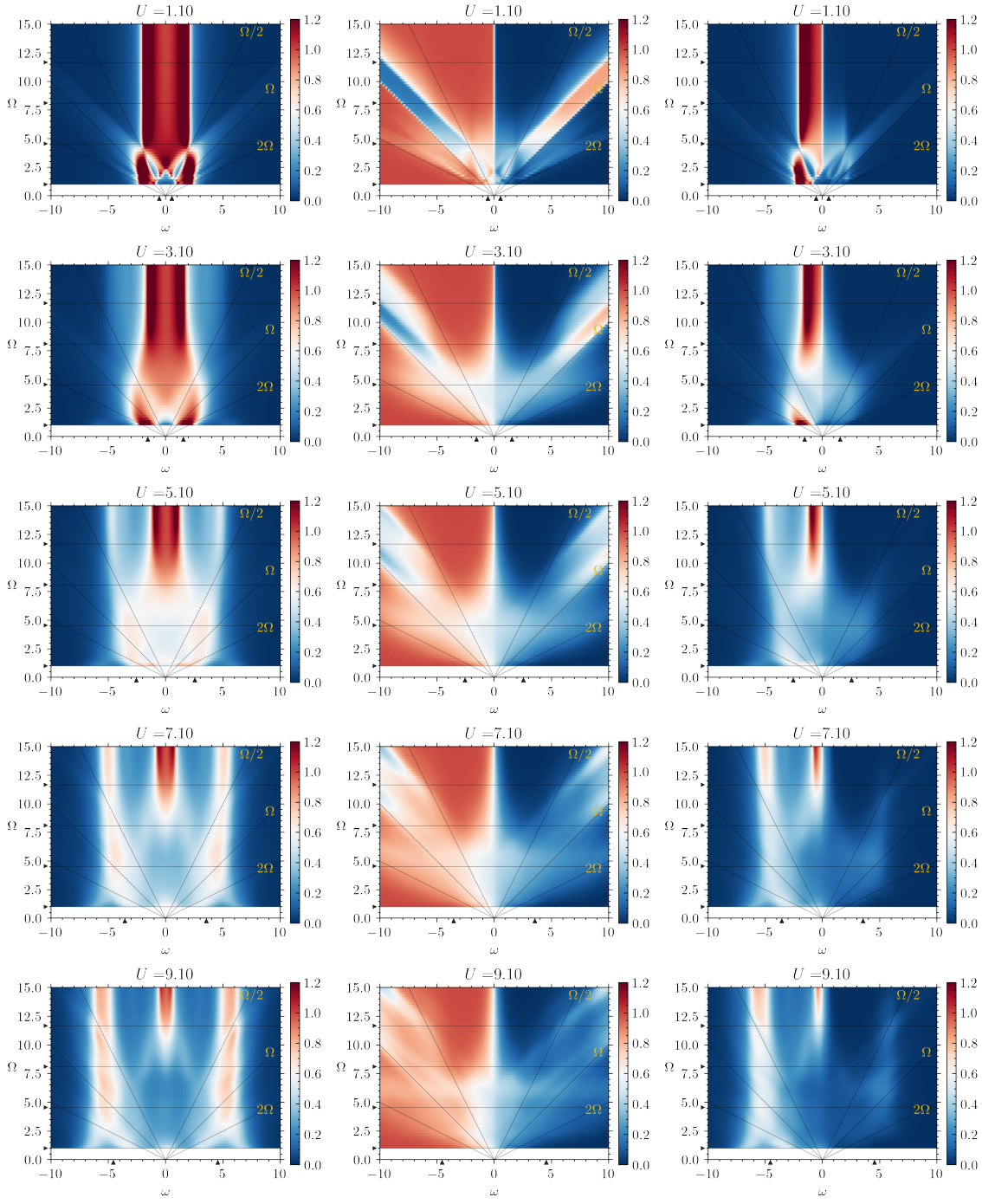

Figure 7.6: (Left column) $-2\mathrm{Im}\,\overline{G}^{R}_{0|AA}(\omega)$, (Middle column) $n_{\mathrm{dist}} = \mathrm{Im}\,\overline{G}^{<}_{0|AA}(\omega)/-2\mathrm{Im}\,\overline{G}^{R}_{0|AA}(\omega)$, (Right column) $\mathrm{Im}\,\overline{G}^{<}_{0|AA}(\omega)$.

7.6.2 Density of states and self-energies with higher harmonics

To get a closer look, we show the time-averaged density of states and higher harmonics of the Floquet Wigner Green's function in Fig. 7.7, Fig. 7.8, Fig. 7.10, Fig. 7.9, Fig. 7.11.The left two columns are imaginary parts of the retarded Floquet Wigner Green's function $\overline{G}^R_n(\omega)$. At the left most column we plot the $-2\mathrm{Im}\,\overline{G}^R_{0|\mathrm{AA}}(\omega)$ in black line, $-2\mathrm{Im}\,\overline{G}^R_{0|\mathrm{BB}}(\omega)$ in red line and $\mathrm{Im}\,\overline{G}^<_{0|\mathrm{AA}}(\omega)$ in gray area. We also plot the effective distribution function $1 + n_\mathrm{d}$ where we shifted a constant for visibility. The blue vertical lines mark the $\pm\Omega/2$. The second column on the left hand side we show $-2\mathrm{Im}\,\overline{G}^R_{n|\eta\eta}(\omega)$ where we shift $n * C$ for each component for visibility. In the third column we show the self energy in Wigner representation and its components in almost the same way.

In Fig. 7.7, the non-interacting or $U = 0.01$ case is shown. The self-energies on the right two columns are zero. From the first column, we can clear see that for low drive frequency $\Omega = 1.0$ there are two bands with $d_s = 1$ density of states that with van Hove singularity at their band edge. The distribution is closed to a step like Fermi-Dirac distribution, but with small peaks caused by the Floquet side bands. For higher drive frequencies $\Omega = 2.78, 4.56, 6.33$ the derivation of the Fermi-Dirac function is bigger. Although a Fermi surface like structure at zero frequency ω, the high/low energy distributions are modified and inverted. This can be understood as $n\Omega$ excitations. One can see that for $\Omega = 4.56$ and $\Omega = 6.33$ the additional peaks or valleys are at the integer multiples of Ω, as we have seen in the density plots Fig. 7.6. From all those figures we can also see a density of state suppression occurs at the $\pm\Omega/2$ or the Floquet Brillouin zone edge. Also for higher frequencies, there are stronger excitation effects, this is expected since the Floquet state is now farther from the adiabatic state.

The higher harmonics of the imaginary part of the retarded Green's function $-2\mathrm{Im}\,\overline{G}^R_{m|\eta\eta}(\omega)$ has a structure that the $m = +1$ harmonics are the mirror of $m = -1$ harmonics, however $+2$ is equal to -2 case. Moreover, as expected, the higher harmonics shrinks when we increase Ω, since the different Floquet replicas have a $m\Omega$ barrier reach each other. The strength of the harmonics also decreases as a function of $|m|$.

In Fig. 7.8, and in Fig. 7.9 we show $U = 3.10$ the density of states and the Green's function Floquet components. This interaction strength is weak in the sense that the Hubbard side peaks are small, but still strong enough for some sizable effects. The interaction generates some spectral broadening which makes everything smoother compare to the noninteracting case especially for the van Hove singularity. The gap at $\Omega/2$ is also partially filled and still visible. On the right hand side now we have non zero self-energies. The imaginary part of the retarded self-energy can be regarded as the damping rate of the single particle state. That at $\Omega = 1.0$ the rate is small around $\omega = 0$ and for $\Omega = 2.78$ the rate has a maximum at $\omega = 0$ indicates a strong suppress of the quasi-particle. Later, a valley is established and becomes deeper at $\omega = 0$ for larger Ω, and the center peak becomes higher. The harmonics of the self-energy behaves similarly as the Green's function. However, the ± 1 modes seem rather identical to each other. We show Ω from 1.00 to 13.44 with step length 1.78.

In Fig. 7.10 and Fig. 7.11 we show $U = 7.10$ case. This interaction strength is strong enough and close to the Mott transition that DMFT and iterated impurity solver can reproduce. Although the details of the transition is model dependent, and we didn't pass transition point here, still we can guess from the relative weight of the center peak and the Hubbard bands. With $U = 7.10$ the local density of states are never looks so closed to the non-interaction case, which one can compare with Fig. 7.7 to verify. And for $\Omega = 1.0$ in Fig. 7.10 we find a 5 peak structure, corresponding to 2 lower and 2 higher Hubbard bands for the non-interacting 2 band, and a center quasi-particle peak. The AA and

BB component are not exactly overlap to each other, this may because of some numerical error. The distribution function not is very smooth for Ω up to 4.56, and most flattened for $\Omega = 4.56$ with a high effective temperature. This is a rather strong heating effect. The $\Omega = 6.33$ in Fig. 7.10 is especially interesting, there it seems the effective temperature is decreasing, and the previous mentioned $\omega = \Omega/2$ slope peaks seem appear inside the center valley.

In Fig. 7.11, the top figure shows that there are two small side peaks. Those small shoulders are the $\Omega/2$ slope peaks that for small Ω from the Hubbard bands and go to the re-appeared center peak at high Ω. They may be better identified from the self-energy plot on the right hand side. For the highest $\Omega = 13.44$ in this figure, one can see that the Fermi-liquid like self-energy that around $\omega = 0$ behaves as ω^2, which is expected because we did not enter into the Mott insulator phase.

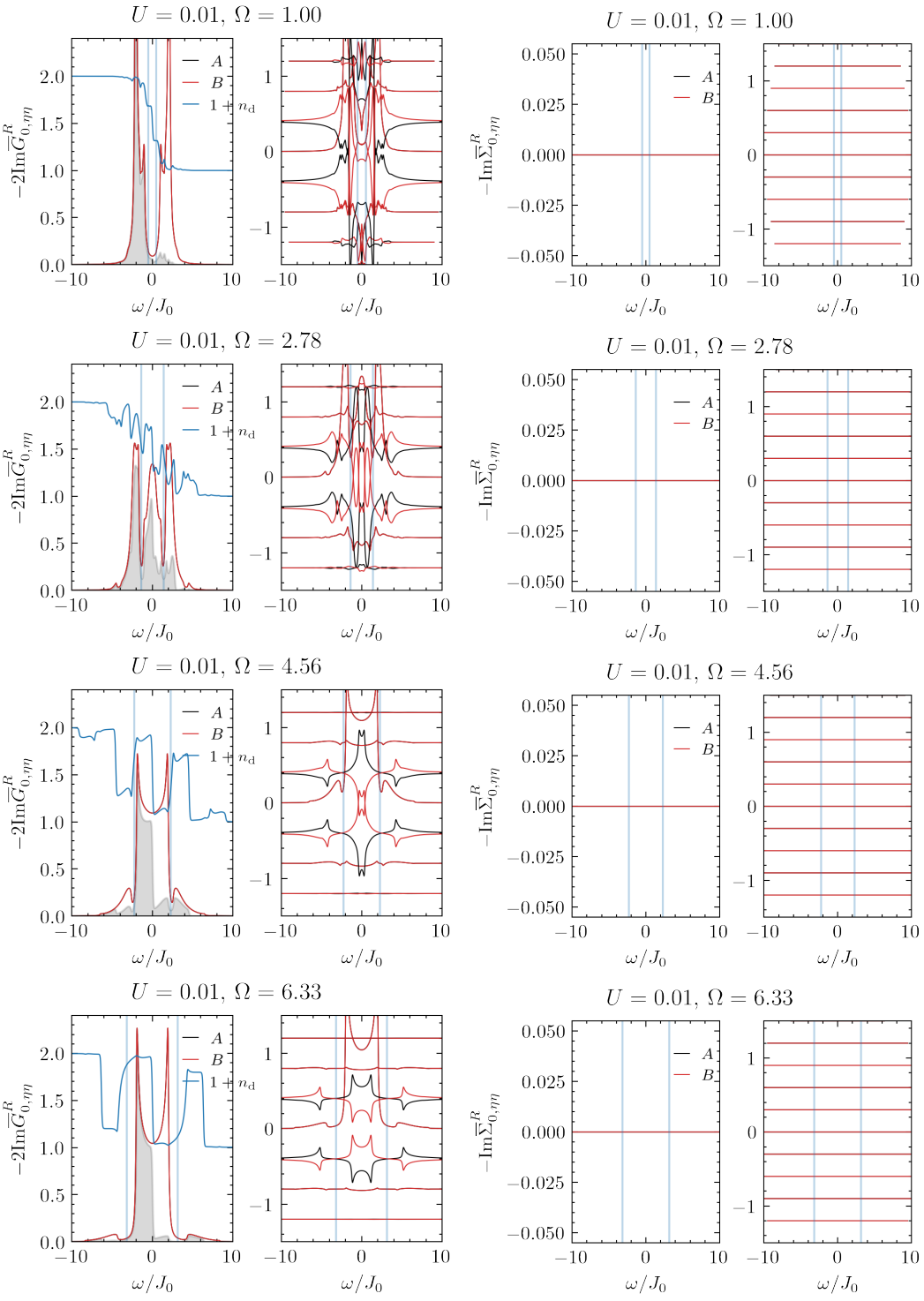

Figure 7.7: (Left two column) Non interacting density of state, from the Wigner-Floquet Green's function, normalized as $-\int \frac{\mathrm{d}\omega}{2\pi} 2\mathrm{Im}\, \overline{G}^R_{0,\mathrm{AA}} = 1$. The gray shaded area is the occupation $\mathrm{Im}\, \overline{G}^<_{0,\mathrm{AA}}$. The components $\overline{G}^R_{m,\eta\eta} + m * C$ are plotted on the right where C is an offset for plot visibility. (Right two column) The self energies, here is zero.

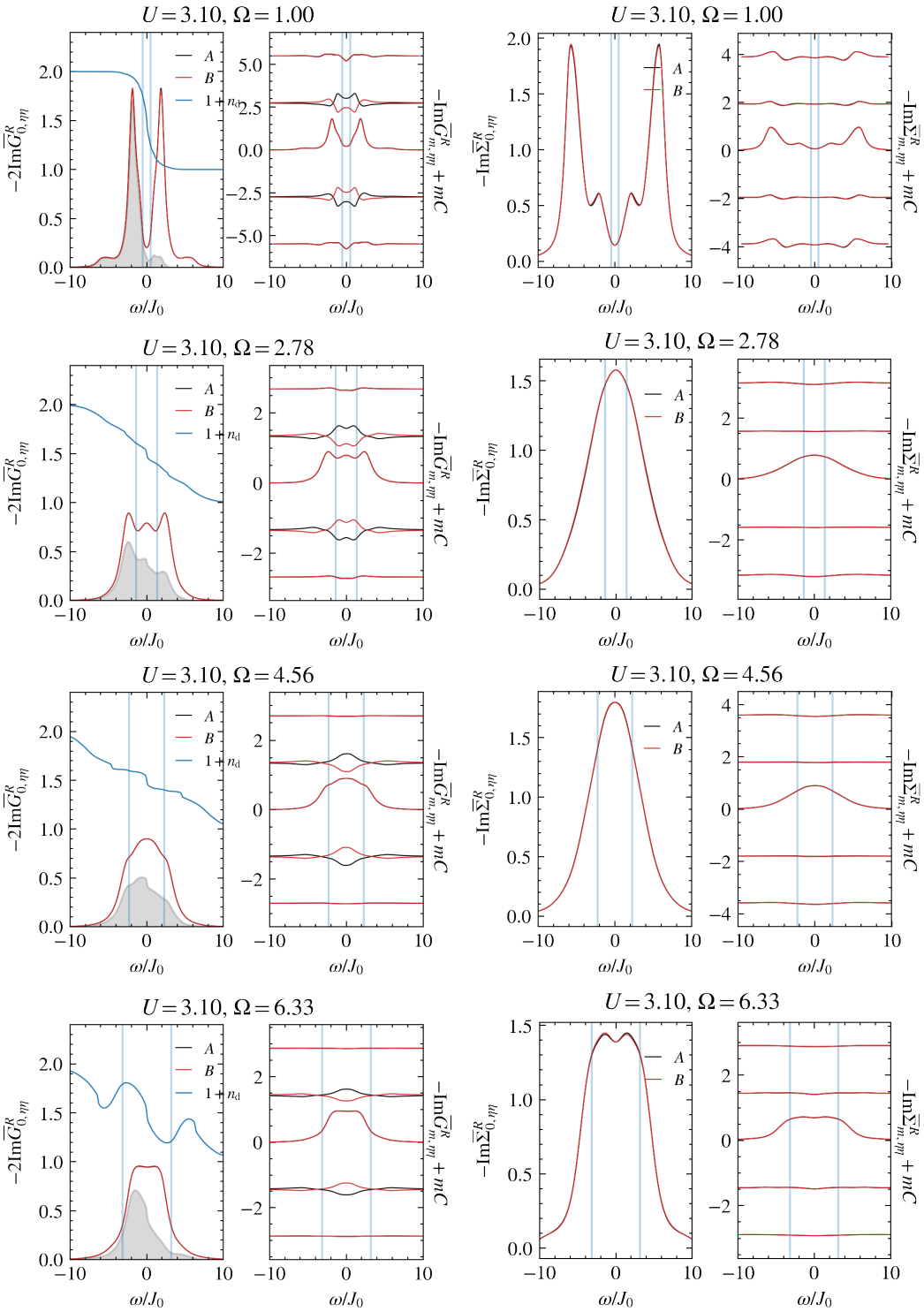

Figure 7.8: (Left two column) Density of state, from the Wigner-Floquet Green's function, normalized as $-\int \frac{\mathrm{d}\omega}{2\pi} 2\mathrm{Im}\,\overline{G}^R_{0,\mathrm{AA}} = 1$. The gray shaded area is the occupation $\mathrm{Im}\,\overline{G}^<_{0,\mathrm{AA}}$. The components $\overline{G}^R_{m,\eta\eta} + m * C$ are plotted on the right where C is an offset for plot visibility. (Right two column) The self energies $-\mathrm{Im}\,\overline{\Sigma^R}_{0,\eta\eta}$ and $-\mathrm{Im}\,\overline{\Sigma}^R_{m,\eta\eta} + m * C$.

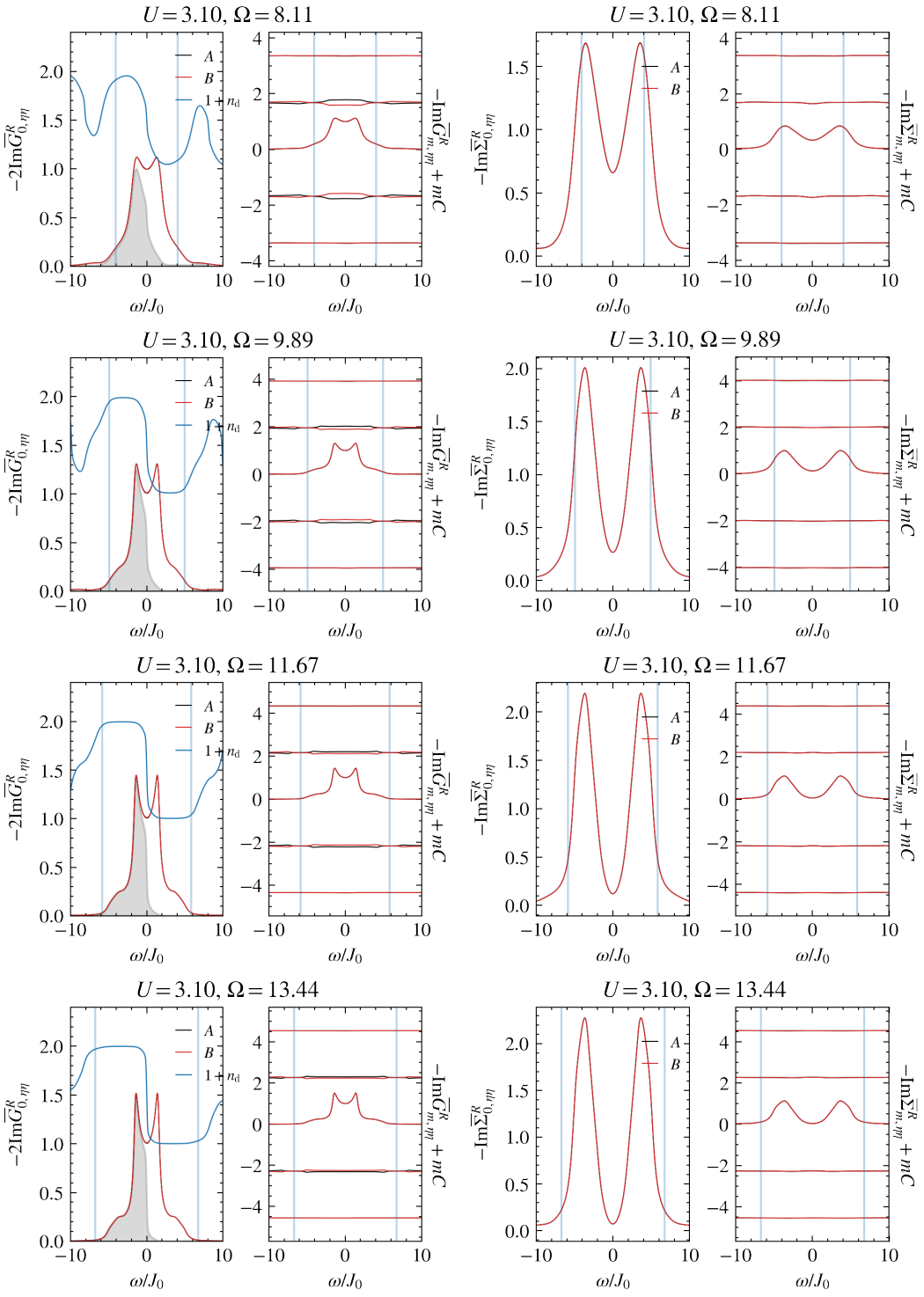

Figure 7.9: (Left two column) Density of state, from the Wigner-Floquet Green's function, normalized as $-\int \frac{\mathrm{d}\omega}{2\pi} 2\mathrm{Im}\,\overline{G}^R_{0,\mathrm{AA}} = 1$. The gray shaded area is the occupation $\mathrm{Im}\,\overline{G}^<_{0,\mathrm{AA}}$. The components $\overline{G}^R_{m,\eta\eta} + m * C$ are plotted on the right where C is an offset for plot visibility. (Right two column) The self energies $-\mathrm{Im}\,\overline{\Sigma^R}_{0,\eta\eta}$ and $-\mathrm{Im}\,\overline{\Sigma}^R_{m,\eta\eta} + m * C$.

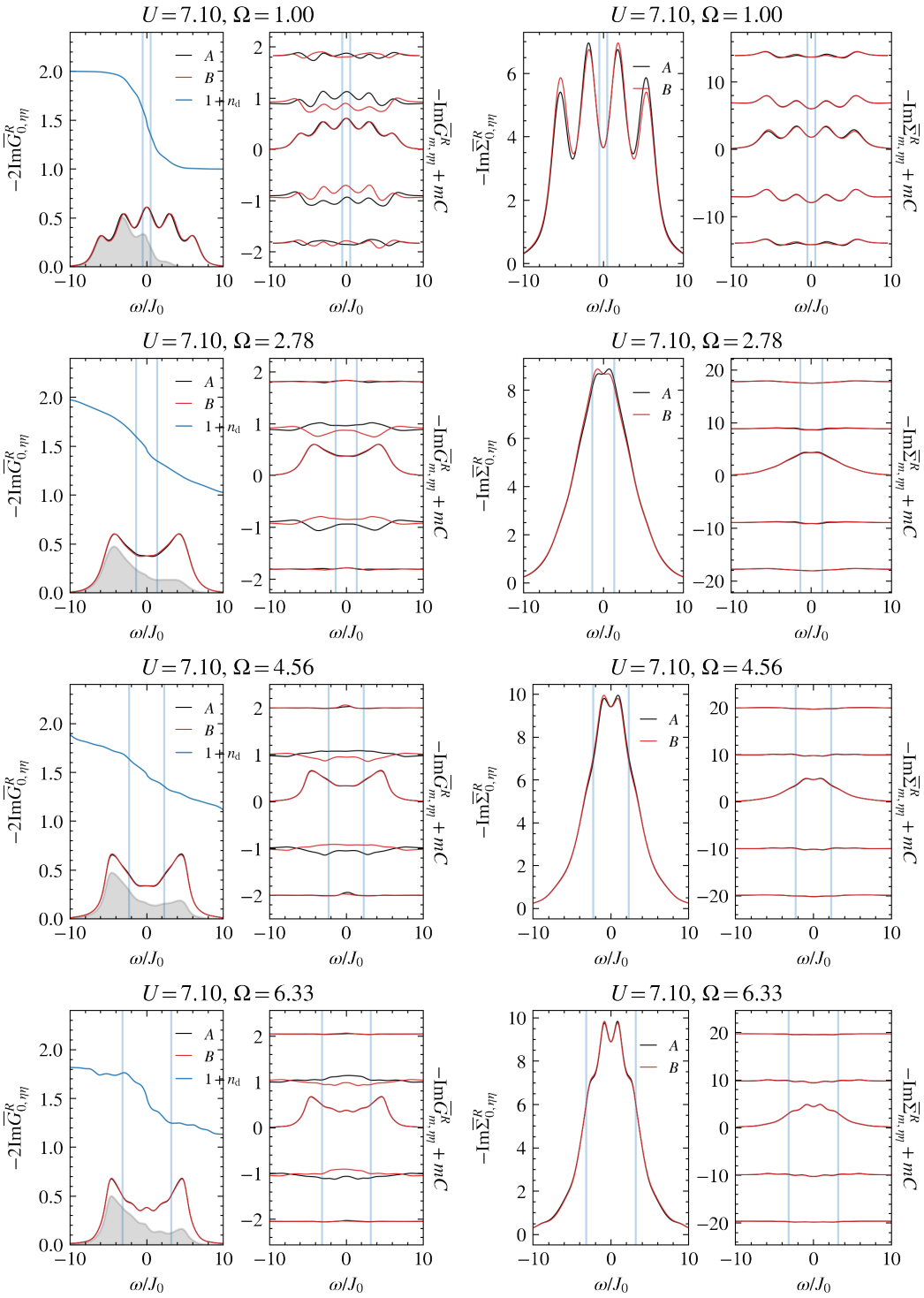

Figure 7.10: (Left two column) Density of state, from the Wigner-Floquet Green's function, normalized as $-\int \frac{\mathrm{d}\omega}{2\pi} 2\mathrm{Im}\,\overline{G}^R_{0,\mathrm{AA}} = 1$. The gray shaded area is the occupation $\mathrm{Im}\,\overline{G}^<_{0,\mathrm{AA}}$. The components $\overline{G}^R_{m,\eta\eta} + m * C$ are plotted on the right where C is an offset for plot visibility. (Right two column) The self energies $-\mathrm{Im}\,\overline{\Sigma^R}_{0,\eta\eta}$ and $-\mathrm{Im}\,\overline{\Sigma}^R_{m,\eta\eta} + m * C$.

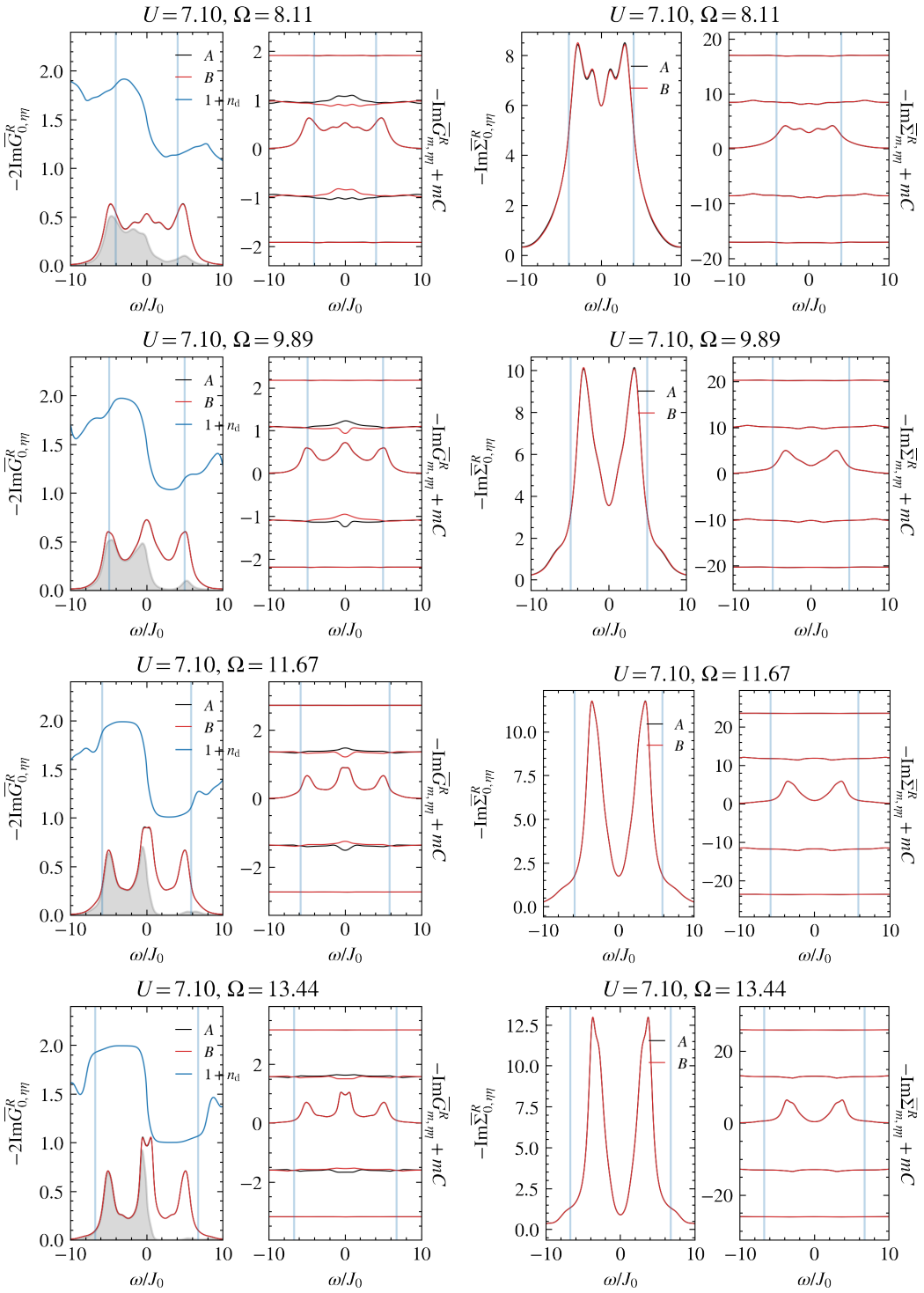

Figure 7.11: (Left two column) Density of state, from the Wigner-Floquet Green's function, normalized as $-\int \frac{\mathrm{d}\omega}{2\pi} 2\mathrm{Im}\,\overline{G}^R_{0,\mathrm{AA}} = 1$. The gray shaded area is the occupation $\mathrm{Im}\,\overline{G}^<_{0,\mathrm{AA}}$. The components $\overline{G}^R_{m,\eta\eta} + m * C$ are plotted on the right where C is an offset for plot visibility. (Right two column) The self energies $-\mathrm{Im}\,\overline{\Sigma^R}_{0,\eta\eta}$ and $-\mathrm{Im}\,\overline{\Sigma}^R_{m,\eta\eta} + m * C$.

7.6.3 Time averaged current

We show the time-averaged current multiplied by the period T, i.e. charge pumped in one period, in Fig. 7.12. Where we compute the current by using the formula that is introduced in the previous chapter in equation (6.24). We repeat the equations here and change the notation to make them consistent within this chapter, we define

$$(\partial_k J'_k)^* = -\mathrm{i}\frac{a_0}{2}J_+(t) + \mathrm{i}\frac{a_0}{2}J_-(t)e^{+ika_0} \tag{7.164}$$

The definition of J_+ and J_- one can find in (7.150). And then we define $\overline{J} = \int_0^T \mathrm{d}t J_{\mathrm{curr}}(t)$ can be computed as

$$\overline{J} = \frac{\mathrm{i}}{a_0 N_k}\sum_k\sum_{mn}\frac{2\pi}{\Omega}\int_{|\omega|\leq\Omega/2}\left([\partial_k J'_k]_{mn}[G^<_{\mathrm{BA}}]_{nm}(\omega,k) + [(\partial_k J'_k)^*]_{mn}[G^<_{\mathrm{AB}}]_{nm}(\omega,k)\right) \tag{7.165}$$

Or in short $\overline{J} = \frac{\mathrm{i}}{aN_k}\sum_k \frac{2\pi}{\Omega}\int_{|\omega|\leq\Omega/2}\mathrm{Tr}_F\left[\partial_k J'_k G^<_{\mathrm{BA}} + (\partial_k J'_k)^* G^<_{\mathrm{AB}}\right](\omega,k)$ with a "Floquet trace" Tr_F. The Green's functions we used is in the Floquet representation and the lesser component is computed as usual by using the local k-independent self-energy and k-dependent non-interacting Green's functions through $G(\omega,k) = [G_0^{-1}(\omega,k) - \Sigma(\omega)]^{-1}$.

The fourier coefficients are

$$[(\partial_k J'_k)^*]_{m-n=0} = \frac{a_0}{2}J_0(-\mathrm{i} + \mathrm{i}\cos(ka_0) + \sin(ka_0)) \tag{7.166}$$

$$[(\partial_k J'_k)^*]_{m-n=-1} = -\frac{a_0}{4}J_1(1 + \cos(ka_0) - \mathrm{i}\sin(ka_0)) \tag{7.167}$$

$$[(\partial_k J'_k)^*]_{m-n=+1} = -\frac{a_0}{4}J_1(1 + \cos(ka_0) - \mathrm{i}\sin(ka_0)) \tag{7.168}$$

Where $[(\partial_k J'_k)^*]_{mn} = [(\partial_k J'_k)^*]_{m-n}$ and $[(\partial_k J_k)^*]_{mn} = ([\partial_k J_k]_{\underline{m}n})^*$

There in Fig. 7.12 two sides of a same data are shown, the $\overline{J}$ vs. U and $\overline{J}$ vs. Ω. One can see that the current is in general reduced by increasing interaction U in this setting. The Ω dependent is more complicated. The noninteracting current has a "S" shape curve, that around $\Omega = 1.1$ there is an enhancement, which can be understood by Floquet side band here is moving away from each other, and the level repulsion becomes weaker. This means the gap, especially at quasi-energy $\Omega/2$ and $\Omega/2$, becomes smaller. This local minimum is lifted when U increases. This kind of behavior is also consistent with the arguments we made in the Section. 6.1.

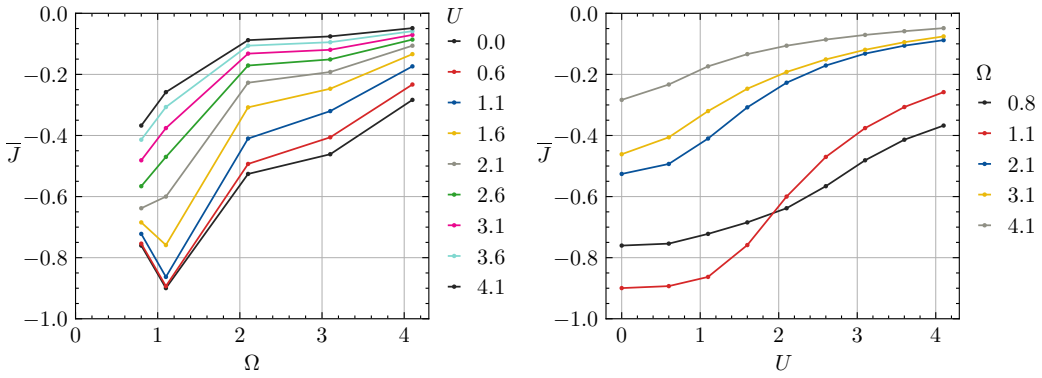

Figure 7.12: (Left) Time averaged current $\overline{J}$ vs. Ω, the legends are for different U. (Right) Time averaged current $\overline{J}$ vs. U, the legends are for different Ω. $\overline{J}$ defined in (7.165).

7.6.4 Time-averaged spectral functions with k dependence

In this section we plot k dependent spectral function $A(\omega, k) = -2\mathrm{Im}\,\overline{G}_0(\omega, k)$ for further references. One can compare them with the Fig. 7.4 and the Fig. 7.5.

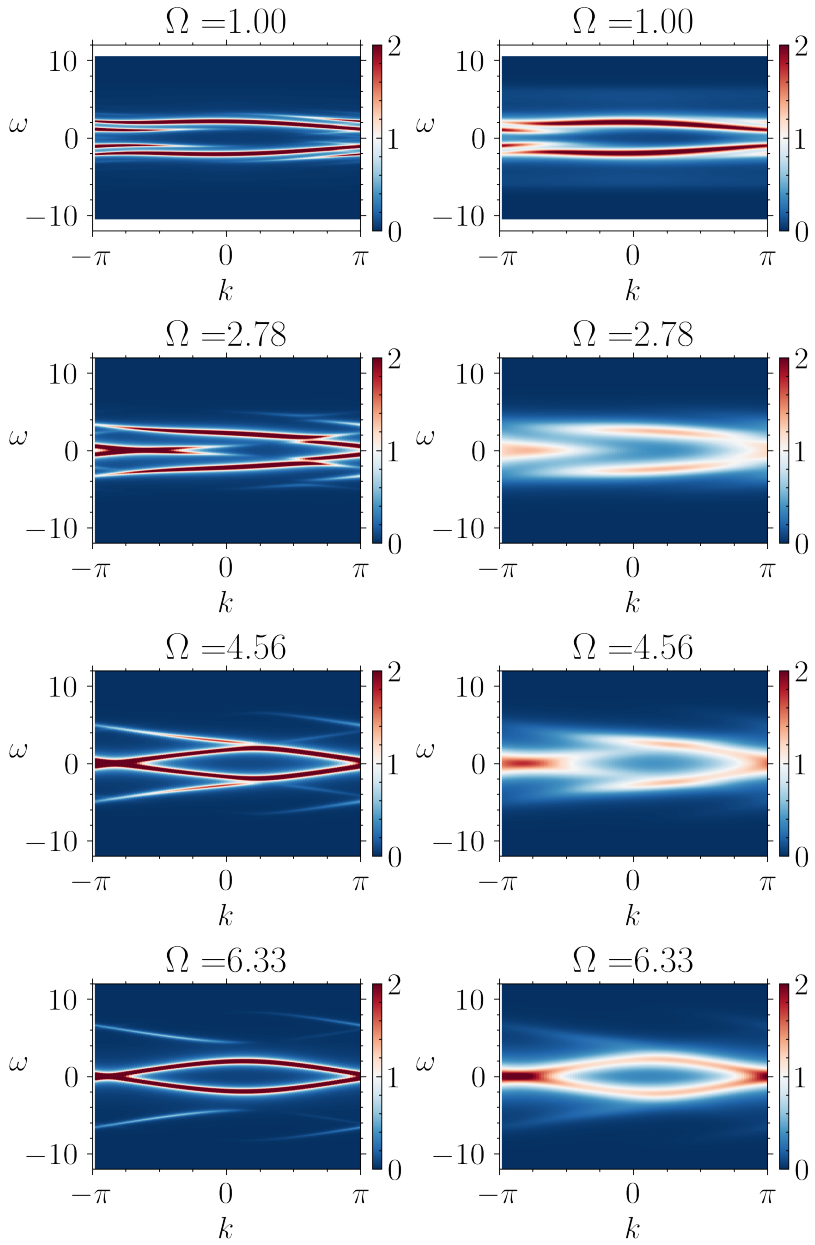

Figure 7.13: Plots of $-2\mathrm{Im}\,\overline{G}^R_{0,\mathrm{AA}}(\omega, k)$ for different Ω. (Left) $U = 1.10$, (Right) $U = 3.10$

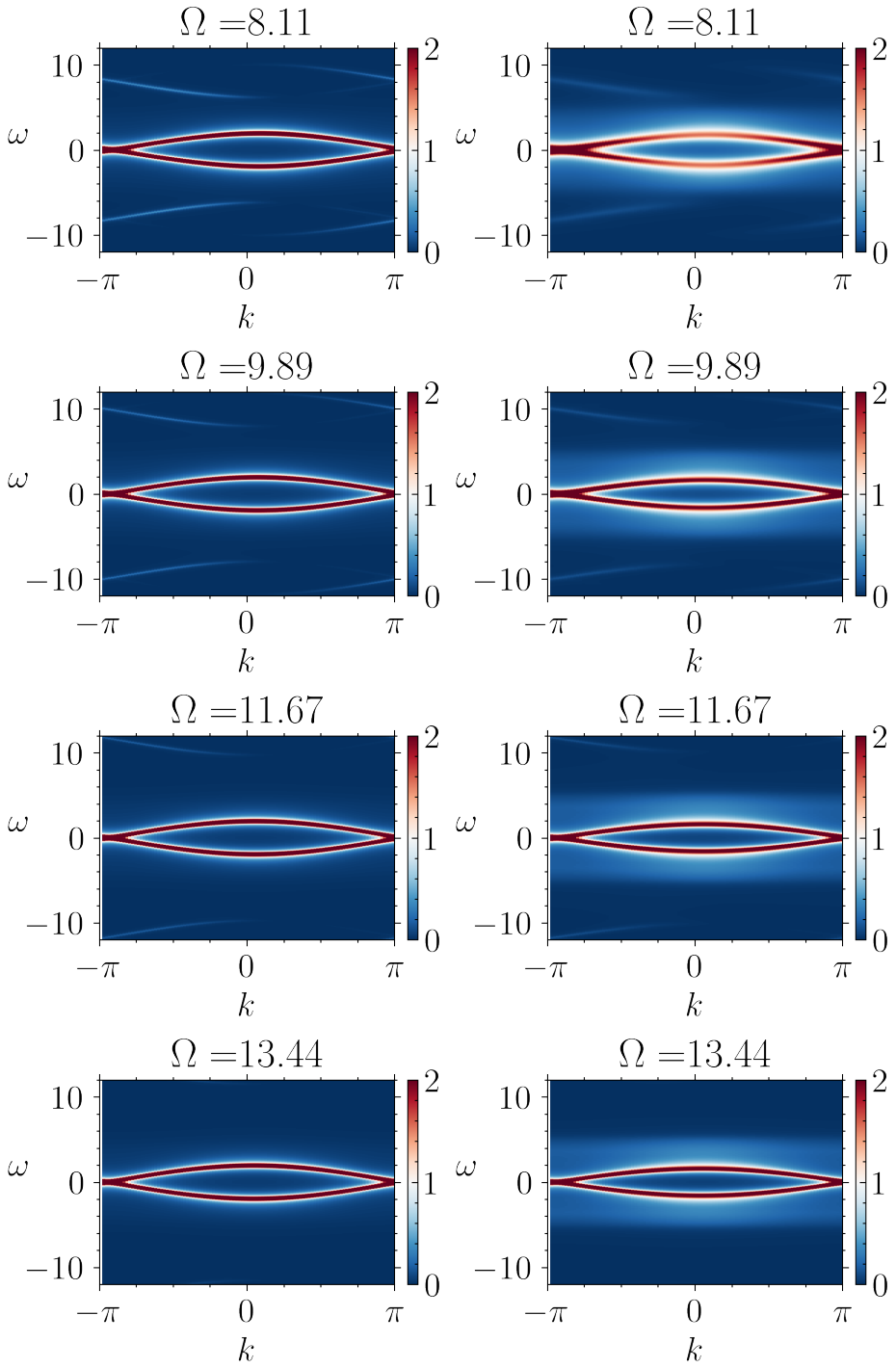

Figure 7.14: Plots of $-2\mathrm{Im}\,\overline{G}^{R}_{0,\mathrm{AA}}(\omega,k)$ for different Ω. (Left) $U = 1.10$, (Right) $U = 3.10$

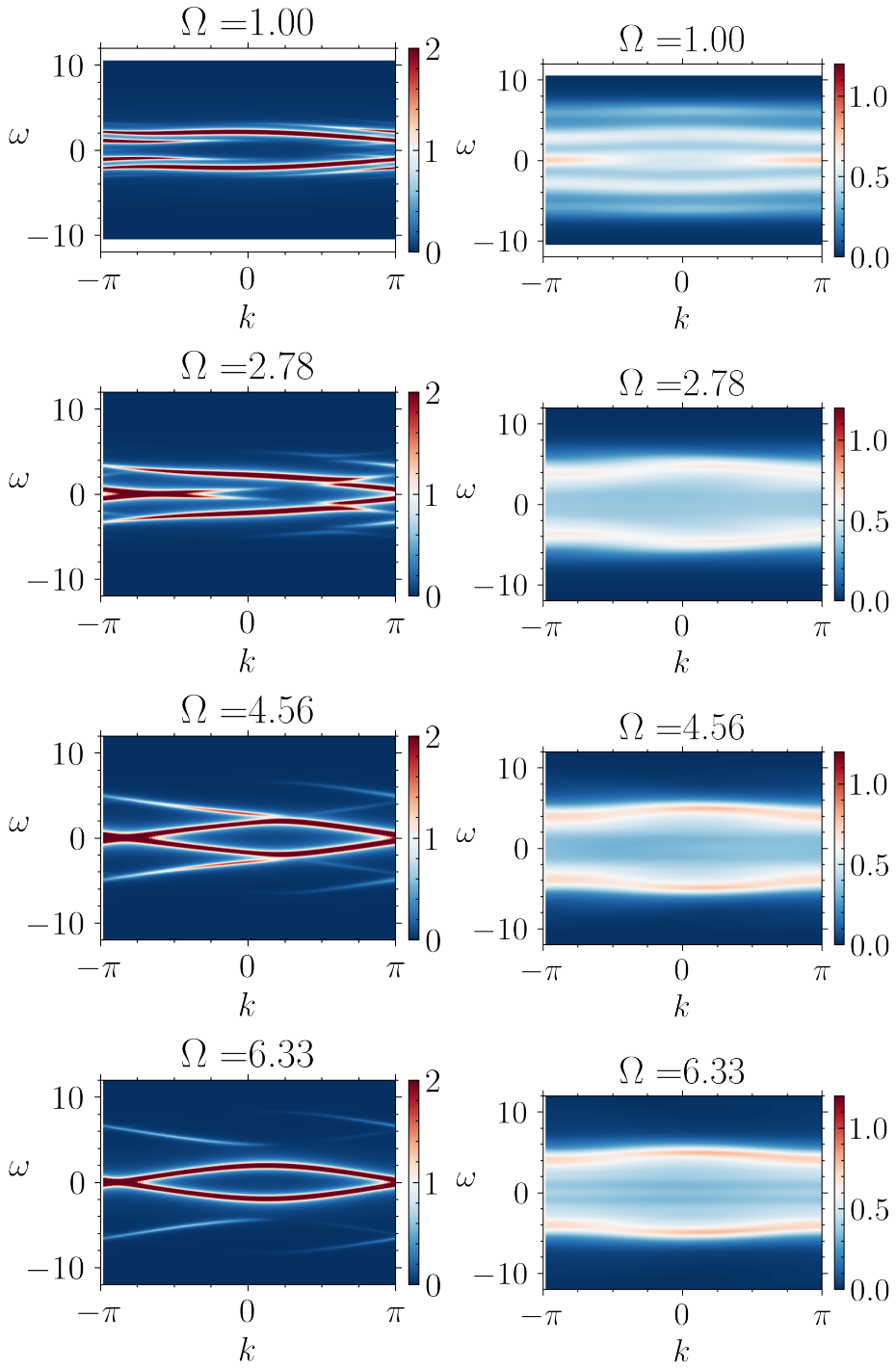

Figure 7.15: Plots of $-2\mathrm{Im}\,\overline{G}^{R}_{0,\mathrm{AA}}(\omega, k)$ for different Ω. (Left) $U = 1.10$, (Right) $U = 7.10$

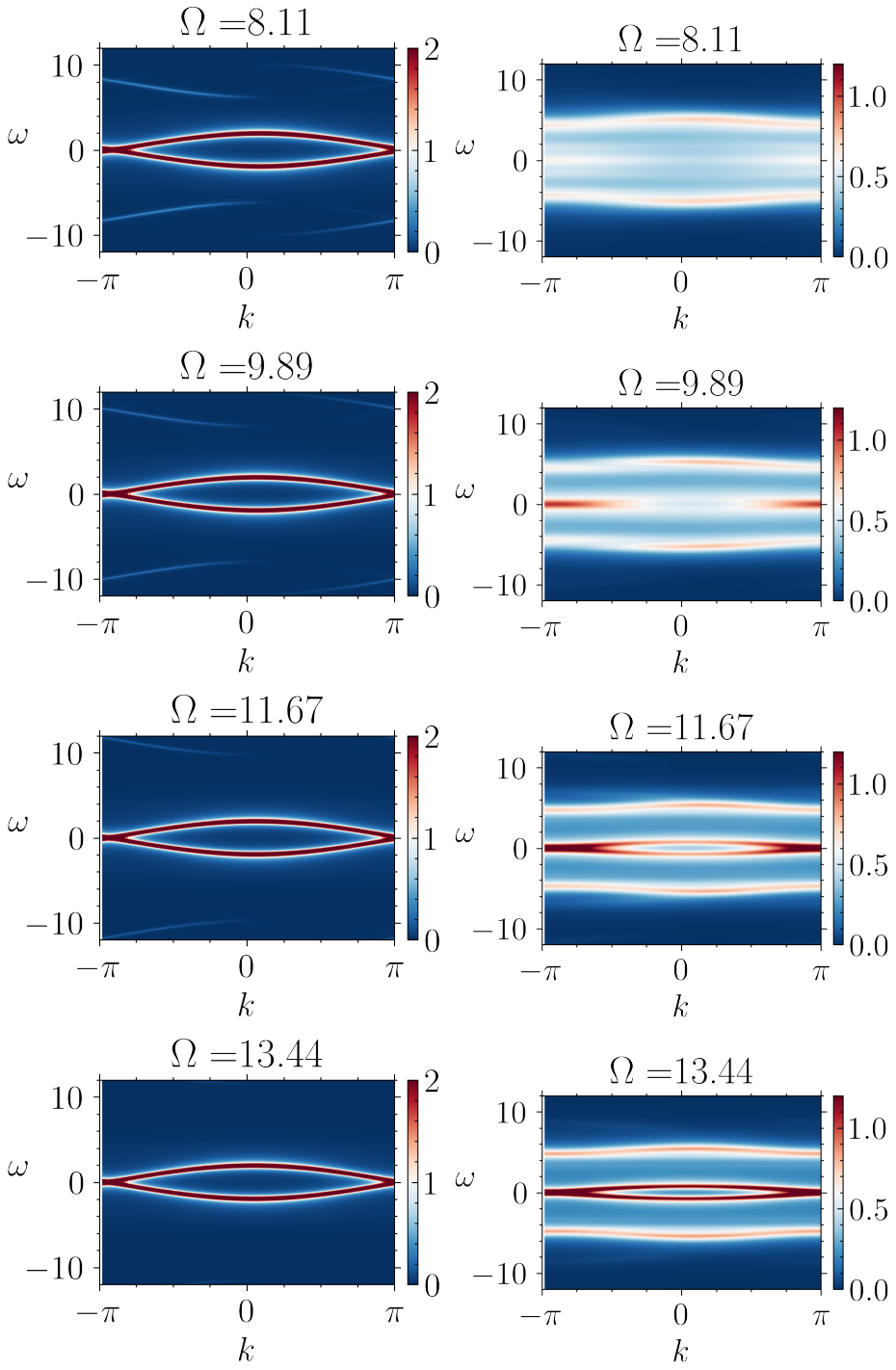

Figure 7.16: Plots of $-2\mathrm{Im}\,\overline{G}^{R}_{0,\mathrm{AA}}(\omega,k)$ for different Ω. (Left) $U = 1.10$, (Right) $U = 7.10$

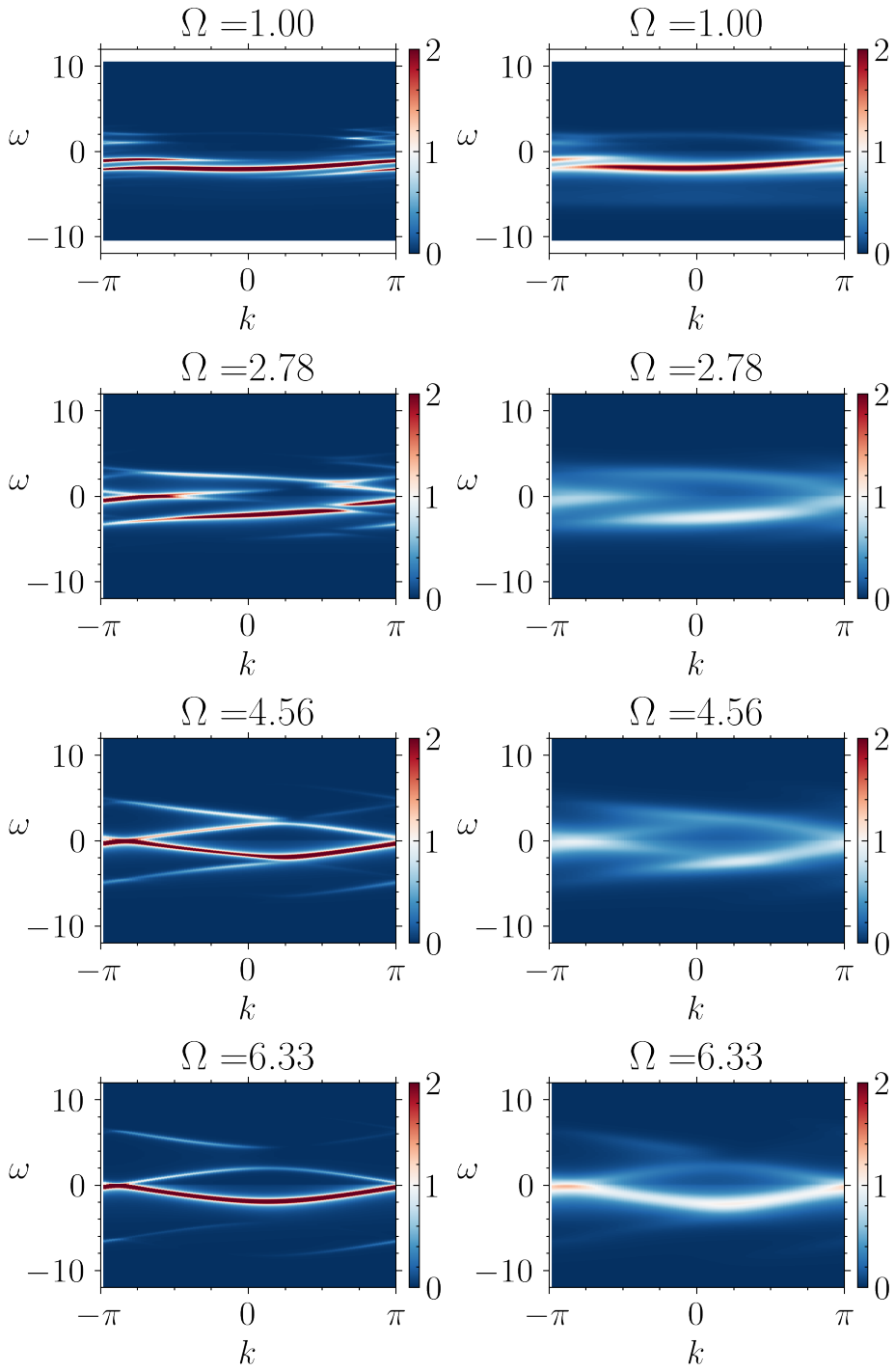

Figure 7.17: Plots of Im $\overline{G}^{<}_{0,\mathrm{AA}}(\omega, k)$ for different Ω. (Left) $U = 1.10$, (Right) $U = 3.10$

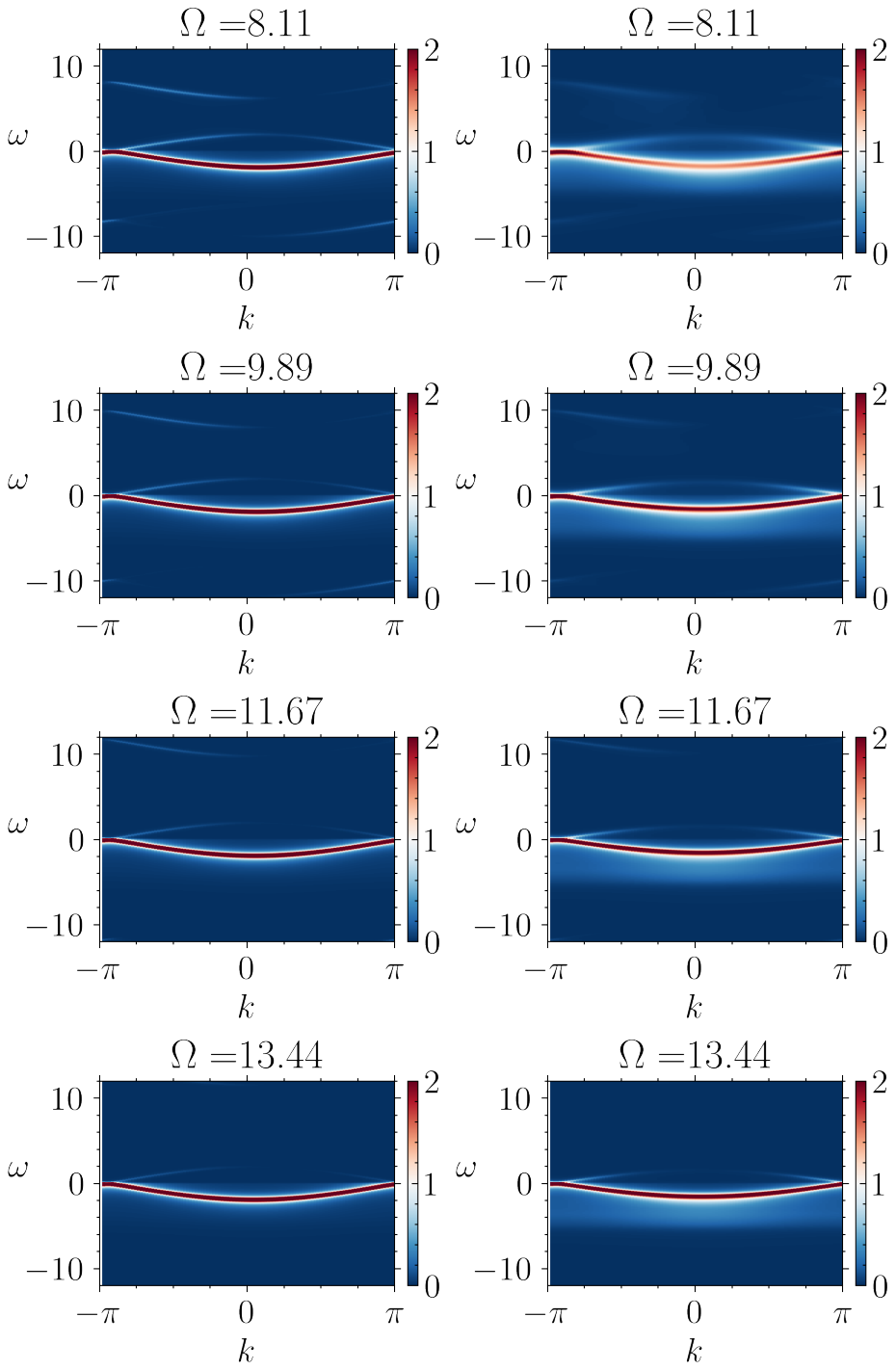

Figure 7.18: Plots of $\mathrm{Im}\,\overline{G}^{<}_{0,\mathrm{AA}}(\omega, k)$ for different Ω. (Left) $U = 1.10$, (Right) $U = 3.10$

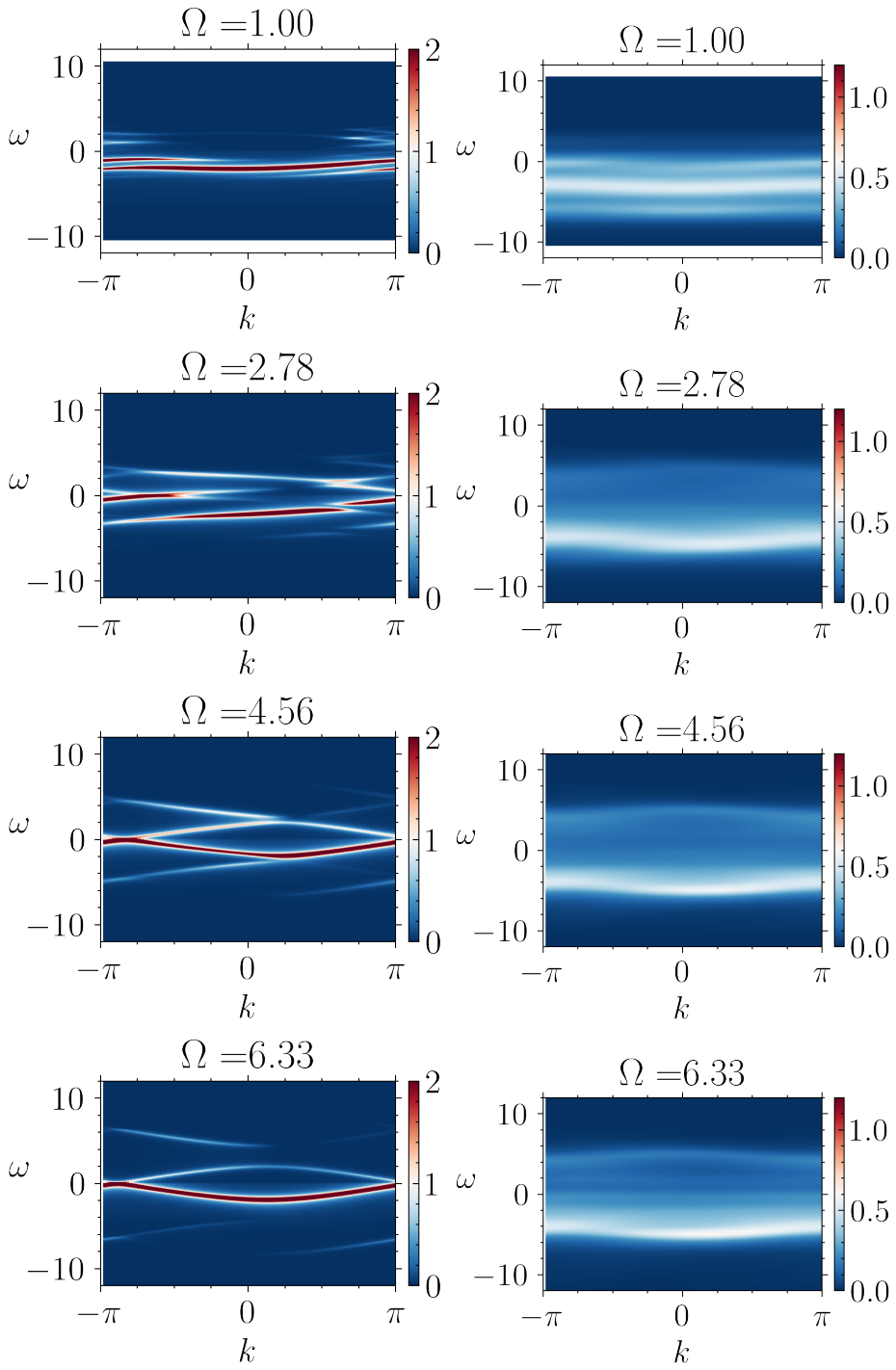

Figure 7.19: Plots of Im $\overline{G}^{<}_{0,\mathrm{AA}}(\omega, k)$ for different Ω. (Left) $U = 1.10$, (Right) $U = 7.10$

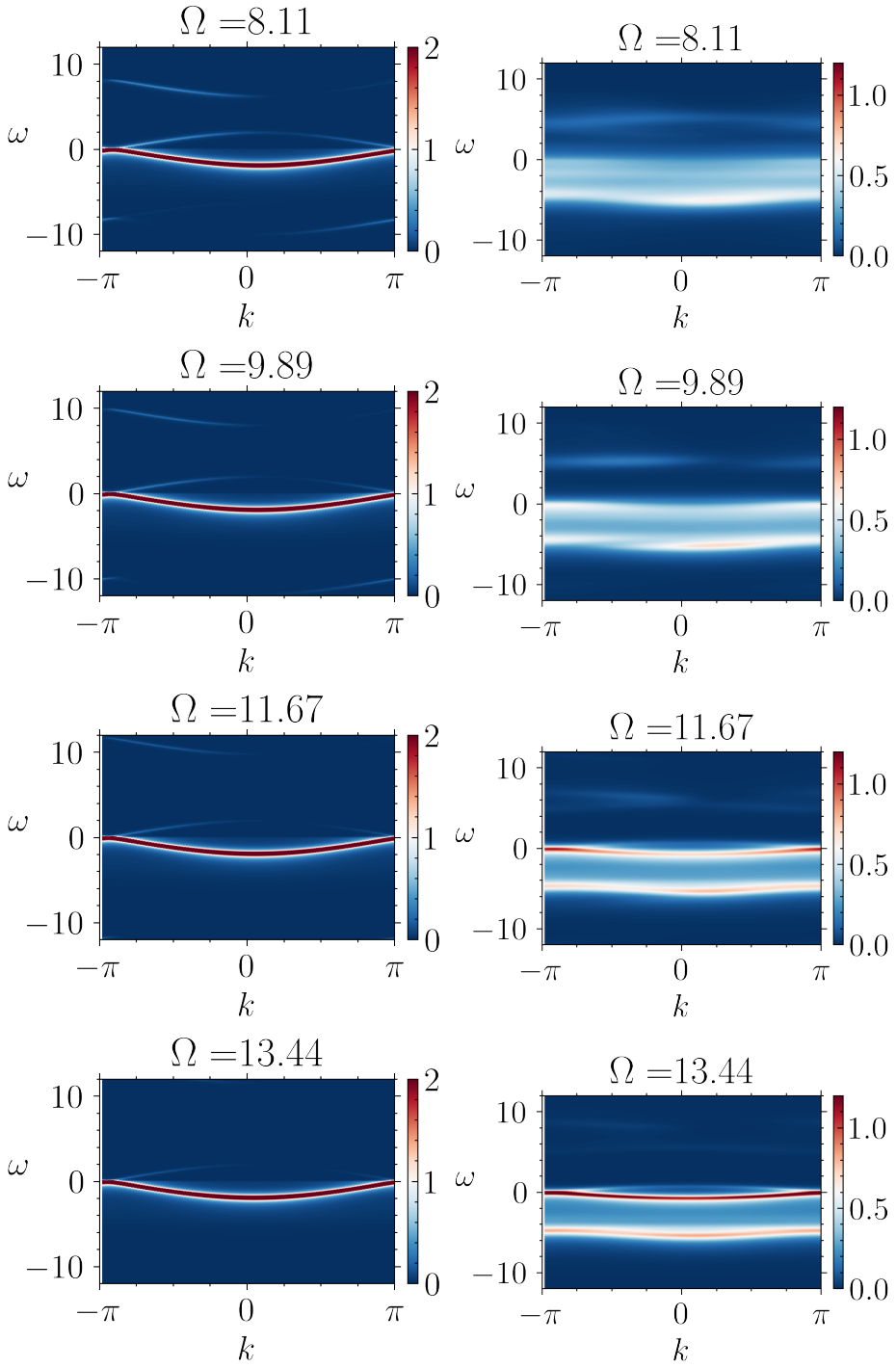

Figure 7.20: Plots of $\mathrm{Im}\,\overline{G}^{<}_{0,\mathrm{AA}}(\omega, k)$ for different Ω. (Left) $U = 1.10$, (Right) $U = 7.10$

7.7 Floquet NCA

Although the iterative perturbation theory (IPT) impurity solver can give qualitative reasonable results, for strong Hubbard interactions or away from half-filling it is usually not efficient even in equilibrium. For strong coupling physics, the non-crossing approximation (NCA) impurity solver becomes the choice. The NCA is a conserving approximation and a hybridization expansion, which is suitable for very large interaction strength, and can be improved systematically. The NCA and its extensions are reliable strong coupling impurity solver with mild numerical cost, and those features applies usually equally well in the studies of periodically driven non-equilibrium real time dynamics, namely Floquet systems. For late time physics which is required for periodically driven non-equilibrium steady state that need to evolve the systems for many periods, the Floquet NCA is especially efficient, origin from its conserving nature. The Floquet NCA can be also applied to periodically driven heavy fermion systems, and multi-orbital problems, where many other methods hard to treat.

Here we review and discuss the non-crossing approximation, which can be treated as an impurity solver for the Floquet DMFT [3].

Recall the single impurity Anderson model (SIAM) read

$$S_{\mathrm{SIAM}} = S_c + S_d + S_{cd} \tag{7.169}$$

where

$$S_d = \int_t \left(\sum_\sigma d_\sigma^\dagger \left(\mathrm{i}\partial_t - \epsilon_d \right) d_\sigma + U n_{d\uparrow} n_{d\downarrow} \right) \tag{7.170}$$

$$S_{cd} = \int_t \sum_{i\sigma} \left(V_i c_{i\sigma}^\dagger d_\sigma + V_i^* d_\sigma^\dagger c_{i\sigma} \right) \tag{7.171}$$

$$S_c = \int_t \left(\sum_{ij\sigma} c_{i\sigma}^\dagger (\mathrm{i}\partial_t - \widetilde{h}_{ij}) c_{j\sigma} + h.c. \right) \tag{7.172}$$

Slave-boson technique, is a parton construction for local impurity. It rewrites d as a composite particle with a constraint, here we consider $U \to \infty$ case, where double occupancy is not possible

$$d_\sigma = b^\dagger f_\sigma, \quad Q \equiv b^\dagger b + \sum_\sigma f_\sigma^\dagger f_\sigma = 1 \tag{7.173}$$

The states of the local Hilbert space are rewritten into slave-boson fields b for the hole and fermion fields f_σ for the singly occupied site in the enlarged space, a projection in the end should be applied. For reviews of its application in Kondo physics see [255]. Similar techniques have a long history, e.g. the Schwinger boson and Abrikosov fermion [266]. They have been successfully applied to spin models [267], Hubbard model and its relatives [8].

7.7.1 NCA equations

The periodically driven system, for instance, the driven SIAM, has been studied by using the non-crossing approximation in the reference [268]. The Keldysh method was applied to the quantum dot transport many years ago, in the 1990s, in the work of Meir and Wingreen [269]. The time-domain version is studied in [270].

The boson-fermion interaction part is

$$S_{fb} = \int_t \sum_{\boldsymbol{k}\sigma} V_{\boldsymbol{k}\sigma} \left(c^\dagger_{\boldsymbol{k}\sigma}(t) f_\sigma(t) b^\dagger(t) + h.c. \right) \tag{7.174}$$

Here we summarize the Floquet-NCA formalism, which can be derived by an "integrated out" procedure, or through the conserving approximation [255], by the derivatives of Γ_Φ

$$\Gamma_\Phi = -\int_{t_1 t_2} \sum_{\boldsymbol{k}\sigma} |V_{\boldsymbol{k}\sigma}|^2 G_{f\sigma}(t_2,t_1) G_{c\boldsymbol{k}\sigma}(t_1,t_2) G_b(t_1,t_2) \tag{7.175}$$

For simplicity here we assume[14]

$$V_{\boldsymbol{k}\sigma} = V \tag{7.176}$$

Which means we can write

$$G_{c\sigma} = \sum_{\boldsymbol{k}} G_{c\boldsymbol{k}\sigma} \tag{7.177}$$

Recall the tensor vertices we defined in the Keldysh method chapter for Schwinger-Keldysh formalism are

$$\gamma^+_{jk} = \begin{pmatrix} 1 & 0 \\ 0 & 0 \end{pmatrix} = +\frac{1}{2}\left(\tau^0 + \tau^3\right)_{jk}, \quad \gamma^-_{jk} = \begin{pmatrix} 0 & 0 \\ 0 & -1 \end{pmatrix} = -\frac{1}{2}\left(\tau^0 - \tau^3\right)_{jk} \tag{7.178}$$

or

$$\gamma^{\mathrm{cl}} \equiv \frac{1}{\sqrt{2}}\begin{pmatrix} 1 & 0 \\ 0 & 1 \end{pmatrix} = \frac{1}{\sqrt{2}}\tau^0, \quad \gamma^{\mathrm{q}} \equiv \frac{1}{\sqrt{2}}\begin{pmatrix} 0 & 1 \\ 1 & 0 \end{pmatrix} = \frac{1}{\sqrt{2}}\tau^1 \tag{7.179}$$

On CTP with tensor vertices the Γ_Φ then reads

$$\Gamma_\Phi = -V \sum_\sigma \gamma_{ij}{}^k G_{f\sigma|ri} G_{c\sigma|js} G_b^{kw} \gamma_{rs}{}^w V \tag{7.180}$$

where a fermionic pesudo-particle (also called pesudo-fermion or spinon) "f" for singly occupied state, "light" slave boson "b" for empty state and conduction electron "c". Note we have a complex boson here. The self-energies are

$$\Sigma_{f\sigma}(t_1,t_2) = -\mathrm{i}\frac{\delta\Gamma_\Phi}{\delta G_{f\sigma}(t_2,t_1)} = \mathrm{i}V^2 G_{c\sigma}(t_1,t_2) G_b(t_1,t_2) \tag{7.181}$$

$$\Sigma_b(t_1,t_2) = \mathrm{i}\frac{\delta\Gamma_\Phi}{\delta G_b(t_1,t_2)} = -\mathrm{i}V^2 \sum_\sigma G_{f\sigma}(t_2,t_1) G_{c\sigma}(t_1,t_2) \tag{7.182}$$

Or on CTP they are

$$\Sigma_{f|ir} = -\mathrm{i}\frac{\delta\Gamma_\Phi}{\delta G_{f\sigma|ri}} = \mathrm{i}V^2 \gamma_{ij}{}^k G_{c\sigma|js} G_b^{kw} \gamma_{rs}{}^w \tag{7.183}$$

$$\Sigma_b^{kw} = \mathrm{i}\frac{\delta\Gamma_\Phi}{\delta G_b^{kw}} = -\mathrm{i}V^2 \sum_\sigma \gamma_{ij}{}^k G_{f\sigma|ri} G_{c\sigma|js} \gamma_{rs}{}^w \tag{7.184}$$

[14] Though a momentum dependent and spin dependent V are possible, we restrict our self to the simplest case that without them.

The extended Hilbert space contains unphysical states which should not affect physical quantities. The physical subspace is the $Q = 1$ space where has a single impurity. Thus, projection is needed after the NCA loop converges. The projection to the sector Q is introduced by the Lagrange multiplier λ though $\lambda(Q-1)$. In practice, one can project [255] by computing the conduction electron self-energy

$$\Sigma_{c\sigma}(t_1,t_2) = -\mathrm{i}\frac{\delta\Gamma_\Phi}{\delta G_{c\sigma}(t_2,t_1)} = \mathrm{i}V^2 G_{f\sigma}(t_1,t_2)G_b(t_2,t_1) \tag{7.185}$$

and then use the T-matrix result [255] for the projected result

$$V^2 G_{d\sigma} = \Sigma_{c\sigma} \tag{7.186}$$

To keep the evolution equations inside the $Q = 1$ sector we need to do further analysis. Define the fugacity [269]

$$\zeta \equiv e^{-i\beta\lambda} \tag{7.187}$$

The fugacity power counting gives

$$G^<_{f,b} \sim O(\zeta), \quad G^>_{f,b} \sim O(1) \tag{7.188}$$

in the $\mathrm{i}\lambda$ ensemble. Thus the equation with different orders of $O(\zeta)$ decouples. We can match the orders, and find that the self-consistent loop can be split into two major steps. The Floquet representation and Floquet Wigner representation can be reached straightforwardly, which we summarize in the Table. 7.1 and Table. 7.2.

Note the quadratic part of the action in the extended space is

$$\begin{aligned} S_f &= \int_t \sum_{\boldsymbol{k}\sigma} c^\dagger_{\boldsymbol{k}\sigma}(t)(\mathrm{i}\partial_t - \epsilon_{\boldsymbol{k}} + \mu)c_{\boldsymbol{k}\sigma}(t) + \sum_\sigma f^\dagger_\sigma(t)(\mathrm{i}\partial_t - \epsilon_f + \mu)f_\sigma(t) \\ S_b &= \int_t b^\dagger(t)\mathrm{i}\partial_t b(t) \end{aligned} \tag{7.189}$$

The d electron spectrum or other physical quantities can be reached by a projection procedure, which can be guaranteed by a conserving approximation in $Q = 1$ sector with Keldysh method. The last step is that the G_d can be computed by

$$G^R_{d\sigma}(\omega) = \frac{Z_{Q=0}}{Z_{Q=1}}\left[G^>_b(t_2,t_1)G^<_{f\sigma}(t_1,t_2) - G^<_b(t_2,t_1)G^>_{f\sigma}(t_1,t_2)\right] \tag{7.190}$$

And in Floquet Wigner representation

$$G^R_{d\sigma}(\omega) = \frac{Z_{Q=0}}{Z_{Q=1}}\int_{\omega'}\left[G^>_{b|n}(\omega')G^<_{f\sigma|m-n}(\omega+\omega') - G^<_{b|n}(\omega')G^>_{f\sigma|m-n}(\omega+\omega')\right] \tag{7.191}$$

$G^> \sim O(1)$	$G^< \sim O(\zeta)$
Initial guess or previous loop gives $G_b^>$	Initial guess or previous loop gives $G_b^<$
$\Sigma_f^>$ by using $G_b^>, G_c^>$	$\Sigma_f^<$ by using $G_b^<, G_c^<$
Σ_f^R by $\Sigma_f^>$, then get G_f^R by Dyson equation	$G_f^<$ by $G_f^R \Sigma_f^< G_f^A$
$G_f^>$ by G_f^R	$\Sigma_b^<$ by using $G_f^<, G_c^>$
$\Sigma_b^>$ by using $G_f^>, G_c^<$	$G_b^<$ by $G_b^R \Sigma_b^< G_b^A$
Σ_b^R by $\Sigma_b^>$, then get G_b^R by Dyson equation	Back to the top
$G_b^>$ by G_b^R	
Back to the top	

Table 7.1: Sketch of the procedures. The $G_c^>, G_c^<$ are inputs and will not be update during the loops. Where we suppressed indices and labels other than Keldysh labels and species labels.

7.7.2 Construction details

Here we partially follow [269]. From the definition of the and the parton form of the d electron.[15]

$$d_\sigma = b^\dagger f_\sigma + \sigma f_{-\sigma}^\dagger a \tag{7.192}$$

Where we have b for the empty state, f for the singly occupied state, and a for the doubly occupied state. The constraint is

$$Q \equiv b^\dagger b + \sum_\sigma f_\sigma^\dagger f_\sigma + a^\dagger a = 1 \tag{7.193}$$

This is because a site can only choose to be empty or singly occupied or doubly occupied, and cannot be, for instance, empty and occupied at the same time. The simplest case of the NCA is that for $U \to \infty$ where the terms contain "a" can be dropped, since the double occupied state are not possible to reach. Thus we have

$$d_\sigma = b^\dagger f_\sigma \tag{7.194}$$

$$Q \equiv b^\dagger b + \sum_\sigma f_\sigma^\dagger f_\sigma = 1 \tag{7.195}$$

Under the above definitions, we can write $Q = n$ partition function on CTP as

$$Z_{Q=n} = \mathrm{Tr}\left[\rho_{Q=n} \hat{T}_C \exp\left\{-\mathrm{i}\int_{C(t)} J_i \hat{\phi}^i\right\}\right] \tag{7.196}$$

[15] See also, for instance, Chapter 9 of [271]

Usual identities	Use in NCA	Further in Floquet
$G^{>}_{f,b} - G^{<}_{f,b} = G^{R}_{f,b} - G^{A}_{f,b}$	$\to G^{>}_{f,b} = G^{R}_{f,b} - G^{A}_{f,b}$	$G^{>}_{mn}(\omega) = G^{R}_{mn}(\omega) - G^{A}_{mn}(\omega)$
$\Sigma^{>}_{f,b} - \Sigma^{<}_{f,b} = \Sigma^{R}_{f,b} - \Sigma^{A}_{f,b}$	$\to \Sigma^{>}_{f,b} = \Sigma^{R}_{f,b} - \Sigma^{A}_{f,b}$	$\Sigma^{>}_{mn}(\omega) = \Sigma^{R}_{mn}(\omega) - \Sigma^{A}_{mn}(\omega)$
$G^{R}_{f,b} = \theta(t_\mathrm{r})[G^{>}_{f,b} - G^{<}_{f,b}]$	$\to G^{R}_{f,b} = \theta(t_\mathrm{r})G^{>}_{f,b}$	$G^{R} = \widetilde{\mathrm{H}}[G^{>}]$
$\Sigma^{R}_{f,b} = \theta(t_\mathrm{r})[\Sigma^{>}_{f,b} - \Sigma^{<}_{f,b}]$	$\to \Sigma^{R}_{f,b} = \theta(t_\mathrm{r})\Sigma^{>}_{f,b}$	$\Sigma^{R} = \widetilde{\mathrm{H}}[\Sigma^{>}]$
$G^{<}_{f,b}(t_1,t_2) =$	$\int_{t_3,t_4} G^{R}_{f,b}\Sigma^{<}_{f,b}G^{A}_{f,b}$	$G^{<}_{mn} = G^{R}_{ml}\Sigma^{<}_{ls}G^{A}_{sn}$
$\Sigma^{>}_{f}(t_1,t_2) =$	$+\mathrm{i}V^2 G^{>}_{b}(t_1,t_2)G^{>}_{c}(t_1,t_2)$	$\to +\mathrm{i}V^2 \int_{\omega',n} \overline{G}_{b\,\vert n}(\omega')\overline{G}_{c\,\vert m-n}(\omega-\omega')$
$\Sigma^{<}_{f}(t_1,t_2) =$	$+\mathrm{i}V^2 G^{<}_{b}(t_1,t_2)G^{<}_{c}(t_1,t_2)$	
$\Sigma^{>}_{b}(t_1,t_2) =$	$-\mathrm{i}V^2 G^{>}_{f}(t_2,t_1)G^{<}_{c}(t_1,t_2)$	$\to -\mathrm{i}V^2 \int_{\omega',n} \overline{G}_{f\,\vert n}(\omega')\overline{G}_{c\,\vert m-n}(\omega+\omega')$
$\Sigma^{<}_{b}(t_1,t_2) =$	$-\mathrm{i}V^2 G^{<}_{f}(t_2,t_1)G^{>}_{c}(t_1,t_2)$	

Table 7.2: Equations used in Floquet NCA. Many indices are suppressed for clarity, they can be restored from the context. The Hilbert transform for the continuous frequencies are defined $\widetilde{\mathrm{H}}[G] \equiv \int_{\omega'} G(\omega,t_\mathrm{a})\frac{1}{\omega-\omega'}$. Where $\overline{G}$ is in the Floquet Wigner representation. Note the last formula for the Floquet-Wigner case, the $m-n$ is because the average time does not depend on the order of t,t'.

In $U \to \infty$ case

$$J_i\hat{\phi}^i = J_{b^\dagger}b^\dagger + J_b b + J_{f^\dagger}f^\dagger + J_f f + J_{d^\dagger}d^\dagger + J_d d \tag{7.197}$$

Where d should be regarded as composite operator and its corresponding source terms are for generating physical correlation functions. Now we assume the initial density matrix is a mix state thermal density matrix with $Q = n$

$$\rho_{Q=n} = \rho_0\delta_{Q,n} = e^{-\beta H_0}\delta_{Q,n} \tag{7.198}$$

Here we also assume that at the initial time only time independent part of non-interacting Hamiltonian contributes, that is the Hamiltonian

$$H_0 = H_b^0 + H_f^0 \tag{7.199}$$

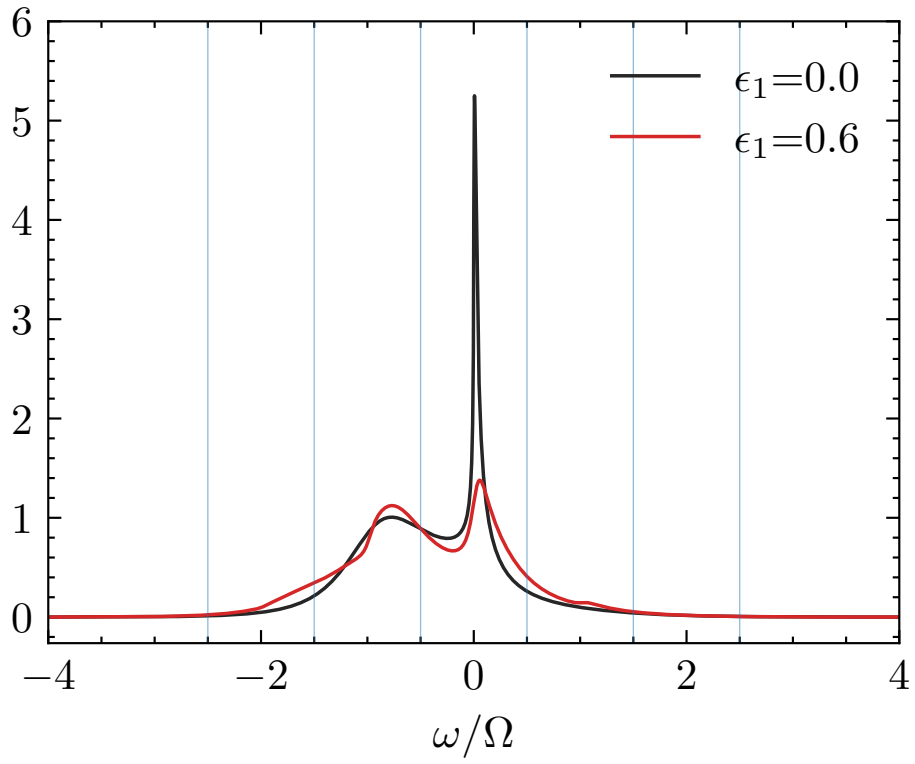

Figure 7.21: Floquet NCA solution for the time averaged spectral function $A_d(\omega)$ for single impurity Anderson model, $\epsilon_f(t) = \epsilon_0 + \epsilon_1 \cos(\Omega t)$, with $\epsilon_0 = -0.5$, $V = \sqrt{0.2}$, $\Omega = 1.0$, total number of Floquet modes $n_f = 15$. The electron bath has a gaussian DoS and the variance σ^2 where $\sigma = 1$. Here we used equal distance mesh, and 2^{10} points in each driven frequency Ω interval. Blue lines are $\Omega/2 + n\Omega$.

where H_b^0 is corresponding to the time independent Hamiltonian of the action S_b, H_f^0 is corresponding to the time independent Hamiltonian of S_f. We repeat the action here

$$\begin{aligned} S_f &= \int_t \left(\sum_{\boldsymbol{k}\sigma} c^\dagger_{\boldsymbol{k}\sigma}(t) \left(\mathrm{i}\partial_t - \epsilon_{\boldsymbol{k}} + \mu \right) c_{\boldsymbol{k}\sigma}(t) + \sum_\sigma f^\dagger_\sigma(t) \left(\mathrm{i}\partial_t - \epsilon_f(t) + \mu \right) f_\sigma(t) \right) \\ S_{fb} &= \int_t V \sum_{\boldsymbol{k}\sigma} \left(c^\dagger_{\boldsymbol{k}\sigma}(t) f_\sigma(t) b^\dagger(t) + h.c. \right) \\ S_b &= \int_t b^\dagger(t) \mathrm{i}\partial_t b(t) \end{aligned} \tag{7.200}$$

where in this section we only assume $\epsilon_f(t)$ can be time-dependent for simplicity. Note that the total Hamiltonian H is commuting with Q

$$[H, Q] = 0 \tag{7.201}$$

thus, Q is conserved.

Now we can use the identity

$$\delta_{Q,n} = \beta \int_{-\pi/\beta}^{\pi/\beta} \frac{\mathrm{d}\lambda}{2\pi} e^{-\mathrm{i}\beta\lambda(Q-n)} = \oint_{\lambda} e^{-\mathrm{i}\beta\lambda(b^\dagger b + \sum_\sigma f_\sigma^\dagger f_\sigma - n)} \tag{7.202}$$

where we defined a short-hand notation $\oint_\lambda = \beta \int_{-\pi/\beta}^{\pi/\beta} \frac{\mathrm{d}\lambda}{2\pi}$. Rewrite [269, 272] $Z_{Q=n}$ to

$$Z_{Q=n} = \oint_{\lambda} e^{\mathrm{i}n\beta\lambda} Z(\lambda) \equiv Z_{[n]} \tag{7.203}$$

Here the $Z_{[n]}$ is a short hand notation for the n-th (for $e^{-\mathrm{i}n\beta\lambda}$) Fourier component of $Z(\lambda)$. Importantly we now have a partition function $Z(\lambda)$ without constraint

$$Z(\lambda) = \mathrm{Tr}\left[e^{-\beta(H_0 + \mathrm{i}\lambda Q)} \hat{T}_C \exp\left\{ -\mathrm{i} \int_{C(t)} J_i \hat{\phi}^i \right\} \right] \tag{7.204}$$

Thus, the $Q = n$ sector partition function can be projected from $Z(\lambda)$ through a Fourier transform. And for $Q = n$ the terms at different order of the "fugacity"

$$\zeta \equiv e^{-\mathrm{i}\beta\lambda} \tag{7.205}$$

Terms except those with total order $O(\zeta^n)$ will be projected out in the end. As we know, the physical subspace is $n = 1$ or $O(\zeta^1)$.

The usefulness of the extended Hilbert space can now be understood, that is

- We can use $Z(\lambda)$ with the convenience that all usual field theoretical techniques can be applied.

Note that one will need to evaluate the projection of the derivatives of the Schwinger functional $\overline{W}(\lambda) = -\mathrm{i} \ln Z(\lambda)$ in the extended space. Without any loss of generality we use $\overline{W}^{(2d)}_{[1]} \equiv \overline{W}^{(dd^\dagger)}_{[1]}$ as an example, where one can replace $(2d)$ to (nd) when it is necessary. The projection to $Q = 1$ can be reached through

$$\overline{W}^{(2d)}_{[1]} = \oint_{\lambda} e^{\mathrm{i}n\beta\lambda} \overline{W}^{(2d)}(\lambda) = -\mathrm{i} \oint_{\lambda} e^{\mathrm{i}n\beta\lambda} \frac{Z^{(2d)}(\lambda)}{Z(\lambda)} \xrightarrow{\mathrm{Im}\,\lambda \to -\infty} -\mathrm{i} \frac{Z^{(2d)}_{[1]}}{Z_{[0]}} \tag{7.206}$$

Here we need to expand $Z(\lambda) = \sum_m e^{-\mathrm{i}m\beta\lambda} Z_{[m]}$, and then expand around $\zeta = e^{-\mathrm{i}\beta\lambda} \to 0$, which can be reached by $\lambda = \mathrm{i}\mathrm{Im}\,\lambda$, $\mathrm{Im}\,\lambda \to -\infty$. Note that we assumed $Z^{(2d)}_{[0]} = 0$ which is satisfied because $Q = 0$ is the case that no physical d impurity is presented.[16] We also used $Z^{(1d)}(\lambda) = 0$, since d is fermionic.

Now define

$$W = -\mathrm{i} \ln Z_{[1]} \tag{7.207}$$

The second functional derivative of Schwinger functional which is legendre transformed directly from

[16] The functional derivatives with auxiliary particles b and f are not necessary 0. Obviously when $Q = 0$, it is possible that $\langle b^\dagger b \rangle_{Q=0} = 1$

$Z_{[1]} = Z_{Q=1}$ is

$$W^{(2d)}_{[1]} = -\mathrm{i}\frac{Z^{(2d)}_{[1]}}{Z_{[1]}} \tag{7.208}$$

Note the difference between $\overline{W}$ and W, and the relation between their functional derivatives is

$$W^{(2d)}_{[1]} = \frac{Z_{[0]}}{Z_{[1]}}\overline{W}^{(2d)}_{[1]} \tag{7.209}$$

which agrees with [269].

The d electron Green's function is

$$G_{d\sigma} = W^{(dd^\dagger)}_{[1]} = \frac{Z_{[0]}}{Z_{[1]}}\overline{W}^{(dd^\dagger)}_{[1]} \tag{7.210}$$

This is achieved by partial derivatives of the sources of the terms

$$J_d d + J_{d^\dagger} d^\dagger \tag{7.211}$$

and then send source terms to zero.

Now we discuss the NCA equations. To reach a set of self-consistent equations, we do power counting in the extended space with the partition function $Z(\lambda)$. A natural choice of the greater and lesser functions is

$$\begin{aligned} G^{>}_{b} &= \overline{W}^{(b_- b^\dagger_+)}_{[0]}, \quad G^{>}_{f\sigma} = \overline{W}^{(f_- f^\dagger_+)}_{[0]} \\ G^{<}_{b} &= \overline{W}^{(b_+ b^\dagger_-)}_{[1]}, \quad G^{<}_{f\sigma} = \overline{W}^{(f_+ f^\dagger_-)}_{[1]} \end{aligned} \tag{7.212}$$

Given that

$$G^{>}_{f,b} \sim O(\zeta), \quad G^{<}_{f,b} \sim O(1) \tag{7.213}$$

This can be roughly understood as where $G^{>}_{f,b}$ is measuring holes, $G^{<}_{f,b}$ is measuring particles. That power counting is consistent with the fluctuation-dissipation theorem in equilibrium with the fugacity entering the Boltzmann weight.

To proceed, we require the order ζ is conserved during the self-consistent loop. From

$$G^{>,<}_{f,b} = G^{R}_{f,b}\Sigma^{>,<}_{f,b}G^{A}_{f,b} \tag{7.214}$$

we know

$$G^{R/A}_{f,b} \sim O(1) \tag{7.215}$$

Now we can match the order of ζ, obviously

$$G^{R}_{f,b} = \theta(t_\mathrm{r})[G^{>}_{f,b} - G^{<}_{f,b}] \to \theta(t_\mathrm{r})[G^{>}_{f,b}] \tag{7.216}$$

In the end we will have Table. 7.2 for NCA equations in the extended space.

To get physical observables we still need projections. The projected retarded impurity Green's

function G_d^R is

$$\begin{aligned} G^R_{d\sigma}(t_1,t_2) &= \theta(t_r)[G^>_{d\sigma} - G^<_{d\sigma}] \\ &= \frac{Z_{[0]}}{Z_{[1]}}\theta(t_r)[G^>_b(t_2,t_1)G^<_{f\,\sigma}(t_1,t_2) - G^<_b(t_2,t_1)G^>_{f\,\sigma}(t_1,t_2)] \end{aligned} \tag{7.217}$$

The projected keldysh impurity Green's function G_d^K can be written as

$$\begin{aligned} G^K_{d\sigma}(t_1,t_2) &= G^>_{d\sigma} + G^<_{d\sigma} \\ &= \frac{Z_{[0]}}{Z_{[1]}}[G^>_b(t_2,t_1)G^<_{f\,\sigma}(t_1,t_2) + G^<_b(t_2,t_1)G^>_{f\,\sigma}(t_1,t_2)] \end{aligned} \tag{7.218}$$

The above projection equations can be simply derived if we neglect the vertex corrections, i.e., we treat f and b are only correlated to themselves, by

$$\begin{aligned} G_{d\sigma}(t_1,t_2) &\sim \langle \hat{T}_C d_\sigma(t_1) d^\dagger_\sigma(t_2)\rangle = \langle \hat{T}_C f^\dagger_\sigma(t_1) b(t_1) b^\dagger(t_2) f_\sigma(t_2)\rangle \\ &\sim \langle \hat{T}_C f_\sigma(t_2) f^\dagger_\sigma(t_1)\rangle \langle \hat{T}_C b(t_1) b^\dagger(t_2)\rangle \\ &= G_{f\,\sigma}(t_2,t_1) G_b(t_1,t_2) \end{aligned} \tag{7.219}$$

The observables thus can be computed. As an example we have shown the time averaged spectral function computed from our code in Fig. 7.21.

7.8 Summary

In this chapter we studied the Rice-Mele Hubbard model by using Floquet-Keldysh dynamical mean-field theory. We computed single-particle observables, the spectral functions and the time-averaged current density. We find that the increasing static Hubbard interaction or the drive frequency will suppress the current. On the other hand, the quasiparticle is only appears for low and high frequencies, but not in the intermediate drive frequencies. In the intermediate drive frequency regime, there are strong heating effects. We also find an interesting $\Omega/2$ slope at relatively strong coupling, which can be related to the topological nature of the model.

Many further works could be done in the future, which we will discuss them in the next section.

Let us summarize this chapter by the following graph.

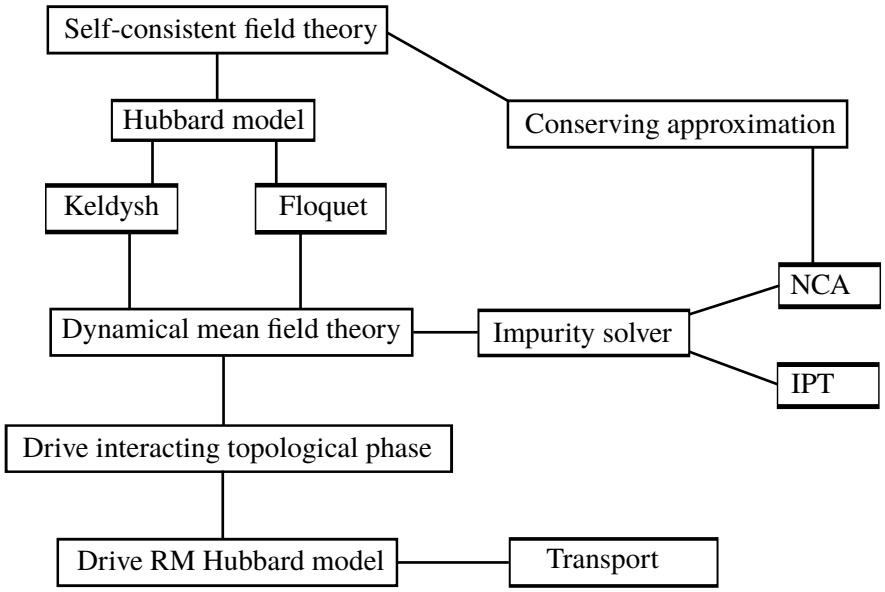

Figure 7.22

7.9 Outlook

Here we provide some outlooks for the future studies.

Several things can be done with the tools in our hands. In principle, we can drive the interaction periodically in an almost arbitrary way, and also include different time dependence for the sites in the unit cell. This is a way to approach the time-dependent dissipation that has been realized in the wave-guide experiment [228] and the transport current can be possibly enhanced by this kind of engineered interaction.

Another thing is if we can choose a more reliable real-time impurity solver for the strong coupling limit rather than the IPT. Since we have the NCA solver for some simple driven system at hand, the NCA solver [3, 273] is promising and can be applied to our problem soon.

In this work, we focus on the Rice-Mele model. The method we used is very general and can be even better to be applied to lattice models in higher dimensions [169], and to many other exotic phases [6], for instance, the Weyl semi-metals, the heavy fermions systems, the high temperature superconductors.

In this work, we studied the Floquet system by using Floquet-Keldysh Green's functions, and DMFT. There are many improvements that can be done in the future, and some of them are very important quantitatively and even qualitatively.

One direction is to use real-time Kadanoff-Baym equations [90]. Since all the computations in this thesis are relying on the non-equilibrium steady states assumption, the validity may need to be checked. Rather than use frequency space Green's functions, one can alternatively solve the Kadanoff-Baym differential equations in time space, where the transient dynamics toward a possible steady-state can be studied.

Last but not least, another question would be if the dynamical mean-field theory is always reliable. The local approximation is exact only for the infinite spatial dimension, or infinite coordination numbers. The momentum dependence, or namely the non-local correlations, can be important in low dimensions in equilibrium. What are their effects out of equilibrium with the periodic drive is an interesting question. It may even be important for the true stable or metastable steady states. For the momentum dependence, we may apply the non-local extensions [77] of the DMFT, and extend them to non-equilibrium. Or we can use other techniques, such as the functional renormalization group [274].

Bibliography

[1] B. A. Bassett, S. Tsujikawa and D. Wands, *Inflation dynamics and reheating*, **78** (2006) 537 (cit. on p. 1).

[2] E. Shuryak, *Strongly coupled quark-gluon plasma in heavy ion collisions*, **89** (2017) 035001 (cit. on p. 1).

[3] H. Aoki et al., *Nonequilibrium dynamical mean-field theory and its applications*, Reviews of Modern Physics **86** (2014) 779, ISSN: 0034-6861 (cit. on pp. 1–3, 42, 52, 62, 107, 110, 115, 120–122, 125–127, 143, 155, 158, 169, 173, 176, 178, 207, 218).

[4] X. Fang, K. Kruse, T. Lu and J. Wang, *Nonequilibrium physics in biology*, **91** (2019) 045004 (cit. on p. 1).

[5] F. Schäfer, T. Fukuhara, S. Sugawa, Y. Takasu and Y. Takahashi, *Tools for quantum simulation with ultracold atoms in optical lattices*, Nature Reviews Physics **2** (2020) 411, ISSN: 2522-5820 (cit. on p. 1).

[6] T. Oka and S. Kitamura, *Floquet Engineering of Quantum Materials*, Annual Review of Condensed Matter Physics **10** (2019) 387 (cit. on pp. 1–3, 112, 218).

[7] G. F. Smoot, *Nobel Lecture: Cosmic microwave background radiation anisotropies: Their discovery and utilization*, **79** (2007) 1349 (cit. on p. 1).

[8] P. A. Lee, N. Nagaosa and X.-G. Wen, *Doping a Mott insulator: Physics of high-temperature superconductivity*, Reviews of Modern Physics **78** (2006) 17 (cit. on pp. 1, 207).

[9] M. Tanabashi et al., *Review of Particle Physics*, Phys. Rev. D **98** (3 2018) 030001, URL: https://link.aps.org/doi/10.1103/PhysRevD.98.030001 (cit. on p. 1).

[10] S. Chatrchyan et al., *Observation of a new boson at a mass of 125 GeV with the CMS experiment at the LHC*, **716** (2012) 30 (cit. on p. 1).

[11] G. Aad et al., *Observation of a new particle in the search for the Standard Model Higgs boson with the ATLAS detector at the LHC*, **716** (2012) 1 (cit. on p. 1).

[12] R. Kogler et al., *Jet substructure at the Large Hadron Collider*, **91** (2019) 045003 (cit. on p. 1).

[13] M. S. Rudner and N. H. Lindner, *Floquet topological insulators: from band structure engineering to novel non-equilibrium quantum phenomena*, (2019), arXiv: http://arxiv.org/abs/1909.02008v1 [cond-mat.mes-hall] (cit. on pp. 2, 3, 68, 107, 112, 178).

[14] F. Harper, R. Roy, M. S. Rudner and S. L. Sondhi,
Topology and Broken Symmetry in Floquet Systems,
Annual Review of Condensed Matter Physics **11** (2019) 345, ISSN: 1947-5454,
arXiv: http://arxiv.org/abs/1905.01317v2 [cond-mat.str-el]
(cit. on pp. 2, 94–97, 107, 114).

[15] A. Eckardt, *Colloquium: Atomic quantum gases in periodically driven optical lattices*,
Reviews of Modern Physics **89** (2017) (cit. on pp. 2, 107, 111, 112, 143).

[16] I. Bloch, J. Dalibard and W. Zwerger, *Many-body physics with ultracold gases*, **80** (2008) 885
(cit. on p. 2).

[17] M. Bukov, L. D'Alessio and A. Polkovnikov, *Universal high-frequency behavior of periodically driven systems: from dynamical stabilization to Floquet engineering*,
Advances in Physics **64** (2015) 139 (cit. on pp. 2, 111, 112).

[18] R. Moessner and S. L. Sondhi, *Equilibration and order in quantum Floquet matter*,
Nature Physics **13** (2017) 424 (cit. on pp. 2, 113, 115).

[19] U. Schollwöck, *The density-matrix renormalization group in the age of matrix product states*,
326 (2011) 96 (cit. on p. 3).

[20] E. Gull et al., *Continuous-time Monte Carlo methods for quantum impurity models*,
Reviews of Modern Physics **83** (2011) 349 (cit. on pp. 3, 170).

[21] G. Cohen, E. Gull, D. R. Reichman and A. J. Millis, *Taming the Dynamical Sign Problem in Real-Time Evolution of Quantum Many-Body Problems*, **115** (2015) 266802 (cit. on p. 3).

[22] A. Alexandru, G. Başar, P. F. Bedaque, S. Vartak and N. C. Warrington,
Monte Carlo Study of Real Time Dynamics on the Lattice, **117** (2016) 081602 (cit. on p. 3).

[23] A. a. Abrikosov, *Methods of Quantum Field Theory in Statistical Physics*,
Dover Publications Inc., 1975, 384 pp., ISBN: 0486632288,
URL: https://www.ebook.de/de/product/1824985/a_a_abrikosov_methods_of_quantum_field_theory_in_statistical_physics.html (cit. on p. 3).

[24] E. Fradkin, *Field Theories of Condensed Matter Physics*, Cambridge University Press, 2016,
856 pp., ISBN: 978-0521764445, URL: https://www.ebook.de/de/product/19864406/eduardo_fradkin_field_theories_of_condensed_matter_physics.html
(cit. on pp. 3, 67, 84, 87, 88, 100).

[25] A. Kamenev, *Field Theory of Non-Equilibrium Systems*, Cambridge University Press, 2011,
356 pp., ISBN: 978-0521760829,
URL: http://www.ebook.de/de/product/14876694/alex_university_of_minnesota_kamenev_field_theory_of_non_equilibrium_systems.html
(cit. on pp. 3, 37, 41–48, 53–55, 58).

[26] J.-B. Z. Claude Itzykson, *Quantum Field Theory*, Dover Publications Inc., 2006, 752 pp.,
ISBN: 0486445682, URL: https://www.ebook.de/de/product/3560335/claude_itzykson_jean_bernard_zuber_quantum_field_theory.html
(cit. on pp. 3, 8, 12, 13).

[27] A. Zee, *Quantum Field Theory in a Nutshell*, Princeton Univers. Press, 2010, 600 pp., ISBN: 0691140340, URL: https://www.ebook.de/de/product/8476766/a_zee_quantum_field_theory_in_a_nutshell.html (cit. on pp. 3, 83, 164).

[28] D. V. S. Michael E. Peskin, *An Introduction To Quantum Field Theory*, Taylor & Francis Inc, 1995, 866 pp., ISBN: 0201503972, URL: https://www.ebook.de/de/product/3595300/michael_e_peskin_daniel_v_schroeder_an_introduction_to_quantum_field_theory.html (cit. on pp. 3, 8, 39, 58, 85).

[29] J. Rammer and H. Smith, *Quantum field-theoretical methods in transport theory of metals*, Reviews of Modern Physics **58** (1986) 323 (cit. on pp. 3, 37, 42, 44, 45, 47, 55, 58, 175).

[30] J. M. Pawlowski, *Aspects of the functional renormalisation group*, Annals of Physics **322** (2007) 2831 (cit. on pp. 5–9, 12, 30, 31).

[31] T. Gasenzer and J. M. Pawlowski, *Functional renormalisation group approach to far-from-equilibrium quantum field dynamics*, Phys. Lett. B 670, 135 (2008) (2007), arXiv: http://arxiv.org/abs/0710.4627v3 [cond-mat.other] (cit. on pp. 5, 30).

[32] C. Kiefer, *Quantum gravity*, Oxford University Press, 2007, ISBN: 9780199212521 (cit. on p. 6).

[33] J. Berges, "Introduction to Nonequilibrium Quantum Field Theory", *AIP Conference Proceedings*, AIP, 2004, arXiv: http://arxiv.org/abs/hep-ph/0409233v1 [hep-ph] (cit. on pp. 7, 8, 21, 24–26, 29, 30, 37, 42–44, 46, 55, 58).

[34] M. Srednicki, *Quantum Field Theory*, Cambridge University Pr., 2007, 664 pp., ISBN: 0521864496, URL: https://www.ebook.de/de/product/5878356/mark_srednicki_quantum_field_theory.html (cit. on pp. 7, 8, 13, 46, 58, 74, 80, 89).

[35] M. Q. Huber and J. Braun, *Algorithmic derivation of functional renormalization group equations and Dyson-Schwinger equations*, (2011), arXiv: http://arxiv.org/abs/1102.5307v2 [hep-th] (cit. on pp. 8, 10, 31).

[36] M. Q. Huber, A. K. Cyrol and J. M. Pawlowski, *DoFun 3.0: Functional equations in Mathematica*, Computer Physics Communications **248** (2019) 107058, arXiv: 1908.02760 [hep-ph] (cit. on pp. 8, 10, 11, 30, 32).

[37] C. D. Roberts and A. G. Williams, *Dyson-Schwinger Equations and the Application to Hadronic Physics*, Prog.Part.Nucl.Phys.33:477-575,1994 (1994), arXiv: http://arxiv.org/abs/hep-ph/9403224v2 [hep-ph] (cit. on p. 8).

[38] R. Alkofer, M. Huber and K. Schwenzer, *Algorithmic derivation of Dyson–Schwinger equations*, Computer Physics Communications **180** (2009) 965 (cit. on p. 10).

[39] M. Moshe and J. Zinn-Justin, *Quantum field theory in the large N limit: a review*, Physics Reports **385** (2003) 69, ISSN: 0370-1573 (cit. on pp. 10, 11).

[40] J. Zinn-Justin, *Quantum Field Theory and Critical Phenomena*, Clarendon Press, 2002, 1080 pp., ISBN: 0198509235, URL: https://www.ebook.de/de/product/3253921/jean_zinn_justin_quantum_field_theory_and_critical_phenomena.html (cit. on p. 10).

[41] E. E. Salpeter and H. A. Bethe, *A Relativistic Equation for Bound-State Problems*, Physical Review **84** (1951) 1232 (cit. on p. 11).

[42] J. C. Ward, *An Identity in Quantum Electrodynamics*, Physical Review **78** (1950) 182 (cit. on p. 13).

[43] Y. Takahashi, *On the generalized ward identity*, Il Nuovo Cimento **6** (1957) 371 (cit. on p. 13).

[44] S. Weinberg, *Quantum Theory of Fields: Volume 2, Modern Applications*, Cambridge University Press, 1996, URL: https://www.ebook.de/de/product/21211459/steven_weinberg_quantum_theory_of_fields_volume_2_modern_applications.html (cit. on pp. 13, 18).

[45] S. Scherer, *Introduction to Chiral Perturbation Theory*, Adv.Nucl.Phys. 27 (2003) 277 (2002), arXiv: hep-ph/0210398 [hep-ph] (cit. on p. 13).

[46] D. Vollhardt and P. Wölfle, *Diagrammatic, self-consistent treatment of the Anderson localization problem ind≤2dimensions*, Physical Review B **22** (1980) 4666 (cit. on pp. 16, 17).

[47] J. Kroha, T. Kopp and P. Wölfle, *Self-consistent theory of Anderson localization for the tight-binding model with site-diagonal disorder*, Physical Review B **41** (1990) 888 (cit. on pp. 16, 17).

[48] J. Kroha, *Diagrammatic self-consistent theory of Anderson localization for the tight-binding model*, Physica A 167, 231 (1990) (2015), arXiv: 1501.05465 [cond-mat.dis-nn] (cit. on p. 16).

[49] H. T. Nieh, P. Sheng and X.-B. Wang, *Ward Identities for Interacting Electronic Systems*, (1998), arXiv: cond-mat/9807313 [cond-mat] (cit. on pp. 16, 17).

[50] H. T. Nieh, L. Chen and P. Sheng, *Ward identities for transport of classical waves in disordered media*, Physical Review E **57** (1998) 1145 (cit. on pp. 16, 17).

[51] H. Kleinert, *Particles and Quantum Fields*, World Scientific Publ., 2016, ISBN: 981474090X, URL: https://www.ebook.de/de/product/25687322/hagen_kleinert_particles_and_quantum_fields.html (cit. on p. 18).

[52] P. Kopietz, L. Bartosch and F. Schütz, *Introduction to the Functional Renormalization Group*, Springer-Verlag GmbH, 2010, ISBN: 364205093X, URL: https://www.ebook.de/de/product/9272946/peter_kopietz_lorenz_bartosch_florian_schuetz_introduction_to_the_functional_renormalization_group.html (cit. on pp. 18, 30, 31).

[53] J. M. Luttinger and J. C. Ward, *Ground-State Energy of a Many-Fermion System. II*, Physical Review **118** (1960) 1417 (cit. on p. 19).

[54] G. Baym and L. P. Kadanoff, *Conservation Laws and Correlation Functions*, Physical Review **124** (1961) 287 (cit. on pp. 19, 22, 27, 28).

[55] G. Baym, *Self-Consistent Approximations in Many-Body Systems*, Physical Review **127** (1962) 1391 (cit. on pp. 19, 22, 27, 28).

[56] J. M. Cornwall, R. Jackiw and E. Tomboulis, *Effective action for composite operators*, Physical Review D **10** (1974) 2428 (cit. on p. 19).

[57] C. Wetterich, *Bosonic effective action for interacting fermions*, Physical Review B **75** (2007) (cit. on pp. 19, 21, 25–27, 156).

[58] J. Berges, *Nonequilibrium Quantum Fields: From Cold Atoms to Cosmology*, (2015), arXiv: http://arxiv.org/abs/1503.02907v1 [hep-ph] (cit. on pp. 21, 24, 26, 37, 43, 44, 52).

[59] L. P. Kadanoff, G. Baym and D. Pines, *Quantum Statistical Mechanics*, Taylor & Francis Inc, 1994, 224 pp., ISBN: 020141046X, URL: https://www.ebook.de/de/product/3596768/leo_p_kadanoff_gordon_baym_david_pines_quantum_statistical_mechanics.html (cit. on pp. 24, 28, 37, 45, 58).

[60] J. Berges, *n-Particle irreducible effective action techniques for gauge theories*, Phys.Rev.D70:105010,2004 (2004), arXiv: http://arxiv.org/abs/hep-ph/0401172v3 [hep-ph] (cit. on p. 29).

[61] M. E. Carrington and Y. Guo, *Techniques for n-Particle Irreducible Effective Theories*, Phys.Rev.D83:016006,2011 (2010), arXiv: http://arxiv.org/abs/1010.2978v2 [hep-ph] (cit. on p. 29).

[62] D. Sénéchal, A.-M. Tremblay and C. Bourbonnais, eds., *Theoretical Methods for Strongly Correlated Electrons*, Springer-Verlag, 2003, 361 pp., ISBN: 0387008950, URL: https://www.ebook.de/de/product/8085697/theoretical_methods_for_strongly_correlated_electrons.html (cit. on p. 30).

[63] G. Stefanucci and R. van Leeuwen, *Nonequilibrium Many-Body Theory of Quantum Systems: A Modern Introduction*, Cambridge University Press, 2013, 620 pp., ISBN: 978-0521766173, URL: http://www.ebook.de/de/product/19864334/gianluca_universit_degli_studi_di_roma_tor_vergata_stefanucci_robert_university_of_jyvaskyla_finland_van_leeuwen_nonequilibrium_many_body_theory_of_quantum_systems.html (cit. on pp. 30, 37, 52).

[64] K. Wilson, *The renormalization group and the ϵ expansion*, Physics Reports **12** (1974) 75 (cit. on p. 30).

[65] K. G. Wilson, *The renormalization group: Critical phenomena and the Kondo problem*, Reviews of Modern Physics **47** (1975) 773 (cit. on pp. 30, 170).

[66] K. G. Wilson, *The renormalization group and critical phenomena*, Reviews of Modern Physics **55** (1983) 583 (cit. on p. 30).

[67] J. Polchinski, *Renormalization and effective lagrangians*, Nuclear Physics B **231** (1984) 269 (cit. on p. 30).

[68] C. Wetterich, *Exact evolution equation for the effective potential*, Physics Letters B **301** (1993) 90 (cit. on p. 30).

[69] J. Berges, N. Tetradis and C. Wetterich,
Non-perturbative renormalization flow in quantum field theory and statistical physics,
Physics Reports **363** (2002) 223 (cit. on pp. 30, 31).

[70] W. Metzner, M. Salmhofer, C. Honerkamp, V. Meden and K. Schönhammer,
Functional renormalization group approach to correlated fermion systems,
Reviews of Modern Physics **84** (2012) 299 (cit. on pp. 30–33, 160).

[71] C. Hille et al., *Quantitative functional renormalization-group description of the two-dimensional Hubbard model*, (2020),
arXiv: http://arxiv.org/abs/2002.02733v1 [cond-mat.str-el] (cit. on p. 30).

[72] L. Corell, A. K. Cyrol, M. Heller and J. M. Pawlowski,
Flowing with the Temporal Renormalisation Group, (2019),
arXiv: http://arxiv.org/abs/1910.09369v1 [hep-th] (cit. on p. 30).

[73] J. Polchinski, *Effective Field Theory and the Fermi Surface*, (1992),
arXiv: http://arxiv.org/abs/hep-th/9210046v2 [hep-th] (cit. on p. 30).

[74] F. B. Kugler and J. von Delft,
Multiloop functional renormalization group that sums up all parquet diagrams,
Phys. Rev. Lett. 120, 057403 (2018) (2017),
arXiv: http://arxiv.org/abs/1703.06505v3 [cond-mat.str-el] (cit. on p. 32).

[75] F. B. Kugler and J. von Delft,
Derivation of exact flow equations from the self-consistent parquet relations,
New Journal of Physics **20** (2018) 123029 (cit. on p. 32).

[76] F. B. Kugler and J. von Delft, *Multiloop functional renormalization group for general models*,
Physical Review B **97** (2018) (cit. on p. 32).

[77] G. Rohringer et al.,
Diagrammatic routes to nonlocal correlations beyond dynamical mean field theory,
Reviews of Modern Physics **90** (2018) (cit. on pp. 32, 155, 218).

[78] J. Schwinger, *Brownian Motion of a Quantum Oscillator*,
Journal of Mathematical Physics **2** (1961) 407 (cit. on p. 37).

[79] L. V. Keldysh, *Diagram technique for nonequilibrium processes*,
Zh. Eksp. Teor. Fiz. **47** (1964) 1515, [Sov. Phys. JETP20,1018(1965)] (cit. on pp. 37, 42).

[80] K.-c. Chou, Z.-b. Su, B.-l. Hao and L. Yu,
Equilibrium and nonequilibrium formalisms made unified, Physics Reports **118** (1985) 1
(cit. on p. 37).

[81] N. Landsman and C. van Weert,
Real- and imaginary-time field theory at finite temperature and density,
Physics Reports **145** (1987) 141 (cit. on pp. 37, 38, 44, 46, 60, 62).

[82] E. A. Calzetta, *Nonequilibrium Quantum Field Theory*, Cambridge University Press, 2008,
URL: https://www.ebook.de/de/product/21387865/esteban_a_calzetta_nonequilibrium_quantum_field_theory.html (cit. on pp. 37, 46).

[83] P. Glorioso and H. Liu,
Lectures on non-equilibrium effective field theories and fluctuating hydrodynamics, 2018,
arXiv: http://arxiv.org/abs/1805.09331v1 [hep-th]
(cit. on pp. 37, 38, 41, 46, 58–61, 63).

[84] J. Rammer, *Quantum field theory of non-equilibrium states*,
Cambridge University Press, 2011, 552 pp., ISBN: 978-0521188005,
URL: http://www.ebook.de/de/product/13945467/jorgen_rammer_quantum_field_theory_of_non_equilibrium_states.html (cit. on p. 37).

[85] M. Bonitz, *Quantum Kinetic Theory*, Springer-Verlag GmbH, 2015, ISBN: 9783319241210,
URL: https://www.ebook.de/de/product/25415930/michael_bonitz_quantum_kinetic_theory.html (cit. on p. 37).

[86] H. Liu and J. Sonner, *Holographic systems far from equilibrium: a review*, (2018),
arXiv: 1810.02367v2 [hep-th] (cit. on p. 38).

[87] P. Glorioso, A. Gromov and S. Ryu, *Effective response theory for Floquet topological systems*,
(2019), arXiv: http://arxiv.org/abs/1908.03217v2 [cond-mat.str-el]
(cit. on pp. 41, 116).

[88] L. M. Sieberer, M. Buchhold and S. Diehl,
Keldysh Field Theory for Driven Open Quantum Systems,
Rep. Prog. Phys. 79, 096001 (2016) (2015),
arXiv: http://arxiv.org/abs/1512.00637v2 [cond-mat.quant-gas]
(cit. on pp. 46, 58).

[89] L. Pitaevskii and E. Lifshitz, *Physical Kinetics*, vol. 10, Butterworth-Heinemann, 1981,
625 pp., ISBN: 978-0750626354, URL: http://www.ebook.de/de/product/3846825/l_p_institute_for_physical_problems_ussr_academy_of_sciences_moscow_ussr_pitaevskii_e_m_lifshitz_physical_kinetics.html (cit. on pp. 47, 55).

[90] A. Eberlein, V. Kasper, S. Sachdev and J. Steinberg,
Quantum quench of the Sachdev-Ye-Kitaev Model, Phys. Rev. B 96, 205123 (2017) (2017),
arXiv: http://arxiv.org/abs/1706.07803v2 [cond-mat.str-el]
(cit. on pp. 52, 218).

[91] J. Berges and D. Mesterházy,
Introduction to the nonequilibrium functional renormalization group, (2012),
arXiv: http://arxiv.org/abs/1204.1489v1 [hep-ph] (cit. on p. 53).

[92] D. Mesterházy, J. Stockemer and Y. Tanizaki, *From quantum to classical dynamics: The relativisticO(N)model in the framework of the real-time functional renormalization group*,
Physical Review D **92** (2015) 076001 (cit. on p. 53).

[93] M. Wais et al., *Quantum Boltzmann equation for strongly correlated systems: Comparison to dynamical mean field theory*, Physical Review B **98** (2018) (cit. on p. 57).

[94] P. Arnold, *Quark-Gluon Plasmas and Thermalization*,
Int.J.Mod.Phys.E16:2555-2594,2007 (2007), arXiv: 0708.0812 [hep-ph] (cit. on p. 58).

[95] M. Crossley, P. Glorioso and H. Liu, *Effective field theory of dissipative fluids*, (2015),
arXiv: 1511.03646 [hep-th] (cit. on pp. 58–61).

[96] L. M. Sieberer, A. Chiocchetta, A. Gambassi, U. C. Täuber and S. Diehl, *Thermodynamic equilibrium as a symmetry of the Schwinger-Keldysh action*, Physical Review B **92** (2015) 134307 (cit. on pp. 58, 61).

[97] H. Bruus and K. Flensberg, *Many-Body Quantum Theory in Condensed Matter Physics: An Introduction*, Oxford Graduate Texts, OUP Oxford, 2004, ISBN: 9780198566335, URL: https://books.google.de/books?id=CktuBAAAQBAJ (cit. on pp. 60, 166).

[98] P. Glorioso and H. Liu, *The second law of thermodynamics from symmetry and unitarity*, (2016), arXiv: 1612.07705 [hep-th] (cit. on p. 61).

[99] S.-K. Jian, S. Yin and B. Swingle, *Universal Prethermal Dynamics in Gross-Neveu-Yukawa Criticality*, Phys. Rev. Lett. 123, 170606 (2019) (2019), arXiv: 1907.12504 [cond-mat.str-el] (cit. on pp. 61, 62).

[100] S. Mathey and S. Diehl, *Absence of Criticality in the Phase Transitions of Open Floquet Systems*, Phys. Rev. Lett. 122, 110602 (2019) **122** (2018), arXiv: http://arxiv.org/abs/1807.02146v2 [cond-mat.stat-mech] (cit. on pp. 61, 62, 120).

[101] S. Mathey and S. Diehl, *Dynamic renormalization group theory for open Floquet systems*, arXiv (2020), arXiv: 2007.09463v1 [cond-mat.stat-mech] (cit. on pp. 61, 62, 115, 120, 124, 125).

[102] R. Shankar, *Renormalization-group approach to interacting fermions*, Reviews of Modern Physics **66** (1994) 129 (cit. on p. 62).

[103] A. Chiocchetta, A. Gambassi, S. Diehl and J. Marino, *Dynamical Crossovers in Prethermal Critical States*, Physical Review Letters **118** (2017) (cit. on p. 62).

[104] C. P. Herzog and D. T. Son, *Schwinger-Keldysh Propagators from AdS/CFT Correspondence*, JHEP 0303 (2003) 046 (2002), arXiv: hep-th/0212072v4 [hep-th] (cit. on p. 62).

[105] B. Swingle, *Unscrambling the physics of out-of-time-order correlators*, Nature Physics **14** (2018) 988 (cit. on pp. 62, 63).

[106] M. J. Klug, M. S. Scheurer and J. Schmalian, *Hierarchy of Information Scrambling, Thermalization, and Hydrodynamic Flow in Graphene*, Phys. Rev. B 98, 045102 (2018) (2017), arXiv: 1712.08813 [cond-mat.str-el] (cit. on p. 63).

[107] J. Maldacena and D. Stanford, *Comments on the Sachdev-Ye-Kitaev model*, Phys. Rev. D 94, 106002 (2016) (2016), arXiv: 1604.07818 [hep-th] (cit. on p. 63).

[108] W. P. Su, J. R. Schrieffer and A. J. Heeger, *Solitons in Polyacetylene*, Physical Review Letters **42** (1979) 1698 (cit. on p. 67).

[109] G. W. Semenoff, *Condensed-Matter Simulation of a Three-Dimensional Anomaly*, Physical Review Letters **53** (1984) 2449 (cit. on p. 67).

[110] G. W. Semenoff, *Canonical Quantum Field Theory with Exotic Statistics*, Physical Review Letters **61** (1988) 517 (cit. on p. 67).

[111] F. D. M. Haldane, *Model for a Quantum Hall Effect without Landau Levels: Condensed-Matter Realization of the "Parity Anomaly"*, Physical Review Letters **61** (1988) 2015 (cit. on pp. 67, 101).

[112] C. L. Kane and E. J. Mele, *Z2Topological Order and the Quantum Spin Hall Effect*, Physical Review Letters **95** (2005) (cit. on p. 67).

[113] M. Konig et al., *Quantum Spin Hall Insulator State in HgTe Quantum Wells*, Science **318** (2007) 766 (cit. on p. 67).

[114] J. E. Moore, *The birth of topological insulators*, Nature **464** (2010) 194 (cit. on p. 67).

[115] D. Hsieh et al., *A topological Dirac insulator in a quantum spin Hall phase*, Nature **452** (2008) 970 (cit. on p. 67).

[116] N. Armitage, E. Mele and A. Vishwanath, *Weyl and Dirac semimetals in three-dimensional solids*, Reviews of Modern Physics **90** (2018) (cit. on pp. 67, 81).

[117] M. Nakahara, *Geometry, Topology and Physics*, Taylor & Francis Ltd, 2003, 596 pp., ISBN: 978-0750306065, URL: http://www.ebook.de/de/product/3646467/mikio_nakahara_geometry_topology_and_physics.html (cit. on pp. 67, 68, 71–73, 75, 76, 92).

[118] B. S. Alexander Altland, *Condensed Matter Field Theory*, Cambridge University Pr., 2010, ISBN: 0521769752, URL: https://www.ebook.de/de/product/10554601/alexander_altland_ben_simons_condensed_matter_field_theory.html (cit. on pp. 67, 80).

[119] M. Fruchart and D. Carpentier, *An Introduction to Topological Insulators*, Comptes Rendus Physique 14 (2013) 779-815 **14** (2013) 779, arXiv: 1310.0255v2 [cond-mat.mes-hall] (cit. on pp. 67, 71, 77, 80, 100).

[120] B. A. Bernevig, *Topological Insulators and Topological Superconductors*, Princeton University Press, 2013, ISBN: 978-0691151755, URL: http://www.ebook.de/de/product/20003958/b_andrei_bernevig_topological_insulators_and_topological_superconductors.html (cit. on pp. 67, 72, 84, 86).

[121] S.-Q. Shen, *Topological Insulators: Dirac Equation in Condensed Matter (Springer Series in Solid-State Sciences)*, Springer, 2017, ISBN: 9789811046063, URL: https://www.amazon.com/Topological-Insulators-Equation-Condensed-Solid-State-ebook/dp/B074XR7KRS?SubscriptionId=0JYN1NVW651KCA56C102&tag=techkie-20&linkCode=xm2&camp=2025&creative=165953&creativeASIN=B074XR7KRS (cit. on p. 67).

[122] E. Witten, *Three Lectures On Topological Phases Of Matter*, La Rivista del Nuovo Cimento, 39 (2016) 313-370 (2015), arXiv: 1510.07698v2 [cond-mat.mes-hall] (cit. on pp. 67, 82, 84, 89, 90).

[123] S. Ryu, A. P. Schnyder, A. Furusaki and A. W. W. Ludwig,
Topological insulators and superconductors: tenfold way and dimensional hierarchy,
New Journal of Physics **12** (2010) 065010 (cit. on pp. 67, 81, 88, 89, 91–93, 96).

[124] X.-G. Wen, *Colloquium : Zoo of quantum-topological phases of matter*,
Reviews of Modern Physics **89** (2017) (cit. on pp. 67, 104).

[125] M. S. Rudner, N. H. Lindner, E. Berg and M. Levin, *Anomalous Edge States and the Bulk-Edge Correspondence for Periodically Driven Two-Dimensional Systems*,
Physical Review X **3** (2013) (cit. on pp. 68, 96–98, 100).

[126] P. A. M. Dirac, *Quantised singularities in the electromagnetic field,*
Proceedings of the Royal Society of London. Series A, Containing Papers of a Mathematical and Physical Character **133** (1931) 60 (cit. on p. 68).

[127] T. T. Wu and C. N. Yang,
Concept of nonintegrable phase factors and global formulation of gauge fields,
Physical Review D **12** (1975) 3845 (cit. on p. 69).

[128] M. V. Berry, *Quantal Phase Factors Accompanying Adiabatic Changes*, Proceedings of the Royal Society A: Mathematical, Physical and Engineering Sciences **392** (1984) 45
(cit. on p. 72).

[129] F. Wilczek and A. Zee, *Appearance of Gauge Structure in Simple Dynamical Systems*,
Physical Review Letters **52** (1984) 2111 (cit. on p. 72).

[130] A. Alexandradinata, X. Dai and B. A. Bernevig,
Wilson-loop characterization of inversion-symmetric topological insulators,
Physical Review B **89** (2014) (cit. on pp. 72, 103).

[131] J. Figueroa-O'Farrill, *Electromagnetic duality for children*, 1998 (cit. on pp. 74, 80).

[132] H. Flanders, *Differential Forms with Applications to the Physical Sciences*,
Dover Publications Inc., 1989, 224 pp., ISBN: 0486661695,
URL: https://www.ebook.de/de/product/3303130/harley_flanders_differential_forms_with_applications_to_the_physical_sciences.html
(cit. on pp. 77, 78).

[133] D. M. Nenno, C. A. C. Garcia, J. Gooth, C. Felser and P. Narang,
Axion physics in condensed-matter systems, Nature Reviews Physics (2020) (cit. on p. 81).

[134] X.-L. Qi, T. L. Hughes and S.-C. Zhang,
Topological field theory of time-reversal invariant insulators, Physical Review B **78** (2008)
(cit. on pp. 81, 83–89, 91).

[135] F. Wilczek, *Two applications of axion electrodynamics*,
Physical Review Letters **58** (1987) 1799 (cit. on p. 81).

[136] A. M. Essin, J. E. Moore and D. Vanderbilt,
Magnetoelectric Polarizability and Axion Electrodynamics in Crystalline Insulators,
Physical Review Letters **102** (2009) (cit. on p. 81).

[137] E. Witten, *Global aspects of current algebra*, Nuclear Physics B **223** (1983) 422
(cit. on p. 82).

[138] E. Witten, *Non-abelian bosonization in two dimensions*, Communications in Mathematical Physics **92** (1984) 455 (cit. on p. 82).

[139] S.-S. Chern and J. Simons, *Characteristic Forms and Geometric Invariants*, The Annals of Mathematics **99** (1974) 48 (cit. on p. 82).

[140] E. Witten, "Quantum Field Theory and the Jones Polynomial", *New Developments in the Theory of Knots*, WORLD SCIENTIFIC, 1990 815 (cit. on p. 83).

[141] M. BOS and V. NAIR, *COHERENT STATE QUANTIZATION OF CHERN-SIMONS THEORY*, International Journal of Modern Physics A **05** (1990) 959 (cit. on p. 83).

[142] G. V. Dunne, *Aspects of Chern-Simons Theory*, (1999), arXiv: hep-th/9902115v1 [hep-th] (cit. on p. 83).

[143] N. Iqbal, H. Liu and M. Mezei, "Lectures on Holographic Non-Fermi Liquids and Quantum Phase Transitions", *String Theory and Its Applications*, WORLD SCIENTIFIC, 2011 (cit. on p. 83).

[144] M. F. Golterman, K. Jansen and D. B. Kaplan, *Chern-Simons currents and chiral fermions on the lattice*, Physics Letters B **301** (1993) 219 (cit. on pp. 83, 84).

[145] X.-L. Qi and S.-C. Zhang, *Topological insulators and superconductors*, Reviews of Modern Physics **83** (2011) 1057 (cit. on pp. 84–88).

[146] E. Witten, *Fermion Path Integrals And Topological Phases*, Rev. Mod. Phys. 88, 35001 (2016) (2015), arXiv: 1508.04715v2 [cond-mat.mes-hall] (cit. on p. 84).

[147] J. Vaeyrynen, *The gradient expansion and topological insulators*, MA thesis: University of Helsinki, 2011, URL: http://ltl.tkk.fi/~teemuo/vayrynen_gradu.pdf (cit. on p. 84).

[148] G. E. Volovik and V. M. Yakovenko, *Fractional charge, spin and statistics of solitons in superfluid3He film*, Journal of Physics: Condensed Matter **1** (1989) 5263 (cit. on p. 84).

[149] E. Fradkin, C. Nayak, A. Tsvelik and F. Wilczek, *A Chern-Simons Effective Field Theory for the Pfaffian Quantum Hall State*, Nucl.Phys. B516 (1998) 704-718 (1997), arXiv: cond-mat/9711087v1 [cond-mat.mes-hall] (cit. on p. 85).

[150] J. Fröhlich and A. Zee, *Large scale physics of the quantum hall fluid*, Nuclear Physics B **364** (1991) 517 (cit. on p. 85).

[151] D. Tong, *Lectures on the Quantum Hall Effect*, (2016), arXiv: 1606.06687v2 [hep-th] (cit. on p. 86).

[152] G. E. Volovik, *The Universe in a Helium Droplet*, Oxford University Press, 2009 (cit. on p. 86).

[153] Z. Wang, X.-L. Qi and S.-C. Zhang, *Equivalent topological invariants of topological insulators*, New Journal of Physics **12** (2010) 065007 (cit. on p. 86).

[154] Z. Wang, X.-L. Qi and S.-C. Zhang,
Topological Order Parameters for Interacting Topological Insulators,
Physical Review Letters **105** (2010) (cit. on p. 86).

[155] Z. Wang and B. Yan, *Topological Hamiltonian as an Exact Tool for Topological Invariants*,
J. Phys.: Condens. Matter 25, 155601 (2013) **25** (2012) 155601,
arXiv: 1207.7341 [cond-mat.str-el] (cit. on pp. 86, 87).

[156] Z. Wang and S.-C. Zhang, *Simplified Topological Invariants for Interacting Insulators*,
Physical Review X **2** (2012) (cit. on p. 86).

[157] R. Roy and F. Harper, *Periodic table for Floquet topological insulators*,
Physical Review B **96** (2017) (cit. on pp. 90, 91, 94–96).

[158] A. Kitaev, *Periodic table for topological insulators and superconductors*, (2009),
arXiv: 0901.2686v2 [cond-mat.mes-hall] (cit. on pp. 91, 92).

[159] A. Altland and M. R. Zirnbauer,
Nonstandard symmetry classes in mesoscopic normal-superconducting hybrid structures,
Physical Review B **55** (1997) 1142 (cit. on p. 91).

[160] F. S. Nathan, *Topological Classification of Floquet-Bloch Systems*,
MA thesis: Niels Bohr Institute, University of Copenhagen, 2015 (cit. on pp. 94, 103).

[161] M. Fruchart, *Complex classes of periodically driven topological lattice systems*,
Physical Review B **93** (2016) (cit. on pp. 94, 96, 97).

[162] S. Yao, Z. Yan and Z. Wang, *Topological invariants of Floquet systems: General formulation, special properties, and Floquet topological defects*, Physical Review B **96** (2017)
(cit. on pp. 94, 96).

[163] X. Liu, F. Harper and R. Roy, *Chiral flow in one-dimensional Floquet topological insulators*,
Physical Review B **98** (2018) (cit. on p. 96).

[164] R. Roy and F. Harper, *Floquet topological phases with symmetry in all dimensions*,
Phys. Rev. B 95, 195128 (2017) (2016), arXiv: 1610.06899v2 [cond-mat.str-el]
(cit. on p. 97).

[165] R. Bott and R. Seeley, *Some remarks on the paper of Callias*,
Communications in Mathematical Physics **62** (1978) 235, ISSN: 0010-3616 (cit. on p. 96).

[166] D. J. Thouless, M. Kohmoto, M. P. Nightingale and M. den Nijs,
Quantized Hall Conductance in a Two-Dimensional Periodic Potential,
Physical Review Letters **49** (1982) 405 (cit. on p. 99).

[167] L. Fu and C. L. Kane, *Time reversal polarization and aZ2adiabatic spin pump*,
Physical Review B **74** (2006) (cit. on p. 99).

[168] T. Fukui, Y. Hatsugai and H. Suzuki, *Chern Numbers in Discretized Brillouin Zone: Efficient Method of Computing (Spin) Hall Conductances*,
J. Phys. Soc. Jpn. 74 (2005) pp. 1674-1677 (2005),
arXiv: cond-mat/0503172v2 [cond-mat.mes-hall] (cit. on pp. 101, 102).

[169] T. Mikami et al., *Brillouin-Wigner theory for high-frequency expansion in periodically driven systems: Application to Floquet topological insulators*, Physical Review B **93** (2016)
(cit. on pp. 102, 112, 120, 125, 178, 218).

[170] R. Yu, X. L. Qi, A. Bernevig, Z. Fang and X. Dai, *Equivalent expression of Z2 topological invariant for band insulators using the non-Abelian Berry connection*, Physical Review B **84** (2011), ISSN: 1098-0121 (cit. on pp. 102, 103).

[171] J. K. Asbóth, L. Oroszlány and A. Pályi, *A Short Course on Topological Insulators*, Springer-Verlag GmbH, 2016, ISBN: 331925605X, URL: https://www.ebook.de/de/product/25029190/janos_k_asboth_laszlo_oroszlany_andras_palyi_a_short_course_on_topological_insulators.html (cit. on pp. 102, 148).

[172] M. Nakagawa, R.-J. Slager, S. Higashikawa and T. Oka, *Wannier representation of Floquet topological states*, Phys. Rev. B 101, 075108 (2020) **101** (2019), arXiv: 1903.12197 [cond-mat.mes-hall] (cit. on p. 103).

[173] F. Nathan and M. S. Rudner, *Topological singularities and the general classification of Floquet–Bloch systems*, New Journal of Physics **17** (2015) 125014 (cit. on p. 103).

[174] W. Chen, *Weakly Interacting Topological Insulators: Quantum Criticality and Renormalization Group Approach*, Phys. Rev. B 97, 115130 (2018) (2018), arXiv: 1801.00697v1 [cond-mat.str-el] (cit. on pp. 103, 143).

[175] P. Molignini, R. Chitra and W. Chen, *Unifying topological phase transitions in noninteracting, interacting, and periodically driven systems*, Eur. Phys. Lett. 128, 36001 (2019) (2019), arXiv: 1912.08819v1 [cond-mat.stat-mech] (cit. on p. 104).

[176] P. Molignini, W. Chen and R. Chitra, *Generating quantum multicriticality in topological insulators by periodic driving*, Physical Review B **101** (2020), ISSN: 2469-9950 (cit. on p. 104).

[177] A. Kitaev, *Anyons in an exactly solved model and beyond*, Annals of Physics **321** (2006) 2 (cit. on p. 104).

[178] X.-G. Wen, *Topological orders and Edge excitations in FQH states*, Advances in Physics, 44, 405 (1995) (1995), arXiv: cond-mat/9506066v2 [cond-mat] (cit. on p. 104).

[179] T. Senthil and M. Levin, *Integer quantum Hall effect for bosons: A physical realization*, (2012), arXiv: 1206.1604 [cond-mat.str-el] (cit. on p. 104).

[180] R. Dijkgraaf and E. Witten, *Topological gauge theories and group cohomology*, Communications in Mathematical Physics **129** (1990) 393 (cit. on p. 104).

[181] X. Chen, Z.-C. Gu, Z.-X. Liu and X.-G. Wen, *Symmetry protected topological orders and the group cohomology of their symmetry group*, Phys. Rev. B 87, 155114 (2013) (2011), arXiv: 1106.4772 [cond-mat.str-el] (cit. on p. 104).

[182] X.-G. Wen, *Choreographed entanglement dances: Topological states of quantum matter*, Science **363** (2019) eaal3099 (cit. on p. 104).

[183] P. Ye, *Gauge theory of strongly-correlated symmetric topological Phases*, Acta Physica Sinica **69** (2020) 077102 (cit. on p. 104).

[184] X. Chen, Z.-C. Gu and X.-G. Wen, *Local unitary transformation, long-range quantum entanglement, wave function renormalization, and topological order*, Physical Review B **82** (2010) 155138 (cit. on p. 104).

[185] F. Verstraete, J. I. Cirac, J. I. Latorre, E. Rico and M. M. Wolf, *Renormalization-Group Transformations on Quantum States*, Physical Review Letters **94** (2005) 140601 (cit. on p. 104).

[186] G. Vidal, *Entanglement Renormalization*, Physical Review Letters **99** (2007) 220405 (cit. on p. 104).

[187] A. Kitaev, *Fault-tolerant quantum computation by anyons*, Annals of Physics **303** (2003) 2 (cit. on p. 104).

[188] P. Weinberg and M. Bukov, *QuSpin: a Python package for dynamics and exact diagonalisation of quantum many body systems part I: spin chains*, SciPost Physics **2** (2017) (cit. on p. 107).

[189] I. L. C. Michael A. Nielsen, *Quantum Computation and Quantum Information*, Cambridge University Pr., 2001, ISBN: 978-1107002173, URL: http://www.ebook.de/de/product/13055864/michael_a_nielsen_isaac_l_chuang_quantum_computation_and_quantum_information.html (cit. on p. 108).

[190] M. A. Sentef, J. Li, F. Künzel and M. Eckstein, *Quantum to classical crossover of Floquet engineering in correlated quantum systems*, Physical Review Research **2** (2020) 033033, arXiv: 2002.12912v2 [cond-mat.str-el] (cit. on pp. 108, 115).

[191] I. Martin, *Floquet dynamics of classical and quantum cavity fields*, Annals of Physics **405** (2019) 101, ISSN: 0003-4916, eprint: 1809.02621v2 (cit. on p. 108).

[192] F. Schlawin, A. Cavalleri and D. Jaksch, *Cavity-Mediated Electron-Photon Superconductivity*, Physical Review Letters **122** (2019) (cit. on p. 108).

[193] S. Ibanez, S. Martinez-Garaot, X. Chen, E. Torrontegui and J. G. Muga, *Shortcuts to adiabaticity for non-Hermitian systems*, Physical Review A **84** (2011) (cit. on pp. 112, 143).

[194] M. Rodriguez-Vega, M. Lentz and B. Seradjeh, *Floquet perturbation theory: formalism and application to low-frequency limit*, New Journal of Physics **20** (2018) 093022 (cit. on p. 112).

[195] D. A. Abanin, E. Altman, I. Bloch and M. Serbyn, *Colloquium : Many-body localization, thermalization, and entanglement*, Reviews of Modern Physics **91** (2019) (cit. on pp. 113, 115).

[196] D. Abanin, W. D. Roeck, W. W. Ho and F. Huveneers, *A Rigorous Theory of Many-Body Prethermalization for Periodically Driven and Closed Quantum Systems*, Commun. Math. Phys. 354, 809-827 (2017) (2015), arXiv: 1509.05386v3 [math-ph] (cit. on p. 114).

[197] D. V. Else, P. Fendley, J. Kemp and C. Nayak, *Prethermal Strong Zero Modes and Topological Qubits*, Physical Review X **7** (2017) (cit. on pp. 114, 115).

[198] N. H. Lindner, E. Berg and M. S. Rudner,
Universal Chiral Quasisteady States in Periodically Driven Many-Body Systems,
Physical Review X **7** (2017) (cit. on p. 115).

[199] A. Herrmann, Y. Murakami, M. Eckstein and P. Werner,
Floquet prethermalization in the resonantly driven Hubbard model,
EPL (Europhysics Letters) **120** (2017) 57001 (cit. on p. 115).

[200] R. Nandkishore and D. A. Huse,
Many-Body Localization and Thermalization in Quantum Statistical Mechanics,
Annual Review of Condensed Matter Physics **6** (2015) 15 (cit. on p. 115).

[201] J. Zhang et al., *Observation of a discrete time crystal*, Nature **543** (2017) 217 (cit. on p. 115).

[202] S. Choi et al.,
Observation of discrete time-crystalline order in a disordered dipolar many-body system,
Nature **543** (2017) 221 (cit. on p. 115).

[203] J. Smits, L. Liao, H. Stoof and P. van der Straten,
Observation of a Space-Time Crystal in a Superfluid Quantum Gas,
Physical Review Letters **121** (2018) 185301 (cit. on p. 115).

[204] J. Rovny, R. L. Blum and S. E. Barrett,
Observation of Discrete-Time-Crystal Signatures in an Ordered Dipolar Many-Body System,
Physical Review Letters **120** (2018) 180603 (cit. on p. 115).

[205] V. Khemani, R. Moessner and S. L. Sondhi, *A Brief History of Time Crystals*, (2019),
arXiv: 1910.10745 [cond-mat.str-el] (cit. on p. 115).

[206] X. Mi et al., *Observation of Time-Crystalline Eigenstate Order on a Quantum Processor*,
(2021), arXiv: 2107.13571 [quant-ph] (cit. on p. 115).

[207] M. Kollar, F. A. Wolf and M. Eckstein,
Generalized Gibbs ensemble prediction of prethermalization plateaus and their relation to nonthermal steady states in integrable systems, Physical Review B **84** (2011) (cit. on p. 116).

[208] H.-J. Schmidt, J. Schnack and M. Holthaus,
Floquet theory of the analytical solution of a periodically driven two-level system,
Applicable Analysis (2018) 1, ISSN: 0003-6811,
arXiv: http://arxiv.org/abs/1809.00558v1 [quant-ph] (cit. on pp. 116, 118).

[209] E. Barnes and S. D. Sarma,
Analytically Solvable Driven Time-Dependent Two-Level Quantum Systems,
Physical Review Letters **109** (2012) (cit. on p. 116).

[210] P. P. Fiziev,
The Heun functions as a modern powerful tool for research in different scientific domains,
(2015), arXiv: 1512.04025v1 [math-ph] (cit. on p. 116).

[211] A. Gangopadhyay, M. Dzero and V. Galitski,
Exact solution for quantum dynamics of a periodically driven two-level system,
Physical Review B **82** (2010) (cit. on p. 116).

[212] A. J. Maciejewski, M. Przybylska and T. Stachowiak, *Full spectrum of the Rabi model*, Phys. Lett. A 378, 1-2, 16-20 (2014) (2013), arXiv: http://arxiv.org/abs/1310.8655v1 [math-ph] (cit. on p. 116).

[213] I. Mendaš, N. Burić, D. Popović, S. Prvanović and M. Radonjić, *Geometric Phase for Analytically Solvable Driven Time-Dependent Two-Level Quantum Systems*, Acta Physica Polonica A **126** (2014) 670 (cit. on p. 116).

[214] A. Messina and H. Nakazato, *Analytically solvable Hamiltonians for quantum two-level systems and their dynamics*, Journal of Physics A: Mathematical and Theoretical **47** (2014) 445302 (cit. on p. 116).

[215] H.-J. Schmidt, *The Floquet theory of the two level system revisited*, Zeitschrift für Naturforschung A **73** (2018) 705, ISSN: 1865-7109, arXiv: http://arxiv.org/abs/1804.01805v1 [quant-ph] (cit. on p. 116).

[216] Q. Xie and W. Hai, *Analytical results for a monochromatically driven two-level system*, Physical Review A **82** (2010) (cit. on p. 116).

[217] E. S. Cheb-Terrab, *Solutions for the general, confluent and biconfluent Heun equations and their connection with Abel equations*, Journal of Physics A: Mathematical and General **37** (2004) 9923 (cit. on p. 116).

[218] L. J. El-Jaick and B. D. B. Figueiredo, *New solutions to the confluent Heun equation and quasiexact solvability*, Applied Mathematics and Computation **256** (2013) 885, ISSN: 0096-3003, arXiv: http://arxiv.org/abs/1311.7677v1 [math-ph] (cit. on p. 116).

[219] R. S. Maier, *On reducing the Heun equation to the hypergeometric equation*, Journal of Differential Equations **213** (2005) 171 (cit. on p. 116).

[220] W. L. Sergei Yu. Slavyanov, *Special Functions: A Unified Theory Based on Singularities (Oxford Mathematical Monographs)*, vol. 193, 3, Oxford University Press; 1 edition (November 16, 2000), 2000 1754, ISBN: 978-0198505730 (cit. on p. 116).

[221] N. Tsuji, T. Oka and H. Aoki, *Correlated electron systems periodically driven out of equilibrium:Floquet+DMFT formalism*, Physical Review B **78** (2008) (cit. on pp. 120–122, 167, 168, 174, 178).

[222] S. Mathey and S. Diehl, *Activating critical exponent spectra with a slow drive*, Phys. Rev. Research 2, 013150 (2020) **2** (2019), arXiv: 1905.03396v2 [cond-mat.stat-mech] (cit. on p. 120).

[223] M. Genske and A. Rosch, *Floquet-Boltzmann equation for periodically driven Fermi systems*, Physical Review A **92** (2015) 062108 (cit. on pp. 120, 176, 177).

[224] M. Genske, *Periodically driven many-body quantum systems: Quantum Ratchets, Topological States and the Floquet-Boltzmann Equation*, PhD thesis: Universität zu Köln, 2017 (cit. on pp. 120, 176).

[225] J. H. Shirley, *Solution of the Schrödinger Equation with a Hamiltonian Periodic in Time*, Physical Review **138** (1965) B979 (cit. on pp. 120, 121, 143).

[226] J. E. Han, *Solution of electric-field-driven tight-binding lattice coupled to fermion reservoirs*, Physical Review B **87** (2013) (cit. on p. 126).

[227] Y. Murakami, N. Tsuji, M. Eckstein and P. Werner, *Nonequilibrium steady states and transient dynamics of conventional superconductors under phonon driving*, Phys. Rev. B 96, 045125 (2017) (2017), arXiv: 1702.02942v3 [cond-mat.supr-con] (cit. on p. 128).

[228] Z. Fedorova, H. Qiu, S. Linden and J. Kroha, *Observation of topological transport quantization by dissipation in fast Thouless pumps*, Nature Communications **11** (2019), ISSN: 2041-1723, arXiv: 1911.03770v3 [quant-ph] (cit. on pp. 131, 139–142, 145, 146, 150, 218).

[229] M. J. Rice and E. J. Mele, *Elementary Excitations of a Linearly Conjugated Diatomic Polymer*, Physical Review Letters **49** (1982) 1455 (cit. on p. 132).

[230] D. J. Thouless, *Quantization of particle transport*, Physical Review B **27** (1983) 6083 (cit. on p. 132).

[231] M. Lohse, C. Schweizer, O. Zilberberg, M. Aidelsburger and I. Bloch, *A Thouless Quantum Pump with Ultracold Bosonic Atoms in an Optical Superlattice*, Nature Phys. 12, 350 (2016) (2015), arXiv: 1507.02225 [cond-mat.quant-gas] (cit. on p. 132).

[232] L. Privitera, A. Russomanno, R. Citro and G. E. Santoro, *Non-adiabatic breaking of topological pumping*, Phys. Rev. Lett. 120, 106601 (2018) (2017), arXiv: 1709.08457 [cond-mat.quant-gas] (cit. on pp. 132, 134, 138, 139, 148).

[233] L. Arceci, L. Kohn, A. Russomanno and G. E. Santoro, *Dissipation assisted Thouless pumping in the Rice–Mele model*, J. Stat. Mech. (2020) 043101 **2020** (2019) 043101, arXiv: 1905.08808 [cond-mat.quant-gas] (cit. on pp. 132, 135).

[234] L. Arceci, *Dissipation effects in driven quantum many-body systems*, PhD thesis, 2019 (cit. on pp. 132, 135).

[235] L. Privitera, *Non-equilibrium aspects of topological Floquet quantum systems*, PhD thesis, 2017 (cit. on pp. 134–136, 138, 139).

[236] B. Höckendorf, A. Alvermann and H. Fehske, *Topological origin of quantized transport in non-Hermitian Floquet chains*, Phys. Rev. Research 2, 023235 (2020) (2019), arXiv: 1911.11413 [cond-mat.mes-hall] (cit. on p. 139).

[237] B. Höckendorf, A. Alvermann and H. Fehske, *Non-Hermitian Boundary State Engineering in Anomalous Floquet Topological Insulators*, Phys. Rev. Lett. 123, 190403 (2019) **123** (2019), ISSN: 0031-9007, arXiv: 1908.01372 [cond-mat.mes-hall] (cit. on p. 139).

[238] B. Höckendorf, A. Alvermann and H. Fehske, *Cutting off the non-Hermitian boundary from an anomalous Floquet topological insulator*, EPL (Europhysics Letters) **131** (2020) 30007, ISSN: 1286-4854 (cit. on p. 139).

[239] P. Schmidt and H. Monien,
Nonequilibrium dynamical mean-field theory of a strongly correlated system, (2002),
arXiv: cond-mat/0202046v1 [cond-mat.str-el] (cit. on pp. 155, 173, 176).

[240] A. Georges, G. Kotliar, W. Krauth and M. J. Rozenberg, *Dynamical mean-field theory of strongly correlated fermion systems and the limit of infinite dimensions*,
Reviews of Modern Physics **68** (1996) 13 (cit. on pp. 155, 157–159, 161, 169, 171–173).

[241] G. Kotliar et al., *Electronic structure calculations with dynamical mean-field theory*,
Reviews of Modern Physics **78** (2006) 865 (cit. on pp. 155, 158, 170).

[242] A. Georges, "Strongly Correlated Electron Materials: Dynamical Mean-Field Theory and Electronic Structure", *AIP Conference Proceedings*, AIP, 2004 (cit. on pp. 155, 166, 167).

[243] D. Vollhardt, A. Avella and F. Mancini,
"Dynamical Mean-Field Theory of Electronic Correlations in Models and Materials",
AIP, 2010 (cit. on pp. 155, 157, 169).

[244] F. H. L. Essler, H. Frahm, F. Göhmann, A. Klümper and V. E. Korepin,
The One-Dimensional Hubbard Model, Cambridge University Press, 2009,
ISBN: 9780511534843, URL:
https://www.amazon.com/One-Dimensional-Hubbard-Model-Fabian-Essler/dp/0511534841?SubscriptionId=AKIAIOBINVZYXZQZ2U3A&tag=chimbori05-20&linkCode=xm2&camp=2025&creative=165953&creativeASIN=0511534841
(cit. on p. 157).

[245] W. Metzner and D. Vollhardt, *Correlated Lattice Fermions ind=∞Dimensions*,
Physical Review Letters **62** (1989) 324 (cit. on p. 158).

[246] J. K. Freericks and V. Zlatić,
Exact dynamical mean-field theory of the Falicov-Kimball model,
Reviews of Modern Physics **75** (2003) 1333, ISSN: 0034-6861 (cit. on pp. 158, 167, 168).

[247] A. I. Lichtenstein and M. I. Katsnelson,
Ab initiocalculations of quasiparticle band structure in correlated systems: LDA++ approach,
Physical Review B **57** (1998) 6884 (cit. on p. 164).

[248] M. Lenk, *DMFT with NCA*, MA thesis: University of Bonn, 2020 (cit. on p. 166).

[249] E. Pavarini, *The physics of correlated insulators, metals, and superconductors lecture notes of the Autumn School on Correlated Electrons 2017*, Forschungszentrum Jülich GmbH, 2017,
ISBN: 9783958062245 (cit. on p. 166).

[250] L. M. Falicov and J. C. Kimball,
Simple Model for Semiconductor-Metal Transitions: SmB6and Transition-Metal Oxides,
Physical Review Letters **22** (1969) 997 (cit. on p. 167).

[251] J. Hubbard, *Electron correlations in narrow energy bands*, Proceedings of the Royal Society of London. Series A. Mathematical and Physical Sciences **276** (1963) 238 (cit. on p. 168).

[252] M.-T. Philipp, M. Wallerberger, P. Gunacker and K. Held,
Mott-Hubbard transition in the mass-imbalanced Hubbard model,
The European Physical Journal B **90** (2017) (cit. on p. 168).

[253] T. Qin and W. Hofstetter, *Nonequilibrium steady states and resonant tunneling in time-periodically driven systems with interactions*, Physical Review B **97** (2018) (cit. on p. 168).

[254] M. Potthoff, *Two-site dynamical mean-field theory*, Phys. Rev. B 64, 165114 (2001) (2001), arXiv: cond-mat/0107502 [cond-mat.str-el] (cit. on pp. 168, 169).

[255] J. Kroha and P. W"olfle, *Fermi and non-Fermi liquid behavior in quantum impurity systems: Conserving slave boson theory*, Acta Phys. Pol. B 29 (12), 3781 (1998) (1998), arXiv: http://arxiv.org/abs/cond-mat/9811074v1 [cond-mat.str-el] (cit. on pp. 170, 207–209).

[256] F. A. Wolf, *Solving dynamical mean-field theory using matrix product states*, 2015, URL: http://nbn-resolving.de/urn:nbn:de:bvb:19-189370 (cit. on p. 170).

[257] A. Dorda, M. Nuss, W. von der Linden and E. Arrigoni, *Auxiliary master equation approach to nonequilibrium correlated impurities*, Physical Review B **89** (2014) 165105 (cit. on p. 170).

[258] O. Parcollet et al., *TRIQS: A toolbox for research on interacting quantum systems*, Computer Physics Communications **196** (2015) 398 (cit. on p. 170).

[259] B. Bauer et al., *The ALPS project release 2.0: open source software for strongly correlated systems*, Journal of Statistical Mechanics: Theory and Experiment **2011** (2011) P05001 (cit. on p. 170).

[260] M. Schüler et al., *NESSi: The Non-Equilibrium Systems Simulation package*, Computer Physics Communications **257** (2020) 107484 (cit. on p. 170).

[261] O. Najera Ocampo, *Study of the dimer Hubbard Model within Dynamical Mean Field Theory and its application to VO2*, Theses: Université Paris Saclay (COmUE), 2017, URL: https://tel.archives-ouvertes.fr/tel-01690699 (cit. on p. 170).

[262] H. A. Bethe, *Statistical theory of superlattices*, Proceedings of the Royal Society of London. Series A - Mathematical and Physical Sciences **150** (1935) 552 (cit. on p. 172).

[263] R. J. Baxter, *Exactly Solved Models in Statistical Mechanics*, DOVER PUBN INC, 2008, 498 pp., ISBN: 0486462714, URL: https://www.ebook.de/de/product/6622293/rodney_j_baxter_exactly_solved_models_in_statistical_mechanics.html (cit. on pp. 172, 174).

[264] A. Lubatsch and J. Kroha, *Optically driven Mott-Hubbard systems out of thermodynamic equilibrium*, Annalen der Physik **18** (2009) 863 (cit. on p. 176).

[265] T. Mikami, *Theory of nonequilibrium steady states in multiband systems in ac-fields and its applications*, PhD thesis: University of Tokyo, 2014 (cit. on p. 178).

[266] A. A. Abrikosov, *Electron scattering on magnetic impurities in metals and anomalous resistivity effects*, Physics Physique Fizika **2** (1965) 5 (cit. on p. 207).

[267] L. Savary and L. Balents, *Quantum spin liquids: a review*, Reports on Progress in Physics **80** (2016) 016502 (cit. on p. 207).

[268] B. H. Wu and J. C. Cao, *Noise of Kondo dot with ac gate: Floquet–Green's function and noncrossing approximation approach*, Physical Review B **81** (2010) 085327 (cit. on p. 207).

[269] N. S. Wingreen and Y. Meir, *Anderson model out of equilibrium: Noncrossing-approximation approach to transport through a quantum dot*, Physical Review B **49** (1994) 11040, ISSN: 0163-1829 (cit. on pp. 207, 209, 210, 213, 214).

[270] T. Lappe, *Non-Markovian Dynamics of Open Bose-Einstein Condensates*, PhD thesis: Rheinische Friedrich-Wilhelms-Universität Bonn, 2021, URL: https://hdl.handle.net/20.500.11811/8961 (cit. on p. 207).

[271] E. Pavarini, *Many-body physics: from Kondo to Hubbard lectures notes of the Autumn School on Correlated Electrons 2015 : at Forschungszentrum Jülich 21-25 September 2015*, vol. 635, Forschungszentrum Jülich GmbH, 2015 092104, ISBN: 9783958060746 (cit. on p. 210).

[272] J. Kroha, P. Hirschfeld, K. Muttalib and P. Wölfle, *Conserving slave boson approach to strongly correlated Fermi systems: Single-impurity Anderson model*, Solid State Communications **83** (1992) 1003 (cit. on p. 213).

[273] M. Eckstein and P. Werner, *Nonequilibrium dynamical mean-field calculations based on the noncrossing approximation and its generalizations*, Physical Review B **82** (2010) (cit. on p. 218).

[274] A. K. Eissing, V. Meden and D. M. Kennes, *Functional renormalization group in Floquet space*, Physical Review B **94** (2016) 245116 (cit. on p. 218).

List of Figures

List of Tables